Exploring the role of *Itch* in human cancer and bone remodelling

Oliver James Read

University of
St Andrews

This thesis is submitted in partial fulfilment for the degree of

Doctor of Philosophy (PhD)

at the University of St Andrews

May 2019

Abstract:

Tight control of post-translational modifications such as ubiquitination is important for cell homeostasis and dysregulation of this process is a common feature in many diseases. *Itch* encodes an E3 ubiquitin ligase that conjugates ubiquitin to a variety of substrates such as Jun B, PKC-θ, PLC- γ1, LATS, TXNIP and p73. In this study both transient and stable knockdown techniques (siRNA and CRISPR respectively) were utilised to explore the role of Itch in both cancer progression and bone remodelling. Transient siRNA-mediated knockdown of *Itch* inhibited cell viability of MiaPaCa-2 and Capan-2 cell lines by ~50% and ~60% respectively compared to both scrambled and untreated controls as determined by SRB. Although siRNA did not increase cell line sensitivity to γ-radiation, doxorubicin, and gemcitabine, it did have an additive effect on resultant survivability. CRISPR-Cas9 mediated stable *Itch* knockdowns in the same cell lines in contrast showed increased sensitivity to the aforementioned treatment regimens however resultant data obtained from cell survival and clonogenicity assays suggested that the $CRISPR^+$ MiaPaCa-2 cells divide faster than both scrambled and parental controls. SWATH-DIA analysis was performed to look for differences in proteome between $CRISPR^+$ and parental MiaPaCa-2 cells. Preliminary data based on isogenic clones suggests potential differences, but additional repeats and further validation is required. Transient *Itch* knockdown in peripheral blood monocytes increased their capacity to differentiate into fully matured osteoclasts ex-vivo: compared to untreated controls, si-Itch treated wells showed higher mean numbers of large $TRAP^+$ cells (mean = 63 and 54 for si-Itch and untreated wells respectively) and multinucleate cells (mean = 25 and 17 for si-Itch and untreated wells respectively) in a 96-well format. Meanwhile CRISPR-mediated knockdown induced a large degree of cellular toxicity in PBMCs. This contrast between stable and transient Itch knockdown prompted discussion of the strengths and weaknesses of each technique and their suitability in different experimental contexts.

Declarations:

Candidate's declaration

I, Oliver James Read, do hereby certify that this thesis, submitted for the degree of PhD, which is approximately 48,000 words in length, has been written by me, and that it is the record of work carried out by me, or principally by myself in collaboration with others as acknowledged, and that it has not been submitted in any previous application for any degree.

I was admitted as a research student at the University of St Andrews in February 2016.

I confirm that no funding was received for this work.

Date Signature of candidate

Supervisor's declaration

I hereby certify that the candidate has fulfilled the conditions of the Resolution and Regulations appropriate for the degree of PhD in the University of St Andrews and that the candidate is qualified to submit this thesis in application for that degree.

Date Signature of supervisor

Permission for publication

In submitting this thesis to the University of St Andrews we understand that we are giving permission for it to be made available for use in accordance with the regulations of the University Library for the time being in force, subject to any copyright vested in the work not being affected thereby. We also understand, unless exempt by an award of an embargo as requested below, that the title and the abstract will be published, and that a copy of the work may be made and supplied to any bona fide library or research worker, that this thesis will be electronically accessible for personal or research use and that the library has the right to migrate this thesis into new electronic forms as required to ensure continued access to the thesis.

I, Oliver James Read, confirm that my thesis does not contain any third-party material that requires copyright clearance.

The following is an agreed request by candidate and supervisor regarding the publication of this thesis:

Printed copy

No embargo on print copy.

Electronic copy

Embargo on all of electronic copy for a period of 1 year on the following ground(s):

- Publication would preclude future publication

Supporting statement for electronic embargo request

Manuscripts are currently in preparation.

Title and Abstract

- I agree to the title and abstract being published.

Date Signature of candidate

Date Signature of supervisor

Underpinning Research Data or Digital Outputs

Candidate's declaration

I, Oliver James Read, hereby certify that no requirements to deposit original research data or digital outputs apply to this thesis and that, where appropriate, secondary data used have been referenced in the full text of my thesis.

Date Signature of candidate

Acknowledgements:

I'd like to thank the following for their help and support throughout my time in St Andrews:

First and foremost I would like to thank my supervisor, Professor David Harrison, for granting me the opportunity of undertaking a PhD project in a subject area I'm passionate about. It is my understanding that my project was seen as a "dark horse" as it was significantly different to the other work performed in our group, however David has both provided encouragement and reinforced my confidence in my work at times as well as listening to any crazy ideas as to where to take the project. I truly feel that this opportunity is a debt I'll never be able to repay.

Dr Paul Reynolds, my secondary supervisor, and Awa Sar who took me through the theory and protocols of some of the genome editing techniques when I was first starting out. If it were not for them allowing me to shadow and utilise their excellent knowledge of the subject matter, my project would have been infinitely more difficult to complete.

Members of the Harrison lab group past and present. Special mention to Peter Mullen, Jen Bré, and Fiona McKissock for all their help with ideas for experiments, methodologies, writing advice and science banter.

The St Andrews Mass Spectrometry and Proteomics Facility for their help with SWATH and mass spec. Most notably Dr Sylvia Synowsky, who took me through the entire process from sample preparation to final analysis.

Breakfast Club (trademark pending) for providing motivation to make it into the office each morning and for fuelling my caffeine and breakfast roll addiction.

Cameron and Doug: "Let your servant be born again from the sea as you were. Bless him with salt, bless him with stone, bless him with steel. What is dead may never die, but rises again, harder and stronger."

And finally, my mother, father, brother, sister and the rest of my family and friends back home for their constant support, regular spot-checks on my sanity, and ceaseless apparent amazement whenever I talk about my project.

For the benefit of anyone reading this, I've refrained from putting in puns that I've been itching to make. Although this passage only begins to scratch the surface, given enough time I'm sure I could have come up with a p-sora of mildly irritating content.

Table of Contents

Table of Figures:

List of Commonly Used Abbreviations:

ALP: alkaline phosphatase
APC: antigen presenting cell
AP-1: activator protein 1
BFR: bone formation rate
Cas: CRISPR associated protein
Cas9n: Cas9 nickase
CMI/DCMI: clomipramine/desmethylclomipramine
CRISPR: clustered regularly interspaced short palindromic repeats
crRNA: CRISPR-RNA
CSC: cancer stem cell
CYLD: cylindromatosis
DNA: deoxyribonucleic acid
DUB: deubiquitinating enzyme
ECM: extracellular matrix
DSB: double stranded break
HDR: homology directed repair
HECT: homologous to E6AP C terminus
g/sgRNA: guide/single guide RNA
IF: immunofluorescence
Ig: immunoglobulin
IHC: immunohistochemistry
IL: interleukin
JNK 1: c-Jun N-terminal protein kinase 1
LATS1: large tumour suppressor homolog 1
Lys: lysine
MAPK (p38α): mitogen activated protein kinase
M-CSF: macrophage colony stimulating factor
MDM2: mouse double minute 2 homolog
MEF: mouse embryonic fibroblast
mRNA: messenger RNA
Ndfip 1: Nedd4 family interacting protein 1
Nedd 4: neural precursor cell expressed developmentally downregulated protein 4
NFAT: nuclear factor of activated T-cells
NF-κβ: nuclear factor-κβ
NHEJ: non-homologous end joining
OPG: osteoprotegrin
PAM: protospacer adjacent motif
PBMC: peripheral blood monocyte
PKC-θ: protein kinase C-θ
PLC-γ1: phospholipase C-γ1
qPCR: quantitative polymerase chain reaction
RANK(L): receptor activated NF-κβ (ligand)
RBR: RING between RING
RING: really interesting new gene
RNA: ribonucleic acid
RNAi: RNA interference
Runx2: runt-related transcription factor 2
shRNA: short hairpin RNA

siRNA: small interfering RNA
Smurf 1: Smad ubiquitination regulating factor 1
SRB: sulforhodamine B
SSB: single stranded break
SWATH MS: sequential windowed acquisition of all theoretical mass spectra
Tab1: TGF-β-activated kinase 1-binding protein 1
TALEN: transcription activator-like endonucleases
TAZ: transcriptional activator with PDZ binding motif
TCR: T-cell receptor
TEAD1-4: TEA domain family member 1-4
T_{FH}: T-follicular helper cell
TGF-β: transforming growth factor β
TGFBR2: TGF-β receptor 2
T_H2: T-helper type 2 cell
TMA: tissue microarray
Tp73/63/53 (p73/63/53): tumour protein 73/63/53
tracrRNA: trans-activating crRNA
TRAF6: TNF receptor-associated factor 6
TRAP: tartrate resistant acid phosphatase
Treg: regulatory T-cell
Trx: thioredoxin
TXNIP: thioredoxin interacting protein
Ub: ubiquitin
Wt: wild type
WWP2: WW domain containing E3 ubiquitin protein ligase 2
YAP-1: yes associated protein-1
ZFN: zinc-finger endonucleases
μ: mean

Chapter 1 – Introduction:

Background:

Ubiquitination is a post-translational process that is crucial for cell homeostasis. It involves the "tagging" of proteins with the molecule ubiquitin (Ub) to dictate the fate of the protein, be it activating a protein to take part in pathway signalling or targeting the protein for degradation by the proteasome. Ubiquitination itself involves an enzyme cascade starting with ubiquitin-activating enzymes (E1), ubiquitin-conjugating enzymes (E2), then ubiquitin ligases (E3) before Ub can be covalently tagged onto the target protein (Figure 1) (Berndsen & Wolberger, 2014; Sluimer & Distel, 2018; Zheng & Shabek, 2017). The consequence of ubiquitin tagging is determined by the number of and the pattern in which Ub molecules are conjugated. In addition to either being mono-ubiquitinated or multi-monoubiquitinated (multiple tagging sites on a single protein), proteins can also be polyubiquitinated with linear or branched Ub chains. Ub molecules can form covalent bonds with each other via their seven lysine (Lys) residues and amino N-terminus (Bernassola et al., 2008; Berndsen & Wolberger, 2014; Sluimer & Distel, 2018). Whichever Lys residue is polyubiquitinated is also an important factor in determining the substrate's fate, for example Lys48 polyubiquitin chains typically signal for degradation via the 26s proteasome. Other consequences of polyubiquitination include changes in intracellular localisation and activation/inhibition of downstream signalling in cellular pathways.

E3 ligases in particular are mainly attributed with target specificity as they are the endpoint of the enzyme cascade: they have been one of the main areas of study. This also makes them attractive candidates for drug discovery, as regulation of E3 ligases is highly implicated in disease (Nalepa, Rolfe, & Harper, 2006; Petroski, 2008). There are three main families of E3 ligases: Homologous to E6AP C terminus (HECT), really interesting new gene (RINGs), and RING between RINGs (RBRs) (Zheng & Shabek, 2017). E3s are responsible for the recruitment of an E2~Ub complex and the target substrate mediating then transferring Ub from E2 to substrate. HECT and RBR E3 ligases perform this function as a two-step transthioesterification mechanism where Ub is transferred from the cysteine active site of the E2 enzyme to a cysteine in the HECT domain before transfer of Ub to the substrate (Berndsen & Wolberger, 2014; Sluimer & Distel, 2018). This is in contrast to RING E3s, which catalyse the direct transfer of Ub from the E2~Ub complex to the substrate (Figure 1).

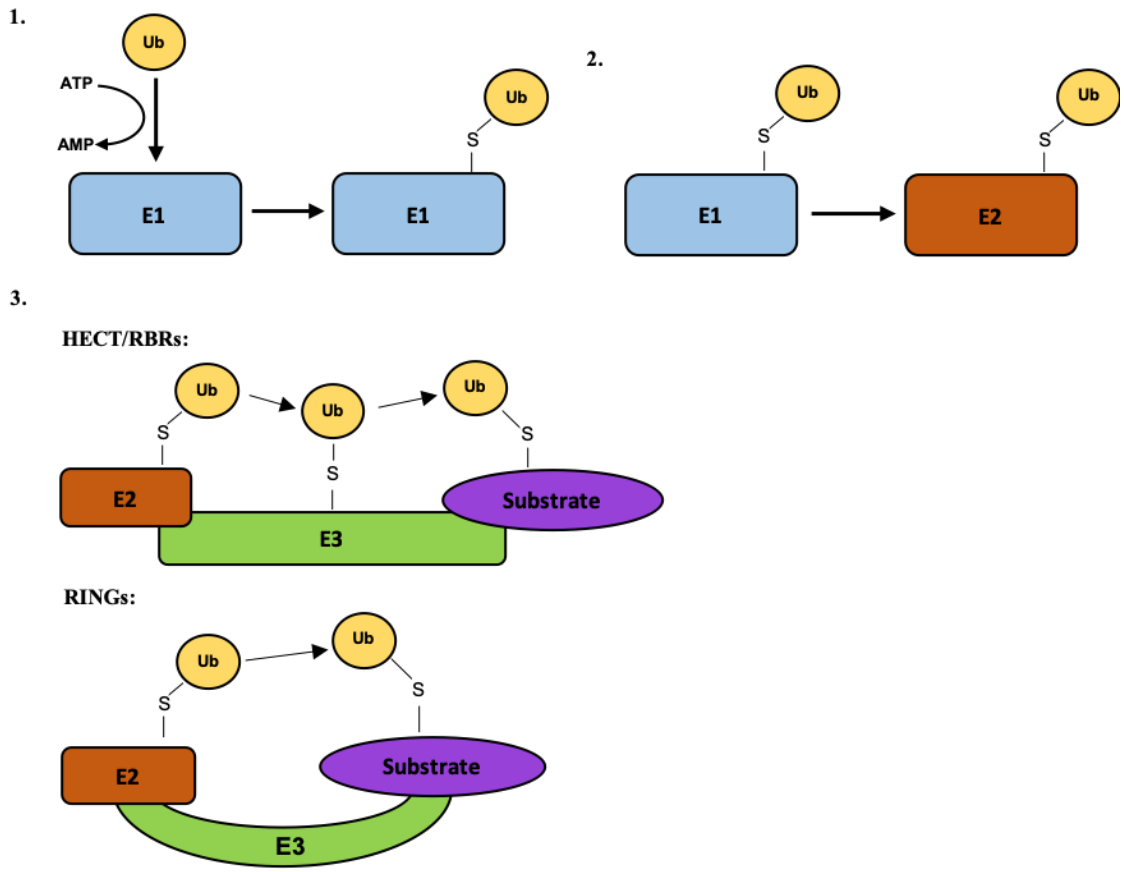

Figure 1: Ubiquitination summary:

(1.) E1 activating enzyme uses ATP to recruit Ub to its active cysteine residue (S). (2.) Ub is transferred from E1 to an E2-conjugating enzyme.(3.) E3 ubiquitin ligases catalyse transfer of Ub from E2 to the substrate. This is done either via a two-step transthioesterification process (HECTs/RBRs) where Ub is first transferred to a cysteine residue on the E3 ligase before being transferred to the substrate, or in the case of RING E3s, is transferred directly to the substrate. Original figure.

Itch – a HECT domain E3 ubiquitin ligase:

The *Itch* gene was first discovered by Perry in non-agouti-lethal 18H mice. These mice had a chromosomal inversion of the *Itch* gene which resulted in the mice displaying various autoimmune characteristics such as chronic interstitial inflammation, alveolar proteinosis, and inflammation of glandular stomach and skin (Perry et al., 1998). The inflamed skin phenotype was what attributed the gene its name as the mice displayed a large degree of scarring due to excessive itching (Fang et al., 2002). *Itch* itself encodes a HECT-domain E3 ubiquitin ligase that belongs to the Nedd4 subfamily (neural precursor cell expressed developmentally downregulated protein 4), one of the more well-studied subgroups of E3-ligases. The Nedd4 subfamily is structurally categorised by a number of WW domains and a single C2 domain positioned more N-terminally to the HECT domain located at the C-terminus (Bernassola et al., 2008; Sluimer & Distel, 2018). Itch in particular has 4 tryptophan (WW) domains between the C2 and HECT domains (Figure 2.).

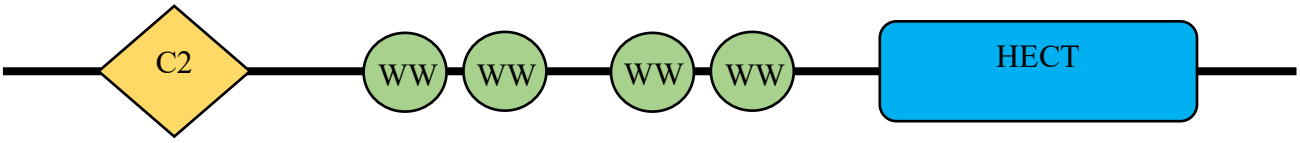

Figure 2: Homologous domain structure of the Itch protein:

The *Itch* gene encodes a HECT E3 ubiquitin ligase that contains the catalytically active HECT domain at the C-terminus, 4 WW domains to facilitate and diversify substrate binding, and a C2 calcium-regulatory domain at the N-terminus. Original figure.

The HECT domain catalyses the transfer of Ub from an E2 conjugating enzyme to the target substrate. C2 domains are usually described as Ca2+ and phospholipid binding domains (Rizo & Südhof, 1998) but can also direct E3 ligases to their substrates as is the case with Smad ubiquitination regulating factor 1 (Smurf1), another Nedd4 family member (Tian et al., 2011). However, whether or not this is the case with Itch is unknown. The four WW domains allow Itch to interact with proline-rich motifs (such as PPxY) on its target substrates. Furthermore, they also play an important role in regulating Itch's enzymatic activity. Itch naturally exists in an autoinhibited closed state (Figure 3-A.) where the central WW domains (notably WW2) bind to the proline-rich motifs in the HECT domain (Gallagher et al., 2006; Riling et al., 2015; Zhu et al., 2017). In this state Itch can associate with an E2 conjugating enzyme but cannot undergo transthioesterification to move Ub to the active site cysteine on the HECT domain. This autoinhibition can be relieved either through the binding of an adaptor protein such as Nedd4 family interacting protein 1 (Ndfip 1) (Figure 3-A.) or by being phosphorylated by c-Jun N-terminal protein kinase 1 (JNK1) (Figure 3-B.).

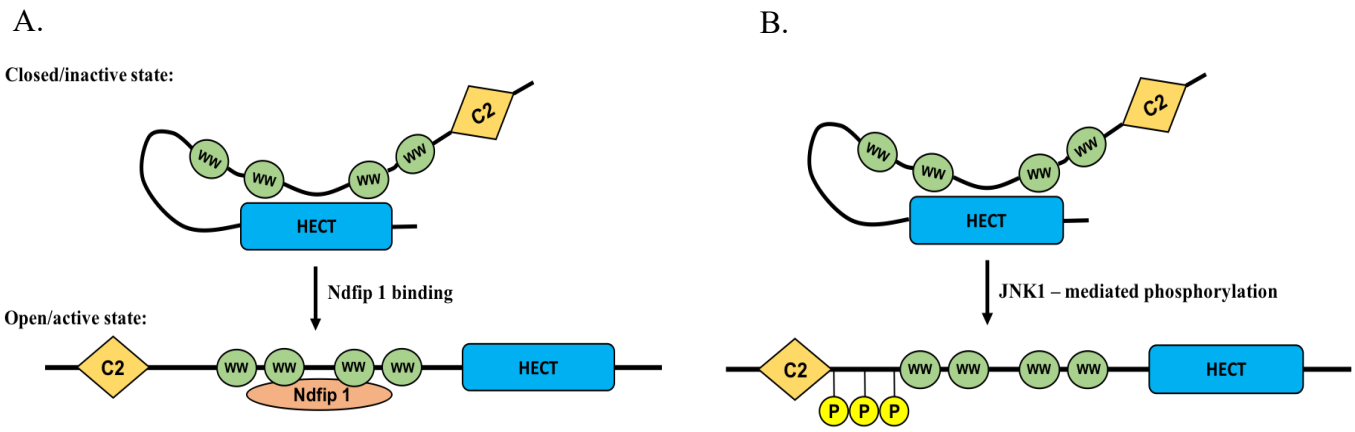

Figure 3: Active and inactive forms of Itch E3 ligase:

Internal WW domains of the Itch protein bind to the HECT domain to keep the E3 ligase in a catalytically inactive state. This prevents the transfer of Ub from E2 to the substrate via the HECT domain. Itch autoinhibition can be relieved either through associating with an adaptor protein e.g. Ndfip 1 (**A.**) or through JNK1-mediated phosphorylation near the N-terminus (**B.**). These interactions allow the WW domains to bind to potential substrates and "frees-up" the active site cysteine residue on the HECT domain to allow Ub to bind to it. Original diagram based on data from: Riling et al., 2015; C. Yang et al., 2006; Zhu et al., 2017.

As previously mentioned, Itch was first identified as a key regulator of the immune response: mice lacking the gene display a severe autoimmune phenotype. This is also mirrored in humans: A study by Lohr's group followed a small, closed group of children of Old-Amish heritage. These children displayed various autoimmune characteristics such as immune infiltrates in lungs, liver and gut as well as showing developmental delay, failure to thrive and dysmorphic features (Lohr et al., 2010). Through autozygosity mapping they discovered that the children had a mutation in the *Itch* gene which resulted in a truncated version of the E3 ligase that lacked the catalytically active HECT domain and WW binding domains. This mutated form of Itch would therefore be unable to bind either an E2 or any of Itch's numerous substrates or adaptor proteins. These phenotypes in mice and humans clarify that *Itch* is a clinically relevant gene worthy of investigation as there does not seem to be any method of redundancy by other HECT E3 ligases in the absence of functioning Itch protein. The first and most obvious topic to address is Itch's role in regulating the immune response and how the autoimmune phenotype could develop in the case of a knockout. Itch exerts its influence over the immune system through various means including regulating lymphocyte activation, differentiation of lymphocytes, and self-tolerance.

Itch in immunity:

T-Cell receptor activation and T-cell anergy:

To generate an immune response a T-lymphocyte or T-cell requires stimulation of the T-cell receptor (TCR) with an antigen from an antigen-presenting cell (APC). This triggers a signalling cascade that leads to clonal expansion of T-cells and an immune response against the antigen. TCR stimulation activates protein kinase C-θ (PKC-θ) and phospholipase C-γ1 (PLC- γ1). PKC-θ activates nuclear factor of activated T-cells (NFAT), which can lead to increased levels of Itch (Figure 4) as discussed below, whilst PLC- γ1 stimulates nuclear factor κ-B (NF-κB) and activator protein-1 (AP-1) (Aki, Zhang, & Liu, 2015; Heissmeyer et al., 2004; Melino et al., 2008; Pardoll, 2012). For T-cell expansion to occur there needs to be co-stimulation at the TCR from the association of both AP-1 and NFAT.

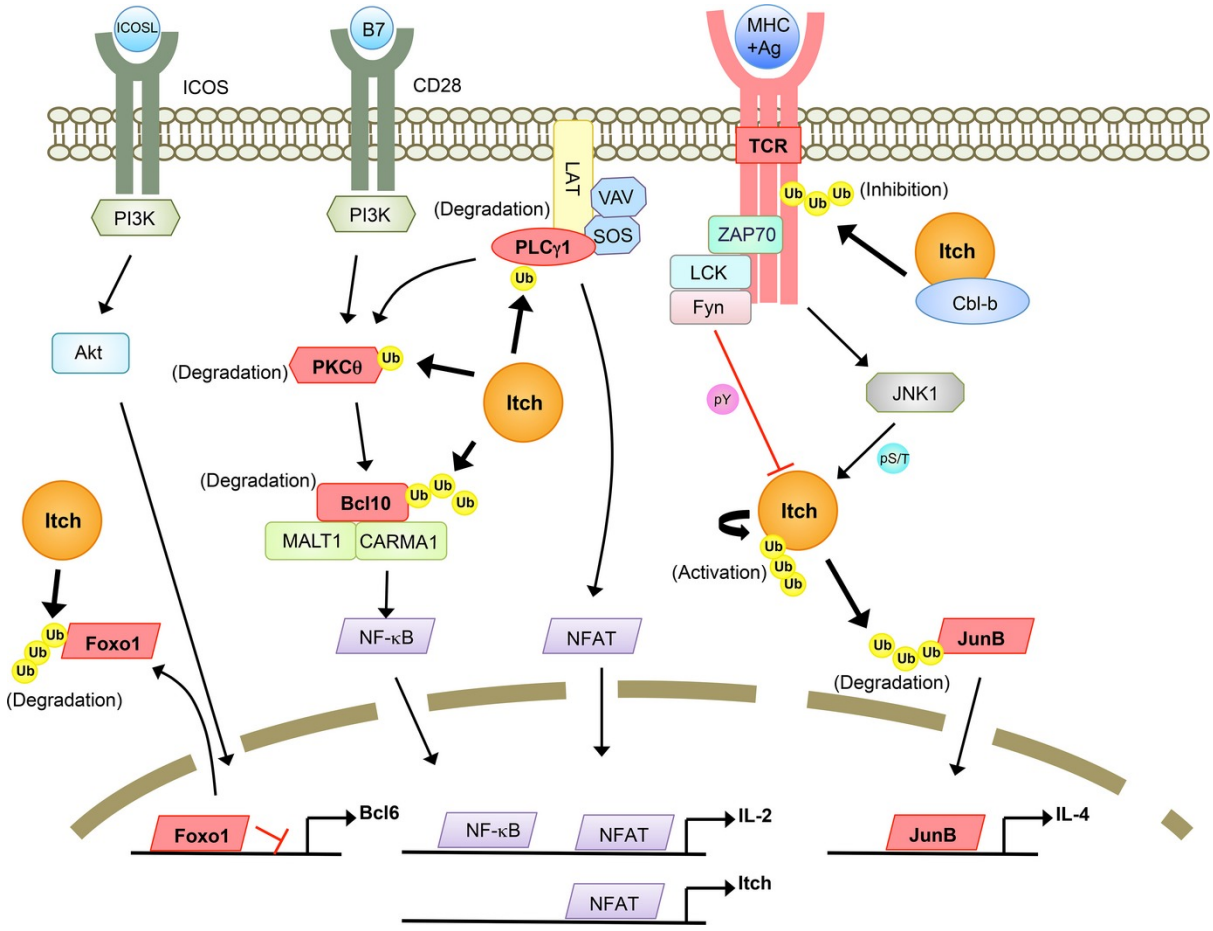

Figure 4: Itch regulation of TCR signalling:

Schematic showing the various ways that Itch (orange) regulates TCR signaling upon interaction with an APC. TCR stimulation causes both NFAT-mediated upregulation of *Itch* expression and JNK1-mediated phosphorylation of Itch protein to activate its E3 ligase activity. Itch then ubiquitinates its substrates (red), for example PLC-γ1 and PKC-θ, to inhibit further TCR signaling and promote anergy of T-cells. Diagram from Aki et al., 2015.

With the surplus peripheral T-cells that circulate in our bodies and such a broad spectrum of antigen targets, how is it that they avoid inadvertently reacting with self-proteins, leading to autoimmunity? Encouragement of T-cell tolerance to self begins with their development in the thymus from haematopoeitic stem cells in a process known as central deletion (Walker & Abbas, 2002). But once they exit this initial screening step, further molecular mechanisms, known as peripheral tolerance mechanisms (Aki et al., 2015; Walker & Abbas, 2002), are required to prevent potential autoimmunity. One of these is known as anergy or "T-cell anergy": the process of rendering a lymphocyte functionally inactive but still alive after interaction with a specific antigen and cell-surface receptors. Itch facilitates T-cell anergy by monoubiquitinating PKC-θ and PLC- γ1 (Figure 4), targeting them for degradation by the proteasome (Heissmeyer et al., 2004). To initiate T-cell clonal expansion and an immune response after formation of the immune synapse and activation of the TCR, there needs to be co-stimulation and activation of NFAT and AP-1. However in the absence of co-stimulation of AP-1, that is when only NFAT is activated, NFAT causes transcriptional upregulation of Itch mRNA levels (Aki et al., 2015; Heissmeyer et al., 2004; Venuprasad et al., 2015). Itch

localises to the immune synapse to downregulate PLC- γ1 and PKC-θ signalling (and thus prevent persistent NF-κB signalling also), which shortens the duration of the immune synapse and promoting anergy.

T-helper type 2 cells:

JunB is a transcription factor that is important for the development of T-helper type 2 cells (T_H2) from activated T-cells. It is also a substrate for polyubiquitination by Itch: upon TCR stimulation, Itch is recruited and phosphorylated by JNK1 to increase its E3 ligase activity and ubiquitinate JunB for degradation by the proteasome (Fang et al., 2002). In *Itch-/-* mice there is a polarization of $CD4^+$ naïve T-cells to differentiated T_H2 cells as shown by increased levels of cytokines interleukin 4 and 5 (IL-4, IL5). Lack of degradation of JunB by Itch causes increased protein stability of JunB in activated T-cells, thus increasing its transcriptional influence on IL-4 and IL-5 promoters which in-turn encourages more naïve T-cells to develop into T_H2 cells (Li et al., 2014). This polarization of naïve T-cells may in part explain the autoimmune phenotype as T_H2 are known to play a main role in the allergic response (Aki et al., 2015; Li et al., 2014) and switching of antibody classes to IgG1, IgA and IgE (Figure 5, Fang et al., 2002) which have been implicated in various inflammatory diseases (Grewe et al., 1998; Williams, Tjota, & Sperling, 2012). Accumulation of JunB in T-cells and polarised T_H2 development is also apparent in *Ndfip 1*-/- knockout mice which showed a similar phenotype to *Itch-/-* mice (Oliver et al., 2006). Ndfip 1 being an adaptor protein is important for changing the conformation of Itch from its inactive to active state by making the WW binding domains and HECT domain available (Riling et al., 2015). Lack of functioning Ndfip 1 means that Itch is kept in its "closed" conformation and therefore cannot ubiquitinate JunB and inhibit T_H2 differentiation. A more recent study has also shown that Itch cooperates with another Nedd 4 family member WWP2 to limit T_H2 differentiation by affecting the strength of TCR signalling (Aki et al., 2018).

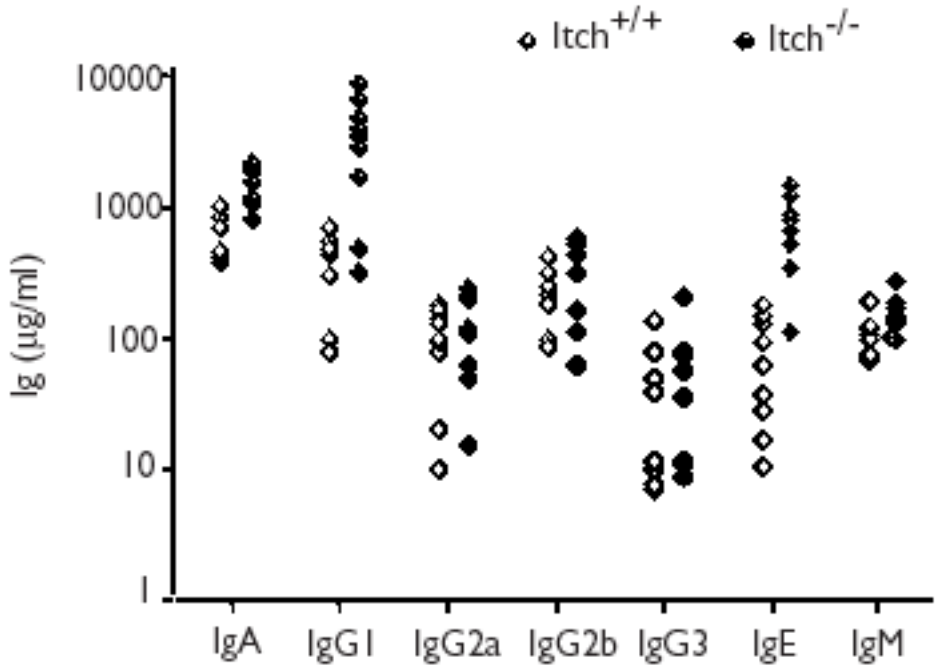

Figure 5: Increased IgA, IgG1 and IgE in Itchy mice:

Serum samples from 10 6-week to 6-month old mice were tested for specific immunoglobulins. Comparison of Itch-/- mice with wild-type revealed a significant increase in classes IgGA (1st column), IgG1 (2nd column), and IgE (6th column). Data from Fang et al., 2002.

T-follicular helper cells and other aspects of immune regulation:

Further evidence of Itch being functionally important in regard to the immune system is in its role in the differentiation of follicular helper T-cells (T_{FH}). *Itch* -/- T-cells were found to be unable to differentiate into T_{FH} cells (Xiao et al., 2014), this prevents the assisted activation of naïve B-cells and the maintenance of germinal centres (Crotty, 2011; Victora & Nussenzweig, 2012) which are key events in the adaptive immune response. A recent study also showed that *Itch* -/- mice have increased protein kinase p38α (MAPK) activity (Theivanthiran et al., 2015), a key inflammatory mediator, due to lack of regulation of Tab1 (TGF-β-activated kinase 1-binding protein 1). This causes p38α autophosphorylation and thus activation of downstream signalling (Ge et al., 2002).

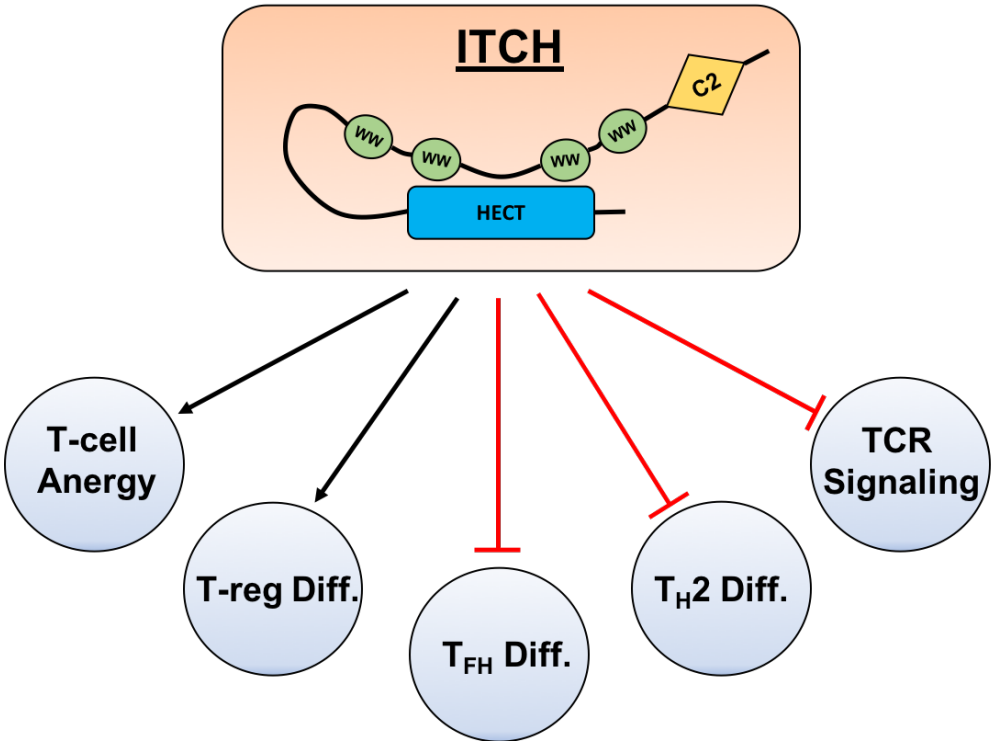

Figure 6: The multifaceted role of Itch in regulating immunity:

Itch E3 ligase activity impacts many pathways linked to regulating the immune system and preventing autoimmunity. Transfer of Ub to proteins associated with specific pathways either upregulates (anergy and Treg differentiation – discussed later) or inhibits them (T_{FH}/T_H2 differentiation and TCR signalling). Original figure.

A wider role for Itch in human pathology?

These are a few examples of the multi-modal way in which Itch modulates the immune response to prevent autoimmunity as seen in the knockout mouse model and humans lacking functional Itch protein (summarised in Figure 6). One of the aspects of cancer cell and tumour survival in a living organism is avoidance of immune surveillance; indeed, immunotherapy i.e. the concept of manipulating the host's immune system to recognise and target tumour tissue is currently one of the most well-researched and promising avenues of cancer research in the modern era (Conroy et al., 2012; Pardoll, 2012). It may be possible that cancer cells utilise E3 ubiquitin ligases such as Itch to manipulate their "visibility" to the immune system and that they may be attractive targets for anti-cancer therapy. However, Itch has several potential substrates that are not limited to immune system regulation. This is in large part due to its ability to interact with several co-factors to promote its E3 ligase activity on specific proteins. Furthermore, the fact that the children described in Lohr's study also showed signs of developmental delay and dysmorphic features heavily implies that Itch plays a larger and wider role in human pathology than exclusively immune system regulation.

The role of Itch in cancer:

In addition to Itch's importance in immune homeostasis, the E3 ligase has been shown to regulate several pathways linked to apoptosis, cell growth, and cell survival (Bernassola et al., 2008; Melino et al., 2008). For this reason, researchers have investigated tumourigenic pathways with Itch substrates that could be impacted by changes in its enzymatic activity. It is now emerging that manipulating Itch activity may be a potent therapeutic strategy for treating cancer in various tissues that show high Itch expression or aberrant signalling of pathways associated with Itch e.g. hippo signalling, p73, and TGF-β (Figure 7). Some labs have already begun to investigate the therapeutic potential of Itch inhibition: the traditionally used anti-depressant clomipramine (CMI) was tested to see if it could increase the sensitivity of lung CSCs (cancer stem cells) to DNA damaging agents including gemcitabine, paclitaxel, and cisplatin (Bongiorno-Borbone et al., 2015). They found that desmethylclomipramine (DCMI - the active metabolite of CMI) did indeed amplify the cytotoxic effect of DNA damaging drugs on lung CSCs when used in combination. In the same investigation they also found similar results through shRNA silencing of Itch in combination with the aforementioned chemotherapeutics. This was done after Rossi's group performed a high throughput drug screen looking for compounds which inhibited Itch function with high specificity compared to other HECT domain E3 ligases. This screen identified CMI to be one of the most specific with significant inhibition of Itch activity (Rossi et al., 2014). CMI Inhibits Itch activity through association with the HECT domain; irreversibly blocking transthiolation of Ub from E2 to E3. However it was noted that in a previous study performed by the same group that CMI/DCMI also blocks autophagic flux which makes cancer cells more susceptible to cytotoxic agents (Rossi et al., 2009). Furthermore, they observed that whilst CMI did not inhibit any of the tested RING E3 ligases it did inhibit E3 activity of E6AP, another HECT domain E3 ligase. Therefore, it is unclear if the results for the cytotoxicity assays seen in the papers investigating CMI/DCMI's effect on Itch levels is indeed due the reduction of Itch activity, inhibition of autophagy, or a combination of both in addition to the degree of specificity to degree of specificity to Itch. They did assess analogous compounds to CMI for efficiency of Itch inhibition however none exceeded the efficacy of DCMI.

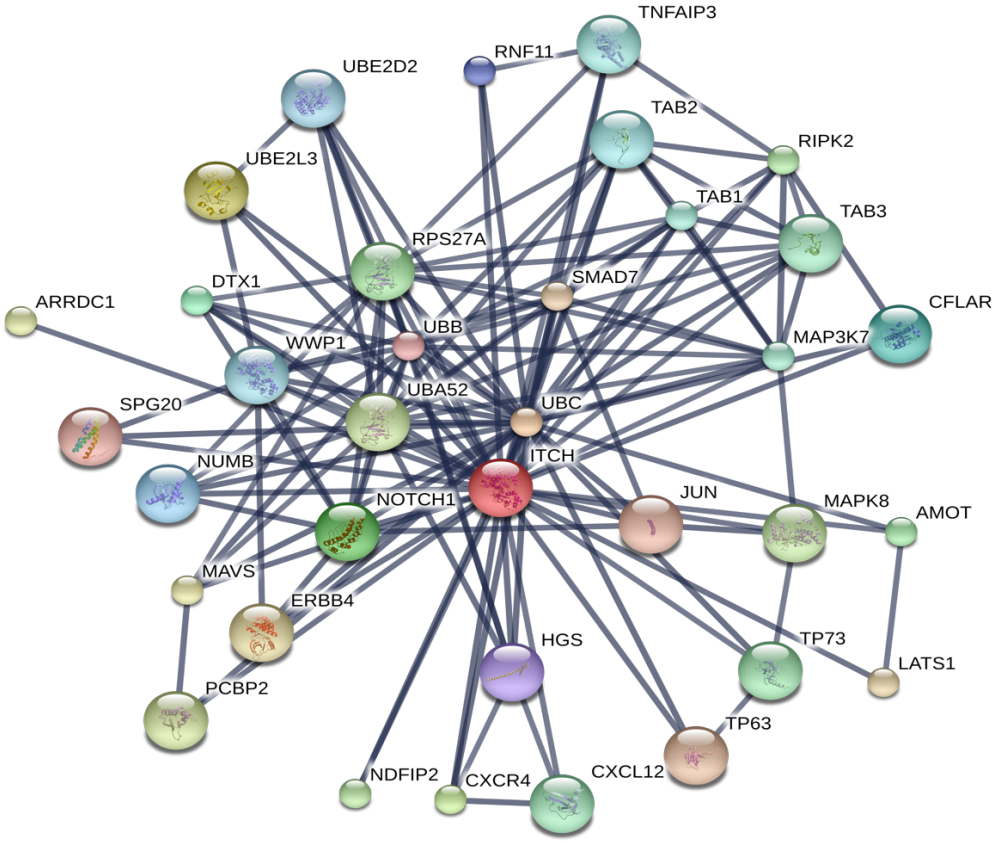

Figure 7: human Itch predicted and known protein interaction network.

Network generated in STRING (search tool for the retrieval of interacting genes/proteins, (Szklarczyk et al., 2015)) showing a confidence view. Each node donates a protein with Itch (red) at the centre and associations as lines between nodes: thicker lines indicate stronger associations. Confidence score restricted to highest (90%) and no more than 50 interactions shown. Proteins listed in order of highest confidence score, proteins in bold are discussed in more detail in the text: UBC: ubiquitin C; UBE_2L3: ubiquitin-conjugating enzyme E_2L3; CXCR4: chemokine (C-X-C motif) receptor 4; NOTCH1: notch 1; DTX1: deltex homologue 1 (*Drosophila*); CFLAR: CASP8 and FADD-like apoptosis regulator; NUMB: numb homologue (*Drosophila*); RNF11: ring finger protein 11; HGS: hepatocyte growth factor-regulated tyrosine kinase substrate; UBB: ubiquitin B; SPG20: spastic paraplegia 20; **JUN**: jun proto-oncogene; **TP63**: tumour protein 63; **SMAD7**: SMAD family member 7; **LATS1**: large tumour suppressor homologue (*Drosophila*); ERBB4: v-erb-a erythroblastic leukemia viral oncogene; MAVS: mitochondrial antiviral signalling protein; ARRDC1: arrestin domain containing 1; PCBP2: poly(rC) binding protein 2; UBA52: ubiquitin A-52 residue ribosomal protein fusion product 1; MAPK8: mitogen-activated protein kinase 8; **NDFIP2**: Nedd4 family interacting protein 2; RIPK2: receptor-interacting serine-threonine kinase 2; RPS27A: ribosomal protein S27a; AMOT: angiomotin; **TP73**: tumour protein 73; CXCL12 chemokine (C-X-C motif) ligand 12; TAB3: TGF-β activated kinase 1; MAP3K7: mitogen activated protein kinase kinase kinase 7; TAB1 TGF-β activated kinase 1; TAB1: TGF-beta activated kinase 1; **TNFAIP3**: tumour necrosis factor, alpha induced protein 1; TAB2: TGF-beta activated kinase 1; **WWP1**: WW domain containing E3 ubiquitin protein ligase 1; UBE2D2: ubiquitin-conjugating enzyme E2D2.

Tumour protein 73 (Tp73/p73):

The transcription factor p73, along with Tp63 (p63), was first identified by Kaghad's group and was found to have strong homology with the tumour-suppressor p53 (Kaghad et al., 1997). It was found to be functionally similar to p53 (which is commonly mutated in cancers), being able to upregulate numerous targets of p53 and is thus a regulator of apoptosis and cell cycle progression. Tp73 and p63 have many splice isoforms (Kaghad et al., 1997; Levrero et al., 2000) which allow variance in function and output. Whether or not p73 specifically acts as a tumour suppressor or an oncogene seems to depend on cellular context and the levels of different isoforms. Splice isoforms that affect the C-terminal, i.e. the TAp73 splice variants, are tumour suppressive, promoting apoptosis and cell cycle arrest signalling cascades whilst the N-terminal splice isoforms, i.e. ΔNp73 are oncogenic as they inhibit apoptosis (Yang et al., 2002). In general *p73* is not mutated in cancer: mice that are heterozygous for *p73* and *p63* show a predisposition to developing tumours in their lifetimes; incidence of lung adenoma was 10% in wild-type, 25% in p63+/-, and 40% in p73+/-, n=40) (Flores et al., 2005). This was especially the case in mice that were also *p53* null where the incidence of tumour develop was additive compared to just p73/63 heterozygosity. Additionally *p73* null mice seem to show severe developmental neural defects such as hippocampal dysgenesis (Yang et al., 2000) along with immune defects. Developmental defects in a *p73* null system would make sense in regards to its role in regulation of apoptosis: apoptosis plays a major role in the development of an organism for example by governing tissue morphology with respect to anatomical axis. Furthermore, several experiments have shown that inhibition of p73 regulators promotes apoptosis, described in more detail below. On the other hand it has been observed that p73 is mutated in neuroblastoma (Kaghad et al., 1997). Additionally in the case of glioblastoma cell lines, knockdown of TAp73 in-vitro reduces chemo resistance and metastasis (Landré et al., 2016) through inhibition of periostin (POSTN) which is a mediator of a variety of cancers such as ovarian and breast (Field et al., 2016; Sung et al., 2016).

Tp73 also differs from p53 in the way that it is degraded. MDM2 has inherent E3 activity; this allows it to degrade p53 (Honda, Tanaka, & Yasuda, 1997; Kubo et al., 2010). Although it can interact with p73 and forced overexpression of MDM2 results in inhibition of p73 function, it does not actually target it for degradation by the proteasome. It is now apparent that MDM2 promotes degradation of p73 through interaction with Itch (Kubo et al., 2010; Wu & Leng, 2015). Pull-down phage displays have shown that Itch is able to interact with the PPxY motif on p73 via its WW binding domains and target it for degradation (Rossi et al., 2005); p53, by contrast lacks the PPxY motif and so cannot interact with Itch. The fact that Itch is a specific inhibitor of p73 (and not p53) function, and p73 upregulating many of the same genes as p53, has made it an attractive candidate among some scientists as a therapeutic target for increasing chemo sensitivity of cancer cell lines (Hansen et al., 2007) since p53 is commonly mutated in disease whilst p73 remains largely unaffected. Hansen and his group reported that MEFs (mouse embryonic fibroblasts) mutant for Itch showed increased cell death by measuring the percentage of hypodiploid cells, annexin expression and changes in membrane potential. They also reported that genetic knockdown of Itch in HeLa cells causes them to have increased sensitivity to doxorubicin treatment (a drug that causes cell-cycle arrest) and that reintroduction of Itch into MEFs with an *Itch* null mutation promoted resistance to treatment (Hansen et al., 2007). This work was consolidated in-vivo by de la Fuente's group (Figure 8: A.): MiaPaCa-2 cells (a pancreatic cell line) were transfected with *Itch*-targeting shRNA and grafted onto xenograft mice and found that this inhibited tumour growth when combined with gemcitabine (de la Fuente et al., 2015) without

any difference in toxicity to the mice (measured by looking at changes in body weight over time, Figure 8: B. & C.). However, in their experiment the combination of shRNA-scrambled and gemcitabine treatment also caused a significant decrease in tumour growth. This is due to the transfection reagent, DAB-Am16, which has been shown to inhibit cell growth (Dufès et al., 2005). Despite being aware of this, no alternative transfection reagent/method of transfection was used as a comparison. Furthermore, neither of these two papers prove that exclusively p73 upregulation (or more specifically, one of its isoforms) is what causes the beneficial result or whether it was the Itch knockdown having a much broader effect on cancer cells than just p73 expression.

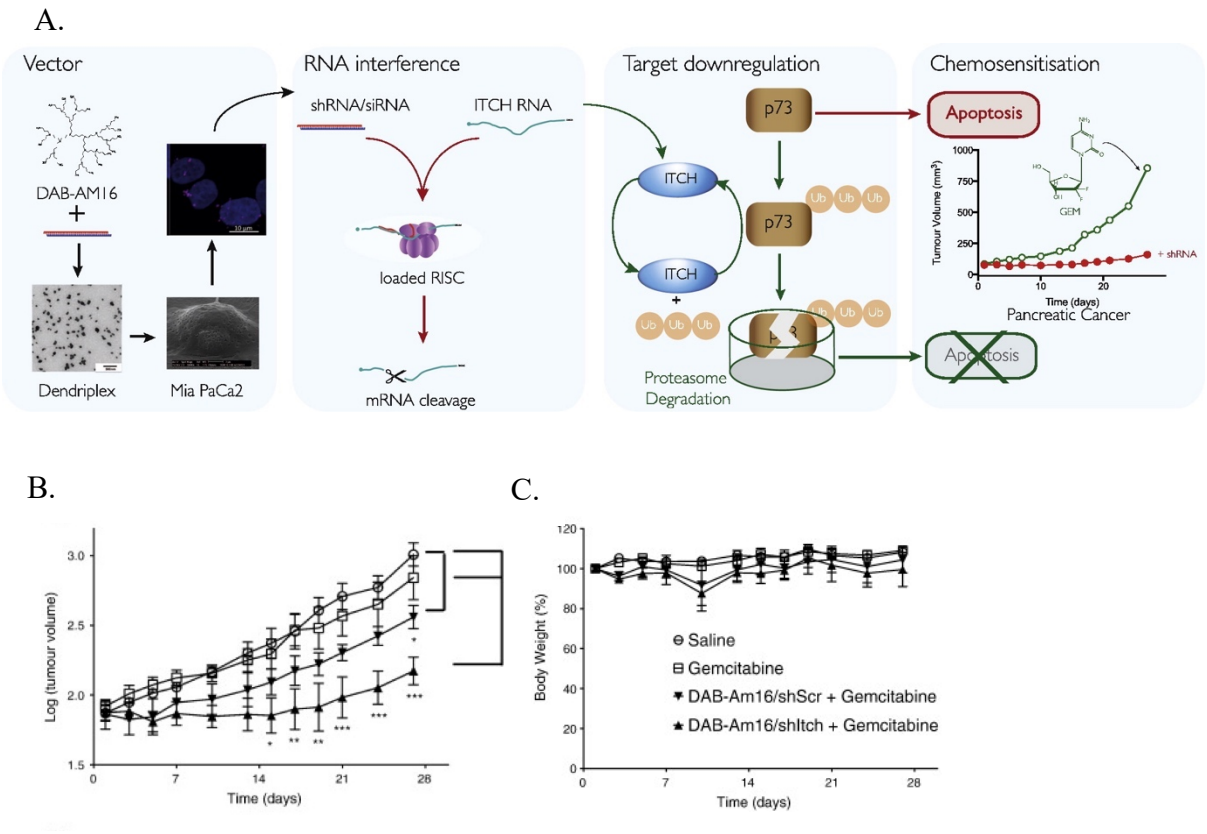

Figure 8: Itch-targeting nanoparticle strategy for increasing the sensitivity of pancreatic cancer to gemcitabine:

A. A nanoparticle vector (DAB-Am16) was developed and used to shuttle *Itch* sh/siRNA into target cells (first and second panel). Itch polyubiquitinates p73, a protein important for regulating the cell cycle and apoptosis and targets it for degradation by the proteasome (third panel). Downregulation of Itch by RNAi-containing nanoparticles increased MiaPaCa-2 xenografted mice to sub-IC50 doses of gemcitabine (last panel). **B.** & **C.** primary data of MiaPaCa-2 xenograft mice; tumour volume and percentage body weight were monitored in mice over a 28 day time-course. Mice treated with DAB-AM16/shItch + Gemcitabine inhibited tumour growth for 17 days (**B.** bottom line) with no statistically significant difference in toxicity to the treated mice (using %-age body weight as a surrogate of mouse health). Diagram and data from De La Fuente et al., 2015.

Thioredoxin-interacting protein:

Oxidative stress is a caused by a loss of balance between production of reactive oxygen/nitrogen species (ROS/RNS) and disposal of species by antioxidants (Visconti & Grieco, 2009). ROS are generated during aerobic respiration by the electron transport chain and consist of hydrogen peroxide (H_2O_2), the hydroxyl ion (OH•) and the superoxide ion (O_2^-; Fridovich, 1978). Accumulation of ROS without sufficient disposal allows the free radicals to disrupt the structure and function of lipids, proteins and DNA, potentially leading to chronic inflammation and cancer (Reuter et al., 2010). Although generation of ROS is initially tumorigenic, as it can inflict DNA damage and potentially cause mutations, cancer cells still have a tolerance threshold of ROS and need to clear them to prevent apoptosis and encourage tumour growth. Thioredoxin-interacting protein (TXNIP), or vitamin-D upregulated protein (VDUP)/thioredoxin binding protein-2 (TBP-2), inhibits the antioxidant thioredoxin (Trx) by directly associating to the redox protein's active site (Junn et al., 2000; Nishiyama et al., 1999). Inhibition of Trx by TXNIP causes increased oxidative stress and leads to the activation of apoptotic signalling cascades by promoting phosphorylation of apoptosis signal-regulating kinase-1 (ASK-1) (Saxena, Chen, & Shalev, 2010). For this reason TXNIP is described as a tumour suppressor and has been observed to be inhibited in various cancers (Butler et al., 2002; Kwon et al., 2010; Nishizawa et al., 2011). TXNIP itself is regulated by Itch as it has 2 PPxY motifs, which allows Itch to bind and polyubiquitinate it for degradation by the proteasome. (Liu et al., 2016; Otaki et al., 2016; Zhang et al., 2010). In particular Zhang's group have already showed that overexpression of Itch causes inhibition of TXNIP expression and conversely that genetic knockdown of Itch using siRNA causes increase in levels of TXNIP (Zhang et al., 2010). Furthermore TXNIP inhibition has also been shown to promote metastasis in melanoma (Goldberg et al., 2003). TXNIP in this case upregulates KISS1 which inhibits metastasis in melanoma cell lines. TXNIP could therefore acts to regulate cancer progression in both early and late stage disease.

Itch and the LATS /Hippo pathway:

The Hippo pathway was first discovered in *Drosophila melanogaster* where flies that were mutant (homozygous loss) for the gene *warts* (*wts*) were observed to have overgrown somatic cells (Justice et al., 1995). Later on many more studies showed that mutations in various other genes including *Salvador* (*sav*), *Hippo* (*hpo*) and *Mob as tumour suppressor* (*mats*) produced the same phenotype (Harvey, Pfleger, & Hariharan, 2003; Lai et al., 2005; Tapon et al., 2002) indicating that these genes might all be involved in the same pathway. The hippo pathway is responsible for regulating apoptosis and organ size in the developing and adult organism and is highly conserved in mammals: knockout of *Mst1/2* (an upstream component of the hippo pathway) causes YAP-1/TAZ (discussed below) activation in hepatocytes and thus liver overgrowth, indicating that the hippo pathway is also important for tissue regeneration in normal systems (Avruch et al., 2011). Because of this, regulation of the hippo pathway is important in regards to tumour progression. The upstream components of the Hippo pathway act by negatively regulating the oncogenic effectors of the pathway *yes associated protein 1* (*YAP-1*) and *transcriptional coactivator with PDZ-binding motif* (*TAZ*), the mammalian homologs of *yorki* (*yki*) (J. Huang, Wu, Barrera, Matthews, & Pan, 2005), causing their phosphorylation and subcellular localization to the cytoplasm rather than the nucleus (Meng, Moroishi, & Guan, 2016). If not regulated, YAP and TAZ translocate to the nucleus where it can activate the co-transcription factor TEA domain family member 1-4 (TEAD1-4) as YAP-1/TAZ cannot directly interact with DNA due to lack of DNA binding domains (DBDs; Zhao et al., 2008). As the hippo pathway is involved in the control of organ size it is not surprising that it is regulated by cell-cell contact (Zhao et al., 2007). YAP

localizes to the nucleus at low cell densities to promote cell division whilst at higher cell densities contact inhibition localizes YAP to the cytoplasm to prevent further growth of tissue. YAP-1 has also been shown to be inhibited on loss of contact with the extracellular matrix (ECM; Zhao et al., 2012) which would then promote anoikis (a form of cell death caused by detachment from the ECM).

Itch regulates the hippo pathway via inhibiting the serine/threonine kinase large tumour suppressor homolog 1 (LATS1 - the mammalian homologue of wts) (Salah, Melino, & Aqeilan, 2011) by targeting it for degradation by the proteasome. LATS1 phosphorylates YAP/TAZ, preventing their localisation to the nucleus and promoting transcription of genes linked to cell growth and survival (Figure 9). The LATS1 protein has two PPxY motifs that Itch can interact with; mutations in both of these motifs prevents Itch-mediated degradation of LATS1 however a mutation in just one of these sites still allows Itch to associate (Salah et al., 2011). Ho et. al. show that Itch acts on LATS1 protein levels in a dose-dependent manner and that treating with a proteasome inhibitor (MG132) blocks this degradation (Ho et al., 2011). To prove the link between Itch, the hippo pathway and cancer, Salah et. al. performed a series of experiments investigating the effect of Itch on the tumour progression of breast cancer cells (Salah, Itzhaki, & Aqeilan, 2014). They showed that Itch is able to enhance the tumour phenotype displayed by MCF10A cells both in-vitro and in-vivo (in-vivo *Itch* overexpression alone was not enough to induce tumorigenesis but it did amplify the phenotype in *H-Ras* transformed cells). *Itch* knockdown inhibits the tumour progression and metastatic ability of these cells: to demonstrate the role of the hippo pathway, and how it interacts with different expression levels of *Itch*, the levels of *LATS1*, and YAP-1/TAZ-affected genes were monitored. The results showed a decrease in *LATS1* expression and p-YAP (phosphorylated YAP), accompanied by an increase in expression of *YAP-1* and YAP-induced genes. Lastly they demonstrated that *YAP-1* knockdown rescues the Itch-mediated tumorigenic phenotype (Salah et al., 2014). Conversely a recent study has shown that Itch can interact and ubiquitinate YAP-1 via the α-arrestins ARRDC1/3 acting as adaptor molecules (J. Xiao et al., 2018). Silencing of ARRDC1/ARRDC3 increased the stability of YAP in clear cell renal carcinoma and promoted the tumourigenic phenotype. Thus via different points of the hippo signalling pathway, Itch can act to both inhibit and promote tumourigenesis.

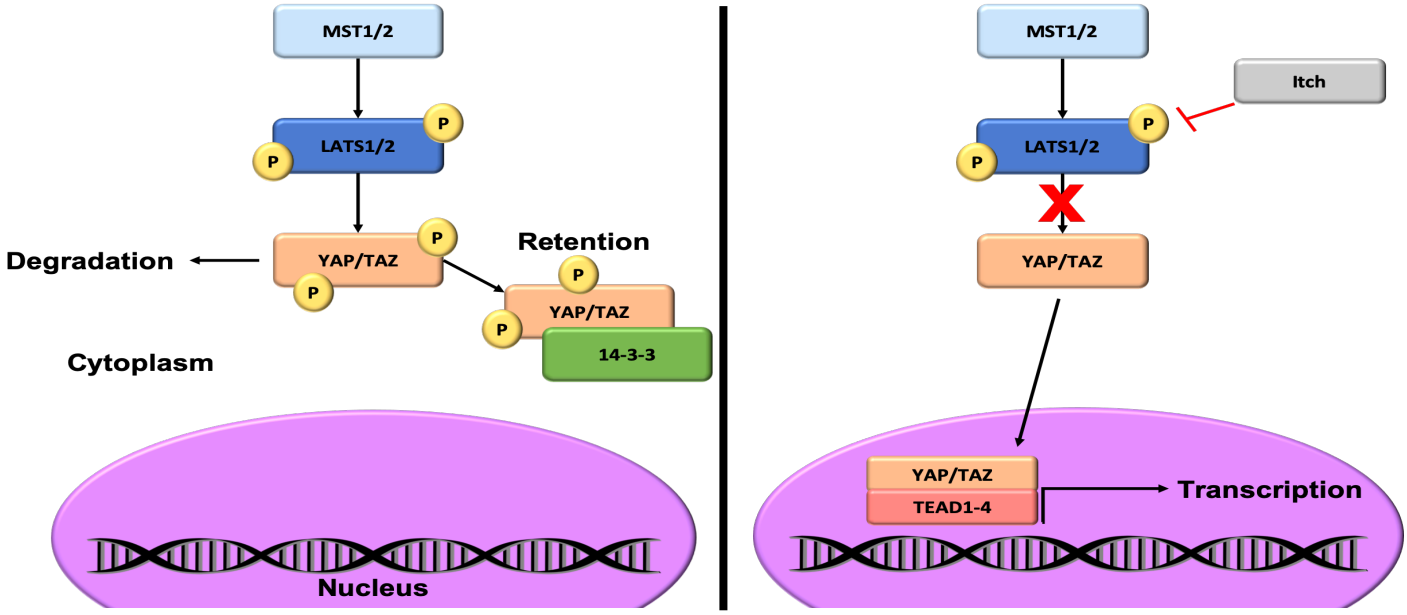

Figure 9: Itch inhibits hippo signalling through ubiquitinating LATS1:

First panel: MST1/2 phosphorylates LATS1/2 which in turn phosphorylates YAP/TAZ. Phosphorylation prevents nuclear localization of YAP/TAZ and prevents their transcriptional activity. YAP/TAZ is instead either degraded or retained in the cytoplasm by 14-3-3. Second panel: Itch ubiquitinates LATS1/2 which targets it for degradation by the proteasome. This limits YAP/TAZ phosphorylation; allowing them to translocate to the nucleus, associate with co-transcription factor TEAD1-4, and upregulating genes linked to cell survival and growth.

Transforming growth factor-β:

Itch is a positive regulator of the transforming growth factor-β (TGF-β) signalling pathway (Park et al., 2015) by targeting Smad7 for ubiquitination. Smad7 is an inhibitory Smad, or i-Smad, that inhibits the signalling activity of the Smad2/Smad4 complex and thus blocks TGF-β signalling: Itch therefore relieves this inhibition of the Smad2/Smad4 complex and promotes TGF-β signalling. Whilst with the other pathways discussed, inhibiting Itch should, in theory, upregulate tumour suppressive molecular mechanisms it is unsure as to what its effect would be in regard to the TGF-β pathway as TGF-β has a broad range of effectors. The role of TGF-β in cancer development seems to be paradoxical: normally TGF-β signalling regulates cell proliferation, differentiation, cell survival and microenvironment (Massagué, 2008) and so is usually a pathway that cancer cells try to downregulate to promote tumourigenesis. Indeed, in many cancers, activators of the pathway are usually inactivated such as Smad4 and TGF-β receptor 2 (TGFBR2; Ikushima & Miyazono, 2010). However TGF-β signalling can also be exploited by cancer cells to promote invasion, metastasis and evasion of the immune system i.e. more late-stage pathological aspects of tumour progression (Fabregat et al., 2014; Massagué, 2008). It would seem, therefore, that there is some form of context-specific selection of outputs from the TGF-β signalling pathway that promotes tumour progression: knocking down tumour suppressive aspects whilst upregulating oncogenic ones. It would be difficult to predict the effect of an Itch knockdown in relation to TGF-β due to its paradoxical role in tumour progression. TGF-β upregulation may be a good preventative measure and may prevent the growth of an early tumour, e.g. cancer stem cells or tumour initiating cells (Iwasaki & Suda, 2009), due to downregulation of pro-survival mechanisms and upregulation of apoptosis. However, in a tumour where tumour suppressive

effects of TGF-β are already inhibited, upregulation of the signal may increase the likelihood of tissue invasion and metastasis.

Another interesting point, linking cancer to immunity, is that the TGF-β pathway facilitates the activities of regulatory T-cells (Tregs). In the human body there are two types of Treg cells; natural Treg cells (nTregs) which are derived from the thymus, and induced or adaptive TReg cells (iTregs) which are induced from naïve $CD4^+$ T-cells via TGF-β signaling and IL-2 (Adeegbe & Nishikawa, 2013; Curotto de Lafaille & Lafaille, 2009). The main role of Treg cells is to suppress the function of normal T-cells, thus preventing autoimmunity and inflammation, especially in areas of increased chemical stress such as the gut. However it has been noted that there is an increased prevalence of Treg cells in the tumour microenvironment and vasculature (Adeegbe & Nishikawa, 2013; Beyer & Schultze, 2009). This is considered one of the barriers of using immunotherapy against cancer cells. TGF-β is required to both induce and maintain Treg cells (Curotto de Lafaille & Lafaille, 2009). The question here is that if Itch normally acts as a positive regulator of the TGF-β pathway, could knockdown/interference of *Itch* in primary cancer tissue samples decrease the amount of Treg cells present in the microenvironment and by extension be able to increase a tumour's sensitivity to immunotherapy? Indeed it has already been shown that silencing TGF-β1 in vitro causes a reduction in Treg cells and reduces tumour volume (Conroy et al., 2012). Furthermore *Itch* -/- naïve T-cells are resistant to Treg suppression and prevents development of iTregs (Venuprasad et al., 2008), however it remains to be seen if these effects can be mirrored by a genetic knockdown of *Itch* explicitly.

Itch in bone remodelling:

Dysregulation of the bone remodelling process can result in debilitating diseases that severely impact patient quality-of-life such as osteoporosis, osteopetrosis, Paget's disease of bone, and rheumatoid arthritis. Bone remodelling entails a delicate balance of bone formation and bone resorption which shifts depending on context for example in the incidence of a bone fracture (formation) or digit formation (resorption). Formation and resorption is governed by osteoblast and osteoclasts respectively therefore study of the molecular mechanisms in which these cells differentiate and perform their respective functions is key to better understand the aforementioned pathologies. Recently Itch has been shown to regulate the activity of both osteoclasts and osteoblasts as discussed below.

Itch and osteoblasts:

Osteoblasts are mononuclear cells differentiated from mesenchymal stem cells typically found in bone marrow through bone morphogenic protein (BMP) signalling (Pittenger et al., 1999; Yamashita, Takahashi, & Udagawa, 2012). They are the cells responsible for synthesising and distributing bone matrix in both endochondral and intramembranous ossification. One-month-old *Itch*-/- mice have been shown to have both increased osteoblast numbers and bone formation rate (BFR) leading to increased bone mass (Zhang & Xing, 2013) hinting to a role of Itch in the terminal differentiation of osteoblasts. Isolation and culture of mesenchymal stem cells from *Itch*-/- displayed increased numbers of osteoblast markers such as *alkaline phosphatase* (ALP) and thus had increased differentiation potential for osteoblast formation. Furthermore they looked at the number of adipocytes formed: another type of cell derived from mesenchymal stem cells that usually have an inverse

relationship with osteoblast numbers (Zhang et al., 2010). The study found that *Itch*-/- mice had fewer adipocytes being formed than wild-type (wt) mice when exposed to adipocyte-inducing media (mean adipocyte formation from bone marrow progenitor cells: 390/well for *Itch-/-* vs 1005/well for wt). *Itch*-/- cells had increased Ub-tagged JunB whilst having similar total JunB protein levels to wt (Zhang & Xing, 2013). Previous literature has confirmed that JunB is an essential transcription factor for the differentiation of osteoblasts from mesenchymal stem cells (L. Zhao et al., 2010). When discussing Itch's role in immune regulation and differentiation of T_H2 cells, Itch ubiquitinates and targets JunB for degradation via the proteasome after JNK1-mediated phosphorylation.

A later study also explored the relation of Itch and osteoblasts in bone fracture repair. Interestingly one initial observation was increased and sustained mRNA expression of several Nedd4 family E3 ligases including *Itch* after an induced tibial fracture in mice (J. Liu et al., 2017). *Itch*-/- mice showed increased expression of osteoblast-related genes after induced fracture such as *runt-related transcription factor 2* (*Runx2*) and *ALP*. They also observed mRNA levels of *receptor activated NF-κB* (RANK) *ligand* (*RANKL*) and *osteoprotegrin* (*OPG*), which are required for bone remodelling as they regulate osteoclastogenesis (Katagiri & Takahashi, 2002; Yamashita et al., 2012).

Itch and osteoclasts:

Osteoclasts are large multinucleated cells that are responsible for the resorption of bone matrix in the remodelling process. They are derived from monocytes, a type of leukocyte, when exposed to RANKL and macrophage colony stimulating factor (M-CSF; Figure 10: A.) which are secreted by osteoblasts and stromal cells in-vivo (Kim & Kim, 2016; Nijweide, Burger, & Feyen, 1986; Yamashita et al., 2012). Osteoblasts also produce OPG, which inhibits osteoclast formation by acting as a competitive inhibitor to RANK on osteoclast precursors (monocyte that is already exposed to M-CSF signalling). In-vivo a context-dependent balance of OPG and RANKL secretion from osteoblasts determines the rate at which osteogenesis and resorption take place at the bone surface. Osteoclast differentiation is dependent on RANKL-induced NF-κB signalling in the presence of M-CSF to trigger transcription of genes for osteoclastogenesis. RANK/RANKL binding triggers a signalling cascade that induces TNF receptor-associated factor 6 (TRAF6), a RING E3 Ub ligase. TRAF6 then auto-ubiquitinates with Lys63 polyubiquitin chains, which promotes NF-κB signalling and osteoclastogenesis (Jin et al., 2008; Lamothe et al., 2007; H. Zhang et al., 2013).

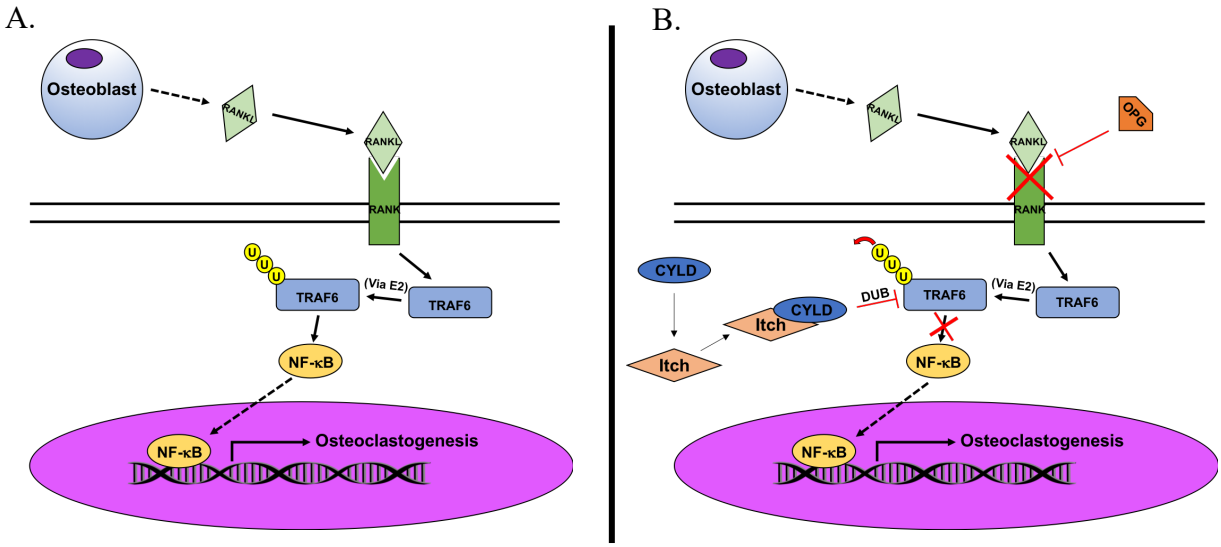

Figure 10: Simplified diagram of RANKL-induced osteoclastogenesis and how it is inhibited: **(A).** RANKL secreted by osteoblasts interacts with RANK on the surface of osteoclast precursors. Intracellular signalling from RANK stimulates autoubiquitination of TRAF6 which allows it to promote NF-κB-mediated transcription of genes associated with mature osteoclast differentiation. **B.** osteoclastogenesis signalling pathway can be inhibited extracellularly through OPG binding to RANK and blocking the receptor. NF-κB also promotes transcription of Itch which can associate with the DUB CYLD. This enzyme complex removes Ub from TRAF6 and prevents further upregulation of NF-κB signalling. Original figure.

Studies looking at *Itch*-/- mice showed increased numbers of osteoclasts compared to wt in response to RANKL signalling (Zhang et al., 2013) and increased levels of bone resorption. Similarly mice treated with CMI to inhibit Itch activity in wt mice also showed increased osteoclastogenesis and bone resorption (Li et al., 2017). *Itch*-/- mice treated with CMI showed no change in osteoclast formation, confirming that the changes in osteoclast numbers in wt mice was strictly due to chemical inhibition of Itch E3 activity. It was thus hypothesised that Itch enzymatic activity negatively regulates osteoclast formation in response to RANKL signalling. NF-κB signalling also induces the upregulation of *Itch* expression thus initiating a negative feedback mechanism to inhibit osteoclastogenesis. However, the thought that Itch would directly act on TRAF6 would seem contrary to Itch's function as an E3 ligase as activated TRAF6 already exists in a self-ubiquitinated state. Instead, Itch associates with the deubiquitinating enzyme (DUB) cylindromatosis (CYLD) (Zhang et al., 2013) to inhibit TRAF6 signalling. As the name implies, DUBs act to remove Ub from target substrates: CYLD deubiquitinates TRAF6 and thus prevents further NF-κB signalling (Figure 10: B.). *CYLD* -/- mice are hypersensitive to RANKL signalling, show persistent NF-κB signalling, and have severe osteoporosis (Jin et al., 2008). TRAF6 is also deubiquitinated by A-20 however, when only A-20 is present (or if *Itch* is absent, preventing the CYLD complex) the process is much slower meaning prolonged NF-κB signalling.

Although *Itch*-/- mice have increased numbers of both osteoblasts and osteoclasts, i.e. cells with seemingly opposing functions, the resultant phenotype (whether or not the mice are

osteoporotic or osteopetrotic) seems to correlate with the age of the organism: young *Itch-/-* mice appear to have greater bone density whilst older mice have lower bone density (Zhang et al., 2013; Zhang & Xing, 2013). Furthermore despite these differences in phenotype it was observed that the ratios of the two cell types in young and old *Itch-/-*mice is unchanged: One could potentially hypothesise that the differing phenotype is due to changes in developmental priorities i.e. in younger mice there is more emphasis for an organism to grow and thus produce more bone matrix whilst at an older age this is not the case.

These findings in mouse models have founded a strong basis ubiquitination and Itch E3 ligase activity are important regulatory factors in bone remodelling, however the question remains as to whether or not this is translatable to humans. As already noted, the children in Lohr's study that are mutant for Itch show stunted growth and dysmorphic features (Lohr et al., 2010) which implies defective bone remodelling machinery. Furthermore, the basis for the study of the effect of CMI on osteoclastogenesis by Li et.al. was after reports of patients being treated with CMI for depression showed a higher incidence of osteoporosis and bone fractures (Vestergaard, Rejnmark, & Mosekilde, 2008) and the small molecular screen by Rossi's group identifying CMI as a specific inhibitor of Itch E3 ligase activity (M Rossi et al., 2014). Itch activity could therefore be a druggable target for the treatment of bone diseases.

CRISPR-Cas9 gene editing – an introduction:

CRISPR (Clustered Regularly-Interspaced Short Palindromic Repeats) is an adaptive immune system employed by various bacteria and archaea that protects against foreign genetic material such as virions. It works by taking a section of the foreign DNA that is directly adjacent to a PAM sequence (protospacer adjacent motif) and incorporating it as a spacer region in the CRISPR locus. Cas (CRISPR-associated protein) proteins are then synthesised along with crRNA (CRISPR-RNA - derived from the incorporated spacer sequences) to recognise and degrade foreign genetic material (Rath et al., 2015; Terns & Terns, 2011). Degradation of foreign nucleic acids is done by the Cas protein introducing breaks in the foreign DNA at sites that are complimentary to the mature crRNA (Jinek et al., 2012).

Since its discovery, the CRISPR-Cas system has been adapted to perform many forms of genetic engineering such as RNAi (RNA interference) by irreversibly knocking down the expression of a gene or inserting genetic material at specific sites in the host genome. One can even perform several genetic edits by using multiple guide-RNA/single guide-RNA (gRNA/sgRNA: a combination of crRNA and tracrRNA) sequences in the same CRISPR array (Cong et al., 2013). Type II CRISPR system uses Cas9 to introduce double stranded breaks at the target site, which are then repaired either by error-prone non-homologous end joining (NHEJ) or homology directed repair (HDR) (Rath et al., 2015). One form of DNA repair can be favoured over the other depending on the design/type of CRISPR-Cas9 system used. Cas9 is conjugated to gRNA to recognise a sequence of 20 base pairs adjacent to a PAM (Mojica et al., 2009). In the case of Cas9, this PAM sequence is "NGG," where N is any base. DNA repair through NHEJ generates insertions or deletions in the host DNA, known as indels: NHEJ machinery either "trims back" or adds bases at either side of the DSB to create blunt-ended DNA ends that are then ligated together (Davis & Chen, 2013). This results in frameshift mutations where the optimal outcome is effective silencing of a gene due to the premature stop codons. HDR meanwhile can be exploited to create precise edits in

genes-of-interest provided template DNA for HDR machinery to act on is included with the Cas9 and sgRNA. However since HDR is inefficient (Pardo et al., 2009), some DSBs will end up being repaired by NHEJ (which is highly efficient), meaning further analysis is required for identification and enrichment of cells which carry the precise edit.

With regard to the RNAi applications of CRISPR this technology does have several advantages over using siRNA or shRNA: it is much more efficient in the knockdown of gene function and is highly specific. The knockdown is also irreversible (which may actually be a disadvantage depending on the context of use) as CRISPR edits host chromosomal DNA which is consequentially inherited by daughter cells. Meanwhile with siRNA the knockdown only persists until the resultant material (i.e. the siRNA) is used up/degraded, or the effect is diluted through cell division (Bartlett & Davis, 2006). For shRNA-mediated knockdown, whilst the silencing effect may persist for an individual cell, the plasmid is not usually passed on to daughter cells upon cell division. Meaning the effect is eventually diluted to the point of non-significance (Rao et al., 2009). shRNA can be stably expressed if the plasmid used has lentiviral or retroviral components which allow it to integrate into host DNA. However, shRNA still only exerts its silencing activity at the mRNA level meaning that not necessarily all transcripts of a gene are affected (which may be an advantage depending on experimental context). Furthermore use of viral constructs for in-vivo application carries risks (Thomas, Ehrhardt, & Kay, 2003), additionally direct transfection of plasmids (and other large nucleic acid constructs) in-vivo can generate a host immune response and localised inflammation (Rao et al., 2009). Meanwhile CRISPR can circumvent the issue of plasmid/viral use through direct injection of a Cas9-sgRNA ribonucleoprotein to mediate gene silencing in-vivo (Fogarty et al., 2017; Ma et al., 2017). It also has advantages over other stable-cell generating techniques such as those which use transcription activator-like endonucleases (TALENs) and zinc-finger endonucleases (ZFNs) in regards to simplicity, cost, and convenience. Cas9 is constant in all CRISPR-related applications and the only variable factor is the short sgRNA which can be easily customisable. Meanwhile TALENs and ZFNs, while powerful and accurate, need to have their DNA-binding proteins/domains specifically designed for a particular gene which is more laborious (Carroll, 2011; Gaj et al., 2013; Joung & Sander, 2013). This makes CRISPR a more attractive option for generation of stable gene-edits in a research environment.

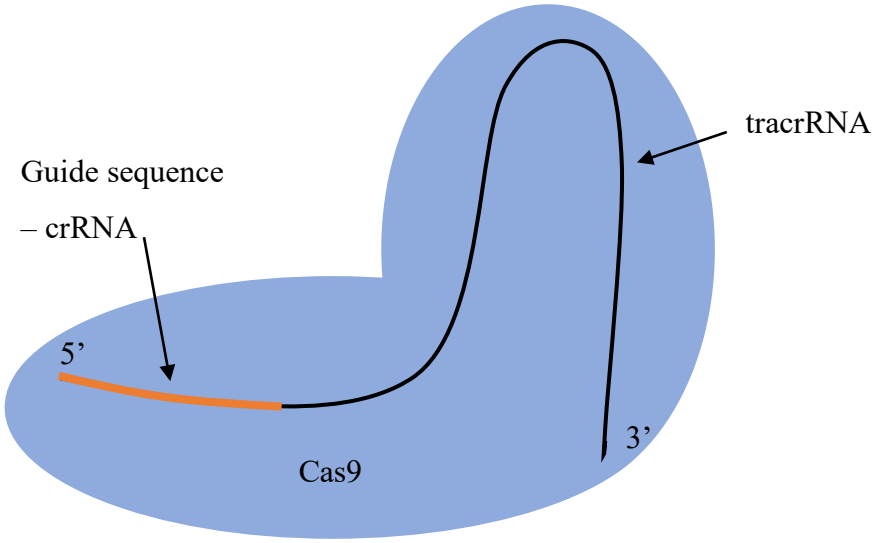

Figure 11: Simple diagram of the Cas9-sgRNA complex:

Cas9 is one example of an endonuclease used in CRISPR applications to create DSBs adjacent to a PAM sequence (NGG in the case of Cas9) in genomic DNA. Cas9 is guided to its targets by sgRNA which is made up of the crRNA guide sequence and tracrRNA backbone. Original figure.

A.

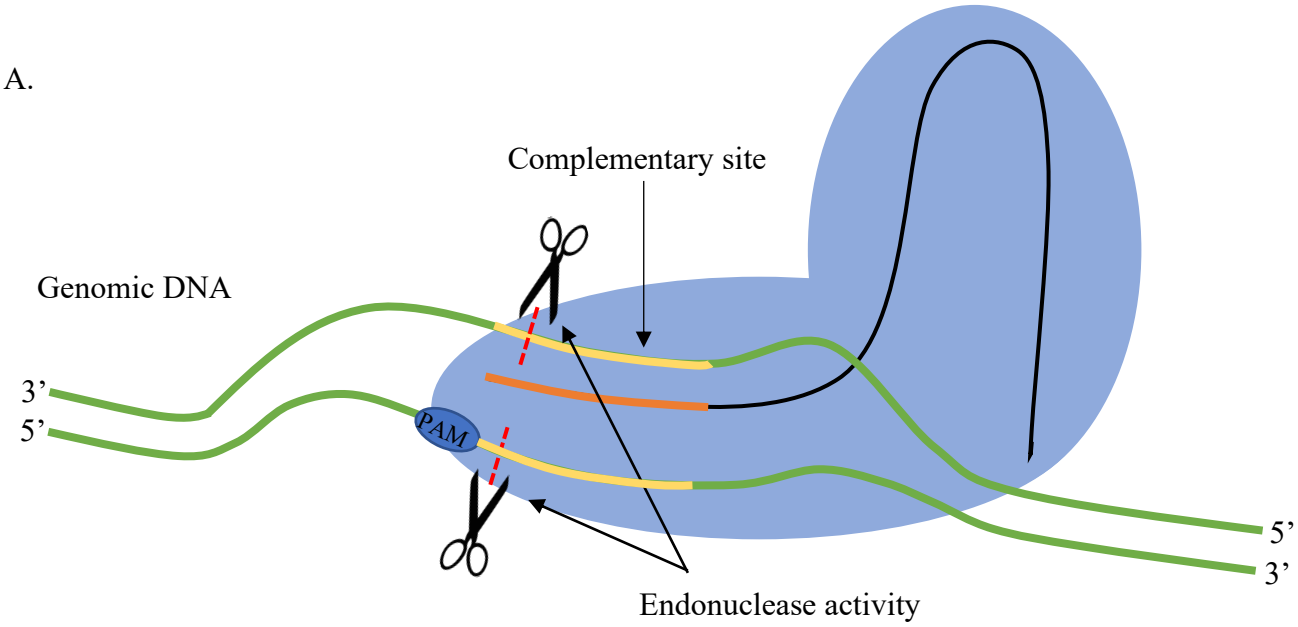
Complementary site
Genomic DNA
3’
5’
PAM
5’
3’
Endonuclease activity

B.

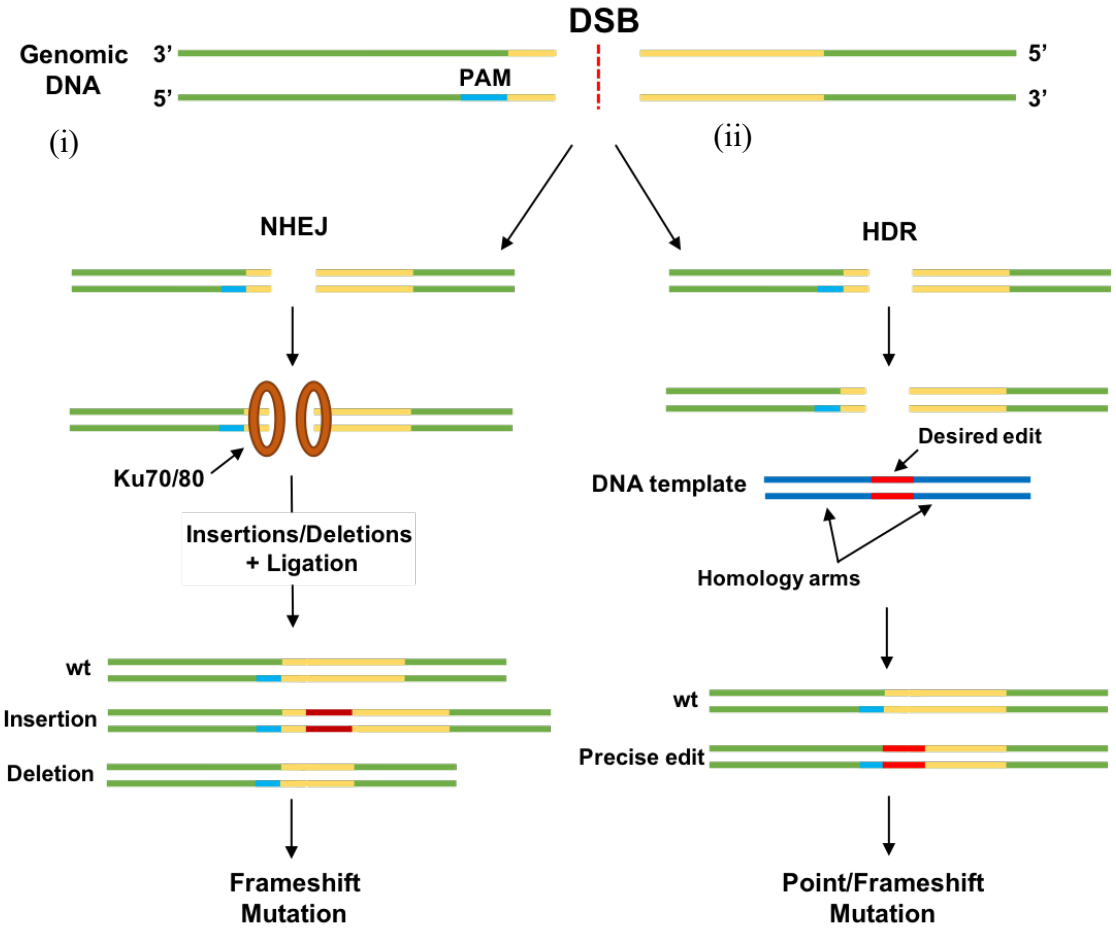
DSB
Genomic DNA
3’
5’
PAM
5’
3’
(i)
(ii)
NHEJ
HDR
Ku70/80
Insertions/Deletions + Ligation
Desired edit
DNA template
Homology arms
wt
Insertion
Deletion
wt
Precise edit
Frameshift Mutation
Point/Frameshift Mutation

Figure 12: Cas9 induces DSBs in host genomic DNA to create knockouts:
A. Cas9 associates with DNA that is complementary to the guide sequence of the sgRNA and induces a DSB 3/4nts downstream of the PAM sequence. **B.** DSBs created by Cas9 endonuclease activity are repaired either through the efficient but error-prone NHEJ pathway or by the less efficient but more accurate HDR which can be exploited to create precise mutations. **(i)** loose ends of genomic DNA are stabilised by Ku70/80 which then recruits NHEJ machinery to either trim-back the DNA or polymerise additional bases to either end of the DSB to regain end compatibility for ligation. This creates random insertions or deletions (termed indels) in the DNA which are different from cell to cell. Indels cause frameshift mutations in genomic DNA. **(ii)** Homology directed repair machinery can be exploited by introducing donor template DNA which is homologous to genomic DNA with the exception of either a small gene edit or potentially larger gene insertions. The result is incorporation of the edit in host DNA that can cause point or frameshift mutations depending on the size of the insert sequence. Original figure.

Traditional CRISPR is not without its limitations however: gRNA typically being 20 bp's long means that there can be a degree of "wobble" base pairing, leading to potential mismatches (extra bases in gRNA or DNA) and off-target mutagenesis (Cornu, Mussolino, & Cathomen, 2017; Cradick et al., 2014; Fu et al., 2013; Hendel et al., 2015). Good gRNA design should, of course, limit the amount of off-target activity but there can be cases where it is unavoidable. One might assume that increasing the length of the gRNA may decrease off target activity however, as discovered by Ran's group, extension of the gRNA, regardless of whether the additional bases matched or mismatched, showed no significant difference in off-target activity than the standard 20bp gRNA (Ran et al., 2013). They did find that off-target activity can be reduced by using a modified CRISPR system that uses dual Cas9n (Cas9 nickase) proteins and two separate gRNAs (Ran et al., 2013). Cas9n is a mutated version of the Cas9 protein that causes a single stranded "nick," rather than DSBs in the target DNA. The dual Cas9n proteins each have their own individual gRNAs targeted at forward and reverse strands of DNA at slight offset of up to 20bp. The offset in nickase activity creates overhangs on each strand of DAN that promotes HDR over NHEJ meaning less-random mutagenesis. This achieves a knockdown that has increased on-target activity due to the requirement of more criteria being fulfilled at the cost of some transfection efficiency compared to traditional CRISPR. Another limitation of CRISPR is the need of a PAM sequence for Cas9 to able to induce DSB in the target gene whilst TALENs and ZFNs are not restricted as to where along the gene their endonuclease activity can take place (Gaj et al., 2013). This is especially the case for Cas variants which require longer PAM sequences (although theoretically lower off-target activity, the number of cut sites is further limited).

Brief summary of project aims:

This project aims to explore the role of Itch in both cancer sensitivity and bone remodelling through means of generating transient and stable *Itch* knockdowns in-vitro through use of siRNA and CRISPR respectively; analysing and interpreting the outcome for each model system. The project also goes on to compare and contrast the methods of genetic knockdown used in experiments. The strength of using a particular gene editing technique is dependent on several factors: Including the pathways being explored and the physiological/morphological consequences of altering them, the time-frame of the experiment and/or project and the nature of the model system being used be it in-vitro or in-vivo.

Based on results from previous studies we hypothesise that genetic knockdown of *Itch* using both transient and stable knockdown strategies will sensitise pancreatic cell lines to current FDA-approved therapeutics. The reason why pancreatic cell lines were chosen was because of the poor survival rate associated with the disease (discussed later) and the lack of effective forms of treatment. Therefore, any additional methods that can supplement and potentiate existing therapeutic approaches to pancreatic cancer are highly researched. An increase in sensitivity may be characterised by an increase in total cytotoxicity or lower dose requirements for the same inhibitory outcome. In a clinical setting a reduction in observable side-effects is also a desirable outcome when testing new forms of treatment however, this is not necessarily an increase in sensitivity and is also difficult to characterise in-vitro.

In the context of Itch's effect on bone remodelling, utilising an ex-vivo approach, we hypothesise that knockdown of *Itch* in monocytes derived from whole blood will increase osteoclastogenesis and thus facilitate osteoclast function in resorbing a bone-like matrix. Once again, both transient and stable approaches will be used before inducing osteoclast development. As previous literature has already confirmed that mice lacking functional Itch protein have differing numbers of osteoclasts compared to wild-type, we wish to assess if this phenomena is also mirrored in a human setting.

Chapter 2 – Materials and Methods

Cell culture:

Media and supplements:

DMEM Glutamax (Cat.No. 31966047), McCoy's 5A modified media (Cat.No. 26600080), and α-MEM (Cat.No. 22571020) - all purchased from ThermoFisher and produced by GibCo. Media was supplemented with FBS (Biowest, Cat.No. S1900-500) to a final concentration of 10% and penicillin/streptomycin (GibCo, Cat.No. 25030-024) to a final concentration of 1%. OPTImem was also purchased from ThermoFisher (Cat.No. 31985062).

Mammalian Cell Culture:

MiaPaCa-2 cells were obtained from frozen stocks and cultured in DMEM. Capan-2 cells were obtained from ATCC and were grown in McCoy's 5A modified media. Cells were incubated at 37°C with 5% CO_2, grown in either T75 or T175 flasks until a confluence of 80-90% was reached. All cell lines used were also tested for the presence of mycoplasma by the Lab Manager. To passage cells, cells were treated with trypsin (GibCo, Cat.No. 25300062) to cause cell detachment from the flask surface, the trypsin was neutralised, then cells were centrifuged at 281 ×g for 5 minutes. The supernatant was discarded and the pellet re-suspended. Cells were then either used for analysis or re-suspended at an appropriate dilution in a new flask. Cells were passaged 10 times before either being disposed of or frozen down and stored in liquid nitrogen; at which point a new batch was thawed.

Isolation of PBMCs from whole blood:

Whole blood (10-20 ml) was taken from a healthy volunteer on 3 occasions (ethics: Appendix 1). The blood was immediately mixed with 10% EDTA solution to prevent blood coagulation (10µl of 10% EDTA solution per 1ml of whole blood). Whole blood was then diluted 1:1 with cold, sterile phosphate-buffered saline (PBS - made from tablets dissolved in dH_2O and autoclaved, ThermoFisher, Cat.No. BR0014G) which was then layered on top of 10 ml of Histopaque-1077 (Sigma Aldrich, Cat.No. 10771) and centrifuged at 800 ×g for 30 minutes (no brake). After the spin the blood separated out into 4 distinct layers (Figure 12). Using a sterile Pasteur pipette, the whitish-pink buffy coat layer containing PBMCs was removed.

PBMCs were then re-suspended in 10 ml cold PBS and centrifuged at 300 g for 10 minutes as an initial wash step, which was then repeated 2-3 times. Cells were then counted and pelleted again before being re-suspended in α-MEM containing 20 ng/ml M-CSF (R&D Systems, Cat.No. 216-MC, carrier-free) to achieve a final cell density of 10^6 cells per ml. PBMC containing media was then dispensed on 6-well plates (1 ml/well) and was topped-up to 3 ml with α-MEM at a final concentration 20 ng/ml m-CSF. Alternatively, PBMCs were resuspended in m-CSF containing medium and aliquoted onto either a plain 96-well plate or a 96-well Osteo Assay Surface plate (Corning, Cat.No. 3988) with an initial cell density of 1000 cells/well in 200 µl.

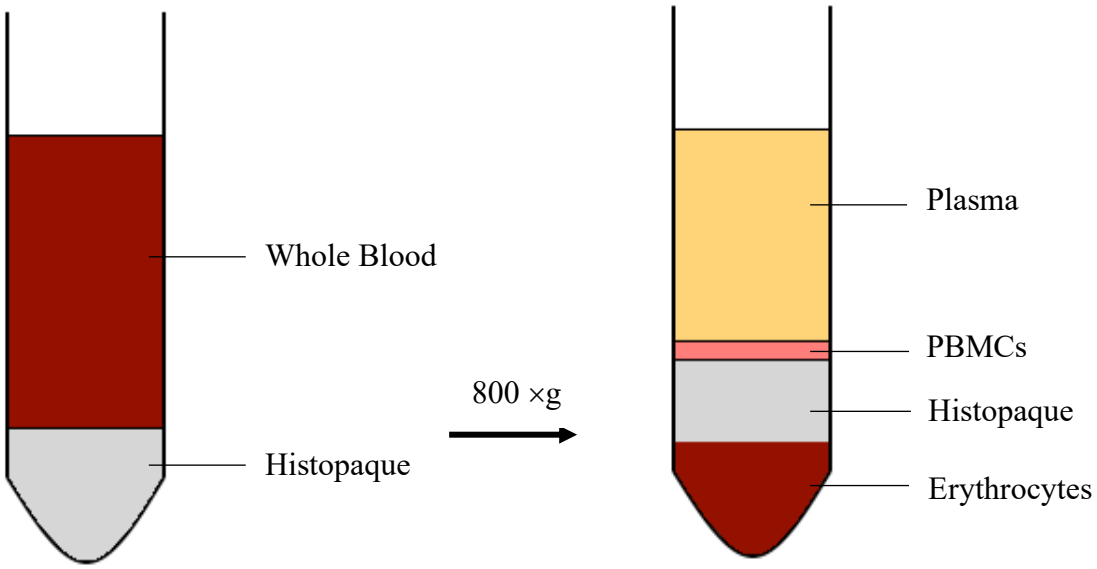

Figure 13: Separation of whole blood by centrifugation using Histopaque:

Upon dilution of whole blood with cold PBS, blood solution is dispensed onto Histopaque in a 50ml tube. The blood is then separated by centrifugation at 800 ×g for 30 minutes. After centrifugation the different components of blood can be seen including Erythrocytes (red blood cells), Leukocytes (PBMCs, T-cells, and B-cells), and blood plasma. Original figure.

Cell Culture of PBMCs:

Once isolated, PBMCs were incubated at 37°C with 5% CO_2 in a humidified incubator. Media was replaced every 3 days with fresh α-MEM containing 20 ng/ml m-CSF. After 7 days of cell culture, media was supplemented with 50ng/ml recombinant RANKL (R&D Systems, Cat.No. 6499-TEC, carrier-free) to encourage differentiation of monocytes into osteoclasts. Media was then replaced every 2 days including fresh cytokines.

Transient Itch knockdown using siRNA:

siRNA design:

Anti-Itch siRNA duplex sequence data was kindly provided by Dr Simon Newman, Nanogenics Ltd and oligonucleotides synthesised by Eurogentec (Table 1).

Name of oligo	Sequence (5'-3')
Anti-Itch_Sense	GCU-GUU-GUU-UGC-CAU-AGA-A
Anti-Itch_AntiSense	UUC-UAU-GGC-AAA-CAA-CAG-C

Table 1: siRNA sense and antisense sequences.

As a negative control a commercial scrambled control from Eurogentec was used. Duplexes were re-suspended in dH_2O to achieve a concentration of 20 μM. Specificity of siRNA was determined through Blast search of the forward and reverse oligonucleotides.

siRNA duplex preparation:

Tubes labelled A and B were, made for each siRNA duplex (4 total for si-Itch and Negative control).

- Tube A: 800 μl OPTImem + 16 μl Lipofectamine RNAiMAX (ThermoFisher, Cat.No. 13778030)
- Tube B: 800 μl OPTImem + 10 ul of 20 μM siRNA duplexes

Each pair of tubes was incubated separately for 5 minutes before the contents from tubes A and B were mixed and incubated for a further 20 minutes at room temperature. This results in 125 nM of siRNA in 1.6 ml. This reaction was scaled up or down depending on the final concentration of siRNA required for particular experiments (some cell lines required a larger final concentration of siRNA for successful knockdown).

siRNA transfection - dish/plate format:

To first verify that the siRNA duplexes could knock-down *Itch* expression we performed forward transfection of siRNA duplexes in cells. Forward transfection involves seeding cells prior to transfection whilst reverse transfection involves seeding cells on top of duplex solution. For western blot verification, firstly $1.5x10^6$ cells were seeded in 10 cm diameter dishes in 10 ml of media. After one day of cell attachment, siRNA duplexes were prepared as above, and the resultant solution was added to the plates drop-by-drop and incubated overnight. After 24 hours transfection, cell lysates were made and protein expression was verified and measured by Western blot. For qPCR verification $5x10^5$ cells were seeded in 6-well plates and before siRNA solution was applied.

Cell-death and functional assays requiring a 96-well plate employed reverse rather than forward transfection. siRNA duplexes were prepared as previously described, 16μl of duplex solution was aliquoted into each well of a 96-well plate (separate plates were used for negative and untreated controls). 100 μl of cell solution with appropriate supplements was then added to each well containing siRNA duplex media (initial cell density dependent on cell line used). After 24 hours of incubation the media was replaced and downstream assays were performed. In experiments where there were supplementary doses of siRNA for a persistent knockdown, siRNA was re-applied at the same concentration 24 and 72 hours after the addition of doxorubicin/gemcitabine or 48 hours after γ-irradiation.

In the case of monocytes already seeded on a 96 well plate (Osteo Assay Surface or otherwise) forward transfection was used and 16 μl of siRNA solution was added to each well already containing supplemented media (α-MEM containing 20 ng/ml m-CSF). After 24 hrs the media was replaced and further supplemented with 50 ng/ml RANKL to see the effects of Itch knockdown on osteoclast differentiation. Freshly prepared siRNA solution was re-applied to the cells at day 3 of RANKL treatment to maintain the knockdown over a 7-day period of time.

Stable Itch Knockdown using CRISPR-Cas9:

sgRNA design:

Forward crRNA design templates were made using 20 base nucleotide sequences from the GeCKOv2 library (Sanjana, Shalem, & Zhang, 2014) and from these the reverse oligos were generated along with additional primer sequences (Table 2). Oligonucleotides were ordered at 50 nmol yield, 5' phosphorylated and unsalted (ThermoFisher).

sgRNA Name	Sequence (5' to 3')
Itch1F	CACCGGTAGTTGTGACTTTGCAGCT
Itch1R	AAACAGCTGCAAAGTCACAACTACC
Itch2F	CACCGGAGTCTGAAGTTGTTACCAA
Itch2R	AAACTTGGTAACAACTTCAGACTCC
Itch3F	CACCGCCAGATCCAAGGATGAAACA
Itch3R	AAACTGTTTCATCCTTGGATCTGGC
Itch4F	CACCGGGTGCTTCTCAGAATGATGA
Itch4R	AAACTCATCATTCTGAGAAGCACCC
Itch5F	CACCGTGAACATGTAGTTTCACCAT
Itch5R	AAACATGGTGAAACTACATGTTCAC
Itch6F	CACCGGACTTGTCAATTTGTCTTGA
Itch6R	AAACTCAAGACAAATTGACAAGTCC
Scramble_F	CACCGCCTAAGGTTAAGTCGCCCTC
Scramble_R	AAACGAGGGCGACTTAACCTTAGGC

Table 2: Oligonucleotides used for sgRNA cloning:

Bases highlighted in red are primer sequences to allow incorporation of sgRNA sequence (in black) into the pLentiCRISPRv2 vector.

Cloning sgRNA into plasmid vector:

The plasmid vector being used for transfection was pLentiCRISPRv2 (Addgene plasmid # 52961) (Sanjana et al., 2014). Restriction maps and gene inserts for all plasmids being used can be viewed in Supplementary Figure 1. Before the crRNA sequences can be inserted into the plasmid vector, the plasmid itself needs to be opened up and the filler sequence removed. The pLentiCRISPRv2 vector (2 µg) was dephosphorylated and digested in a solution of 1 µl FastDigest Esp3I (ThermoFisher, Cat.No. FD0454), 2 µl 2x FastDigest buffer (provided with restriction enzyme), 0.5 µl Calf Intestinal Phosphatase (NEB, Cat.No. M0290 – discontinued as of June 2019), 0.2 µl of 100 mM fresh DTT (Sigma Aldrich, Cat.No. 10197777001) and water up to 20 µl. This reaction was incubated for 30 minutes at 37°C. A 0.8% agarose gel was prepared to visualise the components of the digested plasmid: 0.4g agarose in 50 ml 1x TAE (40 mM Tris base, 20 mM acetic acid and 1 mM EDTA) plus 1 µl of 10 mg/ml ethidium bromide solution. After incubation, 2 µl of loading dye was added to the digested plasmid and was then loaded onto the gel and run at 40 V for 45 minutes (171 mAmp, 16 W). Upon digestion there is a 1.8 kb (filler sequence) band and a 12.8 kb band (plasmid backbone) which was visualised using UV light (Figure 13).

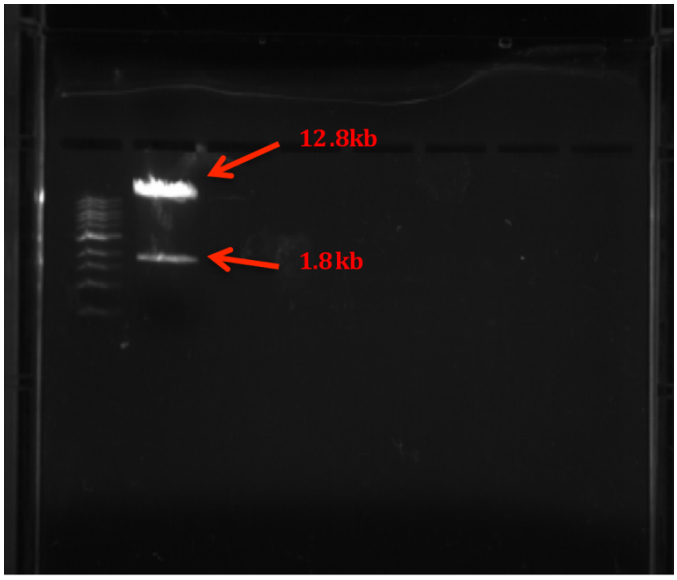

Figure 13: Gel image of digested plasmid:

Plasmid was digested to remove the filler sequence so that sgRNAs could be incorporated into the plasmid backbone. UV exposure revealed a 1.8 kb band and a 12.8 kb band corresponding to the filler sequence and plasmid backbone respectively.

Gel Extraction:

Using a UV source, the 12.8 kb band was excised and weighed; This ensured that it was re-suspended at the correct concentration when it came to the extraction. The plasmid was then purified from the cut-out gel using the QIAquick Gel Extraction Kit (Qiagen Cat.No. 28704). This involves dissolving the gel then isolating DNA from the resulting solution by centrifugation, which results in a 50 µl elute of the digested plasmid in the elution buffer provided with the kit.

Annealing of forward and reverse sgRNA oligonucleotides:

In each case oligonucleotides were resuspended at 1 nmol/µl in d H_2O (Table 3). The pairs of oligos were then annealed in the following reaction: 1 µl forward oligo (1:10 dilution – 0.1 nmol/µl), 1 µl reverse oligo (1:10 dilution – 0.1 nmol/µl), 5 µl NEB buffer 2 (NEB, Cat.No. B7002S), 43 µl water. Annealing reagents were put in a thermocycler with the following steps: 95°C for 5 minutes then ramped down to 25°C at a rate of 6°C/min.

sgRNA Name	yield (nmol)	H_2O volume (µl)
Itch1F	44.2	44.2
Itch1R	46.1	46.1
Itch2F	45.4	45.4
Itch2R	42.4	42.4
Itch3F	41.4	41.4
Itch3R	36.8	36.8
Itch4F	79.7	79.7
Itch4R	35.5	35.5
Itch5F	52.4	52.4
Itch5R	47.7	47.7
Itch6F	69.4	69.4
Itch6R	33.0	33.0

Table 3: Resuspension volumes for sgRNA oligos:

Yield supplied by manufacturer and the appropriate volume of deionised water to re-suspend oligos at 1 nmol/µl.

Ligation of annealed oligos into digested plasmid vector:

Annealed oligos were then ligated to the digested pLentiCRISPv2 vector using the Roche Rapid Ligation Kit (Roche, purchased from Sigma-Aldrich, Cat.No. 11635379001): 5 µl water, 1 µl of a 1:10 dilution of annealed oligos, 2 µl digested gel purified pLentiCRISPRv2, 2 µl 5x DNA dilution buffer, 10 µl 2x digestion buffer, 1 µl ligase. The ligation reaction was incubated overnight at 16°C (for this we used a Lucky Reptile Herp Nursery II Incubator).

Transformation of vector into STBL3 and bacterial expansion:

The ligation mix was then transformed into One Shot STBL3 chemically competent E.coli (Invitrogen, Cat.No. C737303). 5 µl of ligated vector was added to one tube of STBL3 thawed on ice and incubated on ice for 30 minutes. The STBL3s were then heat-shocked at 42°C for 45 seconds before returning to ice for another 2 minutes. 250 µl of LSOC media (provided with the bacteria), pre-warmed to room temperature, was added to each tube of bacteria and incubated at 37°C with shaking at 225 rpm for 1 hour in an Orbital Incubator SI50 (Stuart Scientific). After the incubation period, 200 µl of media was removed from each tube and put on ampicillin-treated agar plates and incubated overnight at 37°C. Due to the presence of ampicillin in the agar the only colonies that should grow on the plate are bacteria that have successfully incorporated a fully ligated plasmid (since lentiCRISPRv2 contains a sequence that codes for ampicillin and carbenicillin resistance). After culturing overnight, colonies were selected (3 per plate) and expanded in 5ml of LB broth supplemented with 100 µg/ml carbenicillin for 15 hours at 37°C with shaking. Carbenicillin was used over ampicillin, as it is more resistant to degradation. Stocks containing a mix of the bacterial media and 80% glycerol were made for potential future use and stored at -80°C.

The rest of the bacterial solution was centrifuged at 1900 ×g for 6 minutes. The supernatant was discarded and DNA was extracted using the QIAprep Spin Mini-prep Kit (Qiagen, Cat.No. 27104). Eluted DNA was quantified using Nanodrop (looking for a 260/280 absorbance ratio of approximately 1.8 for eluted DNA).

Verification of sgRNA incorporation into pLentiCRISPRv2:

Two methods were used for verifying that the insert had been incorporated into the pLentiCRISPRv2 vector: a restriction double digest and plasmid sequencing. A restriction double digest was performed on 1 µg of mini-prep DNA that could then be run on an agarose gel. Additional reagents for the double digest included: 1µl of EcoR1 (NEB, CatNo. R0101S), 1 µl of Nde1 (NEB, Cat.No. R0111S), 2 µl Cutsmart buffer (provided with restriction enzymes), 2 µl of loading dye, then made up to 20 µl with water. Uncut solutions were also made where the restriction enzymes are substituted out for water; this provided a baseline comparison for each sample. Reactions were incubated for 1 hour at 37°C before being loaded onto a 2% agarose gel (with 1 µl EtBr) alongside a 1 kb ladder (NEB, Cat.No. N3232S) and Hyperladder I (Bioline, Cat.No. BIO-33053) and run at 60 V for 55 minutes. The gel was then imaged using a ChemiDoc XRS+ (Bio-Rad), looking for fragments at 154/174 bp, indicating the presence of the sgRNA insert as shown in Figure 14 (A, B, and C).

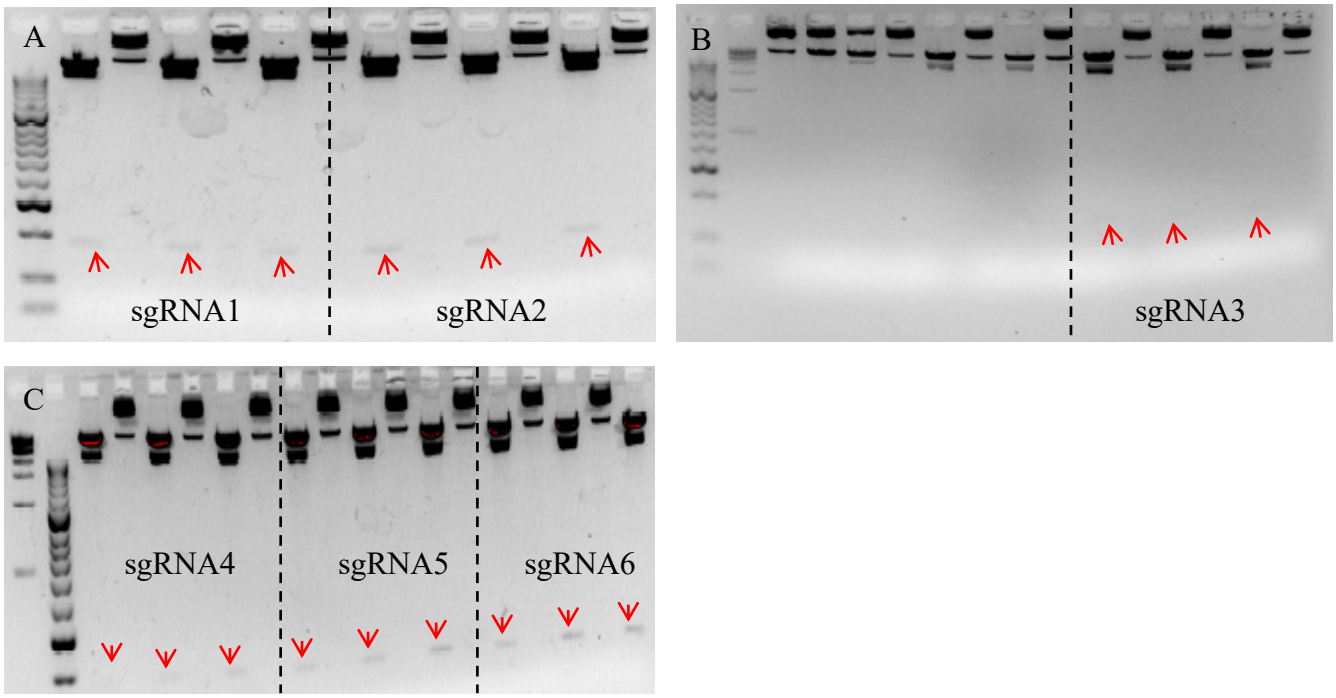

Figure 14: ChemiDoc XRS+ gel images from the restriction double digests:

(**A.**) sgRNA 1 and 2, (**B.**) sgRNA 3, (**C.**) sgRNA 4,5 and 6. Arrows indicate presence of desired bands for each bacterial colony (A,B or C).

Samples where bands were present were sent for sequencing at DNAseq based at the University of Dundee. Mini-prep samples were re-suspended to get 600 ng in 30 µl of water, the sequencing primer used was LKO.1 5' which was diluted from a stock solution (4 µl of a 200 µM stock in 250 µl of water) and 2 µl added to the DNA and water; These were then sent for sequencing. Plasmid sequencing results were returned within one or two days and the sequences were checked to see if they contained the appropriate 20 base pair sgRNA

sequence. The glycerol stocks of the positive hits from both the sequencing and restriction digest were kept and used for DNA maxi-prep.

DNA Maxi-Prep:

The glycerol stocks were then used to create a starter culture of bacteria (scraping of the stock in 3 ml LB and carbenicillin). Only samples that had been validated by both the restriction digest and the plasmid sequencing were used to create the starter cultures (in the case where more than one sample came back positive only one was used). These were cultured for 8 hours at 37°C with shaking before 1 ml was removed and transferred to 200 ml of LB/Carb in a conical flask and cultured overnight at 37°C, shaking at 220 rpm in a New Brunswick I-26 incubator shaker. Culture was then transferred to a 500 ml centrifuge bottle and spun at 6,000 ×g for 15 minutes at 4°C. The supernatant was then discarded and the plasmid was purified using Qiagen's Endo Free Plasmid Maxi Kit (Qiagen, Cat.No. 12163). Resulting protocol yields purified plasmid in a >200 µl suspension, this is then quantified by Nanodrop. Purified DNA was then made into aliquots of 1 µg/µl and stored at -20°C. Maxi preps were also made for the 2 packaging plasmids used in the transfection stage of the CRISPR protocol (see below).

Preparation of lentiviral particles for transduction:

From this point on only plasmids containing sgRNA 1, 2 and 3 were used to create new modified cell lines. To grow lentiviral particles containing the CRISPR-Cas9 system, HEK293T cells were used from frozen stocks. HEK293Ts are a derivative of the HEK293 (Human Embryonic Kidney 293) cell line, one with debatable origin (Stepanenko & Dmitrenko, 2015), that have a temperature sensitive variant of the SV40 antigen, which allows increased production of desired proteins and/or lentivirus. HEK293T cells were plated at a density of $4x10^6$ cells per 10 cm plate and incubated overnight in 10 ml DMEM. 27 µl of Mirus Bio TransIT-LT1 Transfection Reagent (Fisher Scientific, Cat. No. MIR2304) was added to 1.5 ml of pre-warmed OptiMEM and incubated for 20 minutes. A mix of pLentiCRISPRv2 (containing the desired sgRNA sequences targeting *Itch* or containing a scrambled control sequence), PsPAX2 (Addgene plasmid # 12260) and PSDII (also known as pMD2.G - Addgene plasmid # 12259) was prepared (Table 4).

Plasmid	**pLentiCRISPRv2**	**PSPAXII**	**pMD2.G**
Volume of 1 µg/µl plasmid stock (µl)	4.00	3.00	2.00
Amount of plasmid in final solution (µg)	4	3	2

Table 4: plasmids used and volumes of each from maxi-prep stocks.

PsPAX2 and pMD2.G (Supplementary Figure 1) are second-generation packaging plasmids and thus facilitate lentiviral production and transfection in-vitro (PsPAX2 and pMD2.G were gifts from Didier Trono (Addgene plasmid # 12260; http://n2t.net/addgene:12260; RRID:Addgene_12260 and Addgene plasmid # 12259; http://n2t.net/addgene:12259 ; RRID:Addgene_12259). Packaging plasmids were developed to introduce a layer of safety when working with lentiviral vectors since they are derived from HIV-1 (Sakuma, Barry, & Ikeda, 2012). Splitting the lentiviral construct across three plasmids, a packaging construct,

an envelope construct and a transfer construct, acts to prevent the formation of RCLs (Replication competent lentiviruses) (Sakuma et al., 2012). Second generation packaging plasmids are different from first generation packaging plasmids in that they lack certain accessory proteins that are not needed for replication in particular cell lines (Zufferey et al., 1997)

The plasmid mixture was then added to the OPTImem and Mirus solution and incubated for a further 30 minutes. The overall solution was then aliquoted onto the plates of HEK293T cells and incubated overnight. Existing media and replacing with 4ml of fresh media; At this point the cells should start producing lentiviral particles.

After 48 hours total incubation, viral particle-containing media was collected and stored at 4°C. Fresh media (4 ml) was re-applied to the HEK293T cells and placed back in incubation. After 72 hours of exposure to the plasmid mix, the media was once again aspirated from the HEK293T cells and combined with the media from 48 hours. The combined media was passed through a 0.45 μm syringe filter into a tube containing 8 μg/ml polybrene (Sigma-Aldrich, Cat.No. TR-1003): This step acts to separate out any cellular debris contained within the viral media. The viral media could then be used to infect recipient cells.

Transduction of mammalian cell lines:

Prior to lentiviral transduction, $5x10^5$ MiaPaCa-2 or Capan-2 cells were seeded onto 10 cm dishes (two dishes per plasmid of interest). 4 ml of viral media was then added to the recipient cells and kept in the viral incubator for 48 hours. Media was then aspirated and recipient cells were trypsinised using TrypLE Express (Gibco, Cat.No. 12604054). This was then neutralised with either DMEM or McCoy's 5A media (depending on cell line) and centrifuged at 1,200 rpm for 3 minutes in a Heraeus Labofuge 400R. T-75 flasks were prepared containing 20 ml of media (DMEM or McCoy's) treated with puromycin (4 μM, Sigma-Aldrich, Cat.No. 540222). Puromycin acts as a selective pressure: cells that have not incorporated the lentiviral construct will not have puromycin resistance and will have inhibited growth and/or die. The supernatant was discarded and the pellet re-suspended in 5ml of media which was then transferred to the respective T-75 flask. Cells were then cultured with puromycin selection over 4 days, the selection pressure was removed and cells were safe to move back into non-viral incubation after 2 changes of plastic. Downstream applications could then proceed.

Transduction of Primary monocytes:

Viral-particle-containing media from 48 and 72 hours was combined and the media was filtered as previously described (see "*Preparation of lentiviral particles for transduction*" - page: 43). viral media (1.5 ml) of was aliquoted onto 6-well dishes containing monocytes and osteoclast precursors and incubated for 48 hours. Following this incubation period, the viral media was aspirated and the wells washed with PBS. The cells were not trypsinised in this case to minimise the risk of losing cells (primary monocytes do not replicate). Cells were exposed to media containing 1μM puromycin supplemented with M-CSF as before for 4-5 days. During this period of incubation the puromycin-containing media was replaced when there were many dead cells (assessing the morphology of the cells by microscopy). After this period of time the media was replaced with osteoclast differentiation-promoting media (α-MEM containing 20 ng/ml m-CSF and 50 ng/ml RANKL).

Preparation of RNA for qPCR:

Preparation of RNA lysates:

Cells were seeded on 6-well plates and were grown until roughly 80% confluence or 24 hours after siRNA treatment. Media was then aspirated and wells were washed with ice-cold PBS. PBS was removed using an aspirator pump and the plates were placed on-ice at an angle to pool any leftover PBS. This was removed using a fine-tipped pastette. RNA was extracted and isolated using the Quiagen RNEasy Mini Kit (Quiagen, Cat.No. 74104). Lysis solution was prepared by adding 10 µl of β-mercaptoethanol per 1ml of buffer RLT (amount required was calculated beforehand based on number of samples. The β-mercaptoethanol-supplemented RLT is stable at room temperature for up to 1 month). 350 µl of lysis solution was added to each well and wells were gently scraped to detach cells from the plate surface with a sterile cell scraper. Plates were then left for a couple of minutes to lyse and at an angle to pool all the material. Lysates were then transferred to a 1.5 ml Eppendorf tube and labelled appropriately. At this point the lysates can be stored at -80°C if desired. Each lysate was supplemented with 350 µl of 70% ethanol solution (ETOH, 1:1 ratio) and was mixed by pipetting up and down. 700 µl of each sample was transferred to a "RNeasy spin column" (which is already placed inside a 2 ml collection tube) and spun at 10,000 rpm for 15sec in a Heraeus Fresco-21 centrifuge (Thermo). The flow-through was discarded and the column placed back into the collection tube. Any remaining sample was pooled into the corresponding spin column and spun again at 10,000 rpm for 15s. 700 µl of buffer RW1 was added to each spin column and spun at 10,000 rpm for 15s. The flow-through was discarded and spin column placed back into the collection tube. 500µl of buffer RPE (supplemented with ETOH prior to extraction as per Quiagen's instructions) was added to each spin column and spun at 10,000 rpm for 2min. Flow-through was discarded and the column was then placed into a fresh 2 ml collection tube and spun again at 10,000 rpm for 1min. The spin column was removed and placed into a 1.5 ml Eppendorf tube. RNAse-free water (30 µl) was applied directly to the membrane of each spin column which was then spun at 10,000 rpm for 1min to elute the RNA. RNA elute was then stored at -80°C until ready to quantify using Nanodrop (using RNAse-free water as a blank, looking for a 260/280 absorbance ratio of roughly 2.0 for RNA).

cDNA generation by reverse transcription:

Reverse transcription was done as per the instructions of the Quiagen QuantiTect Reverse Transcription Kit (Quiagen, Cat.No. 205311). Template RNA was thawed on ice whilst gDNA Wipeout Buffer, Reverse Transcriptase, RT primers, RT buffer and RNAse-free water were thawed at room temperature. To eliminate any genomic DNA (gDNA) that may be in the sample a gDNA eliminating reaction was set up in 600 µl tubes as described in Table 5 to a total volume of 14 µl. Tubes were flicked to mix the reagents, and centrifuged using an Eppendorf mini spin benchtop centrifuge to pool all of the reagents at the bottom of each tube. Tubes were then incubated in a heat block at 42°C for 2 min then placed immediately on ice.

Component	Amount/reaction
gDNA Wipeout Buffer 7x	2 µl
Template RNA	Variable (up to 1 µg)
RNAse-free water	Variable
Total reaction volume	14 µl

Table 5: gDNA elimination reaction setup.

Reverse transcription master mix was prepared in a separate Eppendorf tube to be dispensed into each of the individual tubes from the gDNA elimination reaction on ice. The volumes per sample are described in Table 6 however excess was usually prepared to account for potential pipetting error. Tubes were flicked and centrifuged, as previously described to mix and pool the whole reaction before initiation.

Reagent	Volume/reaction
QuantiTect Reverse Transcriptase	1 µl
QuantiTect RT Buffer, 5x	4 µl
RT Primer Mix	1 µl
Entire gDNA elimination reaction	14 µl
Total Reaction Volume	20 µl

Table 6: Reverse transcription reaction setup.

To start the reverse transcription reaction each sample was incubated in a heat block at 42°C for 15min. Reverse transcriptase was then inactivated by moving the tubes to a separate heat block at 95°C for 3min. After the 3 minutes the samples were placed on ice to cool down. Once sufficiently cool the samples were spun again to pool all of the sample at the bottom of the tube and then kept at -20°C until needed for qPCR.

Quantitative PCR (qPCR):

qPCR was done using a Quiagen Rotor-Gene Q (Quiagen) qPCR machine with the accompanying software. Tube preparation reagents included Rotor-Gene SYBR Green PCR Kit (Quiagen, Cat.No. 204074) and QuantiTECT Primer Assays (Quiagen) for *GAPDH* and *Itch*. Each individual sample was seeded in quadruplicate for qPCR and was set up as described in Table 7 and was aliquoted into Quiagen Strip Tubes and Caps (Quiagen, Cat.No. 981103). The master mix was prepared separately and aliquoted into tubes before the cDNA was dispensed into individual tubes. Separate master mixes were made for each primer. Additional tubes were made for each run which were either no-template-controls or no-primer-controls to assess for primer specificity.

Reagent	Volume/tube
SYBR Green	12.5 µl
Quantitect Primer Assay	2.5 µl
RNAse-free water	Variable
cDNA	Variable
Total Reaction Volume	25 µl

Table 7: The qPCR tube reaction setup:

The amount of template cDNA specified in the product handbook is ≤100 ng/reaction. We assume from the reverse transcription reaction that all of the template RNA has been converted into cDNA.

Reaction tubes were then loaded into the Rotor-Gene Q and the cycler programmed with the settings described in Table 8, acquiring on the green channel to detect SYBR Green fluorescence.

Step	Time	Temperature
PCR Initial Activation Step	5min	95°C
Two-Step Cycling		
Denaturation	5s	95°C
Annealing/Extension	10s	60°C
Number of Cycles		35-40

Table 8: The qPCR cycling parameters for the Rotor-Gene-Q.

Once the plateaux phase in the reaction for each individual sample had been reached, analysis of relative gene expression (using *GAPDH* as a housekeeping gene) could be performed. Ct values were calculated by the software after designating a threshold value where each of the samples was in the linear phase of the PCR reaction. These values were exported to an Excel spreadsheet where relative *Itch* expression could be calculated for each individual sample (ΔCt) compared to its *GAPDH* expression. Further analysis of this data included mean and standard deviation calculation and normalisation to parental/untreated controls. Data was then copied into GraphPad Prism (version 6.2) to draw graphs and perform a Student's t-test to identify statistically significant differences in mean *Itch* expression between samples.

Preparation of protein lysates for Western Blot:

Cells were seeded on either 10 or 15 cm^2 diameter plates and grown until roughly 80% confluent or 24 hours after siRNA treatment, ensuring that no samples were completely confluent. When the desired confluence was reached the dishes were removed from incubation. A 10 ml aliquot of RIPA lysis buffer (Table 9, "RIPA buffer," 2006) was used to make a lysis solution that was prepared on ice (Table 10).

Reagent	Volume (ml)	Final concentration
5 M NaCl	3	150 mM
0.5 M EDTA, pH 8.0	1	5 mM
1 M Tris, pH 8.0	5	50 mM
NP-40 (IGEPAL CA-630)	1	1.0%
10% sodium deoxycholate	5	0.5%
10% SDS	1	0.1%
dH_2O	84	

Table 9: RIPA buffer preparation and reagents

Reagent	Amount/Volume
RIPA buffer	10 ml
Phosphatase inhibitor 2 (Sigma Aldrich, Cat. No. P5726)	100 µl
Phosphatase inhibitor 3 (Sigma Aldrich, Cat No. P0044)	100 µl
Aprotinin (Sigma Aldrich, Cat. No. SRE0050)	50 µl
cOmplete mini protease inhibitor cocktail (Roche, Cat. No. 11836153001)	1 tablet

Table 10: Reagents used for preparation of the lysis solution

Culture media was decanted and the dishes were washed twice with ice-cold excess PBS to remove any protein-containing media. PBS was then aspirated and the dishes were placed on ice at an angle so that any leftover PBS would run off and could be collected using a fine-tipped Pasteur pipette; This prevents any excess PBS from diluting the lysate if the yield of protein is low. lysis solution was then added to each culture dish; cells were then scraped and left to lyse with the dishes at an angle so that all the lysed material collected at the bottom to make it easier to aspirate. Lysed cells were then transferred to eppendorf tubes and centrifuged at 13,000 rpm for 6 minutes at 4°C in a Heraeus Fresco-21 centrifuge, after which the supernatant was removed and placed in a fresh tube and stored at -80°C until needed.

Bicinchoninic acid assay (BCA assay) to determine protein concentration:

To determine the concentration of protein within lysates a BCA assay was used. 5 µl of protein lysate was diluted in 45 µl of lysis buffer and placed in borosilicate glass tubes (note: lysis buffer used from generating the protein lysates as described before. Buffer is still usable if used within a few days and kept refrigerated, water can be used as an alternative for dilution). Protein standards were prepared (Table 11) using the albumin standard samples provided with the Pierce BCA Protein Assay Kit (Thermo Fisher, Cat No. 23225).

Tube	Final Conc. (µg/ml)	Vol. 2 mg/ml standard (µl)	Vol. dH_2O (µl)
A	0	0.00	50.00
B	100	2.50	47.50
C	150	3.75	46.25
D	200	5.00	45.00
E	500	12.50	37.50
F	1000	25.00	25.00
G	1500	37.50	12.50
H	2000	50.00	0.00

Table 11: BCA assay protein standard preparation:

Protein standards A-H with the final protein concentration, volume of the albumin standard used and the volume of water used for each solution.

In a universal tube 0.5 ml of copper(II) sulfate solution (provided with the kit) was added to 25 ml of bicinchoninic acid solution (provided with the kit). This results in a green solution that was then aliquoted at 1 ml into each of the diluted protein lysate samples and protein standards. The tubes were then placed in a water bath at 60°C for 15 minutes. After incubation the resulting solution in each of the tubes should be purple: the darker the shade, the higher the protein concentration. This was quantified using a Biohit BP800 Microplate Reader (filter: 540 nm) with a pre-prepared algorithm within a spreadsheet to calculate protein concentration (optical densities of the standards provided a standard curve which was then used to estimate protein concentration of each of the test samples). Using the results from the spreadsheet, western blot samples were prepared so as to normalise the concentration of protein between samples by addition of loading buffer (5×) and lysis buffer.

Western blot protocol:

Antibodies used:

Antibody	Species	Supplier	Dilution
Itch (109018)	Rabbit	Abcam	1:10,000
Itch (D8Q6D)	Rabbit	CST	1:1000
β-Actin (8H10D10)	Mouse	CST	1:2000
Cas9 (7A9-3A3)	Mouse	CST	1:1000

Table 12: antibodies for western blots.

Antibodies used throughout the project including species, supplier and dilution used.

Polyacrylamide gel Electrophoresis:

A western blot was performed using the Laemmli method (Laemmli, 1970) which involves using stacking gel to concentrate protein before it enters the resolving gel (reagents for both gels are displayed in Table 13). This is due to the different pH of each of the gels providing different motility to proteins when subject to a current. Samples to be run on the gel were first denatured in a heat block at 60°C for 1 hour whilst a 10% resolving gel and the stacking gel were prepared in vertical electrophoresis apparatus (Table 16). Once samples were loaded

on the gel along with Chameleon Duo protein marker (Licor, Cat.No. 928-60000). Electrophoresis proceeded with an initial step of 35 mA for 35 minutes then 70 mA for over 2 hours.

Solution	Reagents
Resolving gel (10%)	13.5 ml Acrylamide 15 ml 1 M Tris (pH8.85) 0.4 ml 10% SDS 11.1 ml H_2O 0.1 ml TEMED (tetramethylethylenediamine) 0.1 ml AMPS (ammonium persulfate)
Stacking gel	3.6 ml Acrylamide 10 ml 0.375 M Tris (pH6.8) 16 ml H_2O 0.1 ml TEMED 0.1 ml AMPS
Running buffer	9.09 g Tris base (Sigma) 43.26 g Glycine (Sigma) 30 ml 10% SDS dH_2O to 3 L

Table 13: Solutions with relevant reagents and volumes for polyacrylamide gel electrophoresis:

All solutions prepared at room temperature.

Gel transfer:

Transfer buffer was prepared along with the transfer membrane and other components required for transfer. After the run the gel was removed from the electrophoresis apparatus and any sections of the gel that were deemed superfluous were excised. The transfer cassette, including the PVDF transfer membrane (pore size 0.45 μm, Immobilon, Cat. No. IPVH00010), was assembled and the transfer buffer was prepared (Table 14). The cassette was loaded into the transfer tank along with the buffer. Transfer was carried out at 30 V overnight at 4°C with gentle buffer agitation using a magnetic stirrer.

Solution	Reagents
Transfer buffer	12.12 g Tris base 57.68 g Glycine dH_2O to 4 L

Table 14: Solutions used for gel transfer stage in the western blot protocol and the reagents used to prepare them:

All solutions prepared at room temperature.

Primary and secondary antibody staining:

Primary antibodies were diluted in a 50:50 solution of Licor blocking buffer (Licor, Cat.No. 927-40000) and PBS. The transfer cassette was removed from 4°C and the transfer membrane removed, checking to see if the visible bands from the protein marker had successfully transferred from the gel to the membrane. Antibody solution was then applied to the transfer membrane and incubated overnight at 4°C with gentle rocking.

After incubation the membrane was then washed 3×5 minutes with 0.1% PBS-Tween before the secondary antibody solution was applied. Secondary antibodies used were donkey anti-rabbit (CW800 – Licor, Cat.No. 926-32213) and/or donkey anti-mouse (RD680 – Licor, Cat.No. 926-68072) and were both used at a dilution of 1:10,000 in a 50:50 solution of Licor blocking buffer and PBS with 0.1% SDS (to eliminate background and potential non-specific binding). The membrane was incubated with secondary antibody solution and left at room temperature, with gentle rocking, for 45 minutes in the dark: It was then washed again 3×5 minutes with PBS-T followed by 3×5 min washes with just PBS. The membrane was then left to dry on filter paper. Once dry the membrane and bands were imaged and quantified using a Licor Odyssey Scanner (Licor) and Image Studio (Licor). Quantified signal in the red and green channels was then exported to Excel where background correction and normalisation to controls was performed. Data was then copied into GraphPad Prism to draw graphs and search for statistically significant differences in protein level as determined by Student's t-test.

Antibody troubleshooting:

Initially a monoclonal rabbit anti-Itch primary antibody from Abcam was used with a dilution of 1:10,000 (as per the manufacturer's instructions) and mouse β-actin as a loading control with a 1:2000 dilution. Washing, secondary antibody application, and membrane visualisation were performed as previously described.

When visualised using the Licor Odyssey scanner, presence of β-Actin was confirmed as indicated by the red bands at around 42 kDa (Figure 15). However, there was a lack of signal in all of the samples for Itch (band size roughly 103 kDa) including parental and scrambled controls. The presence of β-Actin indicates that there was nothing wrong with the sampling method and that there is indeed protein in the sample meaning that the most likely cause for the lack of Itch signal is linked to the antibodies used.

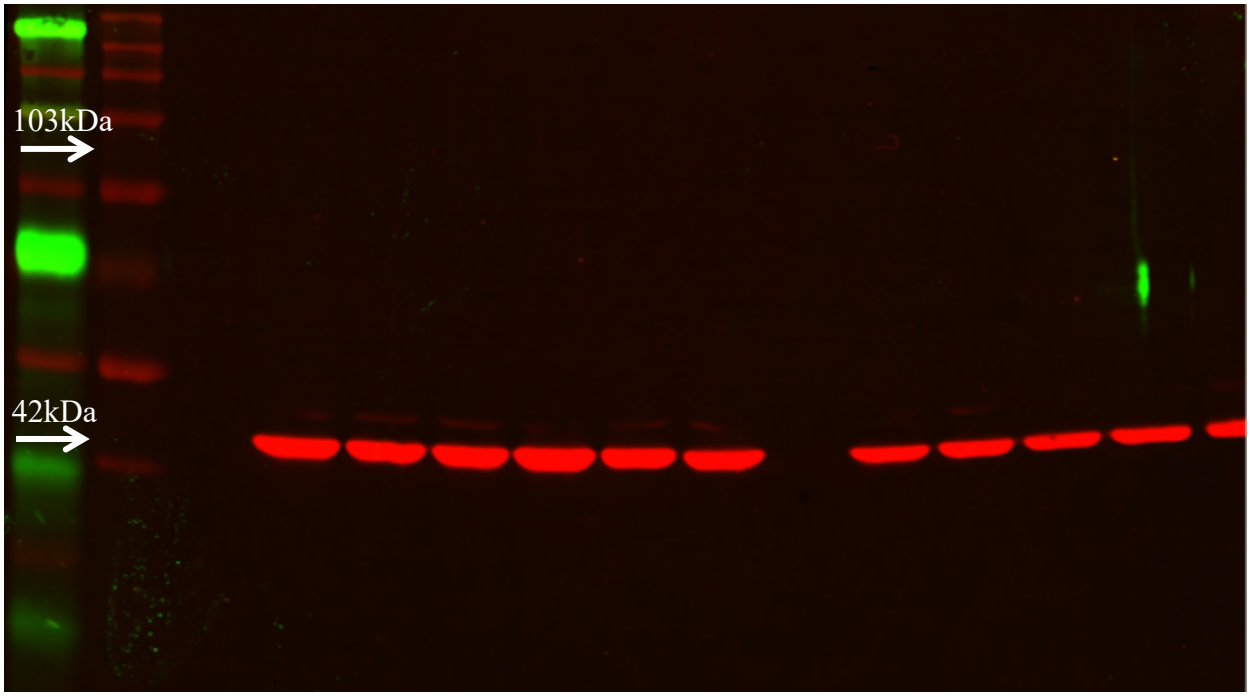

Figure 15: Western blot performed on cell lines:

Red bands show presence of actin loading control, yellow arrow indicates the predicted area one would expect to see Itch (white arrow).

One possible reason that no signal was present was that there is little to no expression of endogenous Itch in the cell types used; This would make it difficult to determine whether the knockout was successful in regards to protein level as there would be no distinguishable base line from which to compare the results. However, previous studies have performed Western blots using MiaPaCa-2 cells and these have been successful (de la Fuente et al., 2015). Another possibility is that the primary antibody was simply too dilute. The dilution used in the protocol was 1:10,000 (based on the manufacturer's instructions) which seemed very low compared to the dilutions typically used for primary antibodies (usually around 1:1000). Lastly, and most simply, the antibody or batch could have been faulty.

To troubleshoot this issue a series of follow-up western blots were performed. To quickly test the dilution theory the membrane was re-blocked and the primary antibody was re-applied at a 1:1000 dilution, however bands could still not be detected (not shown). A new gel was then prepared using existing lysates from three of the four positive control cell lines described in the antibody datasheet: MCF7s, HL60s, and K562s. Each of the lysates along with the protein marker were aliquoted so as to have four replicates of each. Once the transfer step of the Western Blot protocol was completed the membrane was divided into quarters so as to have four sections of membrane each with protein marker and one of each of the positive controls. Each of the membranes were then subjected to different treatments involving the use of different dilutions of Itch primary antibody and different membrane blocking reagents (Table: 15).

Membrane	Primary dilution	Blocking reagent
A	1:1000	50:50 Licor blocking buffer/PBS
B	1:1000	5% Dry Milk powder in PBS
C	1:10,000	50:50 Licor blocking buffer/PBS
D	1:10,000	5% Dry Milk powder in PBS

Table 15: antibody dilutions and blocking conditions for each of the four membranes

The membranes were all treated with the same dilution of secondary antibody (1:10,000) in different blocking agents depending on what was used with the primary antibody. Upon imaging the four membranes (Figure 16) there was still no apparent bands for Itch for any of the samples. After this result we concluded that the batch was faulty, which was later confirmed by Abcam (the manufacturer) at a later date.

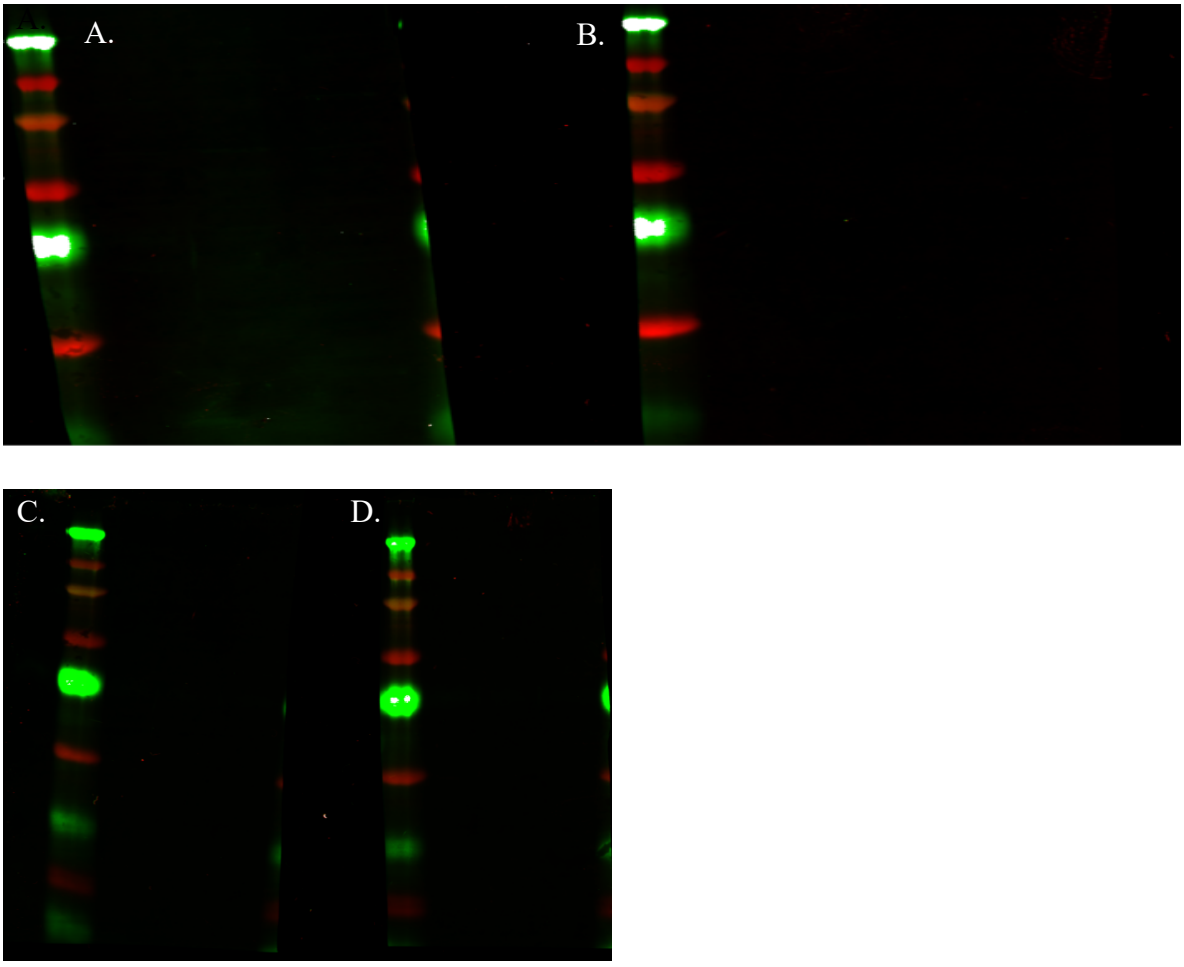

Figure 16: Western blots performed on control cell lines:

Cell lines MCF7, HL60, K562 with different antibody dilutions and blocking agents. Licor blocking buffer, 1:1,000 ab dilution (**A.**) and 1:10,000 ab dilution (**B.)** Dry milk powder 1:1,000 ab dilution (**C.**) and 1:10,000 ab dilution (**D.**).

Cell Survival assays:

Drug Preparation:

Doxorubicin (Sigma Aldrich, Cat.No. 44583) and gemcitabine (Sigma Aldrich, Cat.No. G6423) were made into 10 mM aliquots in 100 µl DMSO (Sigma Aldrich, Cat No. D2660). For cytotoxicity experiments 10/1 µM stock solutions in culture media were made for Capan-2 and MiaPaCa-2 cells respectively. Smaller concentrations were made from various dilutions of these stock solutions. For each experiment a vehicle control was prepared which contained the equivalent dilution of DMSO for the highest drug concentration for each cell line: for Capan-2 cells this was 1:1000 (maximum drug conc. 10 µM) and 1:100,000 for MiaPaCa-2 (maximum drug conc. 100 nM).

Irradiation of cell lines:

Cells were passaged into T25 flasks/6 cm dishes for each test condition and exposed to 0-6 Gy of γ-radiation in a IBL437C Gamma Irradiator (CIS Diagnostic, radioactive source: Cs^{137}). Cells were then immediately passaged, resuspended, counted, and dispensed onto 96 well plates at the densities described below.

SRB and automated cytometry analysis (Celigo):

Cells being treated with chemotherapeutic drugs (i.e. doxorubicin and gemcitabine) were passaged, counted using a haemocytometer, resuspended in fresh media and aliquoted onto 96 well plates to achieve a specific initial cell density (500 cells/well for MiaPaCa-2 cells and 2000 cells/well for Capan-2 cells as determined by a preliminary growth curve experiment). After 24 hours (to allow cells to adhere to the plate surface) cells were subject to increasing concentrations of either gemcitabine or doxorubicin. After 24 hours exposure, drug-containing media was aspirated and replaced with fresh media. Cells subject to radiation had media changed 24 hours after treatment to mimic the conditions of the doxorubicin/gemcitabine treated cells.

Over 4 days of incubation, plates were scanned on Celigo every 24 hours, measuring the change in confluence (percentage cell coverage, Table 16) in each well over time. A sulforhodamine B (SRB) assay was then performed as an end-point measurement of cell survival after 4 days (cytotoxicity assay). Cells were fixed with 50 µl of 25% cold trichloroacetic acid (TCA) solution and incubated for 1 hour at 4°C. Plates were then washed with excess tap water and placed in an oven to dry. 50 µl of SRB staining solution was applied to each well and incubated at room temperature for 45 minutes with gentle rocking. Plates were then washed with excess 1% glacial acetic acid solution and once again placed in an oven to dry. Once dry, wells were incubated with 150 µl of 10 mM, pH 10.5, Tris buffer for 1 hour at room temperature with gentle rocking. Plates were then scanned using the Biohit BP800 Microplate Reader (filter: 540nm – as previously used for BCA protein determination). Absorbance values were recorded for each well and exported to Excel.

Algorithm name: Confluence	
Algorithm type	Texture
Intensity threshold	10
Saturated intensity	4
Precision	High
Diameter (μm)	9
Background correction	Yes
Minimum thickness (μm)	3
Pre-filtering	Minimum cluster size of 500 μm^2

Table 16: Algorithm settings for analysing cell confluence of cell lines.

Solution	Reagents/preparation
25% Trichloroacetic acid (TCA) solution	Dilute 100% stock TCA. Store at 4°C
SRB staining solution	0.4% SRB in 1% acetic acid: dissolve 2 g of SRB in 1% acetic acid and make up to 500 ml. Store at 4°C.
1% glacial acetic acid	Dilute 20 ml stock glacial acetic acid with distilled water up to a final volume of 2 l. Can be stored at room temperature.
10mM Tris buffer (pH 10.5)	Dissolve 1.21 g Tris base in water, adjust pH to 10.5 and make up to a final volume of 1 l. Store at 4°C.

Table 17: Solutions used in SRB protocol.

All solutions prepared at room temperature.

In Excel resultant data was normalised. Both resultant and normalised data was copied into GraphPad prism to draw graphs. Student's t-test was performed to determine statistically significant differences between Itch-targeted cells and control conditions.

Separate graphs were generated to compare samples in the doxorubicin/gemcitabine regimens that had not received the chemotherapeutic but may have received Itch-targeting gene edits or scrambled control. Multiple one-way ANOVAs were used to assess for any statistically significant difference between these negative control conditions.

Clonogenicity (clonogenic) assay:

This was used as a measure of how well cells could form colonies after exposure to different modes of treatment and/or different forms of genetic modification. Cells were passaged and counted as described previously then seeded on either 6- or 24-well plates at 250/125 cells per well respectively. After 24 hours cells were exposed to drug treatment (either gemcitabine or doxorubicin, prepared as previously described) and incubated for 24 hours. Drug-containing media was then removed and replaced with fresh media which was changed every 3-4 days. In the case of radiation; cells were cultured in T25 flasks as previously described before being irradiated and seeded onto plates. After 1 week of incubation post-

treatment plates were scanned on Celigo using a colony identification algorithm (which identifies groups of cells, labelling them as a colony – Table 18).

Algorithm name: Clonogenicity	
Algorithm type	Texture
Intensity threshold	4
Saturated intensity	0
Precision	High
Diameter (μm)	6
Background correction	Yes
Separate touching objects	Yes
Minimum thickness (μm)	12
Pre-filtering	Minimum cluster size of 80,000 μm^2

Table 18: Algorithm settings for analysing clonogenicity of MiaPaCa-2 derived cell lines.

Celigo data was exported as a CSV file which was then copied into GraphPad Prism to draw graphs. Statistically significant differences in clonogenicity between isogenic cell lines were determined via Student's t-test.

Sequential Window Acquisition of all Theoretical Mass Spectra (SWATH):

Lysate preparation:

Lysate preparation for SWATH MS is different to that for western blot preparation. Cells were seeded in 10 cm^2 dishes and were grown until roughly 70% confluence. Once confluent, dishes were either lysed immediately or were treated with 1 Gy δ-radiation and left for 24 hours before lysis. Plates were washed with ice cold PBS twice to remove all traces of media. PBS was aspirated and the dishes were placed at an angle to allow any excess PBS to drain off and be collected using a fine-tip Pasteur pipette. 700 μl of lysis solution (Table 19) was added to each of the dishes and cells were detached from the dish using a cell scraper. The cells were then left to lyse in solution for a couple of minutes.

Reagent	**Supplier**	**Final Concentration**
Ammonium bicarbonate (AmBic)	Sigma	50 mM
Urea	Sigma	8 M
SDC (sodium deoxycholate)	Sigma	4%
TCEP (tris(2-carboxyethyl)phosphine)	Sigma	5 mM

Table 19: Lysis solution reagents and concentrations for SWATH.

Lysate was then transferred to a 1.5 ml Eppendorf tube and stored at -80°C until required. A BCA assay was performed to determine the concentration of protein in each sample which

then allowed us to calculate the volumes required for subsequent reagents needed for SWATH sample preparation.

We wanted to assess the proteomic differences between parental MiaPaCa-2 cells and CRISPR-treated *Itch* knockdown isogenic cell lines and whether treatment with radiation also resulted in difference in proteome. In the initial sample preparation the isogenic cell lines IKO1a, IKO2, and IKO3 were used as biological replicates for the $CRISPR^{+}$ cells. Lysates were also made for samples that were treated 3 days prior with 1 Gy of gamma radiation.

Tryptic digest:

The volume for 60 μg of protein in each lysate was used for the peptide digest. Excess lysis solution was then added to equilibrate the total volumes between each sample. Iodoacetamide was added to a final concentration of 10 mM and incubated for 30 minutes in the dark to alkylate cysteine residues. DTT was then added, to quench the iodoacetamide, to a final concentration of 20 mM and incubated at room temperature for 10 minutes. The urea in the solution then had to be diluted to 1.5 M with AmBic to make it suitable for tryptic digest. 1:50 MS-grade trypsin (Promega, Cat.No. V5280) was then added and incubated overnight at 30°C.

Subsequent aspects of the SWATH protocol were performed in the St Andrews Mass Spectrometry and Proteomics Facility.

C18 salt clean-up:

After isolating peptides, salts need to be removed from the solution before proceeding with mass-spec. However, before this the peptide solution needs to be acidified to remove any detergents: 100% trifluoroacetic acid (TFA) was added to each sample to a final concentration of 0.5%. Acetonitrile (ACN) was then added to each sample to a final concentration of 5%. Salt clean-up was done in Reverse Phase Chromatography Spin Columns (Harvard Apparatus, Cat.No. 74-7242) containing a C18 matrix for this protocol. Before addition of samples, the spin columns had to be washed and equilibrated as follows (all spin steps were done in an Eppendorf Mini Spin benchtop centrifuge):

- 1× wash with 200 μl 100% ACN. Spin at 0.5 rcf for 30s.
- 2× wash with 200 ul 50% ACN. Spin at 0.5 rcf for 30s.
- 3× equilibrate with 5% ACN, 0.5% TFA. spin at 0.5 rcf for 30s.

The sample could then be loaded into the spin column:

- 3× load sample (divide total volume by 3 and roughly add that much to column for each spin), spin at 0.3 rcf for 30sec.
- 5/6× wash with 200 μl 5% ACN, 0.5%TFA. Spin at 0.3 rcf for 30s
- 3× elute with 30 μl 70% ACN, 0.5%TFA. Spin at 1.5 rcf for 30s.

Once all the sample had been eluted each sample was placed in a speedvac to dry.

Spectral library preparation and fractionation:

A spectral library was prepared by making two pooled samples (containing equal amounts of each individual sample) which were processed as previously described. Strong cation-

exchange chromatography (SCX) was used to fractionate one of pooled samples to reduce the complexity of the peptide mixture before Data-Dependent Acquisition (DDA). Ten fractions were generated from this sample.

DDA and Data-Independent Acquisition (DIA) runs:

Both DDA and DIA/SWATH runs were performed on a TripleTOF 5600^{+} instrument (Sciex). Individual samples, pooled sample, and pooled fractions were loaded along with loading buffer and iRT peptides that were spiked into each sample to act as references after detection. Spectral library was generated by performing a DDA run of the pooled sample and SCX fractions. DIA runs were performed afterwards on the 24 individual test samples with 39 windows of variable size (Table 20).

Start m/z (Da)	End m/z (Da)	Margin (Da)	m/z window size (Da)
399.5	419.2	0.5	19.7
418.2	436.2	0.5	18
435.2	450.7	0.5	15.5
449.7	463.4	0.5	13.7
462.4	476.2	0.5	13.8
475.2	488.1	0.5	12.9
487.1	500	0.5	12.9
499	512.3	0.5	13.3
511.3	524.6	0.5	13.3
523.6	536.9	0.5	13.3
535.9	548.8	0.5	12.9
547.8	560.7	0.5	12.9
559.7	572.6	0.5	12.9
571.6	584.1	0.5	12.5
583.1	595.6	0.5	12.5
594.6	607	0.5	12.4
606	618.9	0.5	12.9
617.9	630.8	0.5	12.9
629.8	642.7	0.5	12.9
641.7	655.1	0.5	13.4
654.1	667.8	0.5	13.7
666.8	681	0.5	14.2
680	694.6	0.5	14.6
693.6	709.5	0.5	15.9
708.5	724.3	0.5	15.8
723.3	739.6	0.5	16.3
738.6	754.9	0.5	16.3
753.9	770.7	0.5	16.8
769.7	786.4	0.5	16.7

785.4	803.4	0.5	18
802.4	821.7	0.5	19.3
820.7	841.6	0.5	20.9
840.6	864.2	0.5	23.6
863.2	888.8	0.5	25.6
887.8	915.6	0.5	27.8
914.6	948.3	0.5	33.7
947.3	990.8	0.5	43.5
989.8	1,045.20	0.5	55.4
1,044.20	1,118.70	0.5	74.5
1,117.70	1,250.00	0.5	132.3

Table 20: Variable m/z windows (swaths) used for DIA runs performed on a TripleTOF5600$^+$:

Margin indicates the degree of overlap permitted between each window.

Protein identification, quantification and data analysis:

All subsequent operations were performed Skyline (MacCoss Lab Software) (Maclean et al., 2010). Data from the TripleTOF5600$^+$ was imported into Skyline prior to analysis. Protein identification in DIA runs was based on results found in the spectral library generated from the DDA runs. MS/MS data could then be interpreted to quantify peptide and protein level between individual/groups of samples using the MSstats R-plugin (Choi et al., 2014) or within the Skyline software and exported to Excel. Two different sets of analyses were performed on untreated cells: One comparing all CRISPR-containing (CRISPR$^+$) cells with parental cells for two time points (0 and 3 days), and a second set of group comparisons comparing individual clones (IKO1a, IKO2, and IKO3) against parental cells. Differences in samples in terms of up- or down-regulation of proteins between the groups were displayed as pyramid plots that showed fold change against statistical significance. Fold change cut-off for up-/down-regulation of proteins was set to $\pm Log_2(2)$ fold change and P-value cut-off was set to $-Log_{10}(1.33)$ indicated by dashed horizontal line on each graph. Proteins that exceeded the cut-off points were labelled and colour-coded depending on whether they were up- or down-regulated.

Osteoclast Characterisation:

Tartrate-resistant acid phosphatase (TRAP) staining:

TRAP staining of osteoclasts was performed using the Acid Phosphatase Leukocyte (TRAP) Kit (Sigma Aldrich, Cat.No. 387A). The protocol was adapted slightly to suit plates rather than microscope slides. A citrate/acetone fixing solution was prepared by diluting the concentrated citrate solution (2 ml concentrate in 18 ml deionised water – 10% solution) and then adding 30 ml of stock acetone. Wells were fixed with 50 µl of fixing solution for 30 seconds at room temperature then washed with excess deionised water and left to air-dry. Staining solution was then prepared as described in Table 21. Reagents were added to a glass beaker with constant stirring with a magnetic stirrer.

Reagent	Volume (ml)
Deionised water (pre-warmed to 37°C)	44
Acetate solution	2
Naphthol AS-BI Phosphoric Acid	2
Tartrate Solution	2

Table 21: reagents and volumes for preparation of the TRAP staining solution.

The contents of a single GBC Fast Garnet Salt capsule was then added to the solution and stirred for a further 60s. The solution was then filtered into a separate beaker and then placed in a water bath at 37°C to warm up the staining solution. Once the solution had reached 37°C, 100µl of staining solution was aliquoted onto each well using a multi-channel pipette, plates were then moved to an incubator set at 37°C and kept in the dark for 1-hour. Plates were then washed with excess deionised water for 3 minutes. Acid Haematoxylin solution was aliquoted onto each well (100 µl) and incubated at room temperature for 5 minutes. Plates were washed in excess deionised water for 3 minutes and left to air dry. $TRAP^+$ cells were viewed under a brightfield microscope. Numbers of osteoclasts per well were quantified using cell-count algorithms adjusted for identification of $TRAP^+$ cells and mature osteoclasts on Celigo (Table 22, 23, and 24). All data generated in Celigo was exported as CSV files.

Algorithm name: Osteoclast Confluence	
Algorithm type	Texture
Intensity threshold	7
Saturated intensity	0
Precision	Low
Diameter (µm)	50
Background correction	Yes
Minimum thickness (µm)	8
Pre-filtering	Minimum cluster size of 50 μm^2

Table 22: Algorithm settings for analysing cell confluence of osteoclasts in 96-well plates.

Algorithm name: TRAP Staining	
Algorithm type	Dark object
Intensity threshold	5
Precision	High
Cell Diameter (pixels)	80
Background correction	Yes
Separate touching objects	Yes

Table 23: Algorithm settings for assessing the number of $TRAP^+$ objects in 96-well plates.

Algorithm name: Mature OCs	
Algorithm type	Dark object
Intensity threshold	1
Precision	High
Cell Diameter (pixels)	80
Background correction	Yes
Separate touching objects	No
Pre-filtering	Area >2179 pixels^2

Table 24: Algorithm settings for assessing the number of mature osteoclasts in 96-well plates.

Nuclear staining using Hoechst 33342 to identify multinucleate bodies:

To complement the data produced from TRAP staining of osteoclasts, a nuclear stain was also performed. Each well of a 96-well plate containing TRAP-stained osteoclasts was incubated with 100 µl of 1:10,000 Hoechst solution (Life Technologies, Cat.No. H3570) in PBS for 10 minutes at room temperature, in the dark. The plate was removed from the dark and scanned on Celigo, looking at both brightfield and blue fluorescence channels. The blue and brightfield channels were combined and multinucleate bodies in each well were identified and counted manually. Numbers of multinucleate bodies per well and test conditions were recorded in a spreadsheet.

Data for confluence, trap-staining, mature osteoclast formation, and nuclear staining determined through Celigo was copied into GraphPad Prism where graphs were created. Difference in mean values was tested for statistical significance via Student's t-test.

Chapter 3 – The Effects of Transient *Itch* Knockdown In Pancreatic Cell Lines Using siRNA:

Pancreatic cancer, whilst having a relatively low incidence among other cancer types, is one of highest causes of cancer-related mortality in the world (Ilic & Ilic, 2016; McGuigan et al., 2018; Vincent et al., 2011) with one of the lowest 5-year survival rates, of approximately 5%. This is mainly attributed to the fact that pancreatic cancer is clinically silent until the disease has reached an advanced stage. The only curative treatment of a solid pancreatic tumour is complete surgical resection. This may or may not be accompanied by adjuvant or neo-adjuvant therapy in the form of radiotherapy or chemotherapy. However the effectiveness of these additional forms of treatment is widely debated, particularly with neo-adjuvant therapy: whilst it can help make previously non-resectable tumours resectable, neo-adjuvant therapy delays surgery which remains the only curative method of treatment (Gillen et al., 2010; Ilic & Ilic, 2016). Another issue with pancreatic cancer is that since the disease is usually already at an advanced stage at the time of diagnosis, complete surgical resection is not always possible and the incidence of recurrence is high as it is more likely that the disease has metastasised to secondary sites. Furthermore, since the 5-year survival rate is so low, one must also consider patient quality-of-life following a pancreatectomy and subsequent adjuvant therapy. Pancreatic cancer and pancreatic cell lines are notoriously resistant to standard chemotherapeutic and radiotherapeutic treatment regimens (de la Fuente et al., 2015; Deorukhkar et al., 2010; Krempien & Roeder., 2017) which is why alternative methods need to be considered to potentiate current therapies for pancreatic cancer.

As mentioned, one area of study in terms of sensitising tumours to existing treatment is genetic manipulation and application of synthetic lethality. De la Fuente et al. found that knockdown of *Itch* using si/shRNA via a nanoparticle vector increased sensitivity of xenograft mice to a sub-therapeutic dose of gemcitabine after being transplanted with MiaPaCa-2 cells (a human pancreatic cell line) (de la Fuente et al., 2015). A later study also noted that *Itch* is upregulated in pancreatic cancer tissue biopsies compared to normal pancreatic tissue and correlates with increased cell metastatic potential of pancreatic cell lines (Luo et al., 2016). To explore the role of Itch in pancreatic cancer cell lines siRNA was used to induce a transient (i.e. short-term) knockdown of *Itch* in the pancreatic cell lines MiaPaCa-2 and Capan-2. MiaPaCa-2 cells were used as they have been used with success in previous published studies, Capan-2s was also used as they are p53 wild-type (Deer et al., 2010). Itch specifically targets the p53 homologue p73 for degradation via the proteasome (Rossi et al., 2005; Wu & Leng, 2015) which can facilitate cell-cycle arrest and apoptosis independent of p53 as it can transcriptionally activate many of the same genes (Clarke et al., 1997; Levrero et al., 2000; Annie Yang et al., 2002). However, whereas p53 is commonly mutated in cancer, p73 is not. In pancreatic cancer specifically, the gene mutation frequency of p53 is roughly 70% (Cicenas et al., 2017) This is one of the reasons why *Itch* has been a target of genetic manipulation, as a means to increase cellular p73 stability and thereby promote apoptosis in cancer tissue/cell lines (Bongiorno-Borbone et al., 2015; de la Fuente et al., 2015; Levy et al., 2007; Rossi et al., 2014; Rossi et al., 2005). Since Capan-2 cells are p53 wild-type, we hypothesise that *Itch* knockdown has a reduced effect in increasing sensitivity to therapeutics in this particular cell line compared to MiaPaCa-2s (since MiaPaCa-2s are p53 mutant) as they would be less reliant on p73.

siRNA is a form of RNA-interference (RNAi) that involves generation of an antisense RNA strand that is loaded onto the RNA-interfering silencing complex (RISC). RISC then cleaves the target mRNA thus downregulating gene expression as the mRNA can no longer be translated to protein (Rao et al., 2009; Robb & Rana, 2007). The siRNA can enter a cell either as completely processed siRNA (which can directly associate with RISC) or as long siRNA duplexes (double stranded RNA – dsRNA), which needs to first be processed by Dicer (an endonuclease that cleaves dsRNA to form siRNA) before it can be loaded onto RISC - as determined through *Dicer*-/- studies on mice (Murchison et al., 2005). Entry of siRNA into a cell requires overcoming the hurdle of the plasma membrane blocking unfacilitated siRNAs/dsRNAs from directly entering. This can be achieved through several methods, however in this project Lipofectamine RNAiMax was used. This product utilises lipofection, using lipids to gain passage through the plasma membrane via endocytosis (Felgner et al., 1987). These lipids are generally cationic (positively charged) so that they can more-easily form complexes with anionic (negatively charged) genetic material including siRNAs, dsRNAs and plasmids. siRNA/dsRNA technology provides a convenient tool that can be used to quickly assess the effect of knockdown of specific genes both in-vitro and in-vivo.

However, there is the potential for specific off-target activity where the siRNA/RISC complex associates and cleaves non-target mRNAs. Furthermore siRNA-mediated knockdown is transient meaning that the effect of the knockdown disappears over time as the material is used up, RNAs naturally degrade, or the knockdown effect gets diluted through cell division. Where a more long-lasting knockdown or knockout is desired, alternative gene-editing techniques need to be employed.

This series of experiments aims to test the hypothesis that silencing *Itch* activity in pancreatic cell-lines increases cell-line sensitivity to existing therapeutics including γ-radiation, doxorubicin, and gemcitabine. The reason why these three methods of treatment were used is because each causes DNA damage via different mechanisms which may be important in assessing the relevance of p53 mutational status between the two cell lines being used. Although this investigation technically utilises dsRNA to generate siRNA intracellularly via Dicer, for simplicity we will be referring to the gene-editing technique as siRNA-mediated knockdown.

Results:

Successful transient Itch knockdown in MiaPaCa-2 and Capan-2 cells:

Ability of the siRNA to reduce Itch expression in pancreatic cell lines was assessed by both qPCR and western blot. MiaPaCa-2 and Capan-2 cells were transfected with Itch-targeting siRNA, using Lipofectamine RNAiMax as the transfection reagent, for 24 hours before lysates were taken. Untreated cells, in addition to cells treated with a scrambled siRNA duplex combined with Lipofectamine, were cultured to act as negative controls and confirm that any knockdown activity was solely due to the Itch-targeting duplex. Successful knockdown was determined by analysing the data produced from both western blot (protein level) and qPCR (mRNA level); comparing *Itch* expression in the test cells in relation to that of both negative controls. In MiaPaCa-2 cells we saw over 90% reduction in Itch protein expression compared to untreated cells (Figure 14: A. and B.). This result was also reflected in the qPCR results (Figure 14: C.) where there was a >80% knockdown at the mRNA level. For Capan-2 cells, increasing concentrations of siRNA was used as it was initially observed

that the level of Itch knockdown using the same concentration of siRNA that was used for MiaPaCa-2 cells (12.5nM) was not statistically, or biologically, significant when analysed by western blot. Increasing doses of siRNA were tested and analysed by western blot and qPCR (Figure 14: D., E., and F.). Significant *Itch* knockdown at the protein level was apparent with 25 and 100 nM siRNA (Figure 14: D. & E., columns 4 & 6) with a ~30% reduction in Itch protein, however not for 50 nM (Figure 14: D. & E., column 5). This did not seem to be reflected in the qPCR results as although mean Itch mRNA expression dropped the difference was not statistically significant.

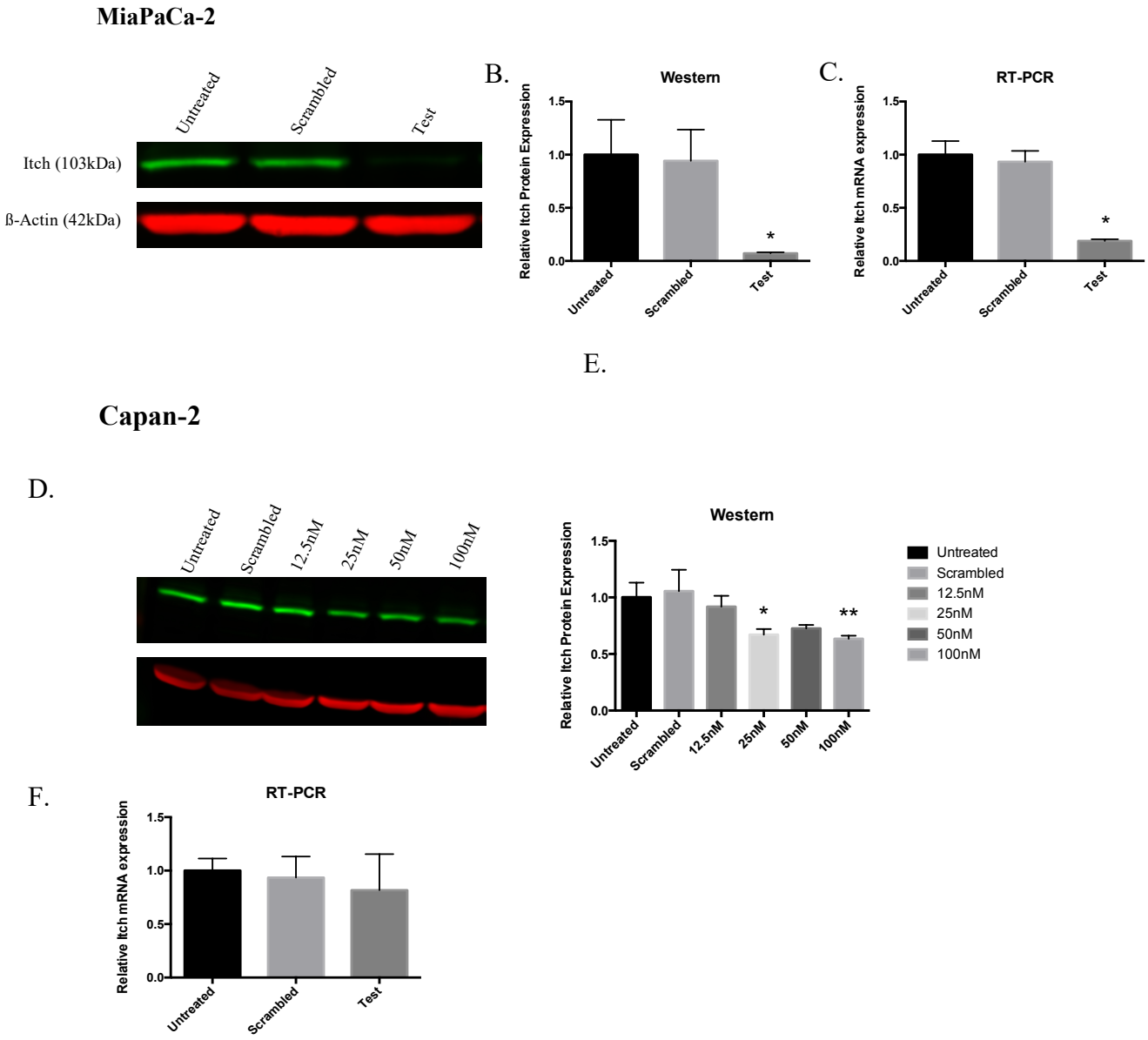

Figure 14: siRNA mediated knockdown of Itch in pancreatic cell lines:

MiaPaCa-2 cells were cultured and subject to either 12.5nM of scrambled siRNA or Itch-targeting siRNA (Test) or were left untreated. After 24 hours media was removed and cells were lysed. Itch (green bands) knockdown by siRNA was confirmed by western blot using β-Actin (red bands) as a loading control (**A.**). Band fluorescence intensity was quantified and analysed in Image Studio (Licor) (**B.**). qPCR was also performed to assess Itch knockdown at the mRNA level (**C.**). Itch knockdown compared to untreated

control was found to be statistically significant at both the protein level (p=0.0393) and mRNA level (p=0.0009). Capan-2 cells were found to be more resistant to siRNA treatment and thus were subject to increasing concentrations of siRNA. Itch knockdown was first confirmed by Western blot (**D.** and **E.**). Statistically significant knockdown was identified with [siRNA] of 25nM (p=0.0342) and 100nM (p=0.034). 25nM concentration was then used for qPCR assessment (**F.**) however the difference in mRNA expression was not statistically significant. Statistical significance in each case was determined by Student's T-test.

An additional experiment was performed to assess the longevity of the silencing effect by siRNA. RNA lysates were taken every 24 hours over a 5-day time course reflective of the duration of the cell survival assays to be carried out. Analysis of relative *Itch* expression by qPCR revealed that even after 5-days post-transfection that there is a significant reduction of *Itch* mRNA (~80%) in MiaPaCa-2 cells compared to those treated with a scrambled control siRNA (Figure 15).

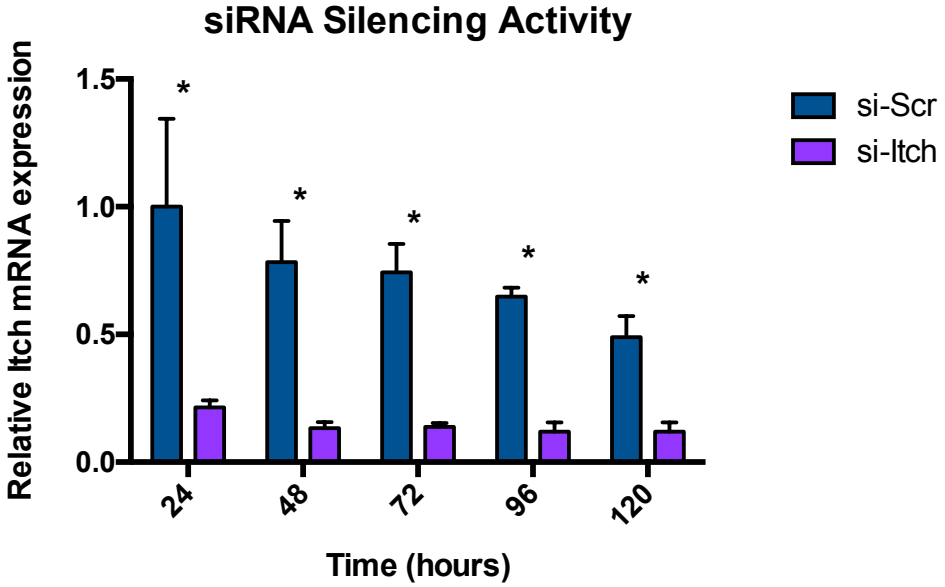

Figure 15: siRNA *Itch* silencing activity persists over a 5-day time course:
qPCR analysis of RNA lysates from MiaPaCa-2 cells treated with either si-Scr or si-Itch taken every 24 hours post-transfection. Student's t-tests detected significant difference at each time point; $p = 3.87\times10^{-3}$, 2.02×10^{-4}, 3.57×10^{-5}, 8.14×10^{-7}, and 1.9×10^{-4} for each time point respectively. No significant difference was observed when comparing the degree of Itch silencing at each time point. Data normalised to Itch expression of first time point of the scrambled control.

Transient Itch knockdown is sufficient for inhibiting cell growth in MiaPaCa-2 cells and is further potentiated by radio- and chemotherapy:

After confirming that Itch had been knocked down by siRNA, cell survivability assays to test the hypothesis that silencing *Itch* increases the sensitivity of pancreatic cell lines to anti-cancer therapeutics including γ-radiation, doxorubicin and gemcitabine. siRNA solution and cells were aliquoted onto 96-well plates. siRNA-containing media was then removed after 24 hours and replaced with drug-containing media for another 24 hours in regard to doxorubicin and gemcitabine treatment. In the case of treatment with γ-radiation, cells were first irradiated and then transfected with siRNA. MiaPaCa-2 cells were then cultured over 4 days; every 24 hours plates were subject to automated cytometry analysis (Celigo) to measure well confluence over time and a sulforhodamine B assay (SRB) was used at the end of the culture period to measure cytotoxicity/cell survival.

For all treatment regimens in MiaPaCa-2 cells, treatment with siRNA (si-Itch) caused a significant decrease in cell viability as indicated by the resultant data for each treatment (Figure 15: A., B., and C., left graphs), including instances where no additional therapeutic was added Figure 15: E. & F.). Resultant cell viability was determined from the raw OD values obtained from the degree of SRB staining in each well. Resultant data for scrambled cells (si-Scr) was similar, if not almost identical, to levels seen for the untreated controls despite the presence of Lipofectamine in these samples. This shows that transient Itch knockdown alone is sufficient to inhibit cell growth and viability.

To correct for the apparent inherent cytotoxicity caused by siRNA-mediated Itch knockdown, SRB data was normalised relative to vehicle control to determine if treatment regimen had any impact on the trend of cell viability as the dose is increased between si-Itch, scrambled, and untreated cells and if there is any increase in sensitivity in combination with siRNA. Upon treatment with γ-radiation, doxorubicin, or gemcitabine cell viability decreases even further. Whilst the trend in relative response remained roughly the same for cells treated with doxorubicin (Figure 16: B., right graph), this was not the case for γ-radiation- or gemcitabine-treated cells. In the case of γ-radiation, relative cell-viability dropped significantly upon reaching 2 Gy which contrasts with what is seen for untreated and scrambled controls (Figure 16: A.). The largest difference was observed in gemcitabine-treated cells; In both the resultant and normalised data there is a significant drop in cell viability of si-Itch cells upon between 7.5-10 nM (Figure 16: C.). However, for either control there is no apparent decrease in cell-viability until between 25-50 nM. Analysis of the curve for the gemcitabine data reveals a shift in IC_{50} si-Itch cells which indicates an increase in sensitivity to gemcitabine (IC50 = 107.6 and 70.12 for untreated and si-Itch respectively).

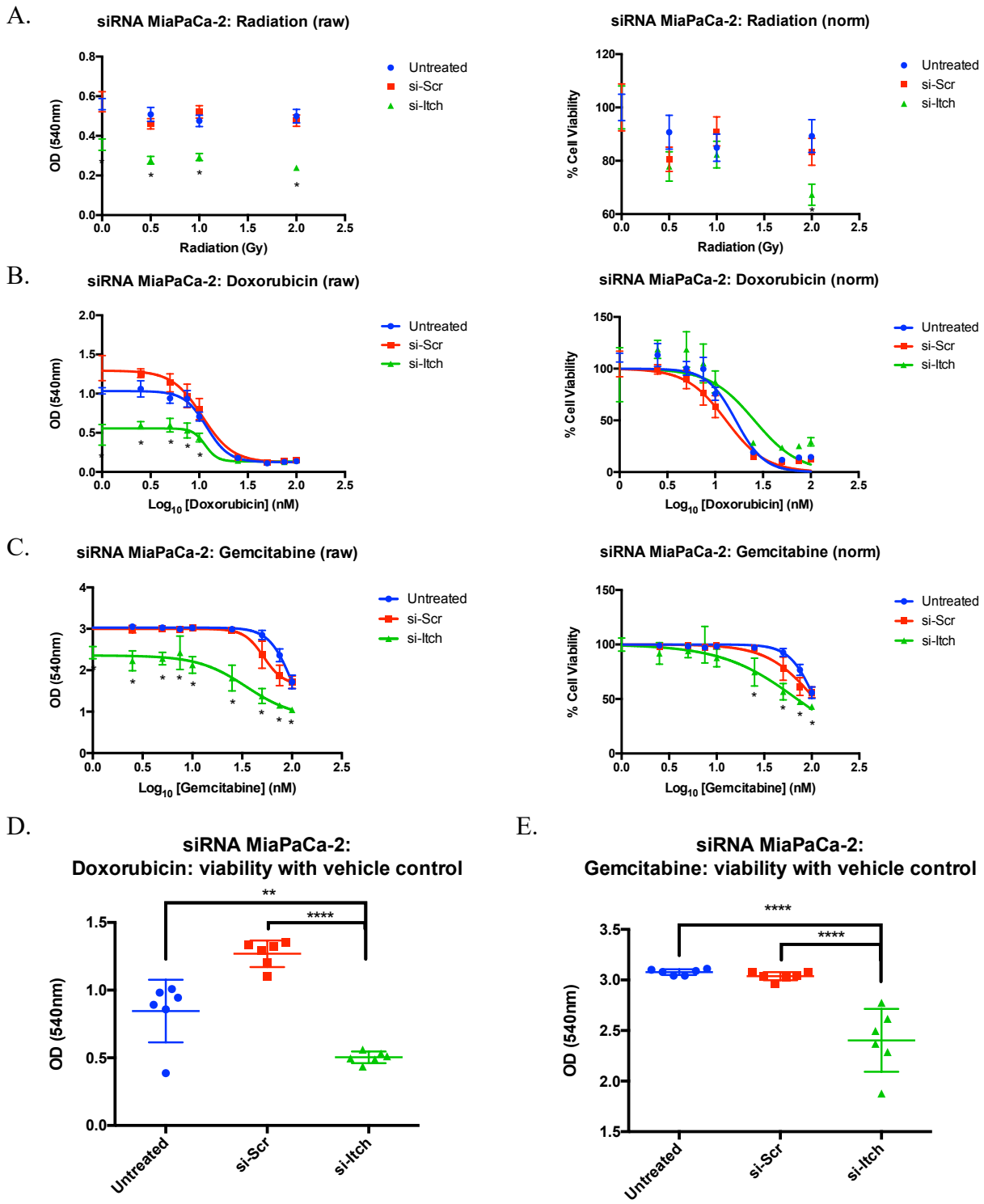

Figure 16: Transient *Itch* knockdown inhibits cell survival which is further potentiated by anti-cancer therapeutics as determined by SRB:

Resultant (left) and normalised (right) SRB cell-survival curves for MiaPaCa-2 cells treated with siRNA in combination with additional treatment. **A.** Cells treated with 0-2 Gy γ-radiation; in resultant data OD readouts for all doses of radiation were statistically significant compared to untreated controls ($p = 3.97\times10^{-12}$, 6.25×10^{-13}, 1.47×10^{-12}, and 1.73×10^{-14} for 0, 0.5, 1, and 2 Gy respectively). Normalised cell viability showed only a significant increase in response for 2 Gy ($p = 2.05\times10^{-8}$). **B.** Cells treated with 0-

100 nM doxorubicin (plotted as $\log_{10}$[doxorubicin]); resultant data showed significant difference for 1, 2.5, 5, 10, and 25 nM doxorubicin ($p = 1.73\times10^{-6}$, 1.61×10^{-6}, 1.44×10^{-5}, 3.78×10^{-5}, and 8.14×10^{-6} respectively). Normalised cell viability showed no significant difference between si-Itch and controls. **C.** Cells treated with 0-100 nM gemcitabine (plotted as $\log_{10}$[gemcitabine]); resultant data showed significant difference for all doses ($p = 1.05\times10^{-6}$, 8.07×10^{-6}, 4.33×10^{-7}, 6.37×10^{-3}, 7.01×10^{-7}, 3.54×10^{-6}, 1.09×10^{-8}, 6.94×10^{-9}, and 2.93×10^{-6} for 1, 2.5, 5, 7.5, 10, 25, 50, 75, and 100 nM respectively). Normalised cell viability showed significant difference between si-Itch and untreated cells for 25, 50, 75 and 100 nM ($p = 1.63\times10^{-3}$, 9.54×10^{-7}, 1.73×10^{-7}, and 3.78×10^{-4} respectively). Data was normalised to a vehicle control in the case for doxorubicin and gemcitabine. Radiation data was normalised to cells that did not receive radiation. An * donates statistically significant difference in mean as determined by Student's t-test. **D.** & **E.** Viability of cells treated with just the vehicle control shows significant decrease in cell viability when just the si-Itch is present compared to both control conditions. Number of asterixis donates degree of statistical significance of a one-way ANOVA between conditions (** = $p < 0.01$, **** = $p < 0.0001$).

Transient Itch knockdown inhibits Capan-2 cell survivability:

When performing calibration plots to optimise the range of drug concentration to use, Capan-2 cells were found to be more resistant to drug treatment compared to MiaPaCa-2 cells (Figure 17: A. & B.). Based on the results displayed in this figure a concentration range of 0-30μM was used for the chemotherapy component of the cytotoxicity assays.

Capan-2 siRNA transfection followed the same protocol as MiaPaCa-2 cells. Similar to the results seen in MiaPaCa-2 cells, siRNA-mediated *Itch* knockdown in Capan-2 cells was sufficient to decrease cell-viability (Figure 18: A., B., & C. left graphs, D. & E.). Once again, results for scrambled control appeared to be in agreement with the results of the untreated control providing further evidence that the engineered siRNA is solely responsible for the decrease in cell viability. A wider range dose of radiation was also used on the assumption that Capan-2 cells may be more resistant to irradiation, as was seen for doxorubicin and gemcitabine. However, for the siRNA experiments the effective inhibitory dose was low (1Gy), and further increase in dose failed to elicit further cytotoxicity (confirmed through biological repeats – Supplementary Figure 2). For both doxorubicin and gemcitabine, addition of chemotherapeutic agent only caused a slight additional decrease in resultant cell survivability, meaning that inhibition occurred over a smaller range of concentrations. Normalisation of results (Figure 18: A., B., & C. right graphs) revealed no increase in sensitivity of si-Itch treated cells compared to si-Scr and untreated cells.

A.

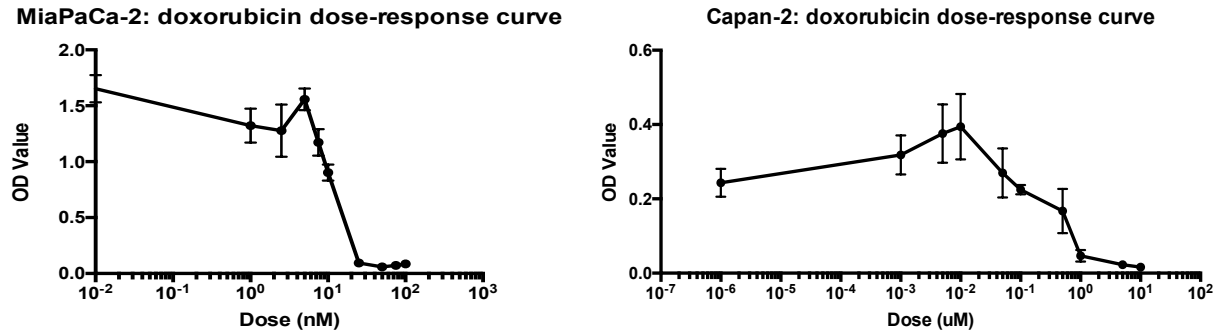

B.

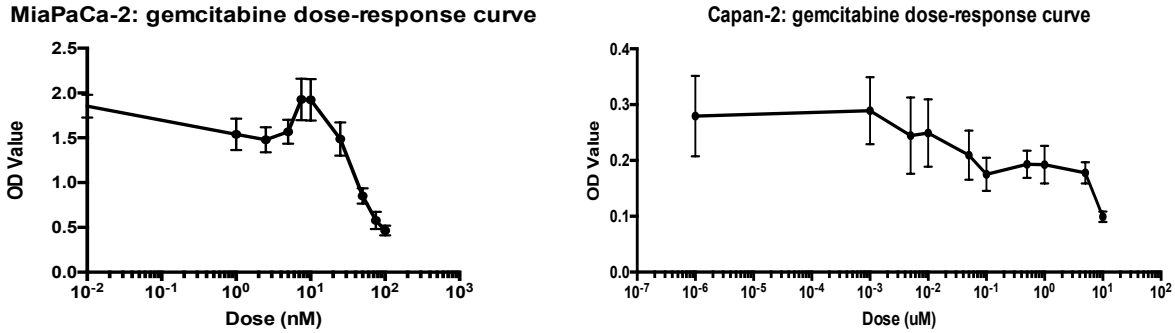

Figure 17: Capan-2 cells are more resistant to doxorubicin/gemcitabine treatment:
SRB dose-response curves of MiaPaCa-2 cells (left) and Capan-2 cells (right) treated with doxorubicin (**A.**) and gemcitabine (**B.**), used to calibrate an appropriate range of drug concentrations to use for future experiments. Compared to MiaPaCa-2 cells, where for both treatment regimens a curve could be established between 0-100nM, Capan-2 cells required higher doses and with a larger concentration range to elicit a suitable dose-response curve (1-10,000 nM). Based on these calibration curves, a concentration range of 0-30 μM was used for Capan-2 cells. Lowest plotted doses represent non-treated negative controls for the purposes of plotting the results on a log scale.

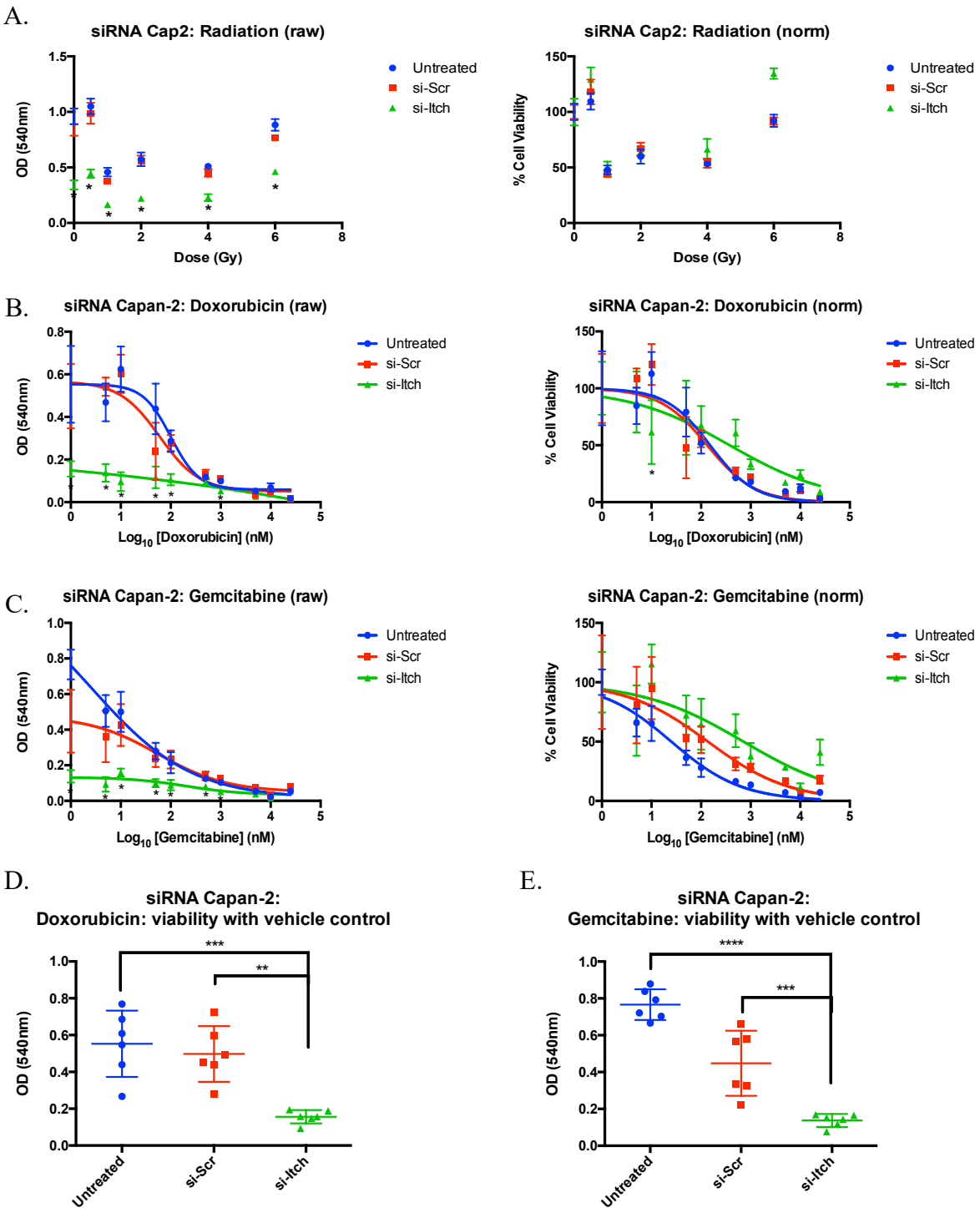

Figure 18: Transient Itch knockdown in Capan 2 cells inhibits cell growth and is potentiated by chemotherapy at lower doses:

Resultant (left) and normalised (right) SRB cell-survival curves for Capan-2 cells treated with siRNA in combination with additional treatment. **A.** Cells treated with 0-6 Gy γ-radiation; in resultant data OD readouts for si-Itch treated cells across all doses of radiation were statistically significant compared to untreated controls ($p = 5.71\times10^{-15}$, 4.17×10^{-115}, 6.83×10^{-14}, 8.97×10^{-13}, 2.46×10^{-14}, and 8.97×10^{-15} for 0, 0.5, 1, 2, 4, and 6 Gy respectively). Normalised cell viability showed no statistically significant increase in

sensitivity of si-Itch cells. **B.** Cells treated with 0-30,000 nM doxorubicin (plotted as $\log_{10}$[doxorubicin] (nM)); resultant data showed significant difference for 1, 5, 10, 50, and 100nM doxorubicin ($p = 3.55\times10^{-4}$, 8.90×10^{-6}, 5.41×10^{-7}, 3.78×10^{-5}, 1.16×10^{-4}, and 1.56×10^{-5} respectively). Only statistically significant increase in sensitivity for normalised data was for 10 nM ($p = 4.14\times10^{-3}$. **C.** Cells treated with 0-30,000 nM gemcitabine (plotted as $\log_{10}$[gemcitabine](nM)); resultant data showed significant difference for si-Itch cells for dose range 1-1000 nM gemcitabine ($p = 1.02\times10^{-7}$, 1.24×10^{-6}, 2.74×10^{-5}, 7.44×10^{-6}, 9.29×10^{-4}, 2.26×10^{-3}, 4.08×10^{-4}, and 2.25×10^{-3} for each dose respectively). Normalised cell viability showed no significant increase in sensitivity upon being treated with siRNA. Data was normalised to a vehicle control in the case for doxorubicin and gemcitabine. Radiation data was normalised to cells that did not receive radiation. An * donates statistically significant difference in mean as determined by Student's t-test. **D.** & **E.** Viability of cells treated with just the vehicle control shows significant decrease in cell viability when just the si-Itch is present compared to both control conditions. Number of asterixis donates degree of statistical significance of a one-way ANOVA between conditions (** = $p < 0.01$, *** = $p < 0.001$, **** = $p < 0.0001$).

Discussion:

siRNA-mediated transient *Itch* knockdown in pancreatic cell lines:

Itch knockdown was achieved in pancreatic cell lines through lipofection of dsRNA. Significant knockdown was seen in MiaPaCa-2 cells using 12.5nM of siRNA, with ~80% reduction in Itch mRNA and ~90% reduction in protein (Figure 14: A., B., and C.). Although the degree of knockdown seen in Capan-2 cells was not as significant as was seen with MiaPaCa-2 cells, there was still a 30% reduction in Itch protein seen when using 25nM siRNA (Figure 14: D., E., and F.), which was viewed as biologically relevant enough for downstream assays. There was almost no difference seen when increasing the concentration of siRNA to 100 nM in Capan-2 cells: any further increase would have increased the number of cytotoxicity assays without adding to discriminatory value of results. During the project it had been noted that Capan-2 cells tended to be more resistant to multiple modes of treatment in regard to toxicity compared to MiaPaCa-2 cells, so it may be that Capan-2 cells are also more refractory to genetic knockdown by lipofection of si/dsRNA as well. Longevity of siRNA silencing activity was also confirmed in MiaPaCa-2 cells which showed an 80% reduction in *Itch* mRNA even at 120 hours post-transfection (Figure 15).

Transient *Itch* knockdown inhibits survivability of pancreatic cell lines:

For both pancreatic cell lines used there was a significant decrease in resultant cell survivability of si-Itch treated cells (as indicated by SRB OD readout) meanwhile levels for scrambled and untreated controls mostly mirrored each other. This indicates that the presence of the Itch-targeting siRNA duplex is sufficient for causing increased cell death in both cell lines regardless of further experimental parameters (i.e. addition of cancer therapeutic), highlighted in Figures 16/17: E. & F. where the only experimental parameter was siRNA transfection. In most cases, additional treatment with radiation or chemotherapeutic drug caused cell survivability to decrease further however this effect was mirrored in both scrambled and untreated controls.

Only in a select few cases did the application of si-Itch significantly increases the sensitivity of cells to either γ-radiation, doxorubicin, or gemcitabine as shown by the relative (normalised) response. The only instances for MiaPaCa-2 cells where there was an increase in sensitivity compared to control samples was with 2 Gy δ-radiation (Figure 16: A.) and low-dose gemcitabine (7.5-10 nM – Figure 16: B.). Capan-2 cells showed no clinically significant difference in relative response for all three modes of treatment when combined with si-Itch. In terms of whether or not the data presented accepts or rejects the hypothesis of *Itch* knockdown sensitising cell lines to treatment is difficult to clarify completely. The differences between the resultant and normalised data for each treatment regimen suggest that decrease in cell viability from *Itch* silencing is independent from any subsequent anti-cancer therapy. Whilst one could say that in the strictest sense the data rejects the hypothesis as a lack of change in relative response (and the pattern of growth) to treatment after siRNA application indicates no change in the sensitivity of both MiaPaCa-2 and Capan-2 cells.

On the other hand, the fact that transfection of Itch-inhibiting siRNA causes such a large decrease in cell survivability could be interpreted to mean that cells have been made more sensitive to cell death in general. The resultant SRB data shows a significant baseline shift in survivability which indicates a shift in cell-fate decisions that favours death as opposed to survival and that any additional treatment has an additive, rather than multiplicative effect. From the experiments performed and the data generated, it would be difficult to classify Itch as an oncogene as nothing was done to assess the metastatic ability of the cells post *Itch* knockdown (for example a wound healing assay). However, the evidence shown does present a strong case that Itch is a potent mediator of cell survival. It would be interesting to assess whether or not a similar phenomenon would be seen in healthy tissue cultured in-vitro after loss of *Itch* function.

Another interesting point is that, as the decrease in survivability is seen in both cell lines, the effect caused by si-Itch is observed regardless of *p53* mutational status. This indicates that the response of cells to transient *Itch* knockdown is not solely due to potential *p73* compensation as previous literature would suggest. Furthermore, these results demonstrate that *Itch* has a more global effect on transcriptome and proteome when it comes to regulating cell fate decisions and managing cytotoxicity, as we would expect from the numerous Itch substrates described previously (Figure 7).

Transient nature of siRNA and its use in-vitro:

A potential weakness identified was that since siRNA was only applied once at the beginning of the experiment, the knockdown may have only been present at the start and that Itch levels may have recovered over the course time due to the transient nature of siRNA (Järve et al., 2007; Rao et al., 2009). One of the concerns with the experimental design was uncertainty about the longevity of the siRNA-mediated knockdown. Previous literature has described that the approximate half-life of siRNAs is about 48 hours as indicated by fluorescent tagging RNAs (Järve et al., 2007; Rao et al., 2009). It may be that knockdown of Itch at the beginning inhibits cell growth/induces apoptosis in cells that take up the siRNA but once the resultant material (siRNA & lipofectamine) is depleted, the cells recover and continue to grow as per normal regardless of the addition of a therapeutic agent. This could explain why resultant survivability of cells exposed to si-Itch is so low, yet the trend seen in response to treatment and the normalised data is similar to the two control conditions. On the other hand, other studies have shown that the longevity of the silencing effect induced by siRNA is more

dependent on the cell doubling time rather than the half-life of siRNA in-vivo and in-vitro with the silencing effect in fast-dividing cells being roughly 5-7 days (Novina et al., 2002; Tuschl, 2002) and potentially persisting for at least 3 weeks in quiescent cells (Omi, Tokunaga, & Hohjoh, 2004; Song et al., 2003). A kinetics-based study by Bartlett and Davis looked at several variables regarding siRNA-mediated silencing activity including siRNA concentration, cell doubling time, number of doses of siRNA, and siRNA half-life (Bartlett & Davis, 2006). They found that the most significant variable to be cell doubling time, the rationale being that the silencing effect gets diluted as cells divide. Despite this they observed that even in fast-dividing cells (doubling time 0.8 days) that luciferase activity (which was stably expressed in each cell line and the target of the knockdown) was restored back to control levels after roughly 7 days. MiaPaCa-2 cells have a doubling time of approximately 40 hours/~1.7 days according ATCC (http://www.lgcstandards-atcc.org/products/all/CRL-1420.aspx?geo_country=gb#characteristics) however confluence based growth curves from Celigo seem to indicate that MiaPaCa-2 doubling time is actually closer to 27 hours (Supplementary Figure 3). In the aforementioned study in cell line with a doubling time of 1.6 days, luciferase was not restored to control levels until roughly 10 days post-transfection. However, at the 5-day mark (endpoint for cell survivability assays in this project) luciferase activity had been restored to about 50% of control levels indicating a degree of loss of silencing activity.

This was addressed by measuring the silencing effect of siRNA over the same timeframe as the cytotoxicity assays (Figure 15) and confirmed that the silencing effect persists in MiaPaCa-2 cells (the fastest dividing cell line of the two used) even after 5 days. Furthermore, cell-survivability experiments were repeated in MiaPaCa-2 cells for all three treatment regimens with supplementary doses of siRNA spaced 48 hours between each application. The preliminary data obtained indicates that there is little to no difference in response to supplementary si-Itch application when compared to single-dose application data across all three modes of treatment (Supplementary Figure 4: A. & C.). There was a slight decrease in cell viability of si-Scr treated cells of the doxorubicin and radiation treatment regimens (however, this was not seen in gemcitabine-treated cells and the effect in irradiated cells was only apparent at low-doses of radiation and to a very minor degree. Combined with the fact that the relative response to treatment appeared to remain unchanged from that seen in the data for single application of siRNA makes it more likely that this phenomenon is likely attributed to toxicity induced by repeated lipofection (Barreau, Dutertre, Paillard, & Osborne, 2006) as opposed to potential off-target activity of the scrambled siRNA.

Alongside the RNA lysates, protein lysates could have also been taken to provide further validation of the silencing effect of siRNA over the 5-day time-course. Another experiment that could be performed could be to assess Impact of si-Itch on cell-line specific doubling time through use of Celigo. Change in the growth-rate can be extrapolated from well confluence data over a specific time-course after application of siRNA (with both scrambled and untreated controls within the same 96-well plate for comparison).

Addressing potential Off-target activity of siRNA:

Although there is strong evidence based on the western blot and qPCR data that there is indeed a significant siRNA-mediated knockdown of Itch in both cell lines (Figure 14: A., B., D., and E.), it would be naïve to ignore the possibility of the siRNA having potential off-target activity. off-target activity is defined as unintended changes to genome expression caused by RNAi (Rao et al., 2009). This can be broken down into specific off-target activity, where the RNAi complex can bind and cleave non-target mRNAs, and non-specific off-target

activity, where the RNAi process causes cytotoxicity or generates an immune response in the case of in-vivo studies. In context of these particular experiments in general cytotoxicity due to lipofection can likely be ruled-out as there was little difference in resultant and normalised cell viability between si-Scr and untreated cells in almost all cases where there was single application of siRNA. It is however possible that si-Itch could have specific off-target activity with gene transcripts other than *Itch*. This may be especially the case for Capan-2 cells where the degree of *Itch* knockdown was minimal even at higher concentrations of siRNA duplex (Figure 14: D., E., & F.). Despite the minimal changes in levels of Itch expression the effect of si-Itch on cell viability was significantly large (Figure 18). With the technology available in our lab it would be difficult to determine whether there was a significant degree of specific off-target activity without outsourcing and utilisation of a high-throughput RNA screening method such as RNA-seq (Chu & Corey, 2012; Nagalakshmi et al., 2008). Performing a BLAST search on the forward and reverse strands of the siRNA duplex reveals candidate mRNAs from genes that may be affected (although none of them had 100% sequence alignments as the returned *Itch* transcripts did). Determination of protein and mRNA levels for these additional genes following si-Itch transfection could be considered as further work to confirm whether or not they are also affected by the knockdown. If any results were deemed significant then the function of said genes and the physiological consequences of their inhibition could be explored further.

Chapter 4 – Stable Knockdown of *Itch* In Pancreatic Cell Lines Using CRISPR-Cas9:

CRISPR gene editing allows irreversible ablation of a gene of interest through sgRNA-guided Cas9 endonuclease activity. After observing that transient *Itch* knockdown inhibits cell survival and has potential synergism in MiaPaCa-2 cells with radiation and gemcitabine, It was hypothesised that a similar response would be seen in a stable knockdown mediated by CRISPR-Cas9.

Results:

Western blot was used to confirm reduction in Itch protein levels for multiple lentiviral constructs in both cell lines (3 for MiaPaCa-2 cells and 2 for Capan-2 cells) before proceeding with cellular cytotoxicity assays. Level of Itch protein was normalised to β-Actin levels and expression was quantified relative to parental untreated cells: in MiaPaCa-2 cells the degree of knockdown seen ranged from 85-95% for all three isogenic cell lines (IKO1a, IKO2, and IKO3 – Figure 19: A.). In Capan-2 isogenic cell lines IKO1a and IKO2 showed 95% and 75% reduction in Itch protein respectively (Figure 19: C.).
Protein expression of Cas9 was also measured as additional confirmation that the plasmid had been successfully incorporated into the cell lines. Both MiaPaCa-2 and Capan-2 cells were found to have significantly increased Cas9 in samples treated with Itch-targeting constructs compared to parental cells (Figure 19: B. & D.) as was expected since Cas-9 is not endogenously expressed in eukaryotic cells. There was no significant difference in expression of Cas9 between scrambled and parental controls identified by western blot. This was contrary to what was anticipated as one would expect the scrambled-treated cells to still express Cas-9 as they were transduced with the same lentiviral construct, albeit with non-targeting sgRNA, and survived selection.

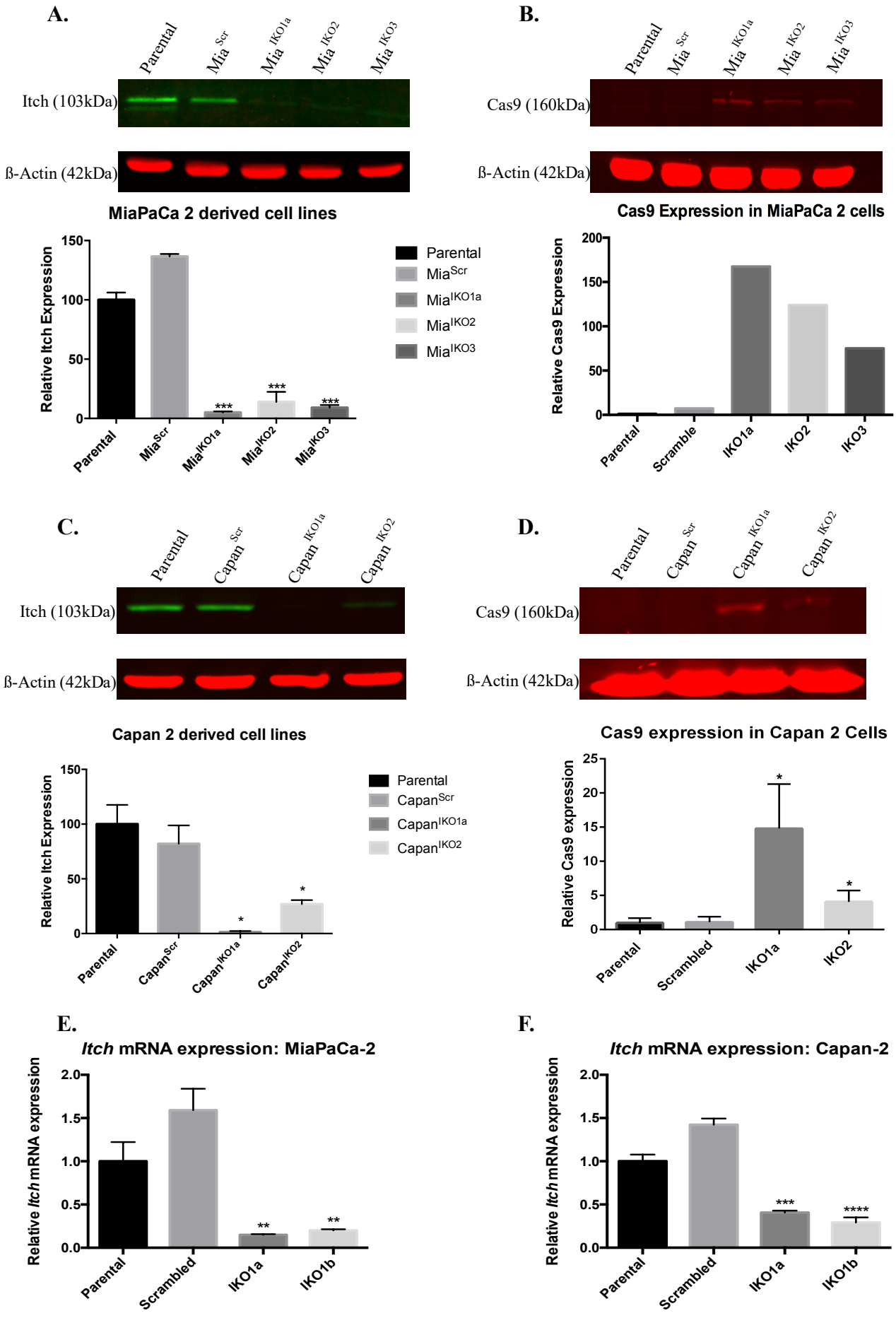
A.
Parental
Mia Scr
Mia IKO1a
Mia IKO2
Mia IKO3
Itch (103kDa)
ß-Actin (42kDa)
MiaPaCa 2 derived cell lines
Relative Itch Expression
Parental
MiaScr
MiaIKO1a
MiaIKO2
MiaIKO3
B.
Cas9 (160kDa)
ß-Actin (42kDa)
Cas9 Expression in MiaPaCa 2 cells
Relative Cas9 Expression
Scramble
IKO1a
IKO2
IKO3
C.
Capan Scr
Capan IKO1a
Capan IKO2
Capan 2 derived cell lines
CapanScr
CapanIKO1a
CapanIKO2
D.
Cas9 expression in Capan 2 Cells
Relative Cas9 expression
Scrambled
E.
Itch mRNA expression: MiaPaCa-2
Relative Itch mRNA expression
IKO1b
F.
Itch mRNA expression: Capan-2

Figure 19: Successful CRISPR-Cas9 mediated knockdown of Itch in pancreatic cell lines: Western blot performed showing the expression of Itch (**A.**) and Cas9 (**B.**) in MiaPaCa-2 cells and the same in Capan-2 cells (**C.** and **D.**) using β-Actin as a loading control. Reduced expression of Itch was observed in all cases where pLentiCRISPRv2 which was accompanied by an inverse expression of Cas9 in the respective cell lines. qPCR was also performed for both cell lines (**E.** and **F.**) to evaluate mRNA expression (using GAPDH as a housekeeping gene). Largest degree of knockdown was seen for construct IKO1a (note: IKO1b is a biological replicate of IO1a). IKO2 and IKO3 had smaller degree of knockdown (Supplementary Figure 5). Difference in mean protein and mRNA level between parental and each individual CRISPR construct was determined by unpaired Student's t-test (number of asterixis dictates the degree of statistical significance; * = $p < 0.05$, ** = $p < 0.01$, *** = $p < 0.001$, **** = $p < 0.0001$).

qPCR was used to quantify mRNA levels of *Itch* as an alternative means of extracting *Itch* expression in isogenic pancreatic cell lines. The largest reduction in *Itch* mRNA was only seen in samples IKO1a and 1b (Figure 19: E. and F.) with a >90% knockdown observed in MiaPaCa-2 cells and 60-70% in Capan-2 cells. Meanwhile for constructs IKO2 and IKO3 mRNA knockdown ranged from 20-40% (Supplementary Figure 5). Although this is not in agreement with the protein data, this may be due to weakness in primer design not being specific for each pLentiCRISPRv2 construct.

CRISPR-mediated Itch knockdown increases MiaPaCa-2 cell line sensitivity to low-dose radiation and doxorubicin:

Cell survivability in response to CRISPR-mediated Itch knockdown in combination with either γ-radiation, doxorubicin, or gemcitabine was quantified using SRB. The same experimental parameters used for the transient knockdown series of experiments were used to provide a means of comparing the two gene editing techniques. To correct for any inherent growth impairment caused by lentiviral infection of MiaPaCa-2 cells, OD values were plotted as resultant data and normalised data when generating SRB curves.

Post-normalisation IKO1a MiaPaCa-2 cells were shown to be more responsive to low-doses of both γ-radiation (0.5-1 Gy) and doxorubicin (5-10 nM) (Figure 20: B. & D.) in addition to higher doses of gemcitabine (50 & 100 nM, Figure 20: F.) as indicated by decrease in normalised OD values compared to scrambled and parental controls. Resultant OD values for γ-irradiated cells was also found to be lower in IKO1a cells compared to parental cells at 0.5 and 1 Gy (Figure 20: A.). Fitting an IC_{50} curve to the normalised data also revealed an increase in sensitivity of IKO1a cells to each mode of treatment compared to parental and scrambled controls (Table 25).

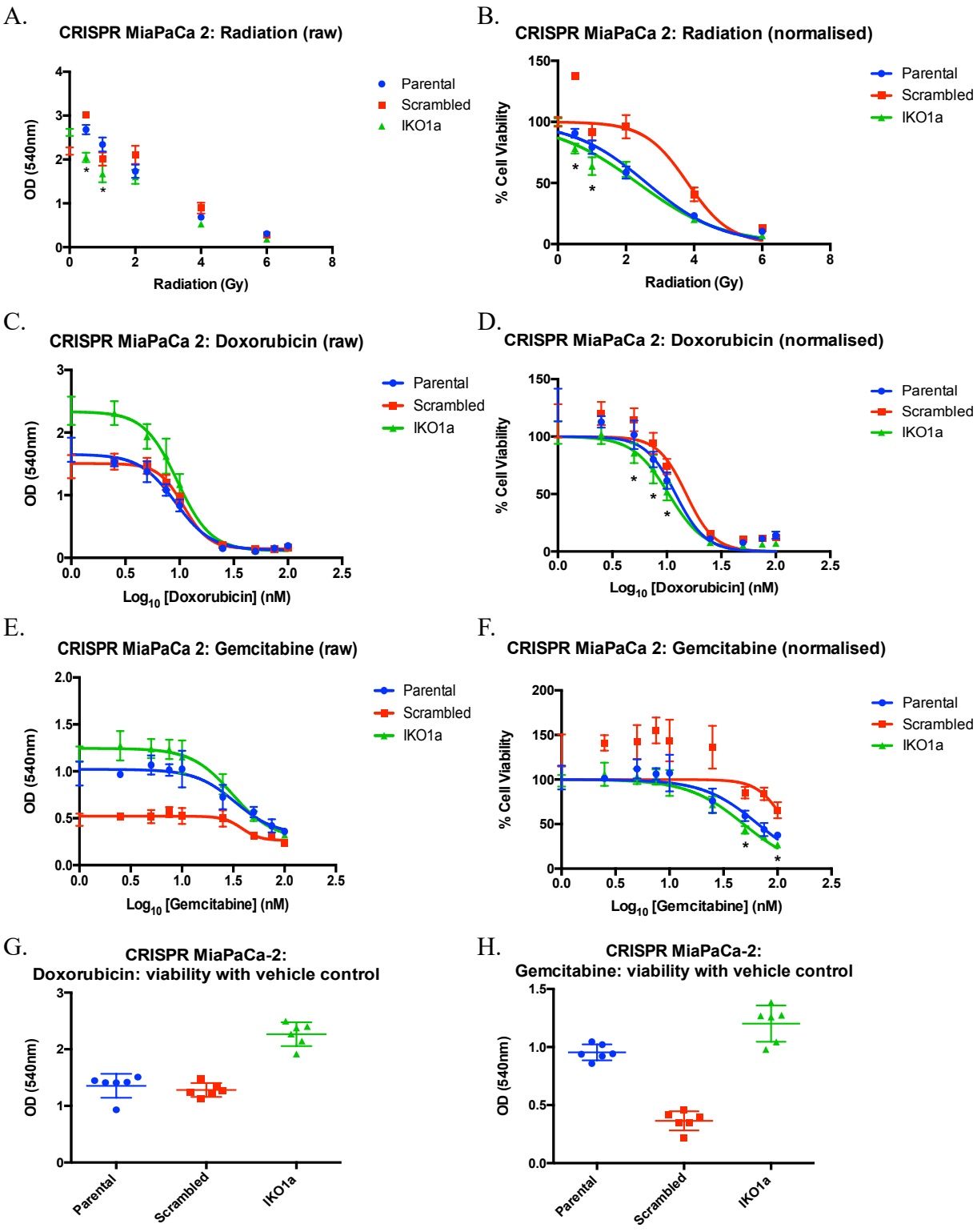

Figure 20: Effect of CRISPR-mediated stable Itch knockdown on MiaPaCa-2 cell sensitivity to therapeutics:

Resultant (left) and normalised (right) SRB cell-survival curves for parental (blue), scrambled (red), and IKO1a (green) MiaPaCa-2 cells in 96-well plates. **A.** Cells treated with 0-6 Gy γ-radiation; in resultant data OD readouts for low doses of radiation (0.5 and 1 Gy) were significantly lower compared to parental cells ($p = 8.44\times10^{-7}$, and 4.59×10^{-15} respectively). Normalised cell viability showed only a significant increase in response for 2 Gy ($p = 2.05\times10^{-8}$). **B.** Cells treated with 0-100 nM doxorubicin (plotted as $\log_{10}$[doxorubicin](nM)); IKO1a cells had higher OD readouts in resultant data compared to both

scrambled and parental controls. Normalised cell viability showed significant increase in sensitivity of IKO1a cells to doxorubicin at doses 5, 7.5 and 10 nM (6.99×10^{-3}, 3.07×10^{-4}, and 5.46×10^{-3} respectively). **C.** Cells treated with 0-100 nM gemcitabine (plotted as $\log_{10}$[gemcitabine](nM)); resultant data once again showed that IKO1a cells had greater OD readouts indicating greater numbers of cells. Normalised cell viability showed IKO1a had greater sensitivity to gemcitabine at doses 50 and 100nM ($p = 3.50\times10^{-4}$, and 7.18×10^{-5}, 1.73×10^{-7} respectively). Data was normalised to a vehicle control in the case for doxorubicin and gemcitabine. Radiation data was normalised to cells that did not receive radiation. An * donates statistically significant difference in mean as determined by Student's t-test. **D.** & **E.** Viability of isogenic cell lines treated with just vehicle control provides further evidence of IKO1a clone being more clonogenic compared to the parental cells as resultant mean OD readout is higher.

	Parental	Scrambled	IKO1a
Radiation (Gy)	2.608	3.811	2.345
Doxorubicin (nM)	12.04	15.06	10.40
Gemcitabine (nM)	65.99	119.8	48.54

Table 25: Summary of IC50s for isogenic cell lines:
Calculated IC50s for each isogenic cell line (colour coded to match previous figure) based on the data in Figure 20. Calibration curves and IC50s determined in GraphPad Prism.

Stable Itch knockdown in MiaPaCa-2 cells increases cell-line clonogenicity:

In almost all experiments involving MiaPaCa-2 cells it was noted that IKO1a cells appeared to grow faster than either control condition (through visual observation during the cytotoxicity experiments). Resultant OD values from the cytotoxicity assays in the doxorubicin and gemcitabine experiments provided evidence that this might be the case in the instances where there was little no drug (Figure 20: C., E., G., & H.). To confirm that the knockdown of *Itch* by CRISPR caused the cells to become more clonogenic a series of clonogenicity assays were performed. An algorithm was designed in Celigo to select for groups of cells above a certain surface area after 1-week incubation (Figure 21: A.).

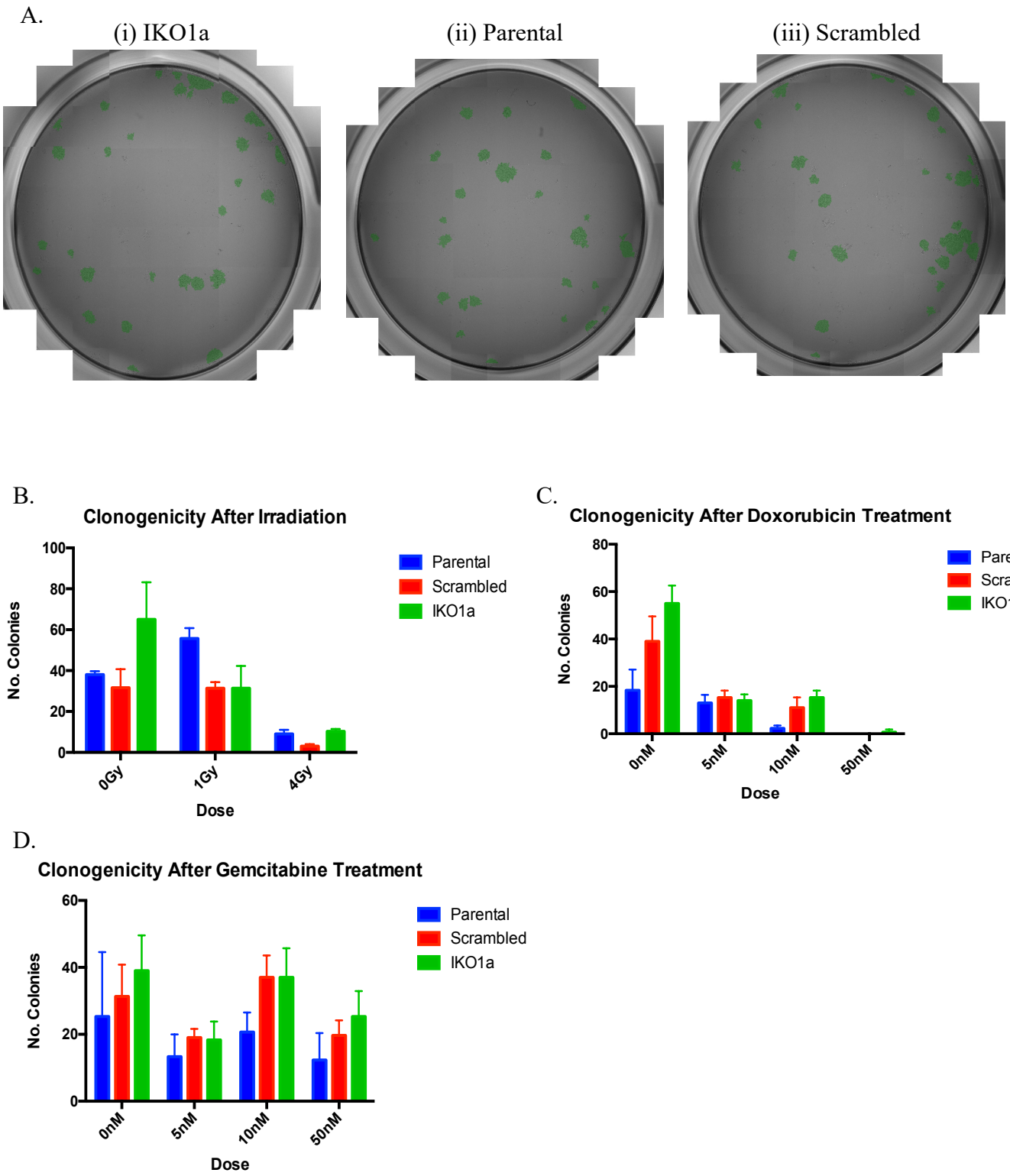

Figure 21: Clonogenicity of MiaPaCa-2 isogenic cell lines:

A. Sample wells of untreated cells with identified colonies in green (images from doxorubicin experiment). Clonogenicity of Parental (blue), Scrambled (red), and IKO1a (green) cells with or without treatment. **B.** Cells were irradiated at either 0, 1 or 4Gy before being distributed at a low cell density on a 6-well plate (250 cells/well). **C.** & **D.** cells were passaged onto 24-plates (125 cells/well) and were treated with either 0, 5, 10 or 50nM doxorubicin/gemcitabine respectively. Drug-containing media was replaced with fresh

media after 24 hours. Number of colonies was determined using a colony count algorithm on Celigo after 1-week incubation post-treatment.

In the absence of any therapeutic agent IKO1a cells showed a greater ability to form colonies after being passaged at low cell density (Figure 21: B., C., & D.) indicating that they are more clonogenic. However, from the data presented and subsequent biological replicates (Supplementary Figure 6) it was difficult to interpret the degree of response of each group of cells to specific treatment regimens. Treatment with 1 Gy of radiation or 10 nM doxorubicin caused the number of colonies formed for IKO1a cells to decrease to levels seen for the two control conditions. This increase in relative response mirrors what was seen for the same doses in the cell survivability assays (Figure 20: B. & D.). However there were instances in the biological replicates where this was not the case (Supplementary Figure 6) but a major weakness in the clonogenicity experiments was reliance on Celigo alone to count colonies which can be erroneous when used to examine plates with larger well sizes as resolution begins to decrease as it scans the periphery of large wells (since it takes individual pictures of different parts of the well then stitches them together).

CRISPR-mediated knockdown of Itch in Capan-2 sensitises cells to gemcitabine:

Capan-2 cells transduced with CRISPR-Cas9 were also assessed for their response to treatment with radio-/chemotherapy after stable *Itch* knockdown. Similar to what was seen with IKO1a MiaPaCa-2 cells, cells appeared more clonogenic as indicated by the increase in resultant OD of untreated cells (Figure 22: G. & H.). Normalisation of the SRB data showed that IKO1a cells are more sensitive to doxorubicin and gemcitabine (Figure 21: D. & F.) with a decrease in IC_{50} for doxorubicin specifically (IC_{50} = 159.8, 114.5, 104.7 nM for parental, scrambled and IKO1a cells respectively). Although there appears to be a shift in IC_{50} in the gemcitabine regimen, an accurate IC_{50} dose could not be calculated from the data.

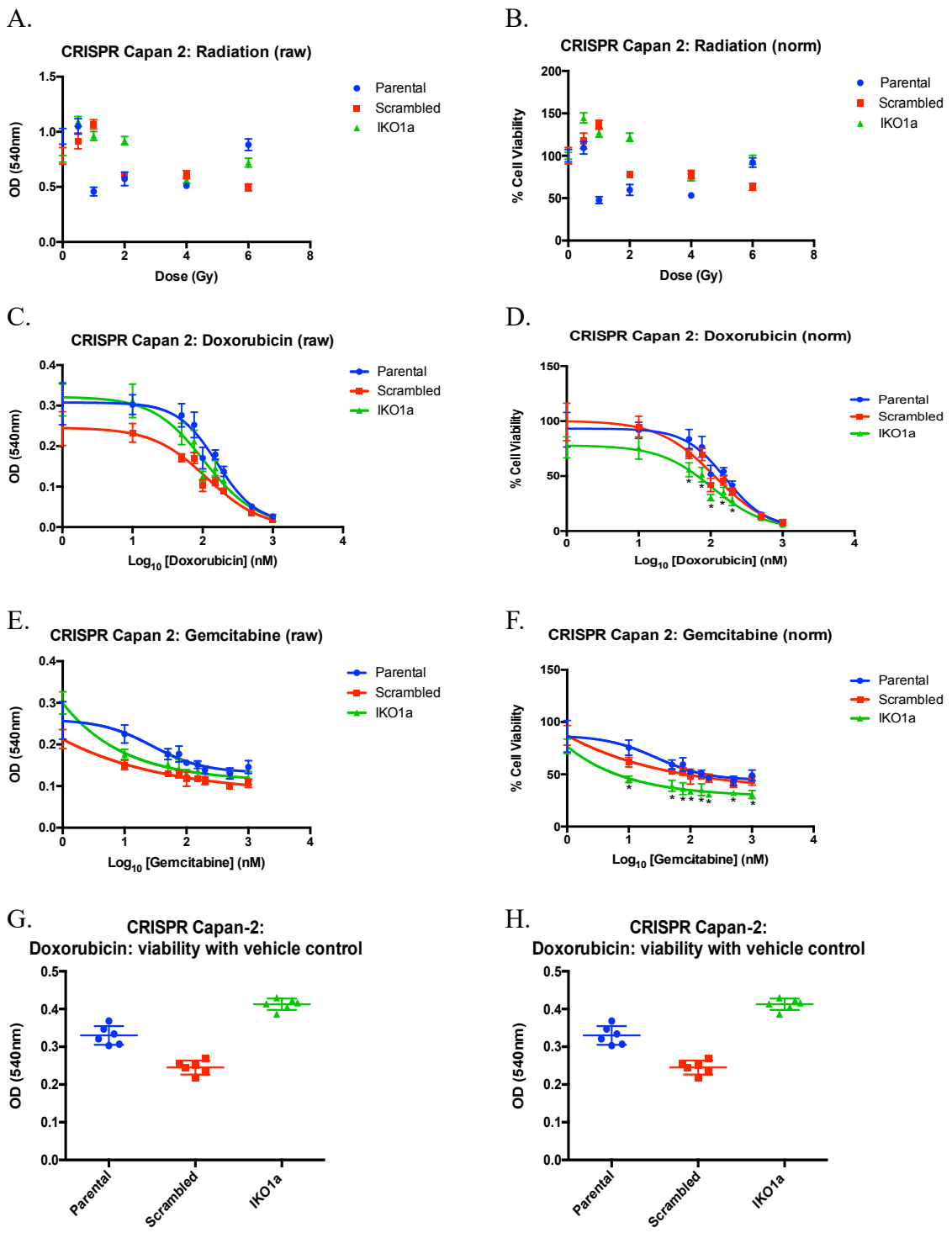

Figure 22: Effect of stable Itch knockdown on Capan-2 response to radio-/chemotherapy: Resultant (left) and normalised (right) SRB cell-survival curves for parental (blue), scrambled (red), and IKO1a (green) Capan-2 cells in 96-well plates. **A.** resultant and normalised data show no difference in response/sensitivity of IKO1a isogenic Capan-2 cells to radiation compared to untreated and scrambled cells. **B.** Cells treated with 0-10,000 nM doxorubicin (plotted as $\log_{10}$[doxorubicin] (nM)); IKO1a cells had comparable OD readouts to parental cells in the resultant data however both exceeded those of scrambled cells. Normalised cell viability showed significant increase in sensitivity of IKO1a cells to doxorubicin at

doses 50, 75, 100, 150, and 200 nM (8.34×10^{-5}, 3.24×10^{-4}, 1.22×10^{-4}, 1.03×10^{-5} and 1.91×10^{-4} respectively). **C.** Cells treated with 0-10,000 nM gemcitabine (plotted as $\log_{10}$[gemcitabine](nM)); resultant data showed no difference in OD readout between isogenic cell lines except at the lowest dose. Normalised cell viability showed IKO1a had greater sensitivity to gemcitabine for all doses above and including 10 nM ($p = 3.02\times10^{-6}$, and 2.67×10^{-5}, 6.15×10^{-5}, 9.53×10^{-8}, 1.51×10^{-4}, 5.37×10^{-7}, 2.02×10^{-4}, and 4.20×10^{-5} respectively). Data was normalised to a vehicle control in the case for doxorubicin and gemcitabine. Radiation data was normalised to cells that did not receive radiation. An * donates statistically significant difference in mean as determined by Student's t-test. **D.** & **E.** Viability of isogenic cell lines treated with just vehicle control provides further evidence of IKO1a clone being more clonogenic compared to the parental cells as resultant mean OD readout is higher.

Screening MiaPaCa-2 isogenic cell lines using SWATH to identify candidate proteins and pathways affected by CRISPR-Cas9:

Sequential windowed acquisition of all theoretical mass spectra (SWATH) or data-independent acquisition (DIA) is a mass-spec technique that allows for almost complete characterisation and quantification of proteomic expression within multiple samples (Gillet et al., 2012; Huang et al., 2015). In contrast to data-dependent acquisition (DDA), which only selects the most abundant fragment ions (precursors) within each cycle if a sample is too complex (has too many precursors), DIA records all fragment ions within a particular m/z (mass/charge ratio) window (typically 25 Da) with several windows stacked to cover a very large mass range each cycle (mass range typically 400-1200 m/z) (Gillet et al., 2012; Vowinckel et al., 2013). DIA then relies on a spectral library consisting of previously defined precursors and proteins identified by past DDA runs to identify and quantify proteins within a sample or across multiple samples (Han et al., 2008; Lam et al., 2007).

To determine any potential changes in MiaPaCa-2 proteome expression due to CRISPR treatment, SWATH-MS was performed on parental, IKO1a, IKO2 and IKO3 cells. In this context SWATH was used to screen for potential protein or pathway candidates that have been up-/downregulated by CRISPR-Cas9 activity. Samples consisted of protein lysates from parental and $CRISPR^+$ cells which were either irradiated or left untreated. A spectral library was created from DDA runs performed on the same TripleTOF5600+ machine. Data extracted from the DIA runs was processed and analysed using Skyline and MsStats (Choi et al., 2014; Maclean et al., 2010) where samples were categorised based on both whether or not they were $CRISPR^+$ and the time-point the lysates were created.

A.

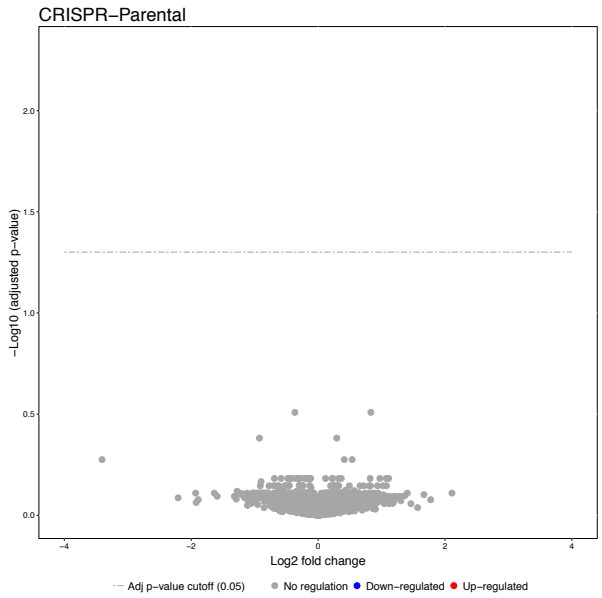

B.

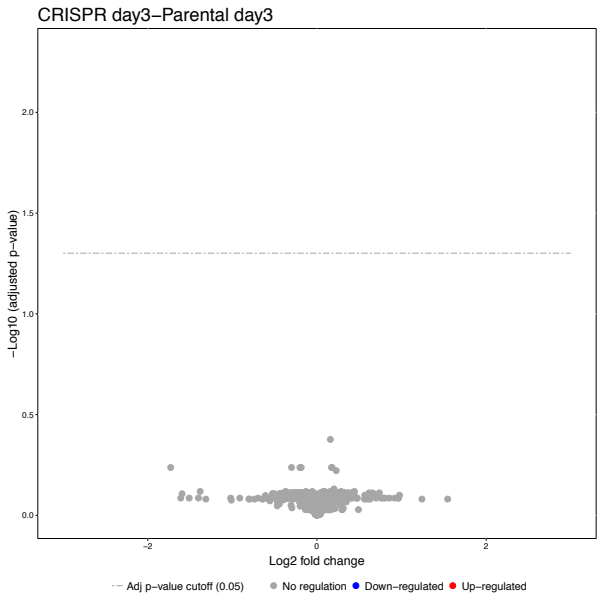

Figure 23: Initial SWATH fold-change analysis of isogenic cell lines:
Pyramid plots displaying log fold-change vs p-value to summarise data analysis of SWATH DIA runs. Samples were grouped based on whether they were CRISPR$^+$ (includes IKO1a, IKO2, and IKO3) or parental. **A.** includes data from all cells that did not receive 1Gy radiation whilst **B.** is from untreated samples from a day 3 time point. Grey dots indicate proteins with non-significant changes in expression. Proteins that would be overexpressed in CRISPR$^+$ samples would show up as red dots (positive log fold-change) whilst those that would be under expressed would show up as blue dots (negative log-fold change). Statistical analysis of DIA data was performed in Skyline with the MsStats R-plugin. Fold change cutoff for up-/down-regulation was set to $\pm Log_2(2)$ fold change and P-value cutoff was set to $-Log_{10}(1.33)$ (indicated by dashed horizontal line on each graph).

Despite the comprehensiveness of the library and the DIA data, there was no statistically significant up- or downregulation of proteins between parental and CRISPR$^+$ cells in both test groups as determined by log fold change vs p-value significance (Figure 23: A. & B.). This would appear to reject the hypothesis of altered expression based on the results seen from the resultant cell survivability of IKO1a cells and clonogenic assays which indicated a change in gene expression due to *Itch* loss resulting in increased survival capabilities even in the absence of treatment and differing responses to low-dose treatment regimens compared to scrambled and parental controls. However, upon re-evaluating the experimental approach and revisiting the SWATH data it was likely that the CRISPR$^+$ group was too complex and contained too much variance as it was a culmination of IKO1a, IKO2, and IKO3 clones. A secondary set of group comparisons and analyses was performed that compared individual

clones against parental cells (Figure 24: A., B., & C.). Re-analysis of the data revealed candidate proteins that were up- or down-regulated in CRISPR^{+} clones compared to parental cells. IKO1a cells were found to have increase fold-change of MBLC1 (metallo-beta lactase domain containing protein 1) and reduced fold-change of IFRD2 (interferon related developmental regulator 2, Figure 24: A.). Whilst IKO2 cells did not seem to have appear to have any statistically significant difference in protein fold-change it was interesting to note that NEK3 (NIMA-related kinase 3) could be up-regulated which was the case in IKO3 cells (Figure 24: B. & C.) IKO3 cells also showed downregulation of TWF1 (twinfillin actin binding protein 1) and DHRS4 (dehydrogenase/reductase 4). Despite these hits, there is not a sufficient number of changes in proteome within groups to perform any form of pathway analysis. This is likely due to the fact that for the secondary analyses there were a lack of replicates to measure and increase the statistical power of the analysis of each individual clone. It is likely that if the experiment was performed again, focusing on individual clones and with more replicates, that more diverse changes in proteome would become apparent, potentially leading to a far more accurate and detailed overview of the effect *Itch* loss has on cells.

A.

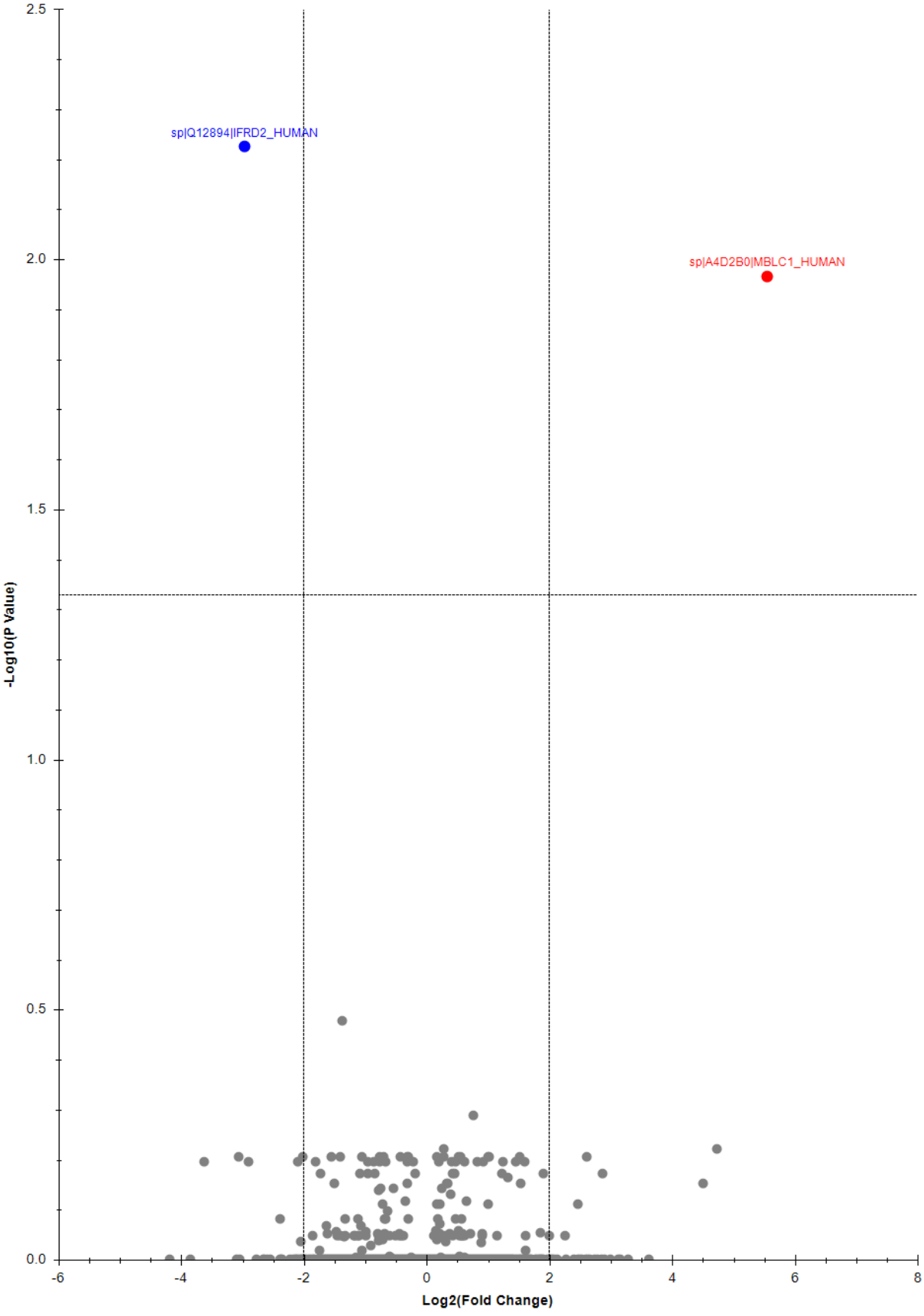
sp|Q12894|IFRD2_HUMAN
sp|A4D2B0|MBLC1_HUMAN
-Log10(P Value)
Log2(Fold Change)
2.5
2.0
1.5
1.0
0.5
0.0
-6
-4
-2
0
2
4
6
8

B.

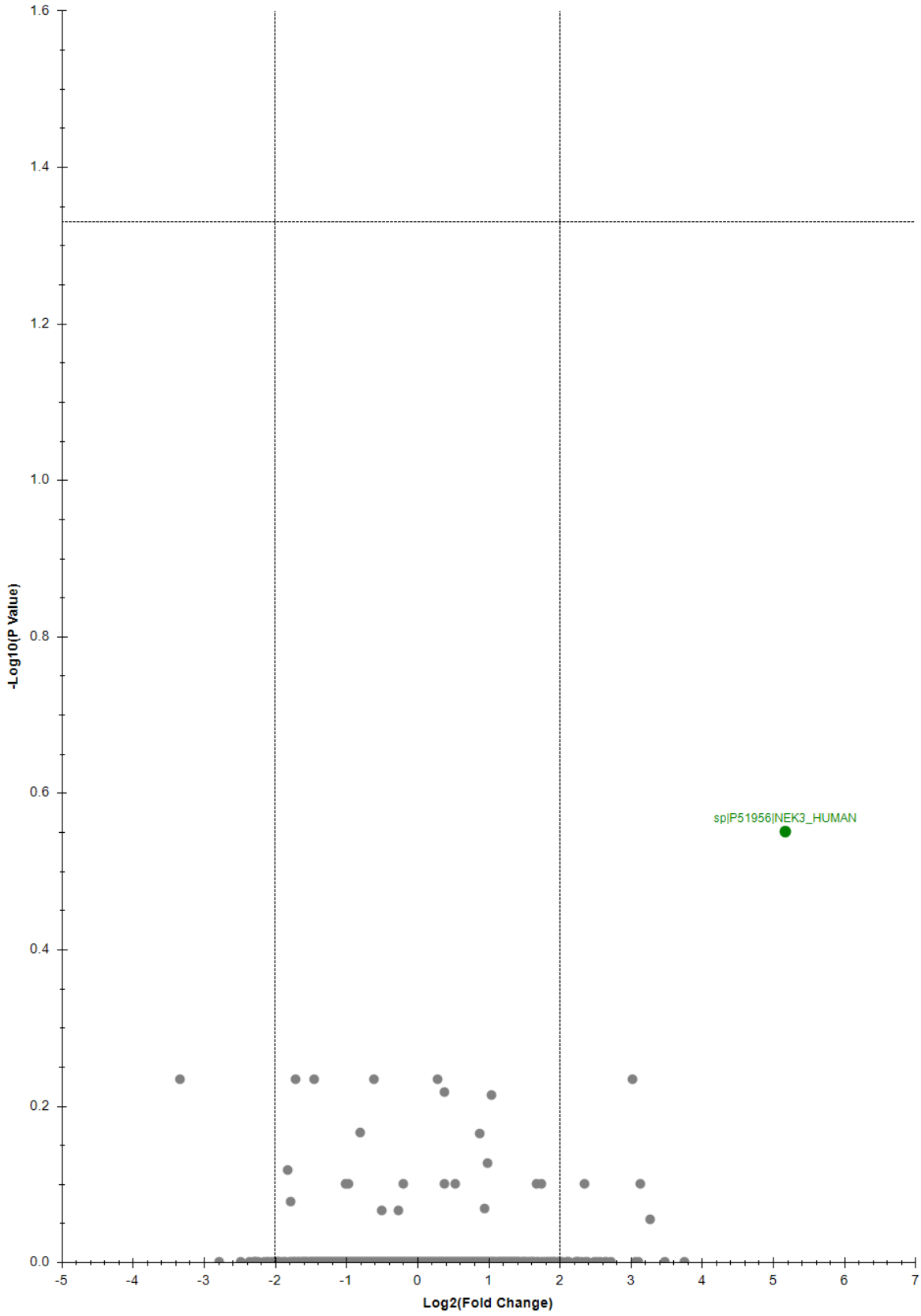
1.6
1.4
1.2
1.0
0.8
0.6
0.4
0.2
0.0
-Log10(P Value)
sp|P51956|NEK3_HUMAN
-5
-4
-3
-2
-1
0
1
2
3
4
5
6
7
Log2(Fold Change)

C.

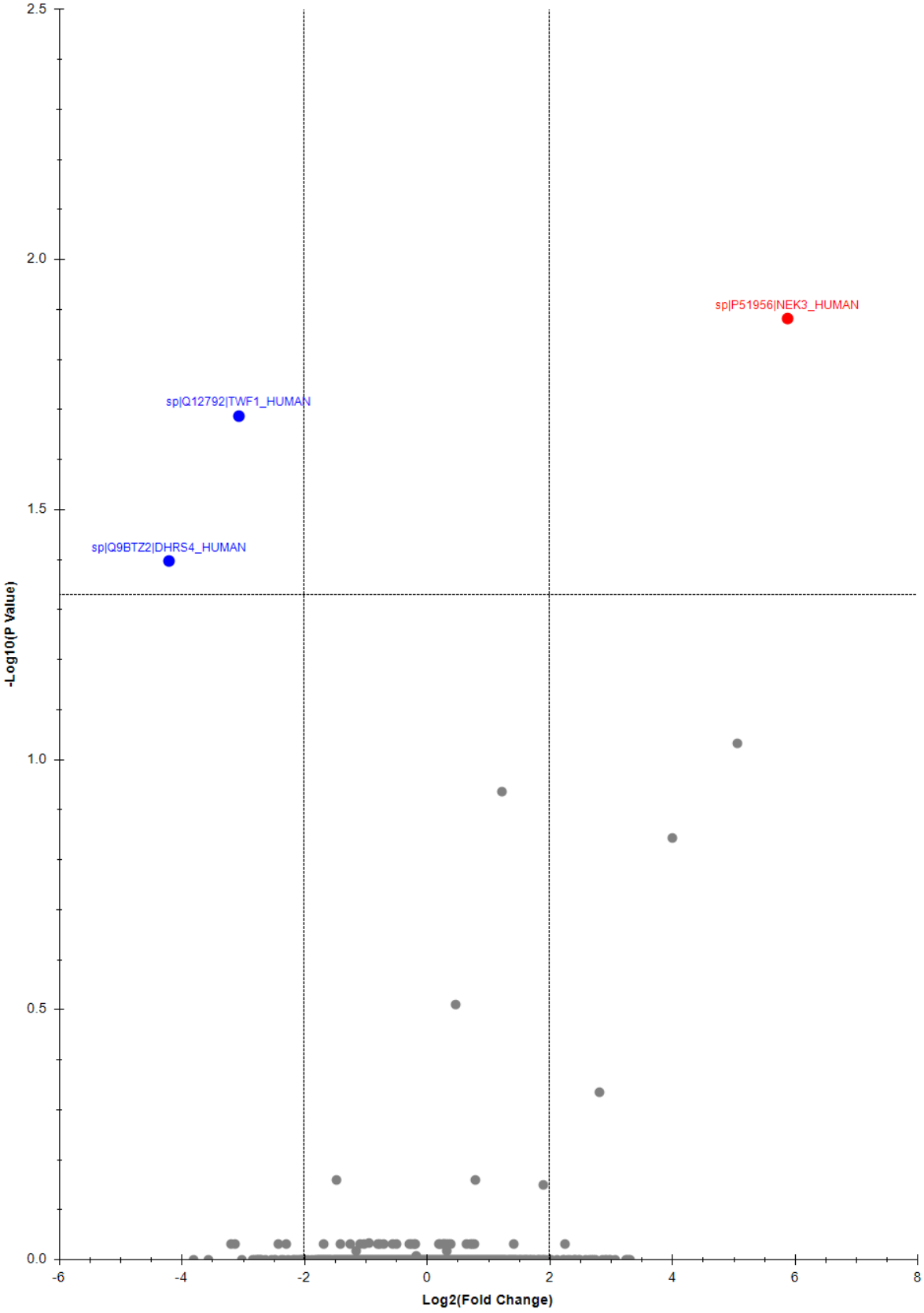
sp|P51956|NEK3_HUMAN
sp|Q12792|TWF1_HUMAN
sp|Q9BTZ2|DHRS4_HUMAN
-Log10(P Value)
Log2(Fold Change)
2.5
2.0
1.5
1.0
0.5
0.0
-6
-4
-2
0
2
4
6
8

Figure 24: Secondary SWATH fold-change analysis of isogenic cell lines reveals potential candidates:

Pyramid plot displaying secondary analysis of SWATH DIA data where the results from individual isogenic cell lines were compared against those of parental cells (plotted as Isogenic cell line vs parental cell line). Dots on the graph represent proteins: blue dots represent proteins that are under-expressed compared to parental cells and red dots represent proteins that are over-expressed. **A.** IKO1a cells showed over-expression of MBLC1 (metallo-beta lactamase domain containing protein 1) and under-expression of IFRD2 (interferon related developmental regulator 2). **B.** Although the analysis suggests that there was no statistically significant difference in protein fold change between IKO2 and parental cells, NEK3 (NIMA-related kinase 3) is highlighted in green as it reoccurs as being upregulated in IKO3 cells and is therefore of particular interest. **C.** IKO3 cells showed upregulation of NEK3 and downregulation of TWF1 (twinfillin actin binding protein 1) and DHRS4 (dehydrogenase/reductase 4) compared to parental cells. DIA data group analysis was performed within the Skyline software. Fold change cutoff for up-/down-regulation was set to $\pm Log_2(2)$ fold change (indicated by vertical lines on each graph) and P-value cutoff was set to $-Log_{10}(1.33)$ (indicated by dashed horizontal line on each graph).

Discussion:

Itch-targeting crRNAs were cloned into a lentiviral plasmid vector for transduction, alongside a scrambled control, into both MiaPaCa-2 and Capan-2 cell lines. Significant *Itch* knockdown in CRISPR$^+$ isogenic cell lines was confirmed by western blot. To determine whether or not these *Itch*-deficient isogenic cell lines would be more sensitive to radiation, doxorubicin and/or gemcitabine, cell survival assays were performed using the same protocol and dose-parameters as was used in the transient *Itch* knockdown experiments. In MiaPaCa-2 derived cell lines, CRISPR-mediated *Itch* knockdown caused an increase in relative response to low doses of radiation and doxorubicin (0.5-1 Gy and 5-10 nM respectively). However, from both the resultant data of the cell survivability assays and the clonogenicity assays IKO1a cells were observed to form greater cell numbers within 96-well plates and form more colonies than parental and scrambled cells (indicating that they may divide faster or more frequently). Meanwhile in Capan-2 cell lines, IKO1a appeared to have an increased relative response to gemcitabine doses ranging from 0.01-1 μM which was contrary to MiaPaCa-2's which showed no change in response. From the 5-day time frame and the resultant data for Capan-2 dose-response curves, it is tenuous to suggest that stable *Itch* knockdown causes Capan-2 cells to be more clonogenic as with MiaPaCa-2 cells (resultant difference in OD of untreated wells was small or non-existent). Furthermore, during culture and experiments it was noted that Capan-2 cells had a much longer doubling time meaning any experiments performed to assess Capan-2 clonogenicity would require a considerable timeframe before any conclusive results could be drawn.

We hypothesised that stable *Itch* knockdown causes cells to adapt to Itch loss of function that may confer a survival advantage. As an attempt to clarify any potential difference in proteome between parental and CRISPR$^+$ cell lines, SWATH-MS was performed to characterise and quantify protein expression. Whilst the first series of analyses performed

revealed no significant differences in protein fold change, comparison of each of the CRISPR+ clones against parental cells revealed a few differences in basal protein levels. Unfortunately, these secondary analyses lacked significant statistical power due to lack of replicates for each of the individual clones. It is likely that there are more differences in proteome caused by loss of *Itch* that could be revealed if the experiment was repeated.

For both cell lines the construct IKO2 showed the smallest degree of Itch knockdown: one could theorise that this could be due to the sgRNA sequence having lower efficacy in terms of Itch knockdown however, this was not pursued as the reduction in *Itch* expression was still significantly large (85/75% reduction in Itch protein for MiaPaCa-2 and Capan-2 cells respectively). Another possible explanation is that the sgRNA sequence for IKO2 had more off-target or mismatch activity in the host genome.

The reason why the term "knockdown" is used over the term "knockout" is due to the fact that there is still a small amount of Itch expression. Most studies that employ CRISPR-Cas9 rely on clonal expansion of genetically identical cells that incorporate the desired gene-edit, usually confirmed by deep sequencing. This results in a population of clones that can then be considered "knockouts." Meanwhile in this investigation the cells have not been tampered with after puromycin selection: this results in a population of cells that are not necessarily clones of each other. This is more representative of an environment in-vivo where gene-edits are introduced into an already living organism rather than generated at conception through crossbreeding of parents with specific genotypes. Furthermore the nature of how CRISPR-Cas9 works in regards to generating indels means that the edit created in one cell is unlikely to be the same as that in another due to different indel lengths, whether the balance leans towards insertions or deletions during there generation, or if the DNA repair mechanism used was different (i.e. HDR rather than NHEJ). What we hoped to obtain, and indeed did, was a mixed population of cells which, on the majority, were negative for Itch expression.

Degree of Itch knockdown at the protein level for all CRISPR^{+} cell lines was very convincing, with both biological significance (inferred from the strength of the Itch bands for CRISPR+ cells compared to parental and scrambled controls) and statistical significance (after quantifying and analysing differences in band fluorescence) (Figure 18: A. and C.). However, this was not necessarily seen for Itch mRNA levels quantified by qPCR. Although this presents a potential weakness in the investigation, characterising CRISPR knockdown/knockout using qPCR has inherent problems that become clearer when referring back to basic principles of the central dogma. For a gene to be expressed DNA must be transcribed to mRNA which is then translated to protein after which it can then perform its function (assuming it is correctly folded and has the appropriate post-translational modifications). Cas9 creates double stranded breaks in DNA which result in indels formed from NHEJ which are random in length between individual cells. As these edits are generated at the DNA level it is highly likely that a viable transcript can be formed resulting in mRNA, albeit a mutated version. It is therefore possible that primers used for qPCR to elicit gene expression for a gene of interest could produce false positive results unless primers were individually tailored for each sgRNA target site (i.e. generating primers that branch the cut site). The main problem with this being that it is not always possible to create suitable primers that branch the cut site dictated by a specific sgRNA due to issues with primer design and stability in the PCR reaction.

With this information in mind it is far more likely that you would see a change in protein expression of your gene of interest. The mutant mRNAs generated from the indels would

likely not translate into a viable protein resulting in their degradation via the proteasome. This would explain why for some of the lentiviral constructs i.e. IKO2 and IKO3 we could see a significantly large reduction in Itch protein (Figure 18: A. and C.) but not in Itch mRNA (Supplementary Figure 5). Reduction in protein level is probably also far more relevant in regard to assessing the functional and physiological consequences of gene-editing techniques rather than strictly looking at mRNA. The major weakness in relying on protein expression is in the case where the basal level of a protein is usually very low as this then becomes difficult to assess any differences between negatives, positives and test conditions through traditional western blot in which case different methods of quantifying protein must be used. Fortunately, in this case basal levels of Itch were suitable enough to provide clarity of gene-editing techniques used in this project.

siRNA data vs CRISPR data - adapting to a life without Itch:

One of the most pressing concerns following the results presented in figures 20 & 22 when compared to the corresponding data of the transient siRNA knockdowns is the degree of response for each experimental condition was significantly different to what was seen for the stable knockdown. Whilst the siRNA-mediated *Itch* knockdown had almost no effect in terms of increasing the sensitivity of cells to additional treatment (with the exception of gemcitabine in MiaPaCa-2 cells) the resultant OD values of the siRNA-treated wells was far lower than that of the si-Scr and untreated cells (for both pancreatic cell lines). In contrast, stable Itch knockdown appeared to increase the sensitivity of both cell lines to all modes of treatment (as indicated by the normalised data and shifts in IC_{50}s – Table 25). Meanwhile the resultant data from both the OD readouts from SRB and the number of colonies identified by Celigo show IKO1a cells are more clonogenic and/or have an increased ability to divide compared to scrambled and parental cells.

The initial question presented why there is such a disparity between each method of *Itch* silencing (transient by siRNA or stable by CRISPR) in terms of cell survivability (i.e. the resultant data). Assuming that *Itch* promotes cell survival as the siRNA data indicates, then one could hypothesise that $CRISPR^+$ cells may have adapted to a "life without Itch".

In the case of a transient knockdown of *Itch*, cell survivability is only impaired temporally as the knockdown effect gradually dissipates. This means that any surviving cells which either temporarily altered their gene expression to cope or did not take up the dsRNA at all (and thus were not subjected to the knockdown) simply recovers the wild-type population (Figure 25). However, this is not the case for cells being treated with CRISPR-Cas9: *Itch* silencing in this system is irreversible so long as the cells are successfully transduced with the lentiviral construct. This means that any cells that survive the initial loss of *Itch* function would need to continually upregulate other proteins (and/or pathways) or acquire further mutations that circumvents the loss-of-function of *Itch* as they are prevented with a more severe "adapt or die scenario". Furthermore, the plasmid used also allows production of a gene that grants antibiotic resistance to puromycin which is used to provide a positive environmental selection pressure for cells that have been successfully transduced - a scenario that is similar in principle to how bacteria acquire antibiotic resistance. The combination of the loss of gene function and the selection pressure could generate cells that would have a survival advantage over the original cell line which would explain the what is observed in the resultant data from the cytotoxicity experiments. This hypothesis combined with the evidence already presented in the results identifies a potential flaw in the use of stable knockdown/knockout gene editing strategies and a caveat in the interpretation of CRISPR data, especially over an extended

investigative timeframe. If stable knockdown/knockout of a gene with unknown function (and consequences if ablated) is desired in-vitro then it may be worth performing transient knockdown first to identify and note any short-term cellular responses. Based on the findings from transient silencing, one can then decide the appropriateness of an irreversible ablation. However, as noted at the start of the discussion, IKO1a cells were more sensitive to radio-/chemotherapy according to the normalised viability data, which was not seen for si-Itch cells. This indicates that there could be potential impairment of pathways associated with coping with cytotoxicity and/or DNA damage resolution. Especially considering that all three modes of treatment exert there cytotoxic effect via inducing DNA damage, albeit via slightly different mechanisms.

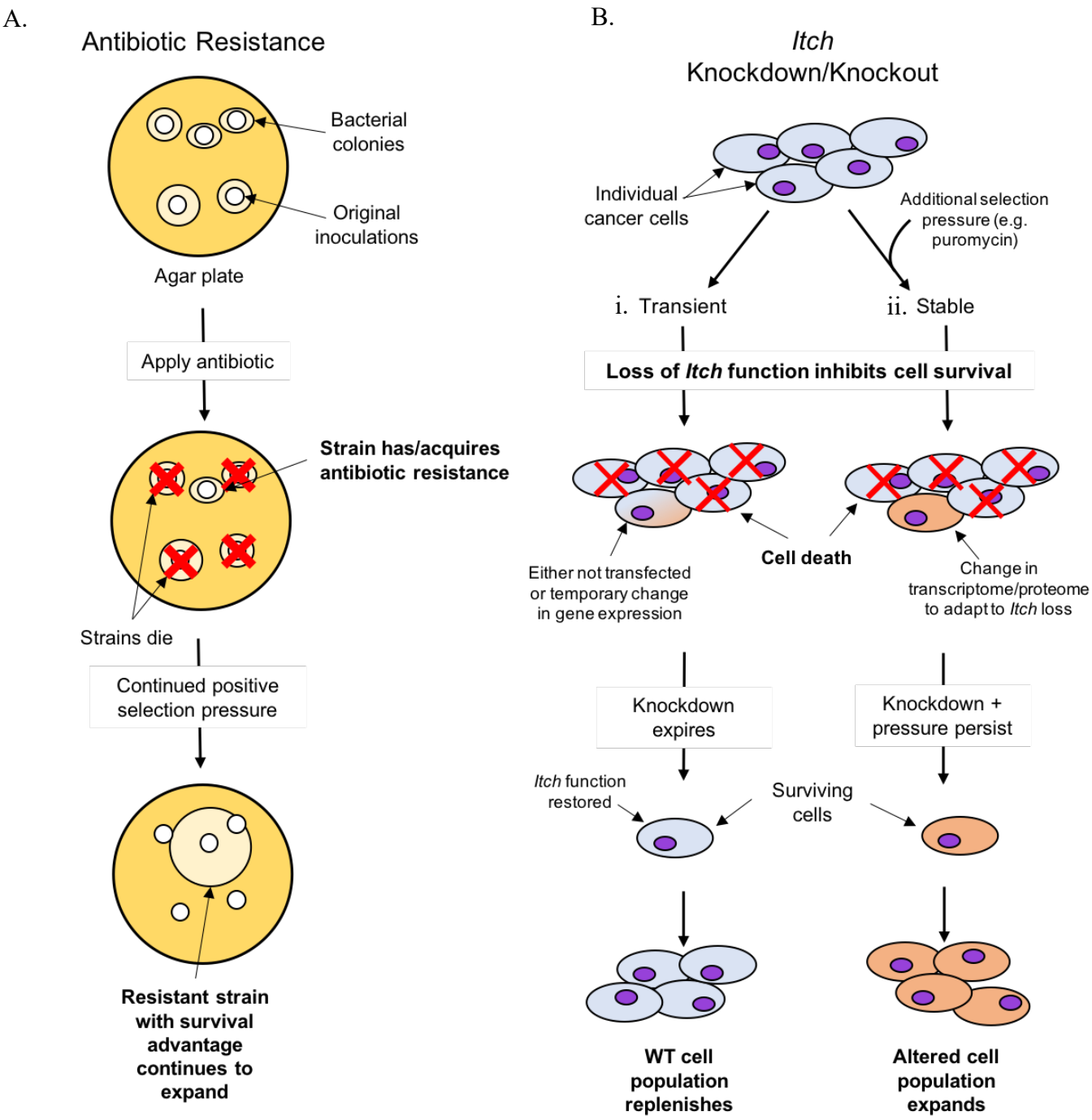

Figure 25: Hypothesis for differing response between transient and stable Itch knockdown/knockout cells – antibiotic resistance analogy:

(**A.**) several bacterial colonies grow from inoculations on an agar plate. When an antibiotic is applied to the dish only strains of bacteria that have or have recently acquired antibiotic resistance are able to survive whilst all none-resistant strains die. Under this positive selection pressure the resistant colony is able to expand further without competition from other strains. This principle could be used to explain the difference between transient and stable Itch knockdown phenotypes and response to radio-/drug therapy (**B.**). In transient *Itch* knockdown (**i.**) *Itch* function is only temporarily impaired in cells that are successfully transfected with siRNA. Over time the knockdown effect either expires in transfected cells or

gets diluted-out as cells divide eventually replenishing the wild-type population as *Itch* function is restored. Meanwhile in a stable knockdown/knockout scenario (**ii.**) As the loss of Itch function is irreversible, cells may need to permanently alter gene expression to survive. Furthermore there may be additional selection pressure in the form of antibiotic resistance genes introduced in the same plasmid used for the stable knockdown/knockout. The resultant surviving population of cells would then be altered to have a survival advantage when compared to wild-type cells.

Better optimisation of SWATH:

Sequential windowed acquisition of all theoretical mass spectra (SWATH-MS) was used to identify any potential changes in protein levels as a result of *Itch* knockdown by CRISPR-Cas9. However, during the first set of analyses, there were no significant differences in protein fold change between parental and CRISPR^{+} cells by the SWATH analysis despite the cell-survivability and clonogenicity experiments indicating otherwise. This was likely due to the fact that all the individual CRISPR^{+} clones were grouped and compared to parental cells which likely added a substantial degree of variance and error. Degree of *Itch* knockdown at protein and mRNA between each clone was different as seen from the western blot and qPCR data (Figure 19). It is therefore possible that each clone could have there own unique proteomic profile. To address this, analysis of individual clones compared to parental cells was performed which discovered differences in fold change for a select few proteins (Figure 24). One example of a potentially interesting protein that was discovered was NEK3. NEK3 was found to be upregulated in IKO3 and potentially upregulated in IKO2 as well. NEK 3 is a member of the NIMA-related serine/threonine-protein kinases that have been reported to be important in both cell cycle regulation and cancer progression (O'Regan et al, 2012; Moniz et al., 2011). Although NEK3 specifically has not been well characterised previously, a recent study reported that NEK3 overexpression is a poor prognostic marker in gastric cancer: 125 out of 168 tissue biopsies showed high immunostaining for NEK3 (Yang et al., 2018). As this is potentially upregulated in two of the *Itch* negative clones it would be interesting to see if there was any molecular or pathway interaction between these two proteins.

However, the statistical power of this second set of analyses was considerably weak due to the lack of replicates. To pull out potentially more candidate proteins and/or pathways effected by CRISPR-mediated *Itch* loss the experiment would likely need repeating with focus on generating sufficient replicate lysates of individual clones and comparing them to those of parental cells. Lack of replicates for each clone would also affect the robustness of the spectral library. Although it has the potential to be very high-throughput, DIA is dependent on spectral libraries that it needs to reference for each precursor within a given m/z window (Ludwig et al., 2018; Schmidlin et al., 2016).

Alternative CRISPR-based approaches:

In this project an early form of CRISPR-Cas9 technology was used where DSBs are generated from an sgRNA-guided Cas9 to encourage indel formation and subsequent stable *Itch* knockdown. Dual nickase Cas9 endonucleases can be used to induce DSBs with greater accuracy and less off-target activity at the cost of some knockdown efficiency (Ran et al., 2013). Additionally, adenine base editors (ABEs) can be conjugated to catalytically inactive Cas9 to enable precise base-editing via conversion of A•T to C•G to introduce/correct point mutations in genomic DNA (Gaudelli et al., 2017; Liang et al., 2017). One particular application of CRISPR-Cas9 that may be interesting to explore in relation to this project is the area of inducible CRISPR-mediated knockouts. Early interpretations of this such as iCRISPR involved transfection of a plasmid encoding transcriptional information for the synthesis of Cas9. Addition of doxycycline induces the expression of Cas9 resulting in DSBs in combination with the relevant sgRNA, which is either incorporated in the same or a separate plasmid, or added at the same time as doxycycline (Dow et al., 2015; González et al., 2014). Inducible CRISPR-Cas9 systems allows one to control the time point at which Cas9 endonuclease activity takes place as well as providing some degree of spatio-temporal control. Obviously, some form of selection would still be needed to isolate cells of interest but this can take place independent of DNA cleavage. The main issue with this particular form of inducible CRISPR-mediated knockout is that it is relatively slow: before any endonuclease activity can take place, Cas9 must first be transcribed and translated after application of doxycycline causing significant delay in silencing activity.

Photosensitive CRISPR-Cas9 systems can also be used as light-dependent inducible system which offers the potential of even greater temporal control (as light can be focussed or filtered in a way to only hit a certain population of cells). This approach relies on a heterodimerisation of photoreactive proteins (such as CRY2 and CIB1) that respond to blue light conjugated to traditional CRISPR components. This has been used as a means of both inducing DSBs via Cas9 endonuclease activity (Nihongaki et al., 2015), and as a means to transcriptionally activate a gene expression via an inactivated dCas9 coupled to a transcriptional activator such as VP64 (Nihongaki et al., 2015; Polstein & Gersbach, 2015). This method also allows one to toggle the system "on-and-off" as light exposure is easily controllable. Although seemingly a very powerful application of inducible CRISPR, it requires specialised equipment for blue light generation usually only found in specialist labs.

iCas is a chemically-inducible form of Cas9 developed by Liu et.al. that allows toggleable activity of Cas9 through supplementation of 4-hydroxytamoxifen (4-HT) (Liu et al., 2016). Multiple hormone binding domains of the oestrogen receptor (ERT2) were fused to Cas9 and upon addition of 4-HT, ERT2 associated Cas9 translocates to the nucleus from the cytoplasm, after which Cas9 can induce DSBs in genomic DNA. Depletion of 4-HT then causes the modified Cas9 to be localised in the cytoplasm where it cannot act, hence the alleged "off" function. However, although the paper mentions iCas' capacity to be switched on or off based on 4-HT dictating the construct's subcellular localisation, it does not necessarily mean that silencing activity would follow the same pattern (i.e. silencing could be turned on and off) if DSB breaks result in indel formation from NHEJ, which is necessary to silence that particular gene irreversibly and in a manner that is also heritable to daughter cells.

The reason why an inducible CRISPR system might be interesting in regard to exploring *Itch* function and particularly its potential role as an oncogene is that one could suddenly "turn-off" Itch and observe the downstream consequences e.g. cell viability. It would be interesting to observe whether or not the response of cells undoing the inducible knockout would mirror that seen in the siRNA-treated cells where *Itch* was only knocked-down transiently. Assuming Cas9 is used (or any DNA-specific Cas variant) this particular method could also better elicit whether the drop in cell survivability upon application of siRNA was due to potential off-targets interactions of the siRNA-RISC complex with other RNAs.

One could adapt the method of a toggleable system with a recently conceived REPAIR-based (RNA editing for A to I replacement) RNA editing system to avoid irreversible gDNA edits. Inactivated Cas13b (dCas13b) conjugated to a crRNA can bind to mRNA rather than DNA (Ali, Mahas, & Mahfouz, 2018; Cox et al., 2017). An attached deaminase (ADAR2) converts adenosine to inosine which is functionally similar to guanine. This means that precise base edits can be made in mRNAs allowing one to perform knockdowns of specific protein isoforms encoded by alternatively spliced mRNA transcripts. Coupling this system with one of the aforementioned methods of induction (biological, chemical, light-based, etc.) would provide a construct that allows toggleable silencing activity that could be stably expressed in cell lines (e.g. via lentiviral or AAV transduction) that would not cause indel formation in gDNA due to DSBs from traditional Cas9 endonucleases. In addition to the knockdown of specific isoforms, one could even incorporate several REPAIR constructs within the same plasmid (for example – a ribonuclear protein approach using lipofection or nucleofection for entry could be used but then this would be transient rather than stable), under control of the same or even separate inducible systems to perform either a more comprehensive, blanket-knockdown of gene expression or being able to influence the levels of several protein isoforms simultaneously. As previously mentioned, technology already exists that allows transcriptional control of target genes through activator/repressor-associated-dCas9 (Gilbert et al., 2013; Maeder et al., 2013; Qi et al., 2013) coupled to photoreactive proteins. Whilst this does achieve toggleable transcriptional control it is restricted by the need of a PAM sequence (for Cas9-DNA binding) which Cas13b does not require.

Additional verification of CRISPR$^+$ cell lines – enzyme mismatch cleavage assay:

In hindsight, one additional form of verification that may have been useful to perform before proceeding with qPCR and Western blot is an enzyme mismatch cleavage (EMC) assay. EMC assays can be used to verify the presence of mutations induced by CRISPR, TALEN and other forms of genome editing (i.e. indels). It is based on the preferential enzymatic cleavage of mismatched DNA over Watson-Crick base pairing (Vouillot, Thélie, & Pollet, 2015). Usually one of two types of mismatch cleavage enzymes is used when verifying indels. CELI is an endonuclease that is found in many plants and within various plant tissues (Oleykowski et al., 1998) and cleaves 3' of the site of mismatch. This led to the development of the commercially available CELII (Surveyor™ nuclease) that is able to detect mismatches due to single base substitutions as well as insertions of various lengths (Qiu et al., 2004). T7E1 (T7 endonuclease 1) is a bacteriophage resolvase whose substrates are dsDNA undergoing some sort of conformational change (e.g. extrahelices, bulges, and kinks) and does not pair well with perfectly Watson-Crick paired DNA (Déclais et al., 1995; Sakurai et al., 2014; Vouillot et al., 2015). Although both enzymes have been shown to work for mutation detection it is reported that T7E1 is more efficient and has a greater signal to background ratio over Surveyor (Sakurai et al., 2014; Vouillot et al., 2015).

In an EMC assay, PCR primers are designed to flank the mutational region of interest (in the case of CRISPR this would be the sgRNA target site), making sure that the site of mutation is offset from the centre of the two primers. Amplification of the target region by PCR from genomic DNA extracts takes place, followed by hybridisation of PCR products. This creates homoduplexes from amplicons where the target site is wild type, and heteroduplexes from amplicons where the target site is mutated in some way. Heteroduplexes have mismatches or extrahelical loops which are more prone to cleavage by EMC enzymes (Vouillot et al., 2015). When gel electrophoresis is performed on the enzyme-treated PCR product, one should see a larger, full-length band from homoduplex DNA, which is wild type, and smaller bands from heteroduplex DNA where the enzyme has cleaved the mismatch site. It is at this point that the importance of the positioning of the mutation site between the two PCR primers comes into play as, if the target site is central to the two primers, only one band will be seen on the gel in heteroduplex DNA: the enzyme will cleave the PCR product centrally, producing two equal-sized bands when visualised on a gel. Alternatively, different sized cleavage products can be viewed using a Bioanalyser alongside the full-length section of DNA (Vouillot et al., 2015). This technique would have allowed provided an initial confirmation step to determine whether or not indels had been created in transduced cells before validating *Itch* protein and mRNA levels.

Chapter 5 – The Effect of Itch Knockdown In Osteoclast Differentiation And Function:

Previous studies have implicated a role for Itch in the regulation of bone remodelling by acting as a negative regulator of the development and function of osteoclasts and osteoblasts (Li et al., 2017; Liu et al., 2017; Zhang et al., 2013; Zhang & Xing, 2013). This part of the project explores the role of Itch in regulation of osteoclast differentiation using a human ex-vivo model. Based on previous work looking at the differentiation potential of monocytes from *Itch*-/- mice a series of experiments was designed to see if this translated to human monocytes derived from whole blood. Thus, the hypothesis is that genetic knockdown of *Itch* in primary human monocytes promotes the differentiation and function of mature osteoclasts. For this investigation whole blood samples were taken from volunteers and used to isolate peripheral blood monocytes (PBMCs) (Henriksen et al., 2012; Marino et al., 2014). After an appropriate cell culture protocol was developed and refined, genetic knockdown of PBMCs was attempted using either previously-validated siRNA or CRISPR-Cas9 before adding RANKL to culture media to promote osteoclast differentiation (Kim & Kim, 2016; Yamashita et al., 2012).

Results:

Successful isolation, culture, and differentiation of primary PBMCs to osteoclasts:

After whole blood was collected and separated into plasma, the buffy coat (containing leukocytes and platelets), and erythrocytes (red blood cells), the buffy coat was extracted using a Pasteur pipette and the cells were washed. Cells were cultured in α-MEM containing 20ng/ml M-CSF to specifically culture monocytes. After 7 days of media was supplemented with 50ng/ml RANKL which was replaced every two days to encourage mature osteoclast differentiation (Figure 26: A.). Mature osteoclasts are morphologically characterised as large multinucleate bodies (due to multiple cells combining) and can be histologically characterised using tartrate resistant acid phosphatase (TRAP) staining (Blumer et al., 2012; Burstone, 1959), which makes cells appear purple/brown. After 7 days RANKL treatment, cells were fixed and stained for TRAP activity (Figure 26: B.).

Successful siRNA-mediated knockdown of *Itch* in primary PBMCs ex-vivo:

After isolation and 7 days of PBMC culture with M-CSF, cells were subject to 12.5 nM siRNA for 24 hours before media was changed. 48 hours post-transfection cell lysates were taken to assess both protein and mRNA levels of Itch to confirm the knockdown. Results from western blot (Figure 27: A. lanes 1, 4 and 5 & B.) showed an average 75% Itch protein knockdown compared to untreated and scrambled controls. This was mirrored by a 80% Itch mRNA knockdown as confirmed by qPCR (Figure 27: C.).

Stable knockdown of Itch by CRISPR-Cas9 was also attempted in a separate batch of PBMCs. After transduction with lentiviral particles $CRISPR^{+}$ there was a large degree of cellular toxicity and cell death. Cells appeared to have burst or damaged nuclei with cellular debris scattered within the cytoplasm as well as in the media (Figure 28). Several cellular structures were adherent to the plate e.g. the plasma membrane, giving the cells a husk-like

appearance. When protein lysates were taken from the affected cells the protein level was too low to be able to tell if the knockdown was successful (Figure 27: A. columns 2 and 3); both CRISPR-Itch and CRISPR-Scr lanes had reduced red fluorescence from β-Actin compared to the other lanes, indicating a significant reduction in total protein. Qualitatively, the level of Itch (green fluorescent bands) for CRISPR-Itch and CRISPR-Scr was so low that any quantification of fluorescence made the samples indistinguishable in terms of Itch protein.

A.

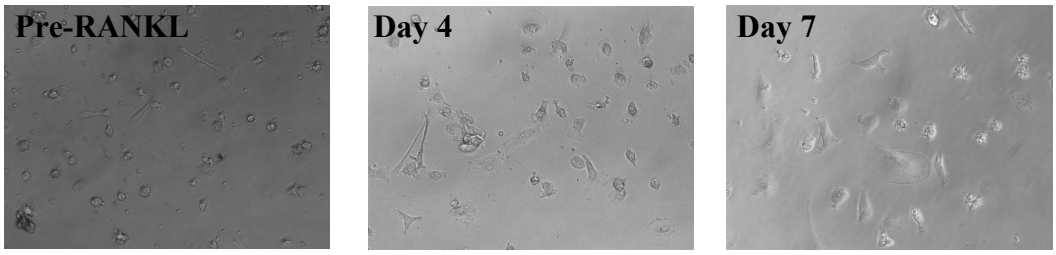

B.

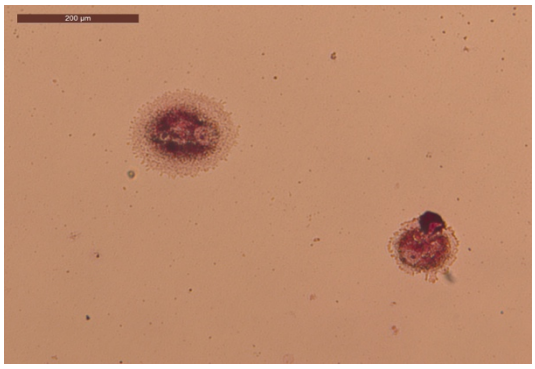

Figure 26: Culture of PBMCs ex-vivo: After isolation from whole blood:

PBMCs were cultured with 20 ng/ml M-CSF for 7days before exposure to 50 ng/ml RANKL. Cells were imaged using an inverted light microscope to monitor osteoclast differentiation (**A.**). After 7days RANKL treatment cells were fixed and stained for TRAP activity (**B.**). TRAP+ cells appear purple/brown.

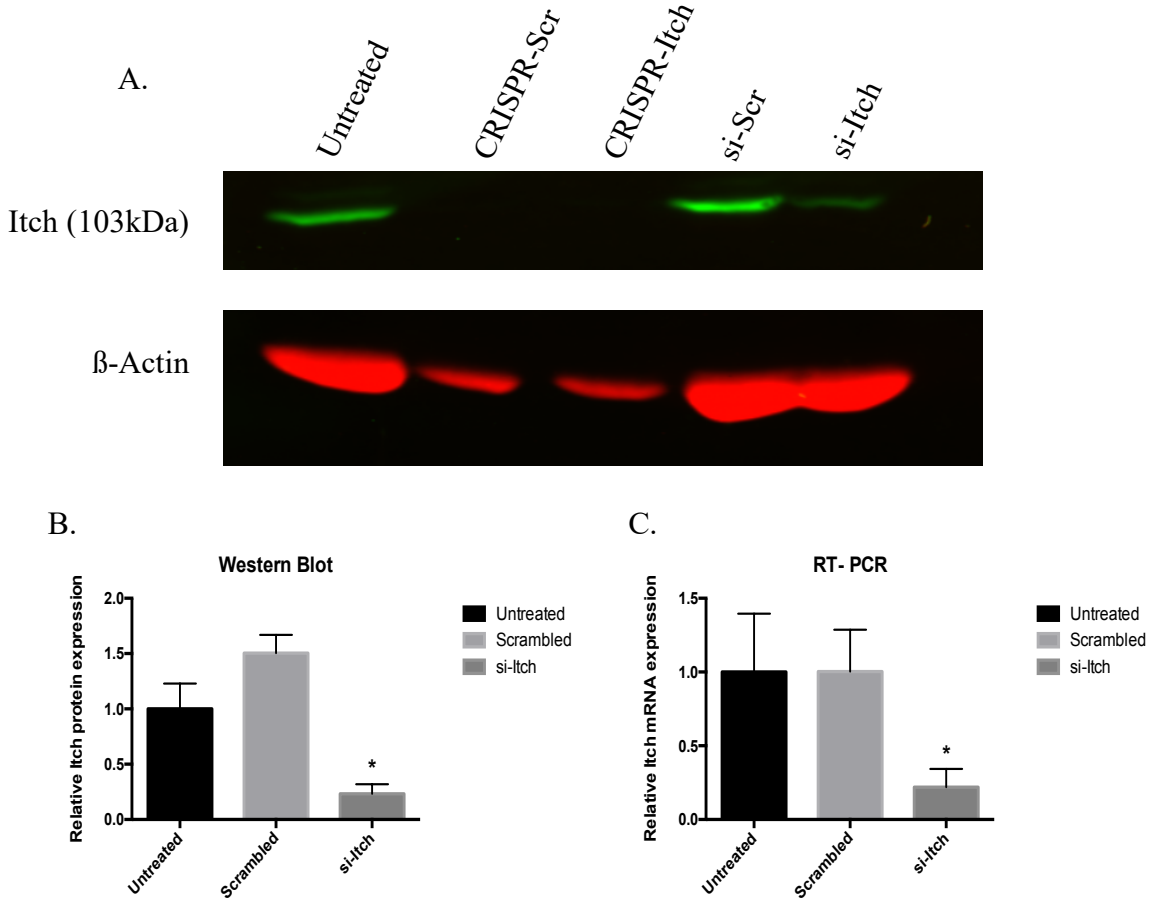

Figure 27: Attempted knockdown of Itch using siRNA and CRISPR-Cas9 in PBMCs:
PBMCs were either incubated with siRNA or CRISPR targeting Itch. **A.** western blot of cells shows successful transient knockdown of Itch in PBMCs compared to a scrambled and negative control (lanes 1, 4, and 5). CRISPR treatment caused cell death in transduced wells, resulting in too little protein being extracted to elicit the degree of Itch knockdown between CRISPR-Itch and CRISPR-Scr (scrambled) (lanes 2 & 3). **B.** quantification of Itch protein relative to untreated controls for siRNA-mediated knockdown. **C.** RT-PCR results showing relative Itch mRNA levels of siRNA-treated PBMCs. GAPDH was used as a housekeeping gene for normalisation of results.

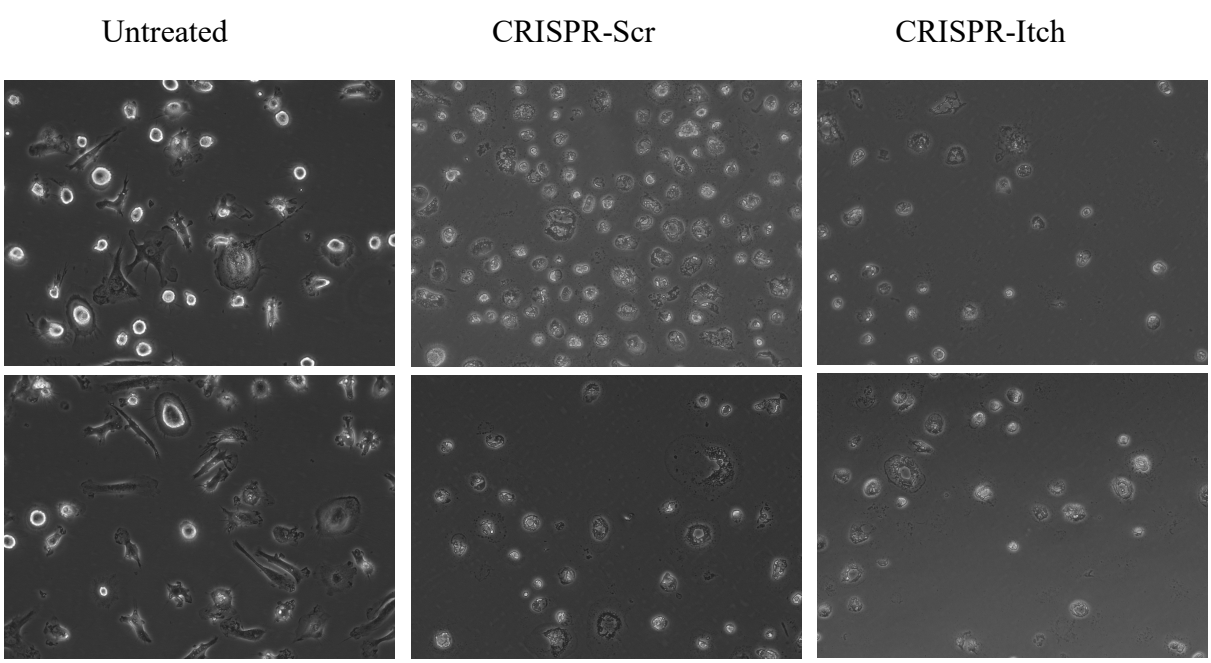

Figure 28: Effect of CRISPR-Cas9 on PBMCs:

Images taken of PBMCs/osteoclasts 14 days post CRISPR treatment. Untreated cells (left) appeared to develop normally, forming large multinucleate cells formed from the fusion of individual osteoclast precursors. However scrambled (middle) and Itch-targeting (right) CRISPR^{+} cells appeared damaged and/or dead with fragmented nuclear material and only some cellular structures remaining adherent to the plate for example the plasma membrane.

Knockdown of *Itch* promotes survival and differentiation of mature osteoclasts ex-vivo:

In order to see if silencing Itch can affect osteoclast differentiation PBMCs were cultured on two types of 96-well plates; either a plain-surface plate or an Osteo-surface Assay Plate (osteo-plate) (Rao et al., 2010). Cells were exposed to siRNA for 24 hours before changing to RANKL-containing media to promote osteoclast differentiation (A supplementary dose of siRNA was applied at day 4 RANKL exposure). As determined using Celigo, it was found that in the regular 96-well plate there was a significant decrease in well confluence for cells that had been treated with scrambled siRNA (Figure 29: A.). No biological, or statistical, difference in confluence was seen between untreated and si-Itch-treated wells. It was hypothesised that this difference in confluence could be due to lipofection toxicity however this same pattern was not seen in the osteo-plate (Figure 29: B.) where confluence averaged at 20% for all three test conditions with little variation. Comparison of percentage confluence between both plates revealed a 10% difference in mean well confluence for untreated and si-Itch wells with no observed difference mean well confluence of scrambled wells between both plate types (Figure 29: C.).

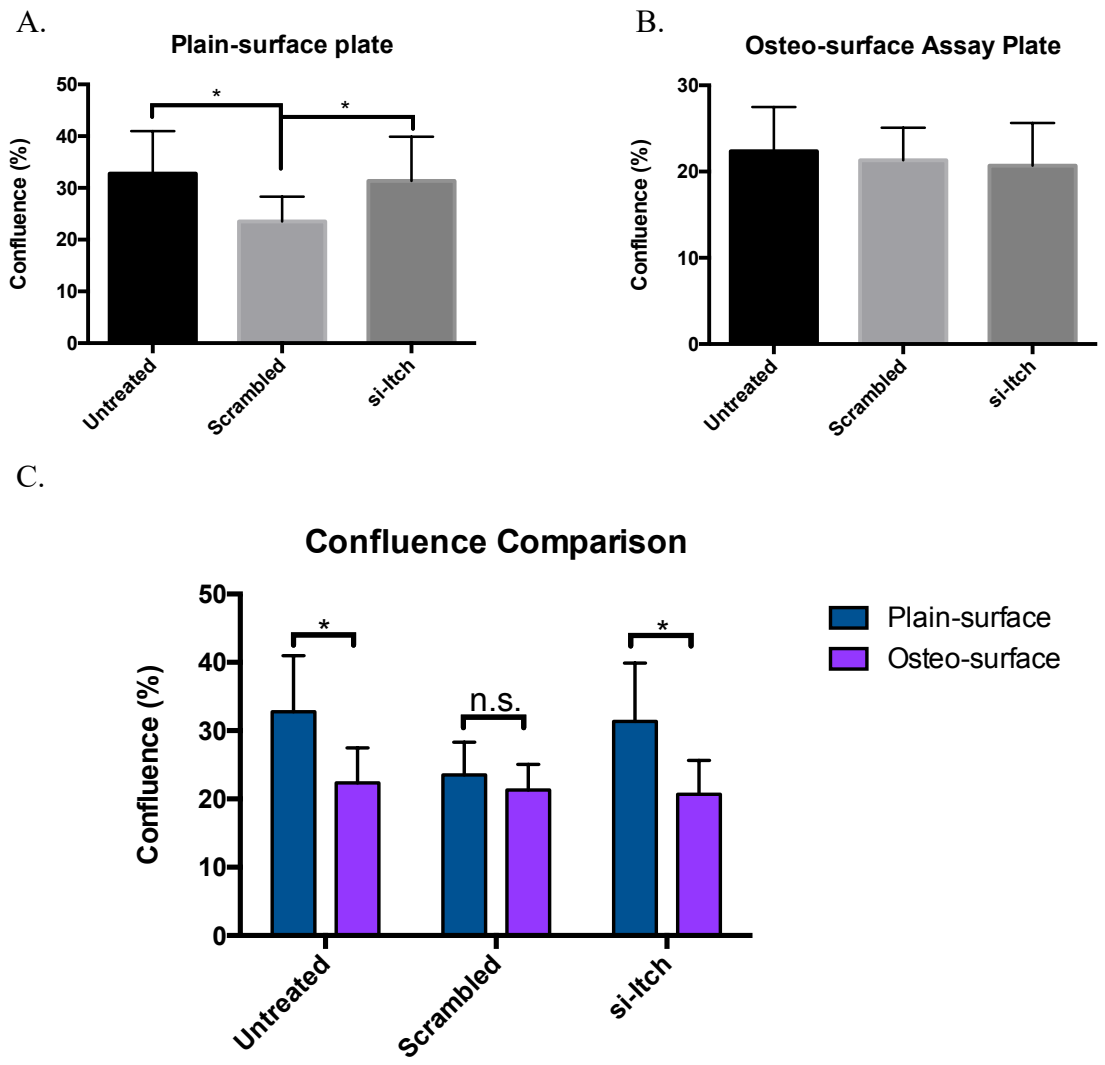

Figure 29: Scrambled siRNA treatment inhibits cell survival of PBMCs and osteoclasts on plain surface plates:

Using Celigo, average well confluence (%) was determined for all test conditions for both plain surface and Osteo-Surface assay plates. In the plain surface plate (**A.**) the average well confluence for the scrambled-treated wells was significantly lower than both the untreated ($p = 0.0001$) and si-Itch wells ($p = 0.0012$). There was no difference observed in the Osteo-Surface plate (**B.**). Mean confluence between plates was also compared and analysed (C.). Mean well confluence in the osteo-surface plate was ~10% lower for both untreated and si-Itch treated wells ($p = 2.33 \times 10^{-5}$ and 2.21×10^{-5} respectively). No significant difference was seen in scrambled-treated wells between both plates. Statistically significant difference in means was calculated using Student's t-test.

Cells were fixed and stained for TRAP activity to confirm the presence of osteoclasts (Figure 30: A.). A cell-counting algorithm was designed in Celigo to identify and record $TRAP^+$ objects in each well of the 96-well plates (Figure 30: B.). Wells treated with scrambled siRNA had lower numbers of $TRAP^+$ cells compared to untreated and si-Itch-treated wells (Figure 30: C.). Interestingly, for the osteo-plate, despite confluence levels across each test condition being comparable (Figure 29: B.), the mean (μ) number of $TRAP^+$ cells for scrambled-treated wells was significantly lower than that of untreated wells ($\mu = 330$ and 449 respectively, $p = 0.0005$). si-Itch treated wells had significantly higher mean for $TRAP^+$ cells ($\mu = 532$, t-test comparing si-Itch vs untreated $p = 0.0048$) (Figure 30: D.).

As previously mentioned, mature, fully differentiated osteoclasts are large multinucleate bodies formed from the fusion of several cells. To determine if siRNA-mediated silencing of *Itch* promotes the formation of mature osteoclasts the same plates were scanned with a second cell-count algorithm that was designed to select for $TRAP^+$ objects above a particular surface-area threshold (Figure 30: E.). In both plain-surface and osteo-surface plates, wells treated with si-Itch had significantly higher numbers of hits ($\mu = 63$ & 9 for plain and osteo-surface plates respectively) indicating an increase in the number of mature osteoclasts compared to the untreated controls ($\mu = 54$ & 4 respectively) (Figure 30: F. & G.). Scrambled-treated wells displayed far lower numbers compared to untreated wells in both plate formats $\mu = 18$ & 2 for plain and osteo-surface plates respectively. Cells on the plain-surface plate were also nuclear-stained with Hoechst33342 and scanned again using a blue fluorescence (461nm emission) and a brightfield filter to identify multinucleate bodies with $TRAP^+$ activity (Figure 30: H.). Concurrent with the previous results, si-Itch treated wells had significantly higher numbers of multinucleate bodies ($\mu = 25$) compared to both untreated ($\mu = 17$) and scrambled-treated ($\mu = 9$) wells (Figure 30: I., t-test comparing si-Itch vs untreated, $p < 0.0001$). These results combined confirm that genetic knockdown of Itch promotes differentiation of PBMCs into mature osteoclasts.

A.

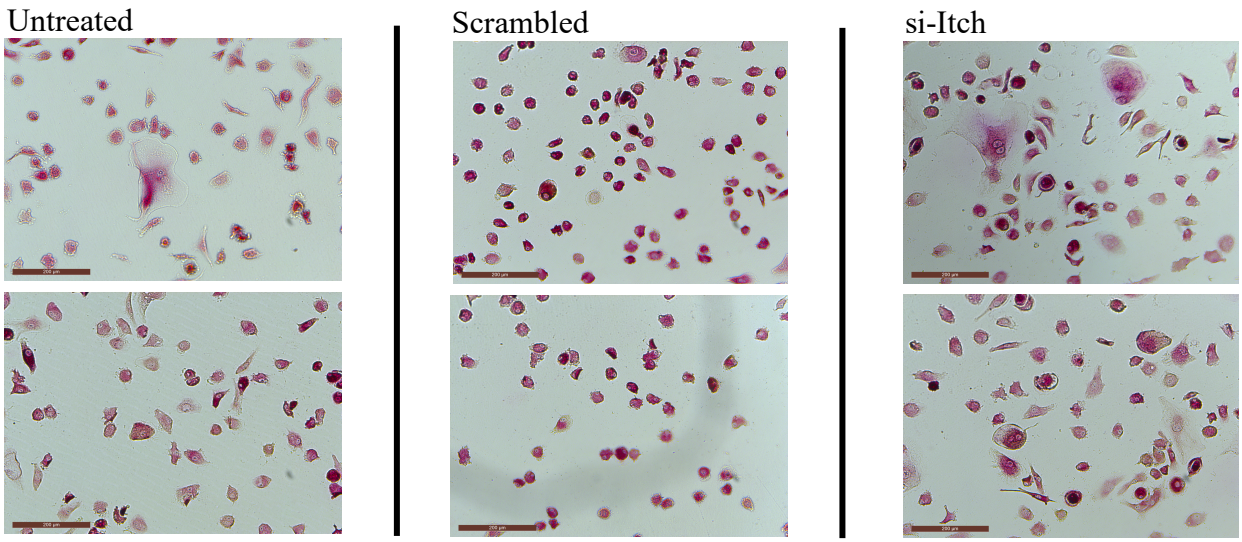
Untreated
Scrambled
si-Itch

B.

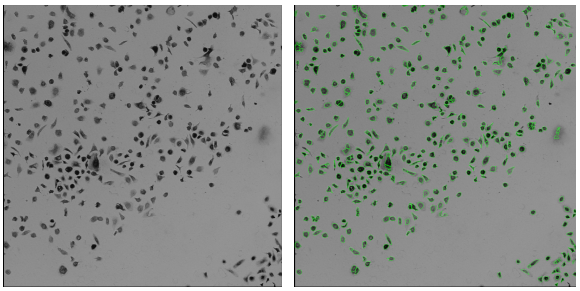

C.

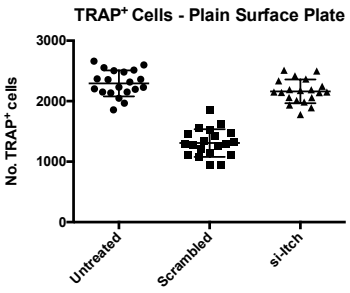
TRAP⁺ Cells - Plain Surface Plate
No. TRAP⁺ cells
3000
2000
1000
0
Untreated
Scrambled
si-Itch

D.

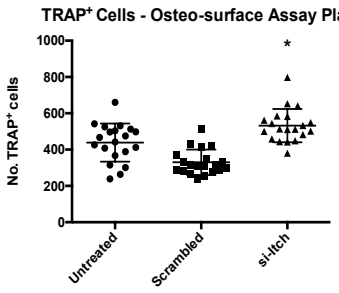
TRAP⁺ Cells - Osteo-surface Assay Plate
No. TRAP⁺ cells
1000
800
600
400
200
0
*
Untreated
Scrambled
si-Itch

E.

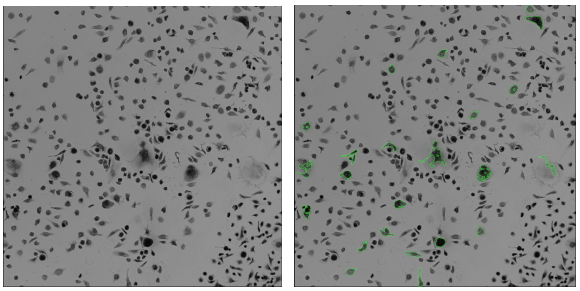

F.

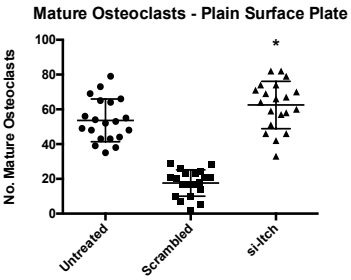
Mature Osteoclasts - Plain Surface Plate
No. Mature Osteoclasts
100
80
60
40
20
0
*
Untreated
Scrambled
si-Itch

G.

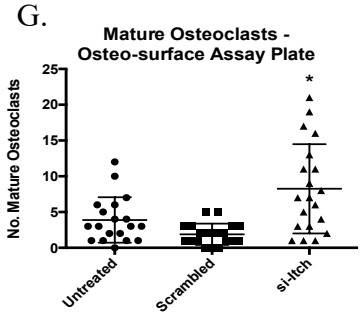
Mature Osteoclasts -
Osteo-surface Assay Plate
No. Mature Osteoclasts
25
20
15
10
5
0
*
Untreated
Scrambled
si-Itch

H.

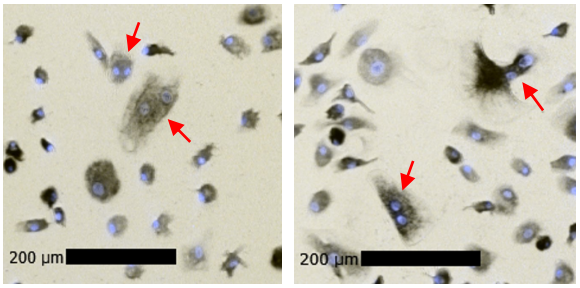
200 µm
200 µm

I.

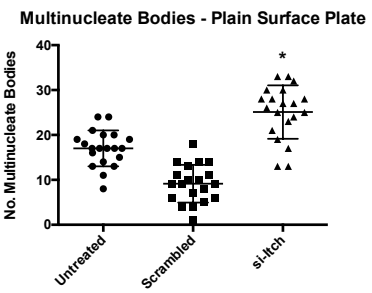
Multinucleate Bodies - Plain Surface Plate
No. Multinucleate Bodies
40
30
20
10
0
*
Untreated
Scrambled
si-Itch

Figure 30: Knockdown of Itch in primary human monocytes increases osteoclast differentiation ex-vivo:

(A.) Osteoclast formation in 96-well plates was verified by TRAP staining for each test condition and imaged under a light microscope (10x magnification); untreated (left), scrambled (middle) and si-Itch (right). After TRAP staining of plates, automated cytometry analysis (Celigo) was used to count $TRAP^+$ cells. Image **B.** shows a section of a well before (left) and after (right) the algorithm was applied, highlighting positive hits in green. This algorithm was then applied to the plain surface plate (**C.**) and the osteo-surface assay plate (**D.**). The difference in mean number of $TRAP^+$ cells between si-Itch and untreated wells was found to be statistically significant in the osteo-surface plate ($p = 0.0048$). Similar algorithm was designed for identification of mature osteoclasts (**E.**). Once again this was applied to both plate types of plate (**F.** and **G.**) and the difference in mean number of mature osteoclasts between si-Itch treated and untreated wells was found to be significant in both plain and osteo-surface plates ($p = 0.0376$ and $p = 0.0099$ respectively). Nuclei of cells on the plain surface plate were stained with Hoechst 33342 (**H.**) to identify multinucleate bodies (red arrows) which were counted for each well (**I.**). Statistically significant difference in mean number of multinucleate cells was seen between untreated and si-Itch treated wells ($p < 0.0001$). Statistically significant difference in means was calculated using Student's t-test.

Discussion:

The aim of this part of the project was to confirm that silencing *Itch* facilitates osteoclast differentiation and function and see whether or not the phenotype in primary human monocytes mirrors what is seen in *Itch*-/- mice (Li et al., 2017; Zhang et al., 2013) whilst also being a more translatable model system.

PBMCs were isolated and cultured from whole blood samples. Any residual T-cells or B-cells that also would have been in the buffy coat would be washed out with media changes as they are non-adherent. Furthermore M-CSF containing media specifically promotes differentiation of monocytes into osteoclast precursors (Marino et al., 2014), meaning that it would be unlikely that any residual T-cells would undergo activation and clonal expansion as the culture conditions lacked critical cytokines for these processes.

Itch knockdown facilitates differentiation of osteoclasts from primary human PBMCs:

After standardising and adapting a protocol for cell culture of PBMCs and their differentiation into osteoclasts, PBMCs were subject to gene silencing techniques to assess the physiological consequences of an *Itch* knockdown. Whilst transient siRNA-mediated silencing was successful, monocytes were refractory to the lentiviral based CRISPR stable knockdown approach. Western blot and qPCR techniques confirmed silencing of Itch at both the protein and mRNA level in siRNA-treated cells. Unlike what was observed with pancreatic cancer cell lines, siRNA-mediated silencing of *Itch* did not affect the survivability of monocytes in-vitro as indicated from the confluence data. If desired this could be re-affirmed using SRB however this would not allow subsequent differentiation-based

experiments. Furthermore, it was observed that lipofection induced toxicity in the si-Scr treated monocytes which was absent in si-Itch treated cells indicating Itch knockdown might be protective against said toxicity. Silencing of *Itch* by siRNA in monocytes and premature osteoclasts increased there ability to differentiate into mature osteoclasts, as indicated by the increased number of multinucleate, $TRAP^+$ bodies present in 96-well plates (Figure 30). The software used was limited in that it was unable to distinguish multiple individual nuclei within a single body. In an ideal scenario one would be able to create an alternative algorithm that would be able to combine recordings of large cellular bodies with multinucleate bodies to get a more absolute number for osteoclastogenesis.

Cellular mechanism for the role of *Itch* in osteoclast differentiation:

Overall these results not only support previous in-vivo and in-vitro data performed in/from mice (wt or *Itch-/-*) but also confirms that the mechanism by which *Itch* effects osteoclastogenisis is also translatable to humans. This opens up an exciting avenue of possible treatment strategies in diseases caused by, or are associated with, dysregulation of bone remodelling for example rheumatoid arthritis and osteoporosis. This aspect of the project also describes a repeatable, robust, and efficient method of siRNA-mediated gene silencing of primary human monocytes for experimentation ex-vivo. Although a small amount of cytotoxicity was observed in scrambled-treated cells, likely due to the transfection method used, there is room for further optimisation to limit further cytotoxicity (for example by comparing different transfection strategies such as electroporation or nanoparticle-mediated delivery).

In an adult organism, upregulation of proteins associated with increased osteoclastogenesis or osteoblastogenesis is usually due to localised inflammation causing persistent NF-κB signalling (Liu et al., 2017; Zhang et al., 2013). In the case of osteoclasts, TRAF6 is required to transduce RANKL/RANK signalling to promote NF-κB transcriptional activation. Although Itch normally acts to regulate the immune response and inflammatory signalling pathways, in this series of experiments there is a lack of external inflammatory agents, with the only additional cytokines being M-CSF and RANKL with the activity of siRNA being intracellular. This reinforces the fact that the action of Itch in regulating osteoclastogenesis specifically, is intrinsic in monocytes rather than strictly extrinsic. To promote NF-κB transcriptional activity, TRAF6 polyubiquitinates itself subsequent to RANKL signal transduction (Lamothe et al., 2007; Zhang et al., 2013). Deactivation of TRAF6 results from a complex formed from Itch and CYLD, a deubiquitinating enzyme (DUB), which acts to remove Ub from activated TRAF6 (Jin et al., 2008). Although this aspect of the project is consistent with the hypothesis that Itch inhibits osteoclast differentiation via inhibition of TRAF6, no steps were taken to completely validate that this mechanism. As there is no evidence to suggest changes in transcription of *CYLD* and *TRAF6* genes in osteoclastogenesis, quantification of mRNA may not be the best approach. Likewise, strictly looking at protein levels may not yield conclusive results in this investigation as whilst levels of Itch change (due to the addition of siRNA) the suggested mechanism involving CYLD and TRAF6 does not involve proteasomal degradation. However, one could look at the levels of polyubiquitinated TRAF6: Zhang's group used the DUB inhibitor N-ethylmaleimide (Emmerich & Cohen, 2015) to block the action of CYLD before enriching for ubiquitinated proteins through a pull-down assay and labelling with an anti-TRAF6 antibody (Zhang et al., 2013). Furthermore, one could attempt to immunoprecipitate CYLD, TRAF6 and Itch in the presence and absence of Itch-targeting siRNA to confirm their interaction (although this does not allow assessment of protein ubiquitination). Whilst targeting Itch directly may seem like

the most attractive strategy for treatment of bone-remodelling dysregulation, Itch has several target substrates and chaperone proteins which may cause off-target activity and side-effects in an in-vivo setting. To achieve a higher degree of on-target activity in this context, a more appropriate strategy may be to modulate TRAF6 signalling or CYLD DUB activity in aims to regulate osteoclastogenesis more specifically.

Effect of lipofection on well confluence and cell survivability:

An interesting observation was the effect the transfection had on average well confluence for each plate. For the plain-surface plate, the wells treated with scrambled siRNA showed a significant decrease in well confluence (Figure 29: A.) which potentially carried over into the TRAP staining data (Figure 30: C.). Meanwhile wells that underwent *Itch* knockdown had similar confluence levels and $TRAP^{+}$ objects to the untreated controls (Figure 29: A. & Figure 30: C. respectively) but having a significantly higher number of mature osteoclasts (Figure 30: F. & I.). One of the possibilities for this difference seen the respective treatment regimens is that lipofectamine confers a certain degree of toxicity to PBMCs/immature osteoclasts, as cytotoxicity due to lipofection has been reported before (Barreau et al., 2006; Zhang et al., 2007). It could be reasonable to think that therefore *Itch* knockdown prevents this apparent lipofectamine toxicity however it is also possible that since the si-Itch treated wells showed higher numbers of more mature osteoclasts, which morphologically are larger and more spread-out (large cell bodies with more finger-like cellular processes protruding from the cell), that those wells would also have greater confluence as they occupy more space. Looking at the cells under a microscope after TRAP staining (Figure 30: A.) showed that si-Itch treated wells had more terminally differentiated cells compared to other wells (pictures taken from plain surface plate). Whether or not the si-Itch treated wells actually had the same number of surviving cells compared to untreated wells would be difficult to assess with the methods used in this project mainly due to the fusion of cells to form mature osteoclasts. One could attempt to count the total number of nuclei as a surrogate for the number of surviving cells at the end of the treatment regimen however, Celigo is unable to distinguish multiple individual nuclei within the same cellular body as separate entities, hence why multinucleate bodies were counted manually after staining and scanning. On the other hand, the effect of treatment on confluence was not seen in the osteo-plate (Figure 29: B.) where all three test conditions had similar degrees of confluence. Furthermore whilst average well confluence for untreated and si-Itch wells was roughly 10% lower in the osteo-plate compared to the plain-surface plate (Figure 29: C.), the average well confluence for the scrambled regimen between both plate types was not significantly different ($\mu = 23.5$ and 21.3 for plain and osteo-plates respectively). Previous literature has reported that osteoclasts cultured on dentine promoted cell survival (Zhang et al., 2013); a similar effect might be taking place with the osteo-plate providing pro-survival factors to seeded cells.

Future optimisation of stable knockdowns in PBMCs:

A difficulty in this investigation was achieving sufficient cell numbers for culture and experimentation. When cultured, numbers of PBMCs do not increase as they cannot divide (van Furth, Raeburn, & van Zwet, 1979). This meant that at the point of seeding onto a surface, monocyte numbers could only decrease; be that due to failure to attach or cell death. One of the challenges in culturing osteoclasts was ensuring sufficient initial cell-densities so that individual pre-osteoclasts could fuse without overpopulating the plates/wells and starving cells of nutrients and/or cytokines.

The obstacle of numbers was perhaps more exaggerated in the attempted CRISPR knockdown: Lentiviral transduction of both scrambled and Itch-targeting sgRNA's with Cas9 caused a significant degree of cell death (Figure 28). The plasmid pLentiCRISPRv2 contains a puromycin selection marker to allowing one to isolate CRISPR^{+} cells (Sanjana et al., 2014) upon addition to culture media. Although the precise mechanism of puromycin's action on prokaryotes and eukaryotes is poorly understood, it is known to interfere with the translation of mRNA to protein (Azzam & Algranati, 1973). To test this to see if addition of puromycin was the cause of the observed apoptotic phenotype, the same concentration was added to untreated PBMCs to see if a similar result was obtained. Although there was a drop in cell number (as expected as the cells did not have the resistance gene), the phenotype was not that of what was seen for the CRISPR-treated cells: dead cells had completely detached (not shown) as opposed to leaving behind what appeared to be a monocyte "husk" which still appeared attached to the cell-culture surface. Furthermore, surviving cells appeared morphologically normal, therefore the phenotype observed for CRISPR-treated cells was likely not due to the addition of puromycin to culture media.

Another possibility is that lentiviral transduction of CRISPR-Cas9 is toxic to monocytes. Previous retroviral gene editing techniques could only work on mitotically active cells (Miller, Adam, & Miller, 1990). The advantage of using HIV-1-derived lentiviral transduction methods is the ability to integrate and edit quiescent cells and thus expand the pool of editable cell lines (Naldini et al., 1996). Although initially this seems to suggest that pLentiCRISPRv2 should be able to silence gene activity in PBMCs, previous work on PBMCs and lentiviral constructs have shown that they are resistant to HIV-1 lentiviral transduction vectors and that it led to an increased cellular toxicity (Mühlebach et al., 2005; Neil et al., 2001; Sirven et al., 2002), however the nature of observed toxicity is not described in the literature. Despite this small lack of clarity, it is far more likely that the cell-death phenotype observed in this investigation is likely due to toxicity caused by the lentiviral vector as opposed to puromycin. Although it has been observed that derivatives of monocytes can be transduced, it is unknown whether osteoclasts specifically can be transduced. Additionally, for the purposes of this series of experiments gene silencing of Itch post-differentiation would not assist in the experimental aims of the project (i.e. whether or not Itch knockdown effects osteoclast differentiation).

In order to generate a stable *Itch* knockdown in PBMCs and their derivatives therefore requires a different approach, most notably a different vector. Cas-9 should still be able to induce guide-mediated double stranded breaks which result in silencing of the target gene provided it can get into the cell and translocate to the nucleus. Potential problems with stable gene-editing technologies such as CRISPR, TALENs, and ZFNs in PBMCs start to become apparent when it comes to identification and enrichment of edited cells for downstream applications. For the generation of mature osteoclasts, a relatively high cell-density of pre-osteoclasts (and by association monocytes) is required so that cells close enough to each other to be able to fuse together to form large multinucleate cells. This makes gene editing techniques that rely on some form of selection pressure (antibiotic resistance genes) or cell sorting (i.e. FACS) to get an enriched culture of edited cells problematic due to the potential loss of un-edited cells. To re-establish a suitable cell density to promote the fusion of premature osteoclasts, cells that have successfully incorporated the edit would likely have to be re-seeded. Although in this series of experiments with transient siRNA no method of determining how many PBMCs taking up the siRNA was used (e.g. fluorescent labelling of RNAs), the fact that a ~75% reduction in *Itch* protein and 80% reduction in *Itch* mRNA was

recorded in a culture of non-dividing cells indicates a high level of transfection efficiency (Figure 27).

An alternative method of silencing *Itch* in PBMCs and osteoclasts would be through the use of small-hairpin-RNA (shRNA). shRNA knockdown involves transfection of cells with a plasmid that can be transcribed in the nucleus by RNA polymerase II/III (without needing to integrate into the host genome) to produce premature gene-targeting shRNAs (Rao et al., 2009). These are then processed like naturally produced microRNAs (miRNA) by Dicer in the cytoplasm before being incorporated into RISC to cleave target mRNAs. shRNA approaches are considered long-lasting compared to traditional siRNA-mediated knockdown methods as the plasmid persists in the transfected cell. Usually shRNA begins to lose its effect when cells divide as the plasmid is not passed on to daughter cells. Over time the silencing effect gets diluted until non-significance compared to wild-type cells. However this would not be an issue in non-dividing cells like PBMCs: due to lack of cell division the longevity of the gene-silencing effect from shRNA would appear stable provided successful transfection and continuous translation of the plasmid. Furthermore plasmids can be engineered to express a marker or reporter gene to confirm uptake and transcription of the plasmid in addition to using western/qPCR to analyse knockdown efficiency (Hong, Zhang, & Cai, 2010). On the other hand, despite siRNA-mediated gene silencing being transient, there is evidence that it can be very long-lasting in quiescent cell-lines as the silencing effect is not diluted upon cell division (Omi et al., 2004; Song et al., 2003).

Assessment of *Itch* knockdown on osteoclast bone-resorptive activity:

Several studies have reported functional assessment of osteoclasts (i.e. resorption of bone matrix) through the use of dentine discs (Henriksen et al., 2012; Marino et al., 2014). These provide a suitable bone-matrix-like substrate that can be cut to specific sizes for cellular assays. Upon distribution of PBMCs onto these discs and differentiation into osteoclasts, their function can be characterised by the formation of "pits" in the dentine due to resorptive activity. Number of pits formed or size of pits can then be used to quantify osteoclast resorptive activity. As a substitute for dentine discs, this project used Corning Osteo-Assay Surface plates: cell culture plates coated with an artificial bone matrix in each well (Rao et al., 2010). To test the hypothesis that *Itch* knockdown increases the resorptive function of osteoclasts, PBMCs were plated onto osteo-plates in parallel with the other experiments. Whilst growth and differentiation was uncompromised between the two types of plates (Mean total well confluence only differed by a maximum of 10% across all conditions – Figure confluence), there was significant loss of cells when it came to staining the wells for TRAP activity, as indicated by the large difference in $TRAP^{+}$ bodies between the osteo-surface and plain-surface plate (Figure 30: A.).

To determine whether or not this was due to technical error during the TRAP staining process or if there is an underlying physiological/cellular mechanism that could cause this apparent loss of cells, both plates were re-analysed with the confluence algorithm post-TRAP staining. In the plain surface plate mean confluence remained unchanged post-TRAP staining regardless of whether the wells had been treated with scrambled siRNA, *Itch*-targeting siRNA, or left untreated (Supplementary Figure 7: A.). However, in the osteo-surface plate confluence of wells post-TRAP staining decreased by over 50% across all three treatment regimens (Supplementary Figure 7: B.) compared to mean well confluence prior to TRAP staining. As both plates were fixed and TRAP-stained in parallel (using the same reagents and protocol) and since the results show no significant change in well confluence in the plain-surface plate caused by this process, one can conclude from the data that osteoclasts are less

adherent to the osteo-surface plate. Furthermore, the fact that there was a ~10% difference in average well confluence in untreated and si-Itch treated wells between the two plate types prior to TRAP staining (Figure 29: C.) further supports the argument that cells are less adherent to the osteo-surface plate. Since there was no difference seen for scrambled wells one can rule-out the possibility that passaging cells onto the osteo plate inhibits cell survival: if this were the case then the cytotoxic effect seen with the scrambled treatment in the plain-surface plate would be additive with any cytotoxic effect that passaging onto the osteo-surface plate would cause thereby decreasing confluence further. This evidence also supports the idea that the osteo-surface may promote cell-survival of attached cells similar to what has been reported with dentine (Zhang et al., 2013).

To perform their function effectively, mature osteoclasts need the combined excretory machinery of many cells to maintain an acidic environment between the osteoclast and bone matrix against a steep concentration gradient (Väänänen et al., 2000). When the bone-resorption process begins, a "sealing zone" is made around the periphery of the osteoclast, leaving a pocket of space to allow the resorbing osteoclast to secrete hydrogen ions and digestive enzymes. One could argue that during this experiment if osteoclasts were actively resorbing the synthetic bone matrix of the osteo-surface plates then adherence to the plate may be weaker than for a regular tissue culture surface as physical attachments are only made at the cells periphery as opposed to throughout the cell body (however formation and degradation of podosomes is a dynamic process). On the other hand, attachment to bone tissue via the sealing zone when actively resorbing tissue needs to be strong as it is important that there is no leakage of hydrogen ions or resorptive enzymes into the extracellular space (Väänänen et al., 2000). Therefore, it is difficult to predict any differences in attachment strength of functionally-active and passive osteoclasts and by extension whether the change in confluence seen pre- and post- TRAP staining in the osteo-surface plate is simply due to it being less adherent without further experimentation. If osteoclasts were actively resorbing the synthetic bone then one would suspect that the resorption pits would still be visible. Wells were washed with a 10% bleach solution as per the protocol described in the literature to remove cells and visualise any pits formed from actively-resorbing osteoclasts (Rao et al., 2010). Unfortunately, when viewed under a light microscope, no pits were observed.

Chapter 6 – Discussion:

Itch is a HECT domain-containing E3 ubiquitin ligase that was originally shown to play an important role in the regulation of the immune system, but has a role in bone formation and in processing several proteins implicated in cancer. This project examined the potential role of Itch in cancer progression and bone remodelling processes as well as critically evaluating different gene-editing techniques within specific experimental contexts.

siRNA-mediated transient knockdown of *Itch* in MiaPaCa-2 and Capan-2 pancreatic cell lines inhibited cell survival significantly independent of any subsequent form of treatment based on resultant OD values from SRB assays. Combination of siRNA-mediated knockdown with chemotherapy or radiotherapy had an additive, rather than amplified, effect on cell death: this was evident from the fact that whilst cell survivability continued to decrease, the normalised response to irradiation, doxorubicin, or gemcitabine remained unchanged compared to controls. Treatment of cells with a scrambled siRNA control had no effect on cell survival (although a minor increase in cell death is seen with repeated lipofection over a short timeframe) indicating that any change in SRB data was solely due to silencing *Itch*.

Following the positive results seen with transient *Itch* knockdown, CRISPR-mediated stable *Itch* knockdowns were generated in MiaPaCa-2 and Capan-2 cells. However stable knockdown of *Itch* did not produce the same results under similar experimental conditions: Whilst the stable knockdown did increase the sensitivity of the cell lines to chemo-/radiotherapy, little-to-no significant difference was seen in the resultant dose-response of either cell lines with evidence to suggest that edited cells may be more clonogenic. It was hypothesised that cells CRISPR$^+$ cells had adapted to the irreversible, long-term loss of *Itch* function which granted a survival advantage compared to scrambled or parental cells. This presents a potential weakness and caveat for the interpretation of data generated from stable knockouts. SWATH MS was used to screen parental and CRISPR$^+$ cells for any differences in proteome that could clarify the observed difference in response. Through analysis of individual clones 5 candidate proteins were either upregulated or downregulated at basal levels compared parental controls. Unfortunately, due to the lack of necessary replicates, this analysis was not robust enough and did not yield enough proteomic differences for any conclusions to be made or pathway analysis to be performed.

It was hypothesised that silencing *Itch* expression in primary human PBMCs increases there ability to differentiate into osteoclasts. Although stable *Itch* knockdown could not be achieved in primary human monocytes, siRNA-mediated transient *Itch* knockdown was confirmed in PBMCs validated by both qPCR and western blot. A series of in-vitro assays confirmed that cells treated with *Itch*-targeting siRNA formed more mature osteoclasts in-vitro.

Targeting Itch as a therapeutic strategy:

In the case of anticancer therapeutics, the fact that transient *Itch* knockdown decreased cell survival and was even synergistic with chemo-/radiotherapy is an exciting prospect as the gene now presents itself as a possible druggable target for small molecule inhibitors. Studies have already shown that *Itch* is upregulated in pancreatic, breast and chronic lymphocytic leukaemia (Luo et al., 2016; Salah et al., 2014; Sampath et al., 2009) and a crystal structure for Itch protein in its inactive/closed state has been resolved (Zhu et al., 2017). Although a crystal structure of active/open Itch has not been determined yet, which could potentially enhance our ability to develop small molecules that specifically block the HECT domain (i.e. the catalytically active site), an alternative biochemical approach for inhibiting Itch utilising the closed structure data could be achieved through blocking the association of adaptor molecules like Ndfip or the phosphorylation sites targeted by proteins such as JNK-1 (Gallagher et al., 2006; Oliver et al., 2006; Zhu et al., 2017). This approach would lock Itch in its inactive state, preventing transthiolation, and ubiquitination of target substrates whilst not effecting *Itch* translational activity. Avoiding inhibition of the HECT domain may also be desirable so as to not exhibit any off-target activity with other HECT domain E3 ligases which could have unpredictable consequences (Fajner, Maspero, & Polo, 2017; Sluimer & Distel, 2018).

Targeting Itch E3 ligase activity may also be a viable therapeutic strategy in the treatment of osteolytic diseases such as arthritis and osteoporosis as well. However, contrary to what would be desired in the treatment of cancer tissue, in this case one would want to increase Itch signalling, specifically in localised areas worst affected by resorptive osteoclast activity. Itch inhibits the formation of both osteoclasts and osteoblasts (Li et al., 2017; Zhang & Xing, 2013), cells with antagonistic functions in balancing the bone remodelling process. This poses a potential issue in specifically targeting one subset of cells in-vivo as both osteoclasts and osteoblasts, despite being derived from different precursors (hematopoietic and myeloid stem cells respectively), differentiation occurs within the same stem-cell niche (Ikeda & Takeshita, 2016). However in the context of age-related disease this may not be a problem: both osteogenesis and osteoclastogenesis is reduced with age in both rodents and humans (Almeida, 2012; Becerikli et al., 2017) meaning bone remodelling and healing processes are reduced in older individuals. As the generation of healthy bone tissue requires the activity of both cell types, upregulating *Itch* signalling in the bone marrow stem-cell niche may be an effective method of preventing weakening of bone tissue, age-related fracture incidences, and facilitating bone healing.

One question in regards to targeting *Itch* as a therapeutic strategy is what effect it could have on the immune system. In *Itch*-/- mice and humans the dominant phenotype is severe autoimmunity (Aki et al., 2018.; Lohr et al., 2010; Perry et al., 1998) therefore could downregulation of *Itch* in mouse models or patients cause a similar phenotype? Although autoimmunity associated with lack of *Itch* is discouraging, this phenotype could solely be due to problems during development of an organism when functional copies of *Itch* are not present. *Itch* is important for regulating key pathways linked to the differentiation of specific immune cell lineages (Aki et al., 2018; Fang et al., 2002; Theivanthiran et al., 2015; Venuprasad et al., 2015) as well as genes involved with foetal development such as Notch and Oct-4 (Chastagner, Israël, & Brou, 2008; Liao et al., 2013; Qiu et al., 2000). But there is little evidence as to the effect of transient Itch knockdown, or temporarily inhibiting Itch

function, in regard to the effect on immunity on a fully developed organism. Although the study by De La Fuente's group showed that inhibiting *Itch* activity in xenograft mice inhibits cancer progression with negligible toxicity, these mice were immunocompromised to allow the graft to take place without inducing an innate immune response and rejecting the transplanted cells (de la Fuente et al., 2015). Additionally, no study has yet been performed to observe the long-term consequences of an induced *Itch* knockout after development. Taking all the above points together it is still unclear to determine the safety of an Itch inhibition therapeutic strategy with regards to its effect on host immunity.

Previous literature has identified several substrates of Itch E3 ligase activity that are linked to cancer development and progression including p73, LATS, TXNIP, and Smad-7 (Hansen et al., 2007; Ho et al., 2011; Levy et al., 2007; Liu et al., 2016; Park et al., 2015). It is therefore difficult to completely characterise which substrates or molecular pathways are responsible for eliciting the recorded response of increased cell death in pancreatic cell lines or whether it is more due to the combination therapy. Further work is required to better understand and elicit possible changes in gene expression and proteome before developing any Itch-targeted therapy. However, in terms of treating cancer, the fact that Itch knockdown/inhibition could have a very wide-spread impact on cellular signalling pathways may be an advantage as it increases the number of potential synthetic-lethal interactions.

It is also unknown as to whether inhibiting *Itch* in healthy cells could cause unwanted toxicity and cell death as is seen in cancer cell lines in-vitro and in-vivo. One of the main safety concerns during translational experiments is possible side-effects due to possible off-target activity of the treatment in question. Although several steps during the are usually taken to limit off-target activity and its associated effects, reaction with healthy tissue is almost an inevitability.

Linking cancer, bone, and *Itch* - cancer-associated osteolysis:

One question presented by this project is can both *Itch*'s effect on cancer progression and bone progression interplay with each other in a more physiological setting? Osteolysis is another term given to active bone resorption by osteoclasts and can sometimes be associated with tumour metastasis, notably in breast and prostate cancer (Goltzman, 2001; Lemma et al., 2017; Marino et al., 2019). Diseased cells which metastasise to bone tissue often release factors that promote osteoclastogeneis for example growth factors, cytokines and a soluble form of RANKL (Goltzman, 2001) whilst inhibiting release of OTP from osteoblasts. This causes increased localised differentiation of osteoclasts from monocytes, thus increasing osteolysis. Although it may seem that manipulating Itch E3 ligase activity may, in the above context, have an effect on cancer-associated osteolysis it is difficult to determine what the overall effect would be. Localised genetic knockdown of *Itch* may decrease cell survivability of any metastasised cells and thus prevent the release of osteoclastogenic factors from cancer cells. On the other hand, we have also shown that knockdown of Itch increases the ability of monocytes to differentiate into osteoclasts, most likely due to persistent TRAF6 ubiquitination. This could mean that even though there would be a reduction in osteoclastogenic factors from any metastasised tumour cells, osteolysis could persist due to increased numbers of mature osteoclasts from precursors. Another important point to consider however is that *Itch* also regulates osteoblast numbers (Zhang & Xing, 2013). If the ratio of osteoblasts to osteoclasts was maintained (and/or if the rate of differentiation) and the ratio of OTP and RANKL was the same, then there may not be any net-difference in bone remodelling. However as mesenchymal stem cells are usually located in bone marrow,

application of any Itch-targeting therapy may be difficult to achieve all the desired effects on all three cell types.

Synthetic Lethality

The hopeful outcome of *Itch* knockdown on cancer cell lines is akin to synthetic lethality i.e. the concept that knockout/knockdown of two genes results in cell death (or growth impairment in regards to synthetic sickness but this is often grouped with synthetic lethality) but loss of function in just one of either gene does not. Synthetic lethality was a concept initially observed by Bridges in *Drosophila melanogasta* (Bridges., 1922) but the term "synthetic lethality," was not coined until a few years later. One of the first instances of genes discovered to be synthetic-lethal in *Drosophila* was the eye pigment genes *deep orange* (*dor*) and *rosy* (*ry*) (Luchessi., 1967). Further advances in synthetic lethality were done in yeast which lead to the development of synthetic lethality screens. One such screen called a synthetic genetic array (SGA) involves crossing a mutant of interest with random mutants plated in wells, looking for synthetic lethal phenotypes (Tong et al., 2001). Another example is synthetic lethal analysis by microarray (SLAM), which is similar to SGA except microarrays, rather than plates, are used to compare the genotype of a transformed and control yeast knockout pool (Ooi, Shoemaker, & Boeke, 2003). Synthetic lethality provides a good framework for the discovery of novel anticancer therapeutics: Where cancer cells are mutant for a specific gene one can perform a screen to look for any potential synthetic lethal interactions; this can be done either through a small molecule screen or a genome-wide knockdown. Treatment based on synthetic lethal genetic interactions can preferentially kill the cells of interest as healthy cells will have only one of two (or several) genes impacted by the treatment regimen and will therefore not yield the genetic lethal phenotype. Synthetic lethal/drug screens also give valuable insight into the molecular mechanisms of cellular pathways, identifying upstream and/or downstream components that were previously unknown. *ataxia telangiectasia and Rad3 related* (*ATR*) is a DNA damage response (DDR) gene that many cancers rely on to cope with oncogenic stress (Bartek, Bartkova, & Lukas, 2007) which was found to be synthetically lethal with various other genes involved in DDR and cell-cycle progression such as *p53*, *ERCC1* and *ATM* (Mohni, Kavanaugh, & Cortez, 2014; Reaper et al., 2011). *ATR* inhibition, either by small molecule treatment or RNA interference (RNAi), is therefore a strong area of interest in terms of anticancer therapy, being shown to be synergistic with gemcitabine in treating pancreatic tumours (Fokas et al., 2012; Mohni et al., 2015) and has gone into phase I clinical trials.

Future direction/experiments:

3D cell culture – a more accurate model of the tumour microenvironment:

For an Itch-targeted therapeutic strategy is to be pursued then it would be necessary to perform further experiments using 3D cell culture. All the experiments performed during this project were all performed within the context of a 2D environment in that cells were cultured and manipulated on flat surfaces. However, this is not necessarily completely representative of disease in-vivo where the tumour grows in a complex 3D microenvironment where additional factors such as vascularisation, immune-interactions, and extracellular matrix (ECM) play large roles in disease progression. In the pancreatic cell line 2D experiments, drugs or any other form of therapy could achieve fairly uniform distribution throughout the entire cell population. However in 3D culture the outermost, proliferative population of cells

is more exposed to any treatment regimen (Jamieson, Harrison, & Campbell, 2015). Treatment methods need to therefore be adapted and/or optimised so that they are able to penetrate to the innermost cells (i.e. the "tumour core"), a feature that would be important to prevent recurrence in a clinical setting.

Multicellular tumour spheroids (MTS) can be developed in a research environment from cell lines to more accurately model 3D tumour architecture and better elicit drug response in-vitro. Previous studies have already noted disparities in the dose-response of cell-lines to several different therapeutics when grown in 3D vs 2D (Melissaridou et al., 2019; Patra et al., 2016; Souza et al., 2018) indicating that bioavailability is a significant factor in assessing the effectiveness of potential therapies. Difference in drug sensitivity could also be attributed to differences in the global gene expression of cells cultured in 3D compared to 2D: Changes in gene expression in 2D cells in generally uniform across the population of cells being tested however, cells grown in 3D show variable expression of specific biomarkers, e.g. stem cell markers, depending on there localisation within the MTS (Jamieson et al., 2015; Melissaridou et al., 2019; Souza et al., 2018).

In contrast to standard 2D cell culture, 3D culturing requires conditions to be that cells preferentially adhere to each other rather than to any culture surface and gradually form MTS'. This can be achieved through a variety of methods however a couple of the more popular examples are the use of either a spinner flask or an ultra-low attachment (ULA) plate. Spinner flasks rely on a magnetically-generated current to maintain constant agitation of cells in media so they cannot form attachments with the flask itself: whilst this is a relatively simple way to get lots of spheroids relatively quickly, the size of multiple MTS' is generally inconsistent and the speed of the flasks needs to be monitored and adjusted over time (as spheroids grow larger, a faster current is needed to prevent them from settling). ULA plates are similar to standard multi-well plates (e.g. 96-well) but surface of each well is coated in a way that prevents cell attachment to the culture surface. Provided that the same number of cells are passaged into each well, MTS' formed in ULA plates should be relatively uniform in size. The main issue with this method is that care needs to be taken when replacing media or applying drug to not accidently aspirate or damage spheroids once they have formed.

Basic dose-response analysis can be extrapolated from changes in spheroid size as growth is limited or as cells die and dissociate from the MTS as their cell-cell attachments weaken. However, this relies on homogenous shape and size of spheroids or precise measurement over multiple time-points to analyse percentage change in size and may be inconsistent between different cell lines due to differences in morphology and/or strength of cell-cell attachments in a normal environment. Melissaridou et.al. assessed clonogenicity and cell viability of cells grown in 3D vs 2D by trypsinising spheroids prior to passaging them onto 12/96 well plates (for clonogenicity and cell viability respectively) (Melissaridou et al., 2019). For cell viability cells were immediately incubated with a commercial fluorescence-based viability assay kit whilst the cells distributed on 12 well plates for assessing clonogenicity were cultured for a further 7 days before crystal violet staining.

Histological or immunological methods can be used to analyse the spatial expression of specific markers within the spheroid as a whole including markers associated with apoptosis, necrosis, hypoxia, and the immune response after fixing and embedding spheroids in paraffin. Additionally, to analyse protein or mRNA by western blot and qPCR respectively, spheroids can be dissociated to create spheroid lysates at the end of the culture period.

Flow cytometry could be a powerful technique for comparative studies of cells grown in 2D vs 3D (Patra et al., 2016). Flow cytometry is able to quantify different molecular and physiological characteristics on a cell-by-cell basis through identification of cell-surface antigens, fluorescent markers (through gene editing or an assay kit that relies on cellular machinery), or cellular staining (e.g. DAPI). differential response to treatment regimens can be readily characterised between cells cultured in 2D and 3D (albeit after spheroid dissociation). In the case of a cytotoxicity assay for example, although it would be difficult to ensure that the number of cells between 2D and 3D culture entering a flow cytometer would be the same, one could measure the proportion of cells that exhibited a specific response to clarify any difference between the two culture techniques. The main limitation of the use of flow cytometry is that a lot of cells are required which means several technical replicate spheroids may be needed for a single experiment. In the study the group circumvented this issue with a microfluidics chamber that could culture 5000 uniformly sized spheroids simultaneously (Patra et al., 2016).

In the context of this project performing gene-edits and assessing the effect of *Itch* knockdown on spheroids adds an additional layer of experimental complexity. If silencing *Itch* decreases cell survivability, as seen in the data in this project, then will it affect the cells' ability to form spheroids for downstream applications. Obviously the effect of *Itch* knockdown on the ability of cells to form spheroids could be an experiment itself: siRNA-mediated transient *Itch* knockdown could be performed prior to passaging cells onto a ULA plate, ability of spheroid formation could then simply be characterised by average spheroid diameter (as an indicator for overall size) under a microscope with image analysis software. If however, genetic knockdown of *Itch* does influence MTS size and thus spheroid formation then in any subsequent comparative cytotoxicity studies transient knockdown would have to be performed after initial formation of spheroids as one would ideally want to begin with MTS' of uniform size. Previously there have been no successful accounts of siRNA-mediated transient gene knockdown of spheroids in-situ. One study however identified that a simple modification to standard 2D transfection protocol overcame this ongoing issue in 3D transfection: they found that use of 10% serum media increased siRNA entry in spheroids as opposed to serum-free OptiMEM that is typically used in for 2D siRNA transfection (Morgan et al., 2018). The exact mechanism of this phenomena is unknown and is interesting as it is the complete opposite of what you see in a 2D context (serum-containing media is ineffective for transfecting cells in 2D culture). Although it was observed that in colorectal cell lines LS174T and SW1463 there was a transient mRNA knockdown of *CTNNB1* (the gene that encodes β-catenin), there was no noticeable decrease in protein. However this may be due to fact that β-catenin has a relatively long half-life particularly in cancer cell lines with upregulated Wnt signalling (Kirschner et al., 2000). If siRNA-mediated transient knockdown of mRNA and protein reduction can be confirmed in MTS' then any of methods of measuring and comparing cytotoxicity in 2D and 3D can be applied. However, if not then an alternative knockdown approach would be required.

shRNA and CRISPR-Cas9 gene editing protocols in 3D spheroids and organoids are effective and well established (Koo, Sasselli, & Clevers, 2013; Matano et al., 2015). However, this approach typically involves the performing transfection/transduction in a 2D context then forming (or re-forming of secondary MTS'/organoids after primary dissociation in some cases) new 3D structures. Although it is unknown how efficient update and efficiency of shRNA/CRISPR in MTS'/organoids would be in-situ, in the context of the experiments being performed in this project the aforementioned method of forming MTS' post-gene edit may be more suitable. However as previously discussed, this line of experiments would best be

performed using an inducible knockdown/knockout system as spheroids grown from IKO1a cells may be drastically different in phenotype and response compared to those that experience a sudden loss of *Itch*. One could transfect/transduce parental cell lines with a plasmid/viral construct designed to mediate gene silencing of *Itch* under the control of a specific stimulus. After application of said stimulus, efficiency of silencing would need to be assessed once again before moving on to any downstream assays. The issue then becomes the ability of the stimulus to penetrate deep enough into the MTS to activate gene-silencing machinery, be it shRNA- or Cas-mediated. Whilst MTS' provide a more representative view of tumour microenvironment and are an overall better in-vitro model over 2D monolayer cultures, there are still significant areas that are lacking compared to a living organism which will have many more complex barriers to overcome in terms of translational therapeutics.

Gene-editing technologies and modern clinical application - overcoming hurdles in translational medicine:

Gene-therapy for treatment of disease is an attractive prospect due to increased specificity compared to drug treatments as well as the having the possibility to target multiple genes within a single application (Bumcrot et al., 2006; Mansoori et al., 2014). Furthermore gene-editing strategies combined with existing drug regimens have the potential for overcoming resistance mechanisms employed by bacteria and cancer cells. However, when discussing the use of genetic manipulation for clinical practice the main factors to consider are whether it is ex-vivo or in-situ, the nature of the edit (transient or stable), efficiency of the system used, and method of delivery.

Ex-vivo gene editing:

Ex-vivo applications of gene therapy presents with fewer complications in terms of patient safety: cells are removed from the patient and edited in the lab, where the correct sequence can then be verified, selected, and expanded before re-introduction into the patient. Stable gene edits are more suited to ex-vivo applications as the modified cells can pass on any changes to daughter cells once re-introduced into the host. Considering the genetic manipulation takes place outside the host, this broadens the range of modification techniques that can be used effectively. Provided accurate verification of the edit being made any of CRISPR, TALEN, shRNA, ZFNs, or viral methods of gene-editing can be used.

As modified cells are recognised as "self" by the hosts immune system it is highly unlikely that an innate immune response will be generated after reintroduction. However, for the very same reason, it is paramount that the modification is verified completely in-vitro through the use of several verification techniques e.g. western blot, qPCR, gene sequencing etc. Obviously different forms of verification would be needed depending on the exact modification being made.

Application of CRISPR in Car-T gene therapy:

One example and recent advancement in the use of ex-vivo genetic manipulation in anticancer therapeutics is the development of Car-T therapy in the treatment of non-solid tumour types such as B-cell acute lymphoblastic leukaemia and non-Hodgkin lymphoma, approved by the FDA in 2017 (Lee & Kim, 2019). Chimeric antigen receptor T cells (or CAR T-cells) are T-cells that have been engineered to express an artificial T-cell receptor that

reprograms their sensitivity and selectivity to more efficiently target tumour tissue (Eyquem et al., 2017; Lee & Kim, 2019; Maus et al., 2013; Newick et al., 2017). T-cells are extracted from the patient and are modified ex-vivo to express a chimeric antigen receptor (CAR). CARs allow T-cells to recognise any cell-surface antigen with high specificity via a single-chain variable fragment derived from an antibody rather than being limited to solely recognising the MHC (major histocompatibility complex).

Since its inception, various labs have been looking into ways to improve and/or adapt CAR-T therapy to increase its efficacy, longevity, or broaden its therapeutic applications. Currently DNA encoding CARs are introduced into the host genome via clinical grade viruses which induces significant cost and concerns of random integration of CAR genes. Roth et.al. employed CRISPR-Cas9 to an insert antigen-targeting CAR into a specific site in the genome through non-viral means (Roth et al., 2018). CRISPR-Cas9 has also been used to simultaneously disrupt the TCR and PDCD1 locus (Ren et al., 2017). Loss of PD-1 (gene product of PDCD1) caused increased antitumour effect in mouse models. Meanwhile the disruption of the TCR complex creates non-alloreactive CAR-T cells (i.e. they do not invoke an innate immune response) allowing the possibility of donor-derived T-cells and preventing graft-versus-host disease (GVHD). In a similar vein, TCR disruption in CAR-T cells has also been achieved through use of TALEN-mediated gene editing (Qasim et al., 2017). These modified cells were then introduced into two infants diagnosed with relapsed refractory CD19+ B cell acute lymphoblastic leukaemia and were found to have remission within 28 days.

Despite these exciting advancements in this technology, CAR-T gene therapy is still limited by the fact that it is only effective in haematological cancers and ineffective or underwhelming in solid tumours, which make up 90% of malignancies (Lee & Kim, 2019; Newick et al., 2017). This is due to several obstacles that solid tumours present that are absent for haematological malignancies namely antigen heterogeneity across different tumour types, tumour microenvironment (TME) hostility, bioavailability, and immune suppression in the TME (Newick et al., 2017). Despite this several groups have already begun attempts to try and circumvent the challenges presented by specific diseases to make CAR-T gene therapy more universal.

In-situ gene editing:

Ex-vivo gene editing is well suited to treatment of diseases where clonal expansion of a single modified cell can produce therapeutically relevant results. This could take the form of modified immune cells (as is the case with Car-T gene therapy) or introduction of cells that can produce healthy protein in a patient that endogenously produces a mutant version (e.g. production of functional CFTR in cystic fibrosis patients). However, there are cases where this approach would not be viable/appropriate, for example in treatment of solid tumours where if gene therapy were to be used it would have to be in-situ. The problem is for in-situ gene editing to become common clinical practice several additional hurdles need to be overcome to ensure effectiveness of treatment and patient safety. As previously discussed, the most likely rationale for genetic manipulation of diseased tissue in-situ is to either correct mutated gDNA or increase its sensitivity to an existing therapeutic (to achieve a pseudo synthetic-lethal affect). However, gene-editing technologies that work within a living organism need to be fulfil the following criteria: they need to be highly specific to diseased tissue with minimal impact on healthy tissue, be able to effectively reach the diseased tissue, and in the case of cancer, be able to penetrate deep enough so as to hit the tumour in its

entirety, and needs to employ a safe yet effective method of delivery that does not invoke the host's innate immune response.

Use of stable gene-editing technologies, such as CRISPR, ZFNs, and TALEN, in this context presents with many potential risks as any cells which take up the edit will be irreversibly changed with genome edits that are also heritable to daughter cells. Whilst with ex-vivo approaches, specific cells are edited and screened outside the patient, with in-situ there is a risk of the gene-editing machinery being introduced into non-target cells which could have unpredictable consequences. Whilst off-target activity is almost non-existent for ZFN- and TALEN-based gene editing (Gaj et al., 2013), previous reports off-target cleavage using CRISPR has been reported extensively (Cradick et al., 2014; Fu et al., 2013; Lin et al., 2014; Ran et al., 2013). Many current projects aiming to improve on this aspect as off-target gDNA cleavage runs the risk of causing random mutagenesis that could have significant clinical consequences. Although ZFNs and TALENs are considered to be lower risk in terms of off-target activity, care would still need to be taken in vector design so as to not transduce/transfect healthy cells with gene-editing machinery.

Transient knockdown of gene function avoids the potential of irreversible genetic changes to healthy tissue, with the associated drawback that several applications may be needed based on the total time-course of the treatment. Transient methods also avoid the possibility of cells adapting to ablation of gene function, as was seen with the experiments in IKO1a cells that lacked functional *Itch*. The results shown in this project demonstrate that, in the case of targeting *Itch*, a more effective therapeutic strategy is to simultaneously knock-down the target gene and apply a synergistic therapeutic. Studies employing transient RNAi-based strategies have been in development for a long time now, achieving positive results (de la Fuente et al., 2015; Judge et al., 2009; Manunta et al., 2013) and several proceeding to clinical trial stages (Chakraborty et al., 2017; Kristen et al., 2019).

Both shRNA and siRNA methods have been used in the aforementioned studies and trials with each having their own associated advantages and disadvantages when compared to the other. shRNAs generally have higher specificity and efficiency over siRNAs as they employ endogenous cellular machinery to generate the RNAi effect; they also have greater longevity as so long as an shRNA plasmid enters the nucleus of a cell it will be continually expressed (Mansoori et al., 2014; Rao et al., 2009). Whilst both siRNAs and shRNA-containing plasmids can induce an interferon response (as introduction of exogenous nucleic material is characteristic of a viral attack) this is less of an issue for shRNA due to low copy numbers required and use of endogenous RNAi machinery for continuous silencing activity rather as opposed to repeated siRNA doses (large dsRNAs in particular invoke a greater immune response). Exogenous siRNAs meanwhile are simpler and cheaper to manufacture (needing only a 19-21bp sense and antisense strands to achieve an effect), and a greater degree of control can be exhibited over their administration: siRNA levels can be "topped-up" when desired, shRNA silencing is constitutive. Control can be exhibited in shRNA by introducing some sort of stimulus-response-based promoter however one would need to ensure the stimulus would not carry additional risks. shRNAs can also induce cellular toxicity by oversaturating the cells endogenous RNAi machinery which siRNA avoids (Grimm et al., 2006).

Vehicles for delivering gene-editing machinery in-situ:

Another area of safety concern in the use of gene-editing strategies in-situ is choosing an appropriate and safe delivery vehicle. Viral particles can transduce cells with DNAs or RNAs

whilst protecting nucleic acid cargo from degradation, alternatively plasmids containing incorporation components can be introduced into cells through lipofection or electroporation. Although viral methods of delivery are generally very efficient and well tolerated in pre-clinical studies there is a stigma surrounding their use in humans due to the potential of random mutagenesis caused by transposon machinery into host genomic DNA (Cornu et al., 2017; Nayerossadat, Maedeh, & Ali, 2012; Thomas et al., 2003) and irreversible genetic alteration of healthy tissue is still an issue.

Plasmids are a popular vector of choice in regard to gene-therapy pre-clinic and can deliver a variety of different gene-editing platforms including protein-coding sequences, CRISPR, TALENs, shRNAs, and ZFNs. Individual cells that are transfected will constitutively express the plasmid for as long as they live and can be inherited if viral components are incorporated (however as mentioned above this may be undesirable in-situ due to safety concerns). Plasmid transcription can also be controlled through a stimulus-responsive transcriptional promotor or repressor. Plasmids can elicit a host immune response, particularly those that are rich in unmethylated CpG motifs: a prevalent feature of bacterial DNA that is not present in vertebrates (Krieg, 2002; Manunta et al., 2011). However, CpG free plasmids can be generated to prevent this in clinical application. Like all exogenous nucleic acids plasmids need to be transfected into cells as they cannot get through the plasma membrane of eukaryotic cells. This can be achieved through methods including intramural injection, lipofection, and electroporation. One example of plasmid gene-editing technologies being taken to clinical trials is in the treatment of melanoma. Intramural injection and/or Electroporation of a plasmid encoding *IL-12* gene was used to treat melanoma patients with distal and local remission recorded to varying degrees (Cha & Daud, 2012; Daud et al., 2008; Mahvi et al., 2007). IL-12 is an immunomodulatory cytokine that potentiates the differentiation of naïve T-cells into T_H1 cells as well as stimulate natural killer (NK) cell activity (Del Vecchio et al., 2007). In this case *IL-12* expression was increased in malignant areas to promote long-lasting antitumor immunity.

A particularly exciting area of study in regard to delivery of gene-editing technologies is the ongoing development of lipid nanoparticles (LNPs). Based on lipofection methods, Cationic LNPs are assembled with anionic nuclear material, such as RNAs or DNA, which is energetically favourable, the LNPs can then easily pass through the anionic plasma membrane of cells via endocytosis (Cornu et al., 2017). LNPs are further modified with protein-based surface antigens or binding domains to increase their selectivity for specific cell types. This technology has been coupled with RNAi technologies to exhibit transient knockdown of target genes to potentiate therapy with minimal toxicity or adverse effects (de la Fuente et al., 2015; Manunta et al., 2011; Yu-Wai-Man et al., 2016). A study by Zuris et.al. also demonstrated that proteins coupled to negatively supercharged proteins can also be incorporated into commercial lipofection reagents (such as Lipofectamine) and delivered into cells successfully (Zuris et al., 2014). Using this approach Zuris' group managed to successfully deliver Cre-recombinase, TALE-proteins, and sgRNA-Cas9 complexes both in-vitro and in-vivo to mouse inner-ear hair cells (however it was found that sgRNA-Cas9 was already sufficiently negatively charged and did not need conjugation of a supercharged protein). This opens up the possibility of developing LNPs that contain proteins rather than just nuclear material. Although commercial lipofection reagents have been reported to induce a degree of toxicity in cells (Barreau et al., 2006) modified LNPs that are specifically targeted to diseased tissue may be circumvent this problem to some degree (i.e. causing lipofection-induced toxicity in target diseased tissue may be therapeutically beneficial).

Concluding Statement:

Gene editing technologies are powerful tools with exciting clinical potential. However, several hurdles in regard to safety-of-use and translation need to be overcome before gene editing can become common medical practice. In a research context gene editing allows the identification and characterisation of disease-linked genes, clarification of biomolecular pathways, and provides a means to mass-produce biological material for research and/or commercial use. Careful selection of which gene-editing techniques to use is essential as each method has associated strengths and weaknesses which dictate their suitability for particular experiments. In this project both siRNA and CRISPR-Cas9 gene-editing techniques have been used to clarify the role of *Itch* in different pathological contexts through a wide range of in-vitro and ex-vivo physiological assays. Furthermore, this project has demonstrated and outlined some of the potential issues surrounding both techniques and how these may be addressed in their experimental specific contexts.

References:

Adeegbe, D. O., & Nishikawa, H. (2013). Natural and induced T regulatory cells in cancer. *Frontiers in Immunology*, *4*, 190.

Aki, D., Li, H., Zhang, W., Zheng, M., Elly, C., Lee, J. H., … Liu, Y.-C. (2018). The E3 ligases Itch and WWP2 cooperate to limit TH2 differentiation by enhancing signaling through the TCR. *Nature Immunology*, *19*(7), 766–775.

Aki, D., Li, Q., Li, H., Liu, Y.-C., & Ho Lee, J. (n.d.). *REVIEW Immune regulation by protein ubiquitination: roles of the E3 ligases VHL and Itch*.

Aki, D., Zhang, W., & Liu, Y.-C. (2015). The E3 ligase Itch in immune regulation and beyond. *Immunological Reviews*, *266*(1), 6–26.

Ali, Z., Mahas, A., & Mahfouz, M. (2018). CRISPR/Cas13 as a Tool for RNA Interference. *Trends in Plant Science*, *23*(5), 374–378.

Almeida, M. (2012). Aging mechanisms in bone. *BoneKEy Reports*, *1*.

Avruch, J., Zhou, D., Fitamant, J., & Bardeesy, N. (2011). Mst1/2 signalling to Yap: gatekeeper for liver size and tumour development. *British Journal of Cancer*, *104*(1), 24–32.

Azzam, M. E., & Algranati, I. D. (1973). Mechanism of puromycin action: fate of ribosomes after release of nascent protein chains from polysomes. *Proceedings of the National Academy of Sciences of the United States of America*, *70*(12), 3866–3869.

Barreau, C., Dutertre, S., Paillard, L., & Osborne, H. B. (2006). Liposome-mediated RNA transfection should be used with caution. *RNA (New York, N.Y.)*, *12*(10), 1790–1793.

Bartek, J., Bartkova, J., & Lukas, J. (2007). DNA damage signalling guards against activated oncogenes and tumour progression. *Oncogene*, *26*(56), 7773–7779.

Bartlett, D. W., & Davis, M. E. (2006). Insights into the kinetics of siRNA-mediated gene silencing from live-cell and live-animal bioluminescent imaging. *Nucleic Acids Research*, *34*(1), 322–333.

Becerikli, M., Jaurich, H., Schira, J., Schulte, M., Döbele, C., Wallner, C., … Behr, B. (2017). Age-dependent alterations in osteoblast and osteoclast activity in human cancellous bone. *Journal of Cellular and Molecular Medicine*, *21*(11), 2773–2781.

Bernassola, F., Karin, M., Ciechanover, A., & Melino, G. (2008). The HECT family of E3 ubiquitin ligases: multiple players in cancer development. *Cancer Cell*, *14*(1), 10–21.

Berndsen, C. E., & Wolberger, C. (2014). New insights into ubiquitin E3 ligase mechanism. *Nature Structural & Molecular Biology*, *21*(4), 301–307.

Beyer, M., & Schultze, J. L. (2009). Regulatory T cells: major players in the tumor microenvironment. *Current Pharmaceutical Design*, *15*(16), 1879–1892. Retrieved from http://www.ncbi.nlm.nih.gov/pubmed/19519430

Blumer, M. J. F., Hausott, B., Schwarzer, C., Hayman, A. R., Stempel, J., & Fritsch, H. (2012). Role of tartrate-resistant acid phosphatase (TRAP) in long bone development. *Mechanisms of Development*, *129*(5–8), 162–176.

Bongiorno-Borbone, L., Giacobbe, A., Compagnone, M., Eramo, A., Maria, R. De, Peschiaroli, A., … De Maria, R. (2015, July 1). Anti-tumoral effect of desmethylclomipramine in lung cancer stem cells. *Oncotarget*, Vol. 6, pp. 16926–16938.

Bumcrot, D., Manoharan, M., Koteliansky, V., & Sah, D. W. Y. (2006). RNAi therapeutics: a potential new class of pharmaceutical drugs. *Nature Chemical Biology*, *2*(12), 711–719.

BURSTONE, M. S. (1959). Histochemical demonstration of acid phosphatase activity in osteoclasts. *Journal of Histochemistry & Cytochemistry*, *7*(1), 39–41.

Butler, L. M., Zhou, X., Xu, W.-S., Scher, H. I., Rifkind, R. A., Marks, P. A., & Richon, V. M. (2002). The histone deacetylase inhibitor SAHA arrests cancer cell growth, up-

regulates thioredoxin-binding protein-2, and down-regulates thioredoxin. *Proceedings of the National Academy of Sciences of the United States of America*, *99*(18), 11700–11705.
Carroll, D. (2011). Genome engineering with zinc-finger nucleases. *Genetics*, *188*(4), 773–782.
Cha, E., & Daud, A. (2012). Plasmid IL-12 electroporation in melanoma. *Human Vaccines & Immunotherapeutics*, *8*(11), 1734–1738.
Chakraborty, C., Sharma, A. R., Sharma, G., Doss, C. G. P., & Lee, S.-S. (2017). Therapeutic miRNA and siRNA: Moving from Bench to Clinic as Next Generation Medicine. *Molecular Therapy. Nucleic Acids*, *8*, 132–143.
Chastagner, P., Israël, A., & Brou, C. (2008). AIP4/Itch regulates Notch receptor degradation in the absence of ligand. *PloS One*, *3*(7), e2735.
Choi, M., Chang, C.-Y., Clough, T., Broudy, D., Killeen, T., MacLean, B., & Vitek, O. (2014). MSstats: an R package for statistical analysis of quantitative mass spectrometry-based proteomic experiments. *Bioinformatics*, *30*(17), 2524–2526.
Chu, Y., & Corey, D. R. (2012). RNA sequencing: platform selection, experimental design, and data interpretation. *Nucleic Acid Therapeutics*, *22*(4), 271–274.
Cicenas, J., Kvederaviciute, K., Meskinyte, I., Meskinyte-Kausiliene, E., & Skeberdyte, A. (2017). KRAS, TP53, CDKN2A, SMAD4, BRCA1, and BRCA2 mutations in pancreatic cancer. *Cancers*.
Clarke, A. R., Howard, L. A., Harrison, D. J., & Winton, D. J. (1997). p53, mutation frequency and apoptosis in the murine small intestine. *Oncogene*, *14*(17), 2015–2018.
Cong, L., Ran, F. A., Cox, D., Lin, S., Barretto, R., Habib, N., … Zhang, F. (2013). Multiplex genome engineering using CRISPR/Cas systems. *Science (New York, N.Y.)*, *339*(6121), 819–823.
Conroy, H., Galvin, K. C., Higgins, S. C., & Mills, K. H. G. (2012). Gene silencing of TGF-β1 enhances antitumor immunity induced with a dendritic cell vaccine by reducing tumor-associated regulatory T cells. *Cancer Immunology, Immunotherapy*, *61*(3), 425–431.
Cornu, T. I., Mussolino, C., & Cathomen, T. (2017). Refining strategies to translate genome editing to the clinic. *Nature Medicine*, *23*(4), 415–423.
Cox, D. B. T., Gootenberg, J. S., Abudayyeh, O. O., Franklin, B., Kellner, M. J., Joung, J., & Zhang, F. (2017). RNA editing with CRISPR-Cas13. *Science (New York, N.Y.)*, *358*(6366), 1019–1027.
Cradick, T. J., Qiu, P., Lee, C. M., Fine, E. J., & Bao, G. (2014). COSMID: A Web-based Tool for Identifying and Validating CRISPR/Cas Off-target Sites. *Molecular Therapy - Nucleic Acids*, *3*, e214.
Crotty, S. (2011). Follicular helper CD4 T cells (TFH). *Annual Review of Immunology*, *29*, 621–663.
Curotto de Lafaille, M. A., & Lafaille, J. J. (2009). Natural and Adaptive Foxp3+ Regulatory T Cells: More of the Same or a Division of Labor? *Immunity*, *30*(5), 626–635.
Daud, A. I., DeConti, R. C., Andrews, S., Urbas, P., Riker, A. I., Sondak, V. K., … Heller, R. (2008). Phase I trial of interleukin-12 plasmid electroporation in patients with metastatic melanoma. *Journal of Clinical Oncology : Official Journal of the American Society of Clinical Oncology*, *26*(36), 5896–5903.
Davis, A. J., & Chen, D. J. (2013). DNA double strand break repair via non-homologous end-joining. *Translational Cancer Research*, *2*(3), 130–143.
de la Fuente, M., Jones, M. C., Santander-Ortega, M. J., Mirenska, A., Marimuthu, P., Uchegbu, I., & Sch??tzlein, A. (2015). A nano-enabled cancer-specific ITCH RNAi chemotherapy booster for pancreatic cancer. *Nanomedicine: Nanotechnology, Biology,*

and Medicine, *11*(2), 369–377.
Déclais, A.-C., Liu, J., Freeman, A. D. J., & Lilley, D. M. J. (2006). Structural Recognition between a Four-way DNA Junction and a Resolving Enzyme. *Journal of Molecular Biology*, *359*(5), 1261–1276.
Deer, E. L., González-Hernández, J., Coursen, J. D., Shea, J. E., Ngatia, J., Scaife, C. L., … Mulvihill, S. J. (2010). Phenotype and genotype of pancreatic cancer cell lines. *Pancreas*, *39*(4), 425–435.
Del Vecchio, M., Bajetta, E., Canova, S., Lotze, M. T., Wesa, A., Parmiani, G., & Anichini, A. (2007). Interleukin-12: biological properties and clinical application. *Clinical Cancer Research : An Official Journal of the American Association for Cancer Research*, *13*(16), 4677–4685.
Deorukhkar, A., Shentu, S., Park, H. C., Diagaradjane, P., Puduvalli, V., Aggarwal, B., … Krishnan, S. (2010). Inhibition of radiation-induced DNA repair and prosurvival pathways contributes to vorinostat-mediated radiosensitization of pancreatic cancer cells. *Pancreas*, *39*(8), 1277–1283.
Dow, L. E., Fisher, J., O'Rourke, K. P., Muley, A., Kastenhuber, E. R., Livshits, G., … Lowe, S. W. (2015). Inducible in vivo genome editing with CRISPR-Cas9. *Nature Biotechnology*, *33*(4), 390–394.
Dufès, C., Keith, W. N., Bilsland, A., Proutski, I., Uchegbu, I. F., & Schätzlein, A. G. (2005). Synthetic anticancer gene medicine exploits intrinsic antitumor activity of cationic vector to cure established tumors. *Cancer Research*, *65*(18), 8079–8084.
Emmerich, C. H., & Cohen, P. (2015). Optimising methods for the preservation, capture and identification of ubiquitin chains and ubiquitylated proteins by immunoblotting. *Biochemical and Biophysical Research Communications*, *466*(1), 1–14.
Eyquem, J., Mansilla-Soto, J., Giavridis, T., van der Stegen, S. J. C., Hamieh, M., Cunanan, K. M., … Sadelain, M. (2017). Targeting a CAR to the TRAC locus with CRISPR/Cas9 enhances tumour rejection. *Nature*, *543*(7643), 113–117.
Fabregat, I., Fernando, J., Mainez, J., & Sancho, P. (2014). TGF-beta signaling in cancer treatment. *Current Pharmaceutical Design*, *20*(17), 2934–2947. Retrieved from http://www.ncbi.nlm.nih.gov/pubmed/23944366
Fajner, V., Maspero, E., & Polo, S. (2017). Targeting HECT-type E3 ligases - insights from catalysis, regulation and inhibitors. *FEBS Letters*, *591*(17), 2636–2647.
Fang, D., Elly, C., Gao, B., Fang, N., Altman, Y., Joazeiro, C., … Liu, Y.-C. (2002). Dysregulation of T lymphocyte function in itchy mice: a role for Itch in TH2 differentiation. *Nature Immunology*, *3*(3), 281–287.
Felgner, P. L., Gadek, T. R., Holm, M., Roman, R., Chan, H. W., Wenz, M., … Danielsen, M. (1987). Lipofection: a highly efficient, lipid-mediated DNA-transfection procedure. *Proceedings of the National Academy of Sciences of the United States of America*, *84*(21), 7413–7417. Retrieved from http://www.ncbi.nlm.nih.gov/pubmed/2823261
Field, S., Uyttenhove, C., Stroobant, V., Cheou, P., Donckers, D., Coutelier, J.-P., … Jat, P. S. (2016). Novel highly specific anti-periostin antibodies uncover the functional importance of the fascilin 1-1 domain and highlight preferential expression of periostin in aggressive breast cancer. *International Journal of Cancer*, *138*(8), 1959–1970.
Flores, E. R., Sengupta, S., Miller, J. B., Newman, J. J., Bronson, R., Crowley, D., … Jacks, T. (2005). Tumor predisposition in mice mutant for p63 and p73: evidence for broader tumor suppressor functions for the p53 family. *Cancer Cell*, *7*(4), 363–373.
Fogarty, N. M. E., McCarthy, A., Snijders, K. E., Powell, B. E., Kubikova, N., Blakeley, P., … Niakan, K. K. (2017). Genome editing reveals a role for OCT4 in human embryogenesis. *Nature*, *550*(7674), 67–73.
Fokas, E., Prevo, R., Pollard, J. R., Reaper, P. M., Charlton, P. A., Cornelissen, B., …

Brunner, T. B. (2012). Targeting ATR in vivo using the novel inhibitor VE-822 results in selective sensitization of pancreatic tumors to radiation. *Cell Death & Disease*, *3*, e441.

Fry, A. M., O'Regan, L., Sabir, S. R., & Bayliss, R. (2012). Cell cycle regulation by the NEK family of protein kinases. *Journal of Cell Science*.

Fu, Y., Foden, J. a, Khayter, C., Maeder, M. L., Reyon, D., Joung, J. K., & Sander, J. D. (2013). High-frequency off-target mutagenesis induced by CRISPR-Cas nucleases in human cells. *Nature Biotechnology*, *31*(9), 822–826.

Gaj, T., Gersbach, C. A., Barbas, C. F., & III. (2013). ZFN, TALEN, and CRISPR/Cas-based methods for genome engineering. *Trends in Biotechnology*, *31*(7), 397–405.

Gallagher, E., Gao, M., Liu, Y.-C., & Karin, M. (2006). Activation of the E3 ubiquitin ligase Itch through a phosphorylation-induced conformational change. *Proceedings of the National Academy of Sciences of the United States of America*, *103*(6), 1717–1722.

Gaudelli, N. M., Komor, A. C., Rees, H. A., Packer, M. S., Badran, A. H., Bryson, D. I., & Liu, D. R. (2017). Programmable base editing of A•T to G•C in genomic DNA without DNA cleavage. *Nature*, *551*(7681), 464–471.

Ge, B., Gram, H., Di Padova, F., Huang, B., New, L., Ulevitch, R. J., … Han, J. (2002). MAPKK-independent activation of p38alpha mediated by TAB1-dependent autophosphorylation of p38alpha. *Science (New York, N.Y.)*, *295*(5558), 1291–1294.

Gilbert, L. A., Larson, M. H., Morsut, L., Liu, Z., Brar, G. A., Torres, S. E., … Qi, L. S. (2013). CRISPR-Mediated Modular RNA-Guided Regulation of Transcription in Eukaryotes. *Cell*, *154*(2), 442–451.

Gillen, S., Schuster, T., Meyer Zum Büschenfelde, C., Friess, H., & Kleeff, J. (2010). Preoperative/neoadjuvant therapy in pancreatic cancer: a systematic review and meta-analysis of response and resection percentages. *PLoS Medicine*, *7*(4), e1000267.

Gillet, L. C., Navarro, P., Tate, S., Röst, H., Selevsek, N., Reiter, L., … Aebersold, R. (2012). Targeted data extraction of the MS/MS spectra generated by data-independent acquisition: a new concept for consistent and accurate proteome analysis. *Molecular & Cellular Proteomics : MCP*, *11*(6), O111.016717.

Goldberg, S. F., Miele, M. E., Hatta, N., Takata, M., Paquette-Straub, C., Freedman, L. P., & Welch, D. R. (2003). Melanoma Metastasis Suppression by Chromosome 6: Evidence for a Pathway Regulated by CRSP3 and TXNIP. *Cancer Res.*, *63*(2), 432–440. Retrieved from http://cancerres.aacrjournals.org/content/63/2/432.abstract?ijkey=be0b434dac4a11a29c55d2c4fa2b0e7b825cd839&keytype2=tf_ipsecsha

Goltzman, D. (2001). Osteolysis and cancer. *The Journal of Clinical Investigation*, *107*(10), 1219–1220.

González, F., Zhu, Z., Shi, Z.-D., Lelli, K., Verma, N., Li, Q. V., & Huangfu, D. (2014). An iCRISPR Platform for Rapid, Multiplexable, and Inducible Genome Editing in Human Pluripotent Stem Cells. *Cell Stem Cell*, *15*(2), 215–226.

Grewe, M., Bruijnzeel-Koomen, C. A. F. ., Schöpf, E., Thepen, T., Langeveld-Wildschut, A. G., Ruzicka, T., & Krutmann, J. (1998). A role for Th1 and Th2 cells in the immunopathogenesis of atopic dermatitis. *Immunology Today*, *19*(8), 359–361.

Grimm, D., Streetz, K. L., Jopling, C. L., Storm, T. A., Pandey, K., Davis, C. R., … Kay, M. A. (2006). Fatality in mice due to oversaturation of cellular microRNA/short hairpin RNA pathways. *Nature*.

Han, X., Aslanian, A., Yates, J. R., & III. (2008). Mass spectrometry for proteomics. *Current Opinion in Chemical Biology*, *12*(5), 483–490.

Hansen, T. M., Rossi, M., Roperch, J. P., Ansell, K., Simpson, K., Taylor, D., … Melino, G. (2007). Itch inhibition regulates chemosensitivity in vitro. *Biochemical and Biophysical*

Research Communications, *361*(1), 33–36.
Harvey, K. F., Pfleger, C. M., & Hariharan, I. K. (2003). The Drosophila Mst Ortholog, hippo, Restricts Growth and Cell Proliferation and Promotes Apoptosis. *Cell*, *114*(4), 457–467.
Heissmeyer, V., Macián, F., Im, S.-H., Varma, R., Feske, S., Venuprasad, K., … Rao, A. (2004). Calcineurin imposes T cell unresponsiveness through targeted proteolysis of signaling proteins. *Nature Immunology*, *5*(3), 255–265.
Hendel, A., Bak, R. O., Clark, J. T., Kennedy, A. B., Ryan, D. E., Roy, S., … Porteus, M. H. (2015). Chemically modified guide RNAs enhance CRISPR-Cas genome editing in human primary cells. *Nature Biotechnology*, *33*(9), 985–989.
Henriksen, K., Karsdal, M. A., Taylor, A., Tosh, D., & Coxon, F. P. (2012). *Generation of Human Osteoclasts from Peripheral Blood*.
Ho, K. C., Zhou, Z., She, Y.-M., Chun, A., Cyr, T. D., & Yang, X. (2011). Itch E3 ubiquitin ligase regulates large tumor suppressor 1 stability [corrected]. *Proceedings of the National Academy of Sciences of the United States of America*, *108*(12), 4870–4875.
Honda, R., Tanaka, H., & Yasuda, H. (1997). Oncoprotein MDM2 is a ubiquitin ligase E3 for tumor suppressor p53. *FEBS Letters*, *420*(1), 25–27.
Hong, H., Zhang, Y., & Cai, W. (2010). In vivo imaging of RNA interference. *Journal of Nuclear Medicine : Official Publication, Society of Nuclear Medicine*, *51*(2), 169–172.
Huang, J., Wu, S., Barrera, J., Matthews, K., & Pan, D. (2005). The Hippo signaling pathway coordinately regulates cell proliferation and apoptosis by inactivating Yorkie, the Drosophila Homolog of YAP. *Cell*, *122*(3), 421–434.
Huang, Q., Yang, L., Luo, J., Guo, L., Wang, Z., Yang, X., … Zhang, Y. (2015). SWATH enables precise label-free quantification on proteome scale. *PROTEOMICS*, *15*(7), 1215–1223.
Ikeda, K., & Takeshita, S. (2016). The role of osteoclast differentiation and function in skeletal homeostasis. *Journal of Biochemistry*, *159*(1), 1–8.
Ikushima, H., & Miyazono, K. (2010). TGFbeta signalling: a complex web in cancer progression. *Nature Reviews. Cancer*, *10*(6), 415–424.
Ilic, M., & Ilic, I. (2016). Epidemiology of pancreatic cancer. *World Journal of Gastroenterology*, *22*(44), 9694–9705.
Iwasaki, H., & Suda, T. (2009). Cancer stem cells and their niche. *Cancer Science*, *100*(7), 1166–1172.
Jamieson, L. E., Harrison, D. J., & Campbell, C. J. (2015). Chemical analysis of multicellular tumour spheroids. *The Analyst*, *140*(12), 3910–3920.
Järve, A., Müller, J., Kim, I.-H., Rohr, K., MacLean, C., Fricker, G., … Helm, M. (2007). Surveillance of siRNA integrity by FRET imaging. *Nucleic Acids Research*, *35*(18), e124.
Jin, W., Chang, M., Paul, E. M., Babu, G., Lee, A. J., Reiley, W., … Sun, S.-C. (2008). Deubiquitinating enzyme CYLD negatively regulates RANK signaling and osteoclastogenesis in mice. *The Journal of Clinical Investigation*, *118*(5), 1858–1866.
Jinek, M., Chylinski, K., Fonfara, I., Hauer, M., Doudna, J. A., & Charpentier, E. (2012). A programmable dual-RNA-guided DNA endonuclease in adaptive bacterial immunity. *Science (New York, N.Y.)*, *337*(6096), 816–821.
Joung, J. K., & Sander, J. D. (2013). TALENs: a widely applicable technology for targeted genome editing. *Nature Reviews Molecular Cell Biology*, *14*(1), 49–55.
Judge, A. D., Robbins, M., Tavakoli, I., Levi, J., Hu, L., Fronda, A., … MacLachlan, I. (2009). Confirming the RNAi-mediated mechanism of action of siRNA-based cancer therapeutics in mice. *Journal of Clinical Investigation*.
Junn, E., Han, S. H., Im, J. Y., Yang, Y., Cho, E. W., Um, H. D., … Choi, I. (2000). Vitamin

D3 Up-Regulated Protein 1 Mediates Oxidative Stress Via Suppressing the Thioredoxin Function. *The Journal of Immunology*, *164*(12), 6287–6295.
Justice, R. W., Zilian, O., Woods, D. F., Noll, M., & Bryant, P. J. (1995). The Drosophila tumor suppressor gene warts encodes a homolog of human myotonic dystrophy kinase and is required for the control of cell shape and proliferation. *Genes & Development*, *9*(5), 534–546.
Kaghad, M., Bonnet, H., Yang, A., Creancier, L., Biscan, J. C., Valent, A., … Caput, D. (1997). Monoallelically expressed gene related to p53 at 1p36, a region frequently deleted in neuroblastoma and other human cancers. *Cell*, *90*(4), 809–819. Retrieved from http://www.ncbi.nlm.nih.gov/pubmed/9288759
Katagiri, T., & Takahashi, N. (2002). Regulatory mechanisms of osteoblast and osteoclast differentiation. *Oral Diseases*, *8*(3), 147–159.
Kim, J. H., & Kim, N. (2016). Signaling Pathways in Osteoclast Differentiation. *Chonnam Medical Journal*, *52*(1), 12–17.
Koo, B.-K., Sasselli, V., & Clevers, H. (2013). Retroviral Gene Expression Control in Primary Organoid Cultures. *Current Protocols in Stem Cell Biology*, *27*(1), 5A.6.1-5A.6.8.
Krempien, R., & Roeder, F. (2017). Intraoperative radiation therapy (IORT) in pancreatic cancer. *Radiation Oncology (London, England)*, *12*(1), 8.
Krieg, A. M. (2002). CPG motifs in bacterial DNA and their immune effects. *Annual Review of Immunology*, *20*(1), 709–760.
Kristen, A. V, Ajroud-Driss, S., Conceição, I., Gorevic, P., Kyriakides, T., & Obici, L. (2019). Patisiran, an RNAi therapeutic for the treatment of hereditary transthyretin-mediated amyloidosis. *Neurodegenerative Disease Management*, *9*(1), 5–23.
Kubo, N., Okoshi, R., Nakashima, K., Shimozato, O., Nakagawara, A., & Ozaki, T. (2010). MDM2 promotes the proteasomal degradation of p73 through the interaction with Itch in HeLa cells. *Biochemical and Biophysical Research Communications*, *403*(3–4), 405–411.
Kwon, H.-J., Won, Y.-S., Suh, H.-W., Jeon, J.-H., Shao, Y., Yoon, S.-R., … Choi, I. (2010). Vitamin D3 upregulated protein 1 suppresses TNF-α-induced NF-κB activation in hepatocarcinogenesis. *Journal of Immunology (Baltimore, Md. : 1950)*, *185*(7), 3980–3989.
LAEMMLI, U. K. (1970). Cleavage of Structural Proteins during the Assembly of the Head of Bacteriophage T4. *Nature*, *227*(5259), 680–685.
Lai, Z.-C., Wei, X., Shimizu, T., Ramos, E., Rohrbaugh, M., Nikolaidis, N., … Li, Y. (2005). Control of cell proliferation and apoptosis by mob as tumor suppressor, mats. *Cell*, *120*(5), 675–685.
Lam, H., Deutsch, E. W., Eddes, J. S., Eng, J. K., King, N., Stein, S. E., & Aebersold, R. (2007). Development and validation of a spectral library searching method for peptide identification from MS/MS. *PROTEOMICS*, *7*(5), 655–667.
Lamothe, B., Webster, W. K., Gopinathan, A., Besse, A., Campos, A. D., & Darnay, B. G. (2007). TRAF6 ubiquitin ligase is essential for RANKL signaling and osteoclast differentiation. *Biochemical and Biophysical Research Communications*, *359*(4), 1044–1049.
Landré, V., Antonov, A., Knight, R., & Melino, G. (2016). p73 promotes glioblastoma cell invasion by directly activating POSTN (periostin) expression. *Oncotarget*, 1–18.
Lee, Y.-H., & Kim, C. H. (2019). Evolution of chimeric antigen receptor (CAR) T cell therapy: current status and future perspectives. *Archives of Pharmacal Research*, 1–10.
Lemma, S., Di Pompo, G., Porporato, P. E., Sboarina, M., Russell, S., Gillies, R. J., … Avnet, S. (2017). MDA-MB-231 breast cancer cells fuel osteoclast metabolism and

activity: A new rationale for the pathogenesis of osteolytic bone metastases. *Biochimica et Biophysica Acta (BBA) - Molecular Basis of Disease*, *1863*(12), 3254–3264.
Levrero, M., De Laurenzi, V., Costanzo, a, Gong, J., Wang, J. Y., & Melino, G. (2000). The p53/p63/p73 family of transcription factors: overlapping and distinct functions. *Journal of Cell Science*, *113 (Pt 1*, 1661–1670.
Levy, D., Adamovich, Y., Reuven, N., & Shaul, Y. (2007). The Yes-associated protein 1 stabilizes p73 by preventing Itch-mediated ubiquitination of p73. *Cell Death and Differentiation*, *14*(4), 743–751.
Li, P., Spolski, R., Liao, W., & Leonard, W. J. (2014). Complex interactions of transcription factors in mediating cytokine biology in T cells. *Immunological Reviews*, *261*(1), 141–156.
Li, X., Sun, W., Li, J., Wang, M., Zhang, H., Pei, L., … Xing, L. (2017). Clomipramine causes osteoporosis by promoting osteoclastogenesis via E3 ligase Itch, which is prevented by Zoledronic acid. *Scientific Reports*, *7*, 41358.
Liang, P., Ding, C., Sun, H., Xie, X., Xu, Y., Zhang, X., … Huang, J. (2017). Correction of β-thalassemia mutant by base editor in human embryos. *Protein & Cell*, *8*(11), 811–822.
Liao, B., Zhong, X., Xu, H., Xiao, F., Fang, Z., Gu, J., … Jin, Y. (2013). Itch, an E3 ligase of Oct4, is required for embryonic stem cell self-renewal and pluripotency induction. *Journal of Cellular Physiology*, *228*(7), 1443–1451.
Lin, Y., Cradick, T. J., Brown, M. T., Deshmukh, H., Ranjan, P., Sarode, N., … Bao, G. (2014). CRISPR/Cas9 systems have off-target activity with insertions or deletions between target DNA and guide RNA sequences. *Nucleic Acids Research*, *42*(11), 7473–7485.
Liu, J., Li, X., Zhang, H., Gu, R., Wang, Z., Gao, Z., & Xing, L. (2017). Ubiquitin E3 ligase Itch negatively regulates osteoblast function by promoting proteasome degradation of osteogenic proteins. *Bone and Joint Research*, *6*(3). Retrieved from http://www.bjr.boneandjoint.org.uk/content/6/3/154.long#ref-11
Liu, K. I., Ramli, M. N. Bin, Woo, C. W. A., Wang, Y., Zhao, T., Zhang, X., … Tan, M. H. (2016). A chemical-inducible CRISPR–Cas9 system for rapid control of genome editing. *Nature Chemical Biology*, *12*(11), 980–987.
Liu, Y., Lau, J., Li, W., Tempel, W., Li, L., Dong, A., … Min, J. (2016). Structural basis for the regulatory role of the PPxY motifs in the thioredoxin-interacting protein TXNIP. *The Biochemical Journal*, *473*(2), 179–187.
Lohr, N. J., Molleston, J. P., Strauss, K. A., Torres-Martinez, W., Sherman, E. A., Squires, R. H., … Puffenberger, E. G. (2010). Human ITCH E3 ubiquitin ligase deficiency causes syndromic multisystem autoimmune disease. *American Journal of Human Genetics*, *86*(3), 447–453.
Ludwig, C., Gillet, L., Rosenberger, G., Amon, S., Collins, B. C., & Aebersold, R. (2018). Data-independent acquisition-based SWATH-MS for quantitative proteomics: a tutorial. *Molecular Systems Biology*, *14*(8), e8126.
Luo, Z.-L., Luo, H.-J., Fang, C., Cheng, L., Huang, Z., Dai, R., … Tang, L.-J. (2016a). Negative correlation of ITCH E3 ubiquitin ligase and miRNA-106b dictates metastatic progression in pancreatic cancer. *Oncotarget*, *7*(2), 1477–1485.
Luo, Z.-L., Luo, H.-J., Fang, C., Cheng, L., Huang, Z., Dai, R., … Tang, L.-J. (2016b). Negative correlation of ITCH E3 ubiquitin ligase and miRNA-106b dictates metastatic progression in pancreatic cancer. *Oncotarget*, *7*(2), 1477–1485.
Ma, H., Marti-Gutierrez, N., Park, W., Wu, J., Lee, Y., Suzuki, K., … Mitalipov, S. (2017). *Correction of a pathogenic gene mutation in human embryos*.
Maclean, B., Tomazela, D. M., Shulman, N., Chambers, M., Finney, G. L., Frewen, B., … Maccoss, M. J. (2010). Gene expression Skyline: an open source document editor for

creating and analyzing targeted proteomics experiments. *BIOINFORMATICS APPLICATIONS NOTE*, *26*(7), 966–968.
Maeder, M. L., Linder, S. J., Cascio, V. M., Fu, Y., Ho, Q. H., & Joung, J. K. (2013). CRISPR RNA–guided activation of endogenous human genes. *Nature Methods*, *10*(10), 977–979.
Mahvi, D. M., Henry, M. B., Albertini, M. R., Weber, S., Meredith, K., Schalch, H., … Sondel, P. (2007). Intratumoral injection of IL-12 plasmid DNA – results of a phase I/IB clinical trial. *Cancer Gene Therapy*, *14*(8), 717–723.
Mansoori, B., Sandoghchian Shotorbani, S., & Baradaran, B. (2014). RNA interference and its role in cancer therapy. *Advanced Pharmaceutical Bulletin*, *4*(4), 313–321.
Manunta, M. D. I., McAnulty, R. J., McDowell, A., Jin, J., Ridout, D., Fleming, J., … Hart, S. L. (2013). Airway deposition of nebulized gene delivery nanocomplexes monitored by radioimaging agents. *American Journal of Respiratory Cell and Molecular Biology*, *49*(3), 471–480.
Manunta, M. D. I., McAnulty, R. J., Tagalakis, A. D., Bottoms, S. E., Campbell, F., Hailes, H. C., … Hart, S. L. (2011). Nebulisation of receptor-targeted nanocomplexes for gene delivery to the airway epithelium. *PloS One*, *6*(10), e26768.
Marino, S., Bishop, R. T., Carrasco, G., Logan, J. G., Li, B., & Idris, A. I. (2019). Pharmacological Inhibition of NFκB Reduces Prostate Cancer Related Osteoclastogenesis In Vitro and Osteolysis Ex Vivo. *Calcified Tissue International*, 1–12.
Marino, S., Logan, J. G., Mellis, D., & Capulli, M. (2014a). Generation and culture of osteoclasts. *BoneKEy Reports*, *3*, 570.
Marino, S., Logan, J. G., Mellis, D., & Capulli, M. (2014b). Generation and culture of osteoclasts. *BoneKEy Reports*, *3*, 570.
Mashal, R. D., Koontz, J., & Sklar, J. (1995). Detection of mutations by cleavage of DNA heteroduplexes with bacteriophage resolvases. *Nature Genetics*, *9*(2), 177–183.
Massagué, J. (2008). TGFβ in Cancer. *Cell*, *134*(2), 215–230.
Matano, M., Date, S., Shimokawa, M., Takano, A., Fujii, M., Ohta, Y., … Sato, T. (2015). Modeling colorectal cancer using CRISPR-Cas9–mediated engineering of human intestinal organoids. *Nature Medicine*, *21*(3), 256–262.
Maus, M. V., Haas, A. R., Beatty, G. L., Albelda, S. M., Levine, B. L., Liu, X., … June, C. H. (2013). T Cells Expressing Chimeric Antigen Receptors Can Cause Anaphylaxis in Humans. *Cancer Immunology Research*, *1*(1), 26–31.
McGuigan, A., Kelly, P., Turkington, R. C., Jones, C., Coleman, H. G., & McCain, R. S. (2018). Pancreatic cancer: A review of clinical diagnosis, epidemiology, treatment and outcomes. *World Journal of Gastroenterology*, *24*(43), 4846–4861.
Melino, G., Gallagher, E., Aqeilan, R. I., Knight, R., Peschiaroli, A., Rossi, M., … Bernassola, F. (2008). Itch: a HECT-type E3 ligase regulating immunity, skin and cancer. *Cell Death and Differentiation*, *15*(7), 1103–1112.
Melissaridou, S., Wiechec, E., Magan, M., Jain, M. V., Chung, M. K., Farnebo, L., & Roberg, K. (2019). The effect of 2D and 3D cell cultures on treatment response, EMT profile and stem cell features in head and neck cancer. *Cancer Cell International*, *19*(1), 16.
Meng, Z., Moroishi, T., & Guan, K.-L. (2016). Mechanisms of Hippo pathway regulation. *Genes & Development*, *30*(1), 1–17.
Miller, D. G., Adam, M. A., & Miller, A. D. (1990). Gene transfer by retrovirus vectors occurs only in cells that are actively replicating at the time of infection. *Molecular and Cellular Biology*, *10*(8), 4239–4242.
Mohni, K. N., Kavanaugh, G. M., & Cortez, D. (2014). ATR pathway inhibition is

synthetically lethal in cancer cells with ERCC1 deficiency. *Cancer Research*, *74*(10), 2835–2845.
Mohni, K. N., Thompson, P. S., Luzwick, J. W., Glick, G. G., Pendleton, C. S., Lehmann, B. D., … Cortez, D. (2015). A Synthetic Lethal Screen Identifies DNA Repair Pathways that Sensitize Cancer Cells to Combined ATR Inhibition and Cisplatin Treatments. *PloS One*, *10*(5), e0125482.
Mojica, F. J. M., Díez-Villaseñor, C., García-Martínez, J., & Almendros, C. (2009). Short motif sequences determine the targets of the prokaryotic CRISPR defence system. *Microbiology (Reading, England)*, *155*(Pt 3), 733–740.
Moniz, L., Dutt, P., Haider, N., & Stambolic, V. (2011). Nek family of kinases in cell cycle, checkpoint control and cancer. *Cell Division*.
Morgan, R. G., Chambers, A. C., Legge, D. N., Coles, S. J., Greenhough, A., & Williams, A. C. (2018). Optimized delivery of siRNA into 3D tumor spheroid cultures in situ. *Scientific Reports*, *8*(1), 7952.
Mühlebach, M. D., Wolfrum, N., Schüle, S., Tschulena, U., Sanzenbacher, R., Flory, E., … Schweizer, M. (2005). Stable Transduction of Primary Human Monocytes by Simian Lentiviral Vector PBj. *Molecular Therapy*, *12*(6), 1206–1216.
Murchison, E. P., Partridge, J. F., Tam, O. H., Cheloufi, S., & Hannon, G. J. (2005). Characterization of Dicer-deficient murine embryonic stem cells. *Proceedings of the National Academy of Sciences of the United States of America*, *102*(34), 12135–12140.
Nagalakshmi, U., Wang, Z., Waern, K., Shou, C., Raha, D., Gerstein, M., & Snyder, M. (2008). The transcriptional landscape of the yeast genome defined by RNA sequencing. *Science (New York, N.Y.)*, *320*(5881), 1344–1349.
Naldini, L., Blomer, U., Gallay, P., Ory, D., Mulligan, R., Gage, F. H., … Trono, D. (1996). In Vivo Gene Delivery and Stable Transduction of Nondividing Cells by a Lentiviral Vector. *Science*, *272*(5259), 263–267.
Nalepa, G., Rolfe, M., & Harper, J. W. (2006). Drug discovery in the ubiquitin–proteasome system. *Nature Reviews Drug Discovery*, *5*(7), 596–613.
Nayerossadat, N., Maedeh, T., & Ali, P. A. (2012). Viral and nonviral delivery systems for gene delivery. *Advanced Biomedical Research*, *1*, 27.
Neil, S., Martin, F., Ikeda, Y., & Collins, M. (2001). Postentry restriction to human immunodeficiency virus-based vector transduction in human monocytes. *Journal of Virology*, *75*(12), 5448–5456.
Newick, K., O'Brien, S., Moon, E., & Albelda, S. M. (2017). CAR T Cell Therapy for Solid Tumors. *Annual Review of Medicine*, *68*(1), 139–152.
Nihongaki, Y., Kawano, F., Nakajima, T., & Sato, M. (2015). Photoactivatable CRISPR-Cas9 for optogenetic genome editing. *Nature Biotechnology*, *33*(7), 755–760.
Nihongaki, Y., Yamamoto, S., Kawano, F., Suzuki, H., & Sato, M. (2015). CRISPR-Cas9-based Photoactivatable Transcription System. *Chemistry & Biology*, *22*(2), 169–174.
Nijweide, P. J., Burger, E. H., & Feyen, J. H. (1986). Cells of bone: proliferation, differentiation, and hormonal regulation. *Physiological Reviews*, *66*(4), 855–886.
Nishiyama, A., Matsui, M., Iwata, S., Hirota, K., Masutani, H., Nakamura, H., … Yodoi, J. (1999). Identification of Thioredoxin-binding Protein-2/Vitamin D3 Up-regulated Protein 1 as a Negative Regulator of Thioredoxin Function and Expression. *Journal of Biological Chemistry*, *274*(31), 21645–21650.
Nishizawa, K., Nishiyama, H., Matsui, Y., Kobayashi, T., Saito, R., Kotani, H., … Ogawa, O. (2011). Thioredoxin-interacting protein suppresses bladder carcinogenesis. *Carcinogenesis*, *32*(10), 1459–1466.
Novina, C. D., Murray, M. F., Dykxhoorn, D. M., Beresford, P. J., Riess, J., Lee, S.-K., … Sharp, P. A. (2002). Erratum: siRNA-directed inhibition of HIV-1 infection. *Nature*

Medicine, *8*(7), 681–686.
Oleykowski, C. A., Bronson Mullins, C. R., Godwin, A. K., & Yeung, A. T. (1998). Mutation detection using a novel plant endonuclease. *Nucleic Acids Research*, *26*(20), 4597–4602. Retrieved from http://www.ncbi.nlm.nih.gov/pubmed/9753726
Oliver, P. M., Cao, X., Worthen, G. S., Shi, P., Briones, N., MacLeod, M., … Yang, B. (2006). Ndfip1 protein promotes the function of itch ubiquitin ligase to prevent T cell activation and T helper 2 cell-mediated inflammation. *Immunity*, *25*(6), 929–940.
Omi, K., Tokunaga, K., & Hohjoh, H. (2004). Long-lasting RNAi activity in mammalian neurons. *FEBS Letters*, *558*(1–3), 89–95.
Ooi, S. L., Shoemaker, D. D., & Boeke, J. D. (2003). DNA helicase gene interaction network defined using synthetic lethality analyzed by microarray. *Nature Genetics*, *35*(3), 277–286.
Otaki, Y., Takahashi, H., Watanabe, T., Funayama, A., Netsu, S., Honda, Y., … Kubota, I. (2016). HECT-Type Ubiquitin E3 Ligase ITCH Interacts With Thioredoxin-Interacting Protein and Ameliorates Reactive Oxygen Species-Induced Cardiotoxicity. *Journal of the American Heart Association*, *5*(1).
Pardo, B., Gómez-Gonzµlez, B., Aguilera, A., & Vespucio, A. (2009). *DNA double-strand break repair: how to fix a broken relationship*.
Pardoll, D. M. (2012). The blockade of immune checkpoints in cancer immunotherapy. *Nature Reviews Cancer*, *12*(4), 252–264.
Park, S., Jung, E.-H., Kim, G.-Y., Kim, B.-C., Lim, J. H., & Woo, C.-H. (2015). Itch E3 ubiquitin ligase positively regulates TGF-β signaling to EMT via Smad7 ubiquitination. *Molecules and Cells*, *38*(1), 20–25.
Patra, B., Peng, C.-C., Liao, W.-H., Lee, C.-H., & Tung, Y.-C. (2016). Drug testing and flow cytometry analysis on a large number of uniform sized tumor spheroids using a microfluidic device. *Scientific Reports*, *6*, 21061.
Perry, W. L., Hustad, C. M., Swing, D. A., O'Sullivan, T. N., Jenkins, N. A., & Copeland, N. G. (1998). The itchy locus encodes a novel ubiquitin protein ligase that is disrupted in a18H mice. *Nature Genetics*, *18*(2), 143–146.
Petroski, M. D. (2008). The ubiquitin system, disease, and drug discovery. *BMC Biochemistry*, *9 Suppl 1*(Suppl 1), S7.
Pittenger, M. F., Mackay, A. M., Beck, S. C., Jaiswal, R. K., Douglas, R., Mosca, J. D., … Marshak, D. R. (1999). Multilineage potential of adult human mesenchymal stem cells. *Science (New York, N.Y.)*, *284*(5411), 143–147.
Polstein, L. R., & Gersbach, C. A. (2015). A light-inducible CRISPR-Cas9 system for control of endogenous gene activation. *Nature Chemical Biology*, *11*(3), 198–200.
Qasim, W., Zhan, H., Samarasinghe, S., Adams, S., Amrolia, P., Stafford, S., … Veys, P. (2017). Molecular remission of infant B-ALL after infusion of universal TALEN gene-edited CAR T cells. *Science Translational Medicine*, *9*(374), eaaj2013.
Qi, L. S., Larson, M. H., Gilbert, L. A., Doudna, J. A., Weissman, J. S., Arkin, A. P., & Lim, W. A. (2013). Repurposing CRISPR as an RNA-Guided Platform for Sequence-Specific Control of Gene Expression. *Cell*, *152*(5), 1173–1183.
Qiu, L., Joazeiro, C., Fang, N., Wang, H. Y., Elly, C., Altman, Y., … Liu, Y. C. (2000). Recognition and ubiquitination of Notch by Itch, a hect-type E3 ubiquitin ligase. *The Journal of Biological Chemistry*, *275*(46), 35734–35737.
Qiu, P., Shandilya, H., D'Alessio, J. M., O'Connor, K., Durocher, J., & Gerard, G. F. (2004). Mutation detection using Surveyor nuclease. *BioTechniques*, *36*(4), 702–707. Retrieved from http://www.ncbi.nlm.nih.gov/pubmed/15088388
Ran, F. A., Hsu, P. D., Lin, C. Y., Gootenberg, J. S., Konermann, S., Trevino, A. E., … Zhang, F. (2013). Double nicking by RNA-guided CRISPR cas9 for enhanced genome

editing specificity. *Cell*, *154*(6), 1380–1389.
Rao, D. D., Vorhies, J. S., Senzer, N., & Nemunaitis, J. (2009). siRNA vs. shRNA: Similarities and differences. *Advanced Drug Delivery Reviews*, *61*(9), 746–759.
Rao, H., Tan, J., Faruqi, F., & Beltzer, J. (2010). *Corning ® Osteo Assay Surface: A New Tool to Study Osteoclast and Osteoblast Differentiation and Function*. Retrieved from https://www.corning.com/media/worldwide/cls/documents/snappshots_CLS_AN_144_osteo_assay.pdf
Rath, D., Amlinger, L., Rath, A., & Lundgren, M. (2015). The CRISPR-Cas immune system: biology, mechanisms and applications. *Biochimie*, *117*, 119–128.
Reaper, P. M., Griffiths, M. R., Long, J. M., Charrier, J.-D., Maccormick, S., Charlton, P. A., … Pollard, J. R. (2011). Selective killing of ATM- or p53-deficient cancer cells through inhibition of ATR. *Nature Chemical Biology*, *7*(7), 428–430.
Ren, J., Liu, X., Fang, C., Jiang, S., June, C. H., & Zhao, Y. (2017). Multiplex Genome Editing to Generate Universal CAR T Cells Resistant to PD1 Inhibition. *Clinical Cancer Research*, *23*(9), 2255–2266.
Reuter, S., Gupta, S. C., Chaturvedi, M. M., & Aggarwal, B. B. (2010). Oxidative stress, inflammation, and cancer: how are they linked? *Free Radical Biology & Medicine*, *49*(11), 1603–1616.
Riling, C., Kamadurai, H., Kumar, S., O'Leary, C. E., Wu, K.-P., Manion, E. E., … Oliver, P. M. (2015). Itch WW Domains Inhibit Its E3 Ubiquitin Ligase Activity by Blocking E2-E3 Ligase Trans-thiolation. *The Journal of Biological Chemistry*, *290*(39), 23875–23887.
RIPA buffer. (2006). *Cold Spring Harbor Protocols*.
Rizo, J., & Südhof, T. C. (1998). C2-domains, structure and function of a universal Ca2+-binding domain. *The Journal of Biological Chemistry*, *273*(26), 15879–15882.
Robb, G. B., & Rana, T. M. (2007). RNA Helicase A Interacts with RISC in Human Cells and Functions in RISC Loading. *Molecular Cell*, *26*(4), 523–537.
Rossi, M, Rotblat, B., Ansell, K., Amelio, I., Caraglia, M., Misso, G., … Melino, G. (2014). High throughput screening for inhibitors of the HECT ubiquitin E3 ligase ITCH identifies antidepressant drugs as regulators of autophagy. *Cell Death & Disease*, *5*, e1203.
Rossi, Mario, De Laurenzi, V., Munarriz, E., Green, D. R., Liu, Y.-C., Vousden, K. H., … Melino, G. (2005). The ubiquitin-protein ligase Itch regulates p73 stability. *The EMBO Journal*, *24*(4), 836–848.
Rossi, Mario, Munarriz, E. R., Bartesaghi, S., Milanese, M., Dinsdale, D., Guerra-Martin, M. A., … Melino, G. (2009). Desmethylclomipramine induces the accumulation of autophagy markers by blocking autophagic flux. *Journal of Cell Science*, *122*(Pt 18), 3330–3339.
Roth, T. L., Puig-Saus, C., Yu, R., Shifrut, E., Carnevale, J., Li, P. J., … Marson, A. (2018). Reprogramming human T cell function and specificity with non-viral genome targeting. *Nature*, *559*(7714), 405–409.
Sakuma, T., Barry, M. A., & Ikeda, Y. (2012). Lentiviral vectors: basic to translational. *Biochemical Journal*, *443*(3).
Sakurai, T., Watanabe, S., Kamiyoshi, A., Sato, M., & Shindo, T. (2014). A single blastocyst assay optimized for detecting CRISPR/Cas9 system-induced indel mutations in mice. *BMC Biotechnology*, *14*, 69.
Salah, Z., Itzhaki, E., & Aqeilan, R. I. (2014). The ubiquitin E3 ligase ITCH enhances breast tumor progression by inhibiting the Hippo tumor suppressor pathway. *Oncotarget*, *5*(21), 10886–10900.
Salah, Z., Melino, G., & Aqeilan, R. I. (2011). Negative regulation of the Hippo pathway by

E3 ubiquitin ligase ITCH is sufficient to promote tumorigenicity. *Cancer Research*, *71*(5), 2010–2020.
Salic, A., Lee, E., Mayer, L., & Kirschner, M. W. (2000). Control of β-catenin stability: Reconstitution of the cytoplasmic steps of the Wnt pathway in Xenopus egg extracts. *Molecular Cell*.
Sampath, D., Calin, G. A., Puduvalli, V. K., Gopisetty, G., Taccioli, C., Liu, C. G., … Plunkett, W. (2009). Specific activation of microRNA 106b enables the p73 apoptotic response in chronic lymphocytic leukemia by targeting the ubiquitin ligase Itch for degradation. *Blood*.
Sanjana, N. E., Shalem, O., & Zhang, F. (2014). Improved vectors and genome-wide libraries for CRISPR screening. *Nature Methods*, *11*(8), 783–784.
Saxena, G., Chen, J., & Shalev, A. (2010). Intracellular shuttling and mitochondrial function of thioredoxin-interacting protein. *The Journal of Biological Chemistry*, *285*(6), 3997–4005.
Schmidlin, T., Garrigues, L., Lane, C. S., Mulder, T. C., van Doorn, S., Post, H., … Altelaar, A. F. M. (2016). Assessment of SRM, MRM ^{3} , and DIA for the targeted analysis of phosphorylation dynamics in non-small cell lung cancer. *PROTEOMICS*, *16*(15–16), 2193–2205.
Sirven, A., Pflumio, F., Zennou, V., Chapuis, B., Zubler, R., & Trono, D. (2002). The human immunodeficiency virus type-1 central DNA flap is a crucial determinant for lentiviral vector nuclear import and gene transduction of human hematopoietic stem cells. *Blood*, *96*(13), 4103–4110.
Sluimer, J., & Distel, B. (2018). Regulating the human HECT E3 ligases. *Cellular and Molecular Life Sciences : CMLS*, *75*(17), 3121–3141.
Song, E., Lee, S.-K., Dykxhoorn, D. M., Novina, C., Zhang, D., Crawford, K., … Shankar, P. (2003). Sustained small interfering RNA-mediated human immunodeficiency virus type 1 inhibition in primary macrophages. *Journal of Virology*, *77*(13), 7174–7181.
Souza, A. G., Silva, I. B. B., Campos-Fernandez, E., Barcelos, L. S., Souza, J. B., Marangoni, K., … Alonso-Goulart, V. (2018). Comparative Assay of 2D and 3D Cell Culture Models: Proliferation, Gene Expression and Anticancer Drug Response. *Current Pharmaceutical Design*, *24*(15), 1689–1694.
Stepanenko, A. A., & Dmitrenko, V. V. (2015). HEK293 in cell biology and cancer research: phenotype, karyotype, tumorigenicity, and stress-induced genome-phenotype evolution. *Gene*, *569*(2), 182–190.
Sung, P.-L., Jan, Y.-H., Lin, S.-C., Huang, C.-C., Lin, H., Wen, K.-C., … Huang, C.-Y. F. (2016). Periostin in tumor microenvironment is associated with poor prognosis and platinum resistance in epithelial ovarian carcinoma. *Oncotarget*, *7*(4), 4036–4047.
Szklarczyk, D., Franceschini, A., Wyder, S., Forslund, K., Heller, D., Huerta-Cepas, J., … Von Mering, C. (2015). STRING v10: Protein-protein interaction networks, integrated over the tree of life. *Nucleic Acids Research*.
Tapon, N., Harvey, K. F., Bell, D. W., Wahrer, D. C. R., Schiripo, T. A., Haber, D. A., & Hariharan, I. K. (2002). salvador Promotes Both Cell Cycle Exit and Apoptosis in Drosophila and Is Mutated in Human Cancer Cell Lines. *Cell*, *110*(4), 467–478.
Terns, M. P., & Terns, R. M. (2011). CRISPR-based adaptive immune systems. *Current Opinion in Microbiology*, *14*(3), 321–327.
Theivanthiran, B., Kathania, M., Zeng, M., Anguiano, E., Basrur, V., Vandergriff, T., … Venuprasad, K. (2015). The E3 ubiquitin ligase Itch inhibits p38α signaling and skin inflammation through the ubiquitylation of Tab1. *Science Signaling*, *8*(365), ra22.
Thomas, C. E., Ehrhardt, A., & Kay, M. A. (2003). Progress and problems with the use of viral vectors for gene therapy. *Nature Reviews. Genetics*, *4*(5), 346–358.

Tian, M., Bai, C., Lin, Q., Lin, H., Liu, M., Ding, F., & Wang, H.-R. (2011). Binding of RhoA by the C2 domain of E3 ligase Smurf1 is essential for Smurf1-regulated RhoA ubiquitination and cell protrusive activity. *FEBS Letters*, *585*(14), 2199–2204.

Tong, A. H., Evangelista, M., Parsons, A. B., Xu, H., Bader, G. D., Pagé, N., … Boone, C. (2001). Systematic genetic analysis with ordered arrays of yeast deletion mutants. *Science (New York, N.Y.)*, *294*(5550), 2364–2368.

Tuschl, T. (2002). Expanding small RNA interference. *Nature Biotechnology*, *20*(5), 446–448.

Väänänen, H. K., Zhao, H., Mulari, M., & Halleen, J. M. (2000). The cell biology of osteoclast function. *Journal of Cell Science*.

van Furth, R., Raeburn, J., & van Zwet, T. (1979). Characteristics of human mononuclear phagocytes. *Blood*, *54*(2). Retrieved from http://www.bloodjournal.org/content/54/2/485.long?sso-checked=true

Venuprasad, K., Huang, H., Harada, Y., Elly, C., Subramaniam, M., Spelsberg, T., … Liu, Y.-C. (2008). The E3 ubiquitin ligase Itch regulates expression of transcription factor Foxp3 and airway inflammation by enhancing the function of transcription factor TIEG1. *Nature Immunology*, *9*(3), 245–253.

Venuprasad, K., Zeng, M., Baughan, S. L., & Massoumi, R. (2015). Multifaceted role of the ubiquitin ligase Itch in immune regulation. *Immunology and Cell Biology*, *93*(5), 452–460.

Vestergaard, P., Rejnmark, L., & Mosekilde, L. (2008). Selective Serotonin Reuptake Inhibitors and Other Antidepressants and Risk of Fracture. *Calcified Tissue International*, *82*(2), 92–101.

Victora, G. D., & Nussenzweig, M. C. (2012). *Germinal Centers*. Retrieved from http://www.annualreviews.org/doi/abs/10.1146/annurev-immunol-020711-075032

Vincent, A., Herman, J., Schulick, R., Hruban, R. H., & Goggins, M. (2011). Pancreatic cancer. *Lancet (London, England)*, *378*(9791), 607–620.

Visconti, R., & Grieco, D. (2009). New insights on oxidative stress in cancer. *Current Opinion in Drug Discovery & Development*, *12*(2), 240–245. Retrieved from http://www.ncbi.nlm.nih.gov/pubmed/19333869

Vouillot, L., Thélie, A., & Pollet, N. (2015). Comparison of T7E1 and surveyor mismatch cleavage assays to detect mutations triggered by engineered nucleases. *G3 (Bethesda, Md.)*, *5*(3), 407–415.

Vowinckel, J., Capuano, F., Campbell, K., Deery, M. J., Lilley, K. S., & Ralser, M. (2013). The beauty of being (label)-free: sample preparation methods for SWATH-MS and next-generation targeted proteomics. *F1000Research*, *2*, 272.

Walker, L. S. K., & Abbas, A. K. (2002). The enemy within: keeping self-reactive T cells at bay in the periphery. *Nature Reviews Immunology*, *2*(1), 11–19.

Williams, J. W., Tjota, M. Y., & Sperling, A. I. (2012). The contribution of allergen-specific IgG to the development of th2-mediated airway inflammation. *Journal of Allergy*, *2012*(Figure 1), 236075.

Wu, H., & Leng, R. P. (2015). MDM2 mediates p73 ubiquitination: a new molecular mechanism for suppression of p73 function. *Oncotarget*, *6*(25), 21479–21492.

Xiao, J., Shi, Q., Li, W., Mu, X., Peng, J., Li, M., … Fan, J. (2018). ARRDC1 and ARRDC3 act as tumor suppressors in renal cell carcinoma by facilitating YAP1 degradation. *American Journal of Cancer Research*, *8*(1), 132–143. Retrieved from http://www.ncbi.nlm.nih.gov/pubmed/29416926

Xiao, N., Eto, D., Elly, C., Peng, G., Crotty, S., & Liu, Y.-C. (2014). The E3 ubiquitin ligase Itch is required for the differentiation of follicular helper T cells. *Nature Immunology*, *15*(7), 657–666.

Yamashita, T., Takahashi, N., & Udagawa, N. (2012). New roles of osteoblasts involved in osteoclast differentiation. *World Journal of Orthopedics*, *3*(11), 175–181.
Yang, A, Walker, N., Bronson, R., Kaghad, M., Oosterwegel, M., Bonnin, J., … Caput, D. (2000). p73-deficient mice have neurological, pheromonal and inflammatory defects but lack spontaneous tumours. *Nature*, *404*(6773), 99–103.
Yang, Annie, Kaghad, M., Caput, D., & McKeon, F. (2002). On the shoulders of giants: p63, p73 and the rise of p53. *Trends in Genetics*, *18*(2), 90–95.
Yang, C., Zhou, W., Jeon, M., Demydenko, D., Harada, Y., Zhou, H., & Liu, Y.-C. (2006). Negative Regulation of the E3 Ubiquitin Ligase Itch via Fyn-Mediated Tyrosine Phosphorylation. *Molecular Cell*, *21*(1), 135–141.
Yang, W. J., Hao, Y. X., Yang, X., Fu, X. L., Shi, Y., Yue, H. L., … Yu, P. W. (2018). Overexpression of Tie2 is associated with poor prognosis in patients with gastric cancer. *Oncology Letters*.
Yu-Wai-Man, C., Tagalakis, A. D., Manunta, M. D., Hart, S. L., & Khaw, P. T. (2016). Receptor-targeted liposome-peptide-siRNA nanoparticles represent an efficient delivery system for MRTF silencing in conjunctival fibrosis. *Scientific Reports*, *6*, 21881.
Zhang, H.-W., Ding, J., Jin, J.-L., Guo, J., Liu, J.-N., Karaplis, A., … Miao, D. (2010). Defects in mesenchymal stem cell self-renewal and cell fate determination lead to an osteopenic phenotype in Bmi-1 null mice. *Journal of Bone and Mineral Research*, *25*(3), 640–652.
Zhang, H., Wu, C., Matesic, L. E., Li, X., Wang, Z., Boyce, B. F., & Xing, L. (2013a). Ubiquitin E3 ligase Itch negatively regulates osteoclast formation by promoting deubiquitination of tumor necrosis factor (TNF) receptor-associated factor 6. *The Journal of Biological Chemistry*, *288*(31), 22359–22368.
Zhang, H., Wu, C., Matesic, L. E., Li, X., Wang, Z., Boyce, B. F., & Xing, L. (2013b). Ubiquitin E3 ligase Itch negatively regulates osteoclast formation by promoting deubiquitination of tumor necrosis factor (TNF) receptor-associated factor 6. *The Journal of Biological Chemistry*, *288*(31), 22359–22368.
Zhang, H., & Xing, L. (2013). Ubiquitin E3 Ligase Itch Negatively Regulates Osteoblast Differentiation from Mesenchymal Progenitor Cells. *STEM CELLS*, *31*(8), 1574–1583.
Zhang, P., Wang, C., Gao, K., Wang, D., Mao, J., An, J., … Yu, L. (2010). The ubiquitin ligase itch regulates apoptosis by targeting thioredoxin-interacting protein for ubiquitin-dependent degradation. *The Journal of Biological Chemistry*, *285*(12), 8869–8879.
Zhang, S., Zhao, B., Jiang, H., Wang, B., & Ma, B. (2007). Cationic lipids and polymers mediated vectors for delivery of siRNA. *Journal of Controlled Release*, *123*(1), 1–10.
Zhao, B., Li, L., Wang, L., Wang, C.-Y., Yu, J., & Guan, K.-L. (2012). Cell detachment activates the Hippo pathway via cytoskeleton reorganization to induce anoikis. *Genes & Development*, *26*(1), 54–68.
Zhao, B., Wei, X., Li, W., Udan, R. S., Yang, Q., Kim, J., … Guan, K.-L. (2007). Inactivation of YAP oncoprotein by the Hippo pathway is involved in cell contact inhibition and tissue growth control. *Genes & Development*, *21*(21), 2747–2761.
Zhao, B., Ye, X., Yu, J., Li, L., Li, W., Li, S., … Guan, K.-L. (2008). TEAD mediates YAP-dependent gene induction and growth control. *Genes & Development*, *22*(14), 1962–1971.
Zhao, L., Huang, J., Guo, R., Wang, Y., Chen, D., & Xing, L. (2010). Smurf1 inhibits mesenchymal stem cell proliferation and differentiation into osteoblasts through JunB degradation. *Journal of Bone and Mineral Research : The Official Journal of the American Society for Bone and Mineral Research*, *25*(6), 1246–1256.
Zheng, N., & Shabek, N. (2017). Ubiquitin Ligases: Structure, Function, and Regulation. *Annual Review of Biochemistry*, *86*(1), 129–157.

Zhu, K., Shan, Z., Chen, X., Cai, Y., Cui, L., Yao, W., … Wen, W. (2017). Allosteric auto-inhibition and activation of the Nedd4 family E3 ligase Itch. *EMBO Reports*, *18*(9), 1618–1630.

Zufferey, R., Nagy, D., Mandel, R. J., Naldini, L., & Trono, D. (1997). Multiply attenuated lentiviral vector achieves efficient gene delivery in vivo. *Nature Biotechnology*, *15*(9), 871–875.

Zuris, J. A., Thompson, D. B., Shu, Y., Guilinger, J. P., Bessen, J. L., Hu, J. H., … Liu, D. R. (2014). Cationic lipid-mediated delivery of proteins enables efficient protein-based genome editing in vitro and in vivo. *Nature Biotechnology*, *33*(1), 73–80.

Appendices:

Appendix 1: Original documentation for MiaPaCa-2 stocks:

MIA PaCa2

218502

ATCC

Product Information Sheet for ATCC ® ™

Product **ATCC-CRL-1420**

Lot Number 59270201

99

Designation: MIA PaCa-2 Description: Pancreatic Carcinoma
Total Cells/mL: 8.3 x 10(5)
Expected Viability: 87.0% to 97.3%
Ampule Passage No.: Unknown
Population Doubling (PDL): N/A
Dilute Ampule Content: 1:10 (T-25) or 1:15 (T-75)
Volume/Ampule: 1 mL
Date Frozen: 06/15/10

A T-25 setup at a dilution of 1:10 reaches approximately 90% confluence in 7 days. A T-75 setup at a dilution of 1:15 reaches approximately 70% confluence in 7 days.

American Type Culture Collection
10801 University Boulevard
Manassas, VA 20110-2209

For technical enquiries in Europe contact:
LGC Standards
E-mail: atcc-tech@lgcstandards.com
Telephone: +44(0)20 8943 8489
Fax: +44(0)20 8943 8405
web site: www.lgcstandards-atcc.org

Appendix 2: Project ethics approval documentation:

University of St Andrews | FOUNDED 1413

University Teaching and Research Ethics Committee

15th January 2018

Professor David Harrison
School of Medicine

Dear Professor Harrison

Thank you for submitting your amendment application which comprised the following documents:

1. Ethical Amendment Application Form

The School of Medicine Ethics Committee is delegated to act on behalf of the University Teaching and Research Ethics Committee (UTREC) and has approved this ethical amendment application. The particulars of this approval are as follows:

Original Approval Code:	MD9202	**Approved on:**	16/10/2012
Amendment 5 Approval Date:	15/01/18	**Approval Expiry Date:**	16/10/2022
Term of Approval	10 YEARS		
Project Title:	Systems pathology of disease		
Researcher(s):	David Harrison, Fiona McKissock, Jennifer Bre, Peter Caie, In Hwa Um, Oliver Read, Ines Nearchou, Christos Gavriel, Nasfytos Dimitriou, Hannah Williams, Mustafa Elshani, Raffaele De Filippis, Mary Kudsy, Mark Bates, Romina Brilla, Nourjahan Khafaga, Sophie Rae, Tsz Chan, Matthew Scott, Beth Gwyther	**Supervisor(s):**	David Harrison

Ethical amendment approval does not extend the originally granted approval period, rather it validates the changes you have made to the originally approved ethical application. If you are unable to complete your research within the original validation period, you are required to write to your School Ethics Committee Convener to request a discretionary extension of no greater than 6 months or to re-apply if directed to do so, and you should inform your School Ethics Committee when your project reaches completion.

Any serious adverse events or significant change which occurs in connection with this study and/or which may alter its ethical consideration, must be reported immediately to the School Ethics Committee, and an Ethical Amendment Form submitted where appropriate.

Approval is given on the understanding that you adhere to the 'Guidelines for Ethical Research Practice' (http://www.st-andrews.ac.uk/media/UTREC/guidelines%20Feb%2008.pdf).

Yours sincerely,

Dr Morven Shearer, Convenor School of Medicine Ethics Committee

School of Medicine Ethics Committee
Medical and Biological Sciences Building, North Haugh, St Andrews, Fife, KY16 9TF, Scotland, UK
Email: medethic@st-andrews.ac.uk Tel No: 01334 463585
The University of St Andrews is a charity registered in Scotland: No SC013532

Appendix 3: TMA ethics approval documentation:

Document Name	QF-TGU-A-SAMREQA VERSION 1.1	Page	1 of 1	Review date	25-Sep-2017

LOTHIAN NRS BIORESOURCE
SAMPLE REQUEST ANSWER FORM

Sample Request number:	SR554
Name of Researcher:	Prof David Harrison
Address of Researcher:	Laboratory Medicine Royal Infirmary of Edinburgh
Study Title:	Expression of candidate prognostic and theranostic biomarkers in a variety of cancer types.
Ethical status:	15/ES/0094
Material Requested	Release and use of the following is approved by Tissue Governance for use in the above study: Sections from various TMA blocks of anonymised archival tissues.

REQUEST AUTHORISED

Date:	25-Sep-2015
Authorised by:	Frances Rae

REQUEST REJECTED

Date:	
Authorised by:	
Reason	

Author : Frances Rae	**Date : 25-Sep-2015**
Authority for Issue : Craig Marshall	**Date : 25-Sep-2015**
Quality Checked : Craig Marshall	**Date : 25-Sep-2015**

Appendix 4: SWATH spectral library summary:

ProteinPilot Controlled Vocabulary Accession (PPCV#)		OR_SCX_IDA_6ug_all.group
	Report Template Version	**1.00 light report**
	Single Column Summary Format Version	**5**
	Identification Yields by False Discovery Rate Analysis	
FDR Analysis	**Identification Yields**	
	Protein level 1% Local FDR	6466
	Protein level 5% Local FDR	**6607**
	Protein level 10% Local FDR	6673
	Protein level 1% Global FDR	**6876**
	Protein level 5% Global FDR	7220
	Protein level 10% Global FDR	7332
	Distinct peptide level 1% Local FDR	49339
	Distinct peptide level 5% Local FDR	**53839**
	Distinct peptide level 10% Local FDR	55792

Distinct peptide level 1% Global FDR	**57826**
Distinct peptide level 5% Global FDR	64153
Distinct peptide level 10% Global FDR	69436
Spectral level 1% Local FDR	184426
Spectral level 5% Local FDR	**199826**
Spectral level 10% Local FDR	206901
Spectral level 1% Global FDR	**214826**
Spectral level 5% Global FDR	238051
Spectral level 10% Global FDR	256226
Corresponding Reported Confidences	
Protein level 1% Local FDR	97.5%
Protein level 5% Local FDR	**91.9%**
Protein level 10% Local FDR	85.5%
Protein level 1% Global FDR	**51.0%**
Protein level 5% Global FDR	12.9%
Protein level 10% Global FDR	10.9%
Distinct peptide level 1% Local FDR	99.4%
Distinct peptide level 5% Local FDR	**96.9%**
Distinct peptide level 10% Local FDR	92.9%
Distinct peptide level 1% Global FDR	**84.6%**
Distinct peptide level 5% Global FDR	38.8%
Distinct peptide level 10% Global FDR	21.8%
Spectral level 1% Local FDR	98.6%
Spectral level 5% Local FDR	**92.8%**
Spectral level 10% Local FDR	84.8%
Spectral level 1% Global FDR	**67.1%**

	Spectral level 5% Global FDR	17.3%
	Spectral level 10% Global FDR	0.1%

Metadata

Metadata		
	Attributes - General	
Attributes - General	Group filename	**OR_SCX_IDA_6ug_all.group**
Attributes - General	Start date	**42822**
Attributes - General	Start time	**03/27/2017 17:39:32**
Attributes - General	User name	**PC08843\MassSpec**
Attributes - General	Internal search identifier number	
	Attributes - Input data	
Attributes - Input data	Number of spectra in search	**399447**

Attributes - Input data	Number of non-empty spectra in search	**399446**
Attributes - Input data	Number of input files	**12**
	Parameters - User settings	
Parameters - User settings	Sample Type	**Identification**
Parameters - User settings	Cysteine Alkylation	**Iodoacetamide**
Parameters - User settings	Digestion	**Trypsin**
Parameters - User settings	Special Factors	**Urea denaturation**
Parameters - User settings	Instrument	**TripleTOF 5600**
Parameters - User settings	Species	
Parameters - User settings	Search Effort	**Rapid**
Parameters - User settings	ID Focus	
Parameters - User settings	Minimum Unused ProtScore	**0**
Parameters - User settings	FDR Analysis	**Yes**

Parameters - User settings	Quantitation	
Parameters - User settings	Background Correction	**No**
Parameters - User settings	Bias Correction	**Yes**
Parameters - User settings	Channel to use as denominator in ratios	
Parameters - User settings	Modified Data Dictionary or Parameter Translation	**No**
	Attributes - Search database	
Attributes - Search database	Database filename	**C:\AB SCIEX\ProteinPilot Data\SearchDatabases \SP_HUMAN_uniprot_ sprot_iRT.fasta**
Attributes - Search database	Number of Proteins in Database	**20204**
Attributes - Search database	Number of proteins searched	**40408**
Attributes - Search database	Number of Residues in Database	**0**
Attributes - Search database	Number of residues searched	**0**

	Attributes - Hardware	
Attributes - Hardware	RAM (MB)	**32675**
Attributes - Hardware	Computer name	**PC08843**
Attributes - Hardware	Number of cores in computer	**18**
Attributes - Hardware	Number of threads (double cores if hyperthreading on)	**36**
	Attributes - Software environment	
Attributes - Software environment	Number of cores licensed to use	**16**
Attributes - Software environment	Operating system	**Windows 7 Professional Service Pack 1 (6.1.7601)**
Attributes - Software environment	ProteinPilot Software Version	**5.0.1.0, 4895**
Attributes - Software environment	Paragon Algorithm Version	**5.0.1.0, 4874**
Attributes - Software environment	Application name	**ProteinPilot(tm) Software**
	Statistics - Protein Summary Table	

Statistics - Protein Summary Table	Percent Confidence of first row in Summary Statistics ID Statistics	**99**
Statistics - Protein Summary Table	Distinct peptides associated with 99% confidence proteins	**66936**
Statistics - Protein Summary Table	Proteins before grouping (99% confidence)	**6307**
Statistics - Protein Summary Table	Proteins detected (99% confidence)	**5606**
Statistics - Protein Summary Table	Spectra associated with 99% confidence proteins	**237379**
Statistics - Protein Summary Table	Percent Confidence of first row in Summary Statistics ID Statistics	**95**
Statistics - Protein Summary Table	Distinct peptides associated with 95% confidence proteins	**68295**
Statistics - Protein Summary Table	Proteins before grouping (95% confidence)	**7361**
Statistics - Protein Summary Table	Proteins detected (95% confidence)	**6557**
Statistics - Protein Summary Table	Spectra associated with 95% confidence proteins	**239729**
Statistics - Protein Summary Table	Percent Confidence of first row in Summary Statistics ID Statistics	**66**

Statistics - Protein Summary Table	Distinct peptides associated with 66% confidence proteins	**68759**
Statistics - Protein Summary Table	Proteins before grouping (66% confidence)	**7663**
Statistics - Protein Summary Table	Proteins detected (66% confidence)	**6794**
Statistics - Protein Summary Table	Spectra associated with 66% confidence proteins	**240387**
Statistics - Protein Summary Table	Percent Confidence of first row in Summary Statistics ID Statistics	**10**
Statistics - Protein Summary Table	Distinct peptides associated with 10% confidence proteins	**69945**
Statistics - Protein Summary Table	Proteins before grouping (10% confidence)	**8587**
Statistics - Protein Summary Table	Proteins detected (10% confidence)	**7332**
Statistics - Protein Summary Table	Spectra associated with 10% confidence proteins	**242263**
	Parameters - Search Dimension Factors	
Parameters - Search	Number of segments the input data are broken into	**106**

Dimension Factors		
Parameters - Search Dimension Factors	Number of searches per segment (2 for Thorough, 1 for Rapid)	**1**
Parameters - Search Dimension Factors	Number of apparent sub-searches in group file	**106**
Parameters - Search Dimension Factors	Do reversed search	**TRUE**
Parameters - Search Dimension Factors	Do separate searches for each plex in MS1 quantitation	**FALSE**
Parameters - Search Dimension Factors	Maximum number of hypotheses to keep per spectrum	**15**
	Parameters - Identification - Mass accuracy	
Parameters - Identification - Mass accuracy	MS1 initial mass error tolerance type	**dalton**
Parameters - Identification - Mass accuracy	MS1 initial mass error tolerance value	**0**

Parameters - Identification - Mass accuracy	MS2 initial mass error tolerance type	**dalton**
Parameters - Identification - Mass accuracy	MS2 initial mass error tolerance value	**0**
Parameters - Identification - Mass accuracy	MS1 final mass error standard deviation type	**dalton**
Parameters - Identification - Mass accuracy	MS1 final mass error standard deviation value	**0**
Parameters - Identification - Mass accuracy	MS2 final mass error standard deviation type	**dalton**
Parameters - Identification - Mass accuracy	MS2 final mass error standard deviation value	**0**
	Parameters - Identification - Multi-precursor search	
Parameters - Identification - Multi-precursor search	Use multi-precursor search function	**TRUE**
Parameters - Identification - Multi-precursor search	Maximum number of different precursor masses to try to match to in the Fraglet stage when doing multi-precursor search	**5**

Parameters - Identification - Multi-precursor search	Maximum dynamic range gap of secondary precursors vs primary precursor in the Fraglet stage when doing multi-precursor search	**10**
Parameters - Identification - Multi-precursor search	Maximum number of different precursor masses to try to match to in the Taglet stage when doing multi-precursor search	**1**
Parameters - Identification - Multi-precursor search	Maximum dynamic range gap of secondary precursors vs primary precursor in the Taglet stage when doing multi-precursor search	**3**
	Parameters - Identification - Charge ambiguity	
Parameters - Identification - Charge ambiguity	First charge state to consider when precursor z is not determined	**2**
Parameters - Identification - Charge ambiguity	Probability of first charge state to consider when precursor z is not determined	**1**
Parameters - Identification - Charge ambiguity	Second charge state to consider when precursor z is not determined	**3**
Parameters - Identification - Charge ambiguity	Probability of second charge state to consider when precursor z is not determined	**1**

Parameters - Identification - Charge ambiguity	Third charge state to consider when precursor z is not determined	**4**
Parameters - Identification - Charge ambiguity	Probability of third charge state to consider when precursor z is not determined	**1**
Parameters - Identification - Charge ambiguity	Fourth charge state to consider when precursor z is not determined	
Parameters - Identification - Charge ambiguity	Probability of fourth charge state to consider when precursor z is not determined	
	Parameters - Protein Grouping	
Parameters - Protein Grouping	Use Bayesian protein confidence calculation	**TRUE**
Parameters - Protein Grouping	Use peptide FDR analysis to recalibrate peptide confidences	**TRUE**
Parameters - Protein Grouping	In mid-Pro Group, minimum Intersection ProtScore to be in Same Group	**4**
Parameters - Protein Grouping	In mid-Pro Group, minimum Unused ProtScore to keep a Group	**0**
Parameters - Protein Grouping	In mid-Pro Group, keep competitor proteins with ProtScore units from winner	**6**
Parameters - Protein Grouping	In final Pro Group, minimum Intersection ProtScore to be in same group	**1**

Parameters - Protein Grouping	In final Pro Group, minimum Unused ProtScore to keep a group	**0**
Parameters - Protein Grouping	In final Pro Group, keep competitor proteins with ProtScore units from winner	**2**
	Parameters - Quantitation - processing	
Parameters - Quantitation - processing	Do isobaric quant background correction algorithm	**FALSE**
Parameters - Quantitation - processing	Normalize the central tendency of protein ratios to be unity	**TRUE**
Parameters - Quantitation - processing	Compute protein-level ratios from the median of peptide ratios	**TRUE**
Parameters - Quantitation - processing	Quant threshold setting no longer used	**-1**
Parameters - Quantitation - processing	Use measures for quantitation if signal to noise is greater than	**9**
	Parameters - Quantitation - curation	
Parameters - Quantitation - curation	Maximum number of labels allowed on a peptide for it to be used for quantitation	**35**

Parameters - Quantitation - curation	Include extreme ratios in the protein ratio calculation if the fraction of peptides from a protein having extreme ratios is greater than	**0**
Parameters - Quantitation - curation	Exclude quantitation data if identification confidence does not pass a threshold value	**TRUE**
Parameters - Quantitation - curation	Exclude quantitation data if a minimum intensity is not passed	**TRUE**
Parameters - Quantitation - curation	Exclude quantitation data based on discordant peptide logic	**TRUE**
Parameters - Quantitation - curation	Exclude quantitation data using sharing logic	**TRUE**
Parameters - Quantitation - curation	Minimum protein confidence to consider a protein confident and capable of excluding spectra as shared	**1**
Parameters - Quantitation - curation	Minimum peptide percent confidence from a confident protein to consider a spectrum shared	**15**
Parameters - Quantitation - curation	Minimum peptide confidence to be used for quantitation	**15**
Parameters - Quantitation - curation	Consider a peptide discordant if joint feature probability less than	**0**

	Parameters - Non-functional	
Parameters - Non-functional	Show results only for distinct peptides, suppressing redundancy	**FALSE**
Parameters - Non-functional	Do not store MS1 level data	**FALSE**
	Statistics - Processing Times - Start&Stop Clock Times	
Statistics - Processing Times - Start&Stop Clock Times	Start time - Search	**03/27/2017 17:39:32**
Statistics - Processing Times - Start&Stop Clock Times	End time - Search	**03/27/2017 21:54:20**
Statistics - Processing Times - Start&Stop Clock Times	Start time - Identification algorithm stages	**03/27/2017 21:10:39**
Statistics - Processing Times - Start&Stop Clock Times	End time - Identification algorithm stages	**03/27/2017 21:49:48**
Statistics - Processing Times - Start&Stop Clock Times	Start time - Signal processing stage	**03/27/2017 17:39:54**

Statistics - Processing Times - Start&Stop Clock Times	End time - Signal processing stage	**03/27/2017 21:10:27**
Statistics - Processing Times - Start&Stop Clock Times	Start time - Waiting stage	**03/27/2017 21:10:27**
Statistics - Processing Times - Start&Stop Clock Times	End time - Waiting stage	**03/27/2017 21:10:39**
Statistics - Processing Times - Start&Stop Clock Times	Start time - Fraglet Algorithm search stage	**03/27/2017 21:11:35**
Statistics - Processing Times - Start&Stop Clock Times	End time - Fraglet Algorithm search stage	**03/27/2017 21:20:20**
Statistics - Processing Times - Start&Stop Clock Times	Start time - Mid-Pro Group Algorithm stage	
Statistics - Processing Times - Start&Stop Clock Times	End time - Mid-Pro Group Algorithm stage	
Statistics - Processing Times - Start&Stop Clock Times	Start time - Taglet Algorithm search stage	

Statistics - Processing Times - Start&Stop Clock Times	End time - Taglet Algorithm search stage	
Statistics - Processing Times - Start&Stop Clock Times	Start time - Final Pro Group Algorithm stage	**03/27/2017 21:20:20**
Statistics - Processing Times - Start&Stop Clock Times	End time - Final Pro Group Algorithm stage	**03/27/2017 21:49:48**
Statistics - Processing Times - Start&Stop Clock Times	Start time - FDR analysis stage	**03/27/2017 21:49:52**
Statistics - Processing Times - Start&Stop Clock Times	End time - FDR analysis stage	**03/27/2017 21:54:20**
	Statistics - Processing Times - Duration in Real Clock Times	
Statistics - Processing Times - Duration in Real Clock Times	Clock time duration - Full search (min)	**255**
Statistics - Processing Times - Duration in Real Clock Times	Clock time duration - Identification algorithm stages (min)	**39**

Statistics - Processing Times - Duration in Real Clock Times	Clock time duration - Signal processing stage (min)	**211**
Statistics - Processing Times - Duration in Real Clock Times	Clock time duration - Waiting stage (min)	**0**
Statistics - Processing Times - Duration in Real Clock Times	Clock time duration - Fraglet Algorithm stage (min)	**9**
Statistics - Processing Times - Duration in Real Clock Times	Clock time duration - Mid-Pro Group Algorithm stage (min)	
Statistics - Processing Times - Duration in Real Clock Times	Clock time duration - Taglet Algorithm stage (min)	
Statistics - Processing Times - Duration in Real Clock Times	Clock time duration - Pro Group Algorithm stage (min)	**29**
Statistics - Processing Times - Duration in Real Clock Times	Clock time duration - FDR Analysis (min)	**4**
Statistics - Processing Times - Duration in Real Clock Times	Clock time not accounted for in measured stages	**1**

	Statistics - Processing Times - Duration in CPU Time	
Statistics - Processing Times - Duration in CPU Time	CPU time duration - Signal Processing stage (min)	
Statistics - Processing Times - Duration in CPU Time	CPU time duration - Fraglet Algorithm stage (min)	**113**
Statistics - Processing Times - Duration in CPU Time	CPU time duration - Mid-Pro Group Algorithm stage (min)	
Statistics - Processing Times - Duration in CPU Time	CPU time duration - Taglet Algorithm stage (min)	
Statistics - Processing Times - Duration in CPU Time	CPU time duration - Pro Group Algorithm stage (min)	**72**
	Statistics - Processing Times - Percent by Stage	
Statistics - Processing Times - Percent by Stage	Percent of clock time - Identification Algorithm stages	**0**
Statistics - Processing Times - Percent by Stage	Percent of clock time - Signal Processing stage	**1**

Statistics - Processing Times - Percent by Stage	Percent of clock time - Waiting stage	**0**
Statistics - Processing Times - Percent by Stage	Percent of clock time - Fraglet Algorithm stage	**0**
Statistics - Processing Times - Percent by Stage	Percent of clock time - Mid-Pro Group Algorithm stage	
Statistics - Processing Times - Percent by Stage	Percent of clock time - Taglet Algorithm stage	
Statistics - Processing Times - Percent by Stage	Percent of clock time - Pro Group Algorithm stage	**0**
Statistics - Processing Times - Percent by Stage	Percent of clock time - FDR Analysis	**0**
	Statistics - Processing Rate - Clock (Sec/Spectrum)	
Statistics - Processing Rate - Clock (Sec/Spectrum)	Clock time rate (sec/spect) - Full Search	**0**

Statistics - Processing Rate - Clock (Sec/Spectrum)	Clock time rate (sec/spect) - Identification Algorithm stages	**0**
Statistics - Processing Rate - Clock (Sec/Spectrum)	Clock time rate (sec/spect) - Signal processing stage	**0**
Statistics - Processing Rate - Clock (Sec/Spectrum)	Clock time rate (sec/spect) - Waiting stage	**0**
Statistics - Processing Rate - Clock (Sec/Spectrum)	Clock time rate (sec/spect) - Fraglet Algorithm stage	**0**
Statistics - Processing Rate - Clock (Sec/Spectrum)	Clock time rate (sec/spect) - Mid-Pro Group Algorithm stage	
Statistics - Processing Rate - Clock (Sec/Spectrum)	Clock time rate (sec/spect) - Taglet Algorithm stage	
Statistics - Processing Rate - Clock (Sec/Spectrum)	Clock time rate (sec/spect) - Pro Group Algorithm stage	**0**
Statistics - Processing Rate - Clock (Sec/Spectrum)	Clock time rate (sec/spect) - FDR Analysis	**0**

	Statistics - Processing Rate - CPU (Sec/Spectrum)	
Statistics - Processing Rate - CPU (Sec/Spectrum)	CPU time rate (sec/spect) - Signal processing stage	
Statistics - Processing Rate - CPU (Sec/Spectrum)	CPU time rate (sec/spect) - Fraglet Algorithm stage	**0**
Statistics - Processing Rate - CPU (Sec/Spectrum)	CPU time rate (sec/spect) - Mid-Pro Group Algorithm stage	
Statistics - Processing Rate - CPU (Sec/Spectrum)	CPU time rate (sec/spect) - Taglet Algorithm stage	
Statistics - Processing Rate - CPU (Sec/Spectrum)	CPU time rate (sec/spect) - Pro Group Algorithm stage	**0**
	Statistics - Processing Rate - Clock (Sec/Spectrum/DB Protein)	
Statistics - Processing Rate - Clock (Sec/Spectrum/DB Protein)	Clock time rate (sec/spect/DB protein) - Full search	**0**

Statistics - Processing Rate - Clock (Sec/Spectrum/DB Protein)	Clock time rate (sec/spect/DB protein) - Identification algorithm stages	**0**
Statistics - Processing Rate - Clock (Sec/Spectrum/DB Protein)	Clock time rate (sec/spect/DB protein) - Signal processing stage	**0**
Statistics - Processing Rate - Clock (Sec/Spectrum/DB Protein)	Clock time rate (sec/spect/DB protein) - Waiting stage	**0**
Statistics - Processing Rate - Clock (Sec/Spectrum/DB Protein)	Clock time rate (sec/spect/DB protein) - Fraglet Algorithm stage	**0**
Statistics - Processing Rate - Clock (Sec/Spectrum/DB Protein)	Clock time rate (sec/spect/DB protein) - Mid-Pro Group Algorithm stage	
Statistics - Processing Rate - Clock (Sec/Spectrum/DB Protein)	Clock time rate (sec/spect/DB protein) - Taglet Algorithm stage	

Statistics - Processing Rate - Clock (Sec/Spectrum/DB Protein)	Clock time rate (sec/spect/DB protein) - Pro Group Algorithm stage	**0**
Statistics - Processing Rate - Clock (Sec/Spectrum/DB Protein)	Clock time rate (sec/spect/DB protein) - FDR Analysis	**0**
	Statistics - Processing Rate - CPU (Sec/Spectrum/DB Protein)	
Statistics - Processing Rate - CPU (Sec/Spectrum/DB Protein)	CPU time rate (sec/spect/DB protein) - Signal processing stage	
Statistics - Processing Rate - CPU (Sec/Spectrum/DB Protein)	CPU time rate (sec/spect/DB protein) - Fraglet Algorithm stage	**0**
Statistics - Processing Rate - CPU (Sec/Spectrum/DB Protein)	CPU time rate (sec/spect/DB protein) - Mid-Pro Group Algorithm stage	

Statistics - Processing Rate - CPU (Sec/Spectrum/DB Protein)	CPU time rate (sec/spect/DB protein) - Taglet Algorithm stage	
Statistics - Processing Rate - CPU (Sec/Spectrum/DB Protein)	CPU time rate (sec/spect/DB protein) - Pro Group Algorithm stage	**0**
	Statistics - Extent of Distribution - Fundamental	
Statistics - Extent of Distribution - Fundamental	Distribution factor - CPU vs. clock time - Signal processing stage	
Statistics - Extent of Distribution - Fundamental	Distribution factor - CPU vs. clock time - Fraglet Algorithm stage	**13**
Statistics - Extent of Distribution - Fundamental	Distribution factor - CPU vs. clock time - Mid-Pro Group Algorithm stage	
Statistics - Extent of Distribution - Fundamental	Distribution factor - CPU vs. clock time - Taglet Algorithm stage	
Statistics - Extent of Distribution - Fundamental	Distribution factor - CPU vs. clock time - Pro Group Algorithm stage	**2**
	Statistics - Extent of Distribution - vs Segments	

Statistics - Extent of Distribution - vs Segments	Ratio of distribution factor to number of search segments - Signal processing stage	
Statistics - Extent of Distribution - vs Segments	Ratio of distribution factor to number of search segments - Fraglet Algorithm stage	**0**
Statistics - Extent of Distribution - vs Segments	Ratio of distribution factor to number of search segments - Mid-Pro Group Algorithm stage	
Statistics - Extent of Distribution - vs Segments	Ratio of distribution factor to number of search segments - Taglet Algorithm stage	
Statistics - Extent of Distribution - vs Segments	Ratio of distribution factor to number of search segments - Pro Group Algorithm stage	**0**
	Statistics - Extent of Distribution - vs Licensed Cores	
Statistics - Extent of Distribution - vs Licensed Cores	Ratio of distribution factor to number of licensed cores - Signal processing stage	
Statistics - Extent of Distribution - vs Licensed Cores	Ratio of distribution factor to number of licensed cores - Fraglet Algorithm stage	**1**
Statistics - Extent of Distribution - vs Licensed Cores	Ratio of distribution factor to number of licensed cores - Mid-Pro Group Algorithm stage	

Statistics - Extent of Distribution - vs Licensed Cores	Ratio of distribution factor to number of licensed cores - Taglet Algorithm stage	
Statistics - Extent of Distribution - vs Licensed Cores	Ratio of distribution factor to number of licensed cores - Pro Group Algorithm stage	**0**
	Statistics - Search Segmentation	
Statistics - Search Segmentation	Average number of spectra per segment	**3768**
Statistics - Search Segmentation	Standard deviation of number of spectra per segment	**100**
Statistics - Search Segmentation	Maximum number of spectra per segment	**3968**
Statistics - Search Segmentation	Minimum number of spectra per segment	**3640**
	Attributes - Input data filenames	
Attributes - Input data filenames	Filename of Input File 1	**D:\5600+ data\Ollie Reid\IDA\OR_170324_IDA_6ug_all_iRT.wiff**
Attributes - Input data filenames	Filename of Input File 2	**D:\5600+ data\Ollie Reid\IDA\OR_IDA_6ug_all.wiff**

Attributes - Input data filenames	Filename of Input File 3	**D:\5600+ data\Ollie Reid\SCX\Ollie_Reid_SCX01_iRT_8ul.wiff**
Attributes - Input data filenames	Filename of Input File 4	**D:\5600+ data\Ollie Reid\SCX\Ollie_Reid_SCX02_iRT_8ul.wiff**
Attributes - Input data filenames	Filename of Input File 5	**D:\5600+ data\Ollie Reid\SCX\Ollie_Reid_SCX03_iRT_8ul.wiff**
Attributes - Input data filenames	Filename of Input File 6	**D:\5600+ data\Ollie Reid\SCX\Ollie_Reid_SCX04_iRT_8ul.wiff**
Attributes - Input data filenames	Filename of Input File 7	**D:\5600+ data\Ollie Reid\SCX\Ollie_Reid_SCX05_iRT_8ul.wiff**
Attributes - Input data filenames	Filename of Input File 8	**D:\5600+ data\Ollie Reid\SCX\Ollie_Reid_SCX06_iRT_8ul.wiff**
Attributes - Input data filenames	Filename of Input File 9	**D:\5600+ data\Ollie Reid\SCX\Ollie_Reid_SCX07_iRT_8ul.wiff**
Attributes - Input data filenames	Filename of Input File 10	**D:\5600+ data\Ollie Reid\SCX\Ollie_Reid_SCX08_iRT_8ul.wiff**
Attributes - Input data filenames	Filename of Input File 11	**D:\5600+ data\Ollie Reid\SCX\Ollie_Reid_SCX09_iRT_8ul.wiff**
Attributes - Input data filenames	Filename of Input File 12	**D:\5600+ data\Ollie Reid\SCX\Ollie_Reid_SCX10_iRT_8ul.wiff**

Supplementary Figures:

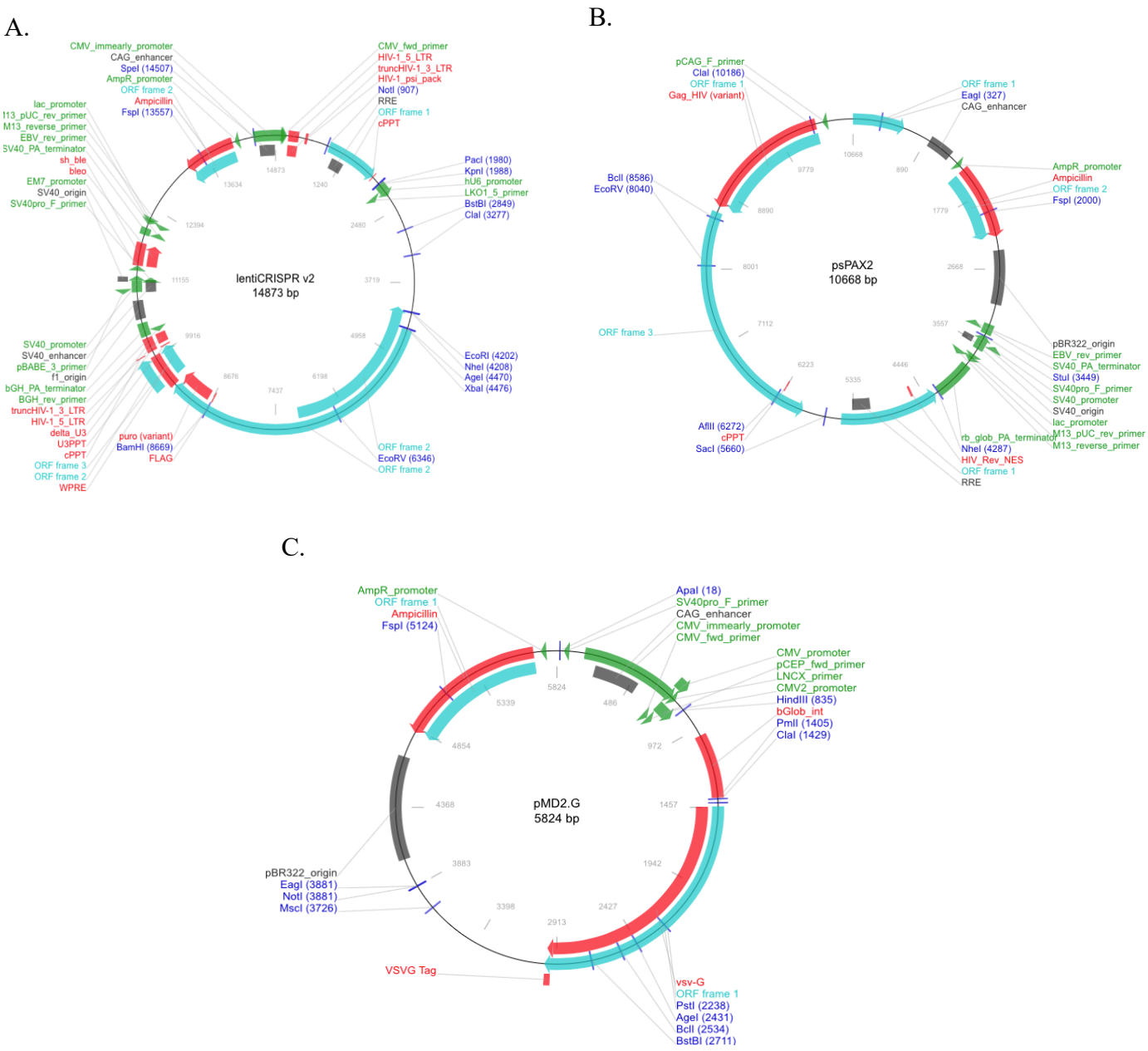

Supplementary Figure 1: plasmids used in the generation of CRISPR$^+$ cell lines: sequence maps for pLentiCRISPRv2 (**A.**) and packaging plasmids psPAX2 (**B.**) and pMD2 (**C.**) used for the transduction of cells during the project. Maps from addgene (https://www.addgene.org).

A.

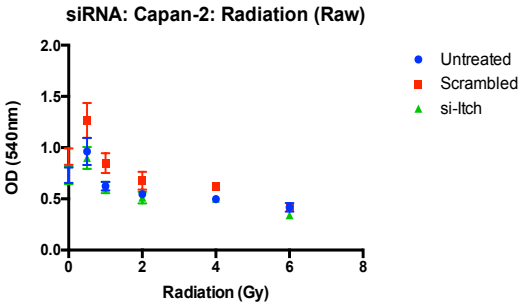
siRNA: Capan-2: Radiation (Raw)
OD (540nm)
Radiation (Gy)
Untreated
Scrambled
si-Itch

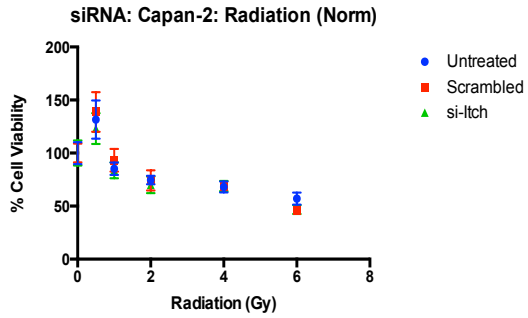
siRNA: Capan-2: Radiation (Norm)
% Cell Viability
Radiation (Gy)
Untreated
Scrambled
si-Itch

B.

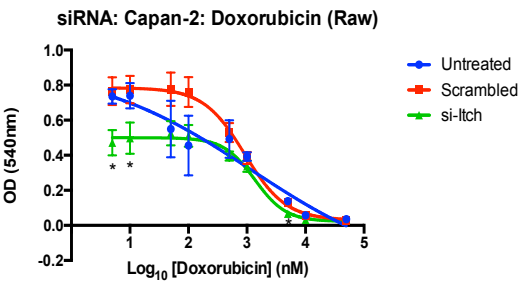
siRNA: Capan-2: Doxorubicin (Raw)
OD (540nm)
Log10 [Doxorubicin] (nM)
Untreated
Scrambled
si-Itch

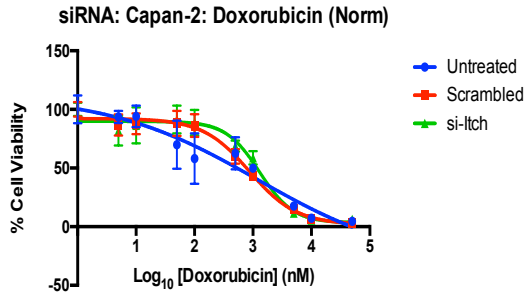
siRNA: Capan-2: Doxorubicin (Norm)
% Cell Viability
Log10 [Doxorubicin] (nM)
Untreated
Scrambled
si-Itch

C.

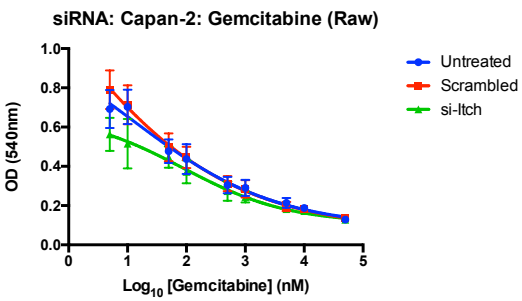
siRNA: Capan-2: Gemcitabine (Raw)
OD (540nm)
Log10 [Gemcitabine] (nM)
Untreated
Scrambled
si-Itch

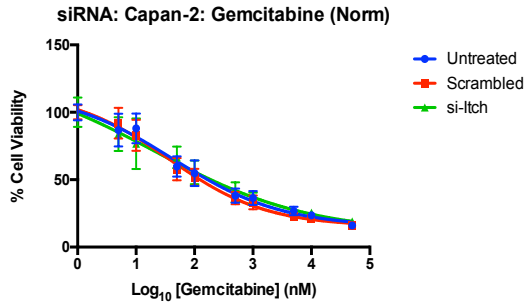
siRNA: Capan-2: Gemcitabine (Norm)
% Cell Viability
Log10 [Gemcitabine] (nM)
Untreated
Scrambled
si-Itch

D.

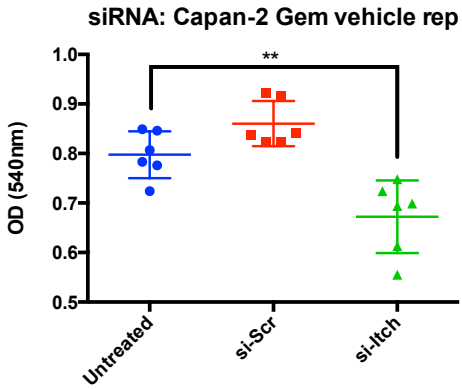
siRNA: Capan-2 Gem vehicle rep
OD (540nm)
**
Untreated
si-Scr
si-Itch

E.

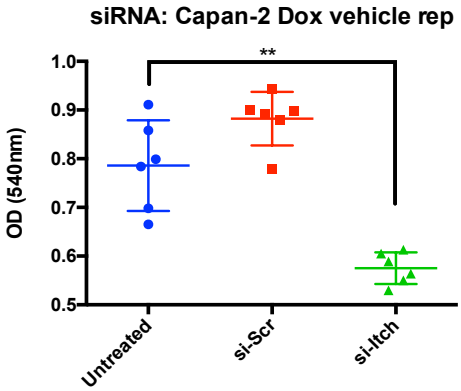
siRNA: Capan-2 Dox vehicle rep
OD (540nm)
**
Untreated
si-Scr
si-Itch

Supplementary Figure 2: Biological repeat of Capan-2 siRNA-mediated transient *Itch* knockdown cell survival experiments:

Resultant (left) and normalised (right) SRB cell-survival curves for Capan-2 cells treated with siRNA in combination with additional treatment. **A.** Cells treated with 0-6 Gy γ-radiation; for both resultant and normalised data there was no statistically significant differences between samples. **B.** Cells treated with 0-25,000 nM doxorubicin (plotted as $\log_{10}$[doxorubicin]); resultant data showed significant difference for 5 and 10 nM ($p = 1.60\times10^{-5}$, and 4.12×10^{-4} respectively). No significant increases in sensitivity was observed. **C.** Cells treated with 0-25,000 nM gemcitabine (plotted as $\log_{10}$[gemcitabine]); no statistically difference was seen for both resultant and normalised data. Data was normalised to a vehicle control in the case for doxorubicin and gemcitabine. Radiation data was normalised to cells that did not receive radiation. An * donates statistically significant difference in mean as determined by Student's t-test. **D.** & **E.** Viability of cells treated with just the vehicle control shows significant decrease in cell viability when just the si-Itch is present compared to untreated cells (** = $p < 0.01$). Number of asterixis donates degree of statistical significance of a one-way ANOVA between conditions.

A.

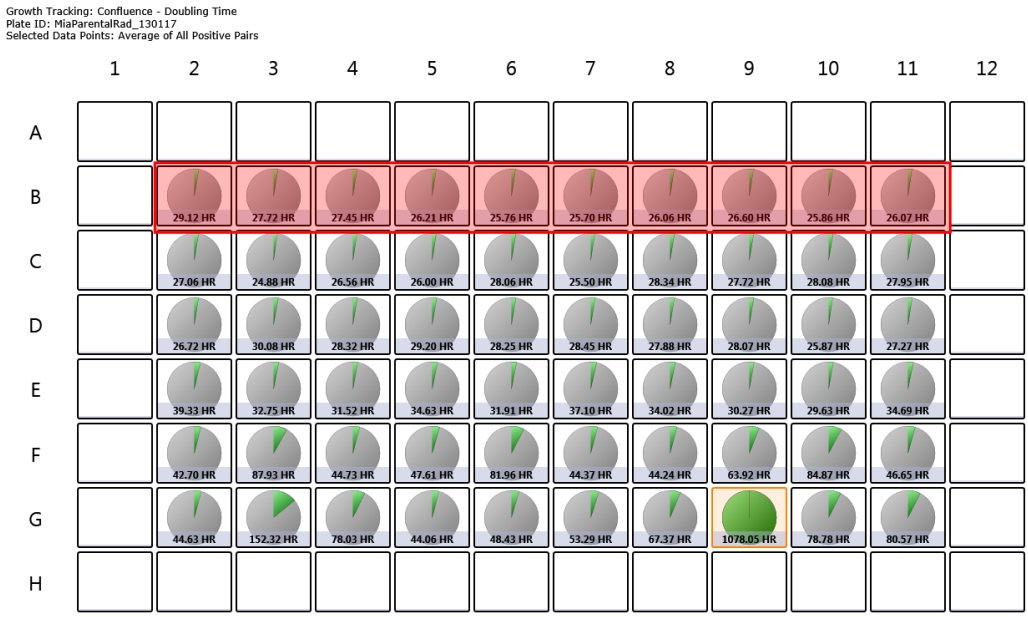

B.

	Data Set		
	1	2	3
Doubling Time (Hours)	29.44	29.12	30.29
	26.79	27.72	21.44
	36.43	27.45	37.73
	23.38	26.21	43.27
	31.18	25.76	36.28
	36.64	25.7	35.97
	33.65	26.06	36.96
	34.5	26.6	24.85
	25.85	25.86	29.27
	24.21	26.07	30.14
Mean	**30.21**	**26.66**	**32.62**
Std.Dev	**5.00**	**1.11**	**6.59**
Median	**30.31**	**26.14**	**33.13**
		Mean All	**29.83**
		Std.Dev All	**5.28**
		Median All	**28.42**

Supplementary Figure 3: Summary analysis of MiaPaCa-2 basal doubling time in-vitro:

Confluence data generated every 24 hours of the cytotoxicity experiments on Celigo was analysed to produce doubling times for each well (A.). Data sets were obtained from 0Gy treated MiaPaCa-2 cells (example data set highlighted in red – appears as data set 2 in following table). To estimate doubling time of MiaPaCa-2 cells in hours statistical analysis was performed on 3 doubling time data sets generated from 3 independent experiments (B.). Mean, standard deviation, and median doubling time was generated both for each individual data set and across all data sets.

A.

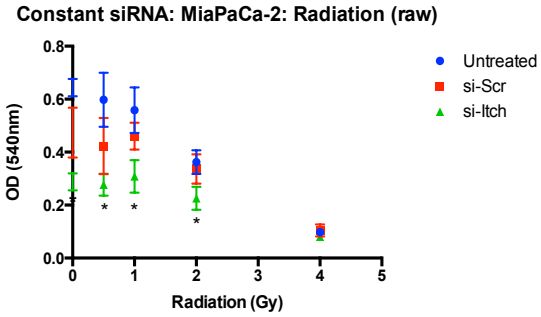
Constant siRNA: MiaPaCa-2: Radiation (raw)
OD (540nm)
Radiation (Gy)
Untreated
si-Scr
si-Itch

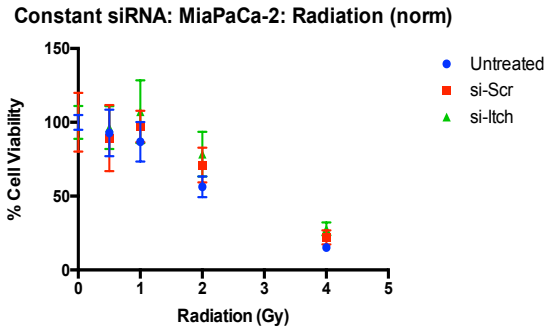
Constant siRNA: MiaPaCa-2: Radiation (norm)
% Cell Viability
Radiation (Gy)
Untreated
si-Scr
si-Itch

B.

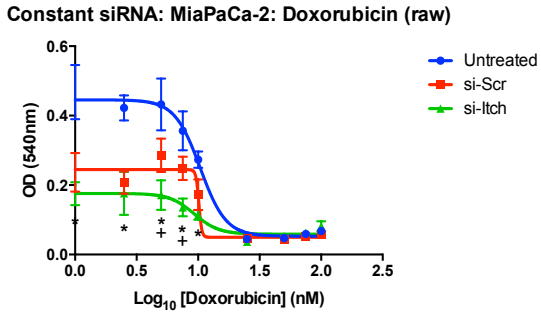
Constant siRNA: MiaPaCa-2: Doxorubicin (raw)
OD (540nm)
Log10 [Doxorubicin] (nM)
Untreated
si-Scr
si-Itch

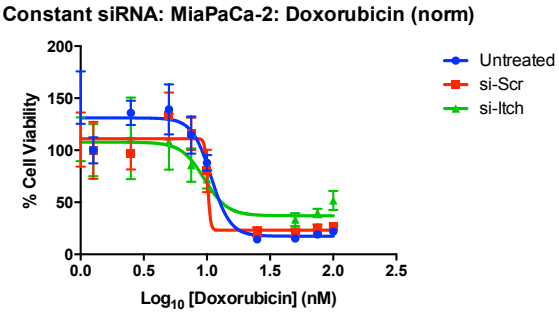
Constant siRNA: MiaPaCa-2: Doxorubicin (norm)
% Cell Viability
Log10 [Doxorubicin] (nM)
Untreated
si-Scr
si-Itch

C.

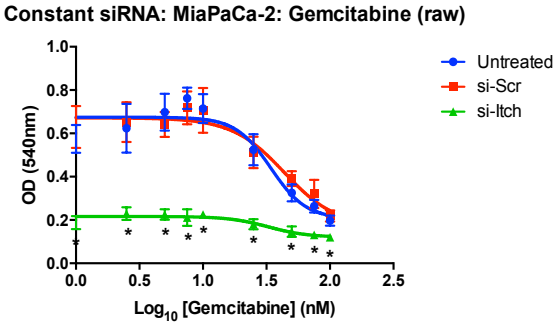
Constant siRNA: MiaPaCa-2: Gemcitabine (raw)
OD (540nm)
Log10 [Gemcitabine] (nM)
Untreated
si-Scr
si-Itch

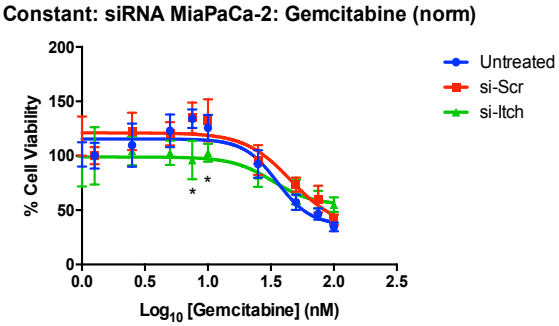
Constant: siRNA MiaPaCa-2: Gemcitabine (norm)
% Cell Viability
Log10 [Gemcitabine] (nM)
Untreated
si-Scr
si-Itch

D.

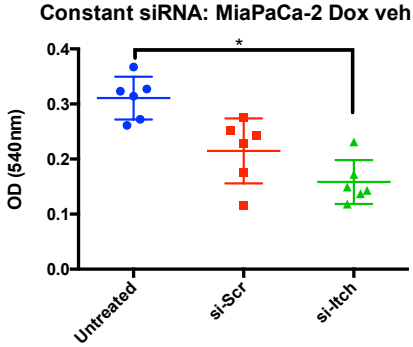
Constant siRNA: MiaPaCa-2 Dox vehicle
OD (540nm)
Untreated
si-Scr
si-Itch

E.

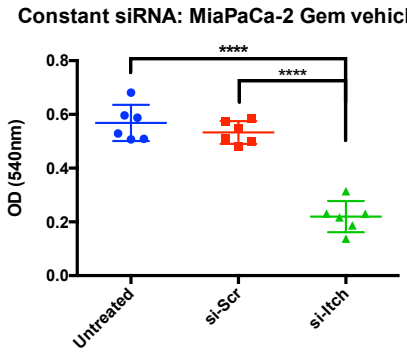
Constant siRNA: MiaPaCa-2 Gem vehicle rep
OD (540nm)
Untreated
si-Scr
si-Itch

Supplementary Figure 4: Continuous transient *Itch* knockdown of MiaPaCa-2 cells inhibits cell survival:

Resultant (left) and normalised (right) SRB cell-survival curves for MiaPaCa-2 cells treated with siRNA in combination with additional treatment. A secondary dose of siRNA was applied at 48 hours post-treatment. **A.** Cells treated with 0-4 Gy γ-radiation; resultant data showed significant reduction in OD readout in si-Itch cells compared to si-Scr for doses 0, 0.5, 1, and 2 Gy ($p = 1.40\times10^{-5}$, 7.88×10^{-4}, 1.01×10^{-5}, and 1.02×10^{-4} respectively – scrambled was chosen to compare against in this case as the OD values were closer to those of si-Itch). No statistically significant increase in sensitivity was observed upon normalisation of the data. **B.** Cells treated with 0-100 nM doxorubicin (plotted as $\log_{10}$[doxorubicin]); resultant data showed significant difference for 1, 5, 2.5, 5, 7.5 and 10 nM between si-Itch and untreated cells ($p = 7.25\times10^{-6}$, 7.93×10^{-6}, 2.22×10^{-5}, 5.08×10^{-6}, 5.59×10^{-8}, and 3.45×10^{-3} respectively). Significant difference was also seen when compared to si-Scr for doses 5 & 7.5 nM ($p = 1.47\times10^{-3}$ and 6.51×10^{-5} respectively). No significant increases in sensitivity was observed upon normalising the data. **C.** Cells treated with 0-100 nM gemcitabine (plotted as $\log_{10}$[gemcitabine]); resultant data showed significant reduction in OD readout for si-Itch across all doses of gemcitabine ($p = 1.05\times10^{-7}$, 8.58×10^{-6}, 1.31×10^{-7}, 1.00×10^{-9}, 9.06×10^{-9}, 5.95×10^{-7}, 2.92×10^{-6}, 2.93×10^{-6}, and 5.16×10^{-5} for each dose respectively - compared against untreated control). Increase in sensitivity of si-Itch was seen at 7.5 and 10 nM gemcitabine ($p = 8.15\times10^{-4}$ and 2.89×10^{-3} respectively. Data was normalised to a vehicle control in the case for doxorubicin and gemcitabine. Radiation data was normalised to cells that did not receive radiation. An * donates statistically significant difference in mean as determined by Student's t-test. **D.** & **E.** Viability of cells treated with just the vehicle control shows significant decrease in cell viability when just the si-Itch is present compared to untreated cells. Number of asterixis donates degree of statistical significance of a one-way ANOVA between conditions (* = $p < 0.05$, **** = $p < 0.0001$).

A.

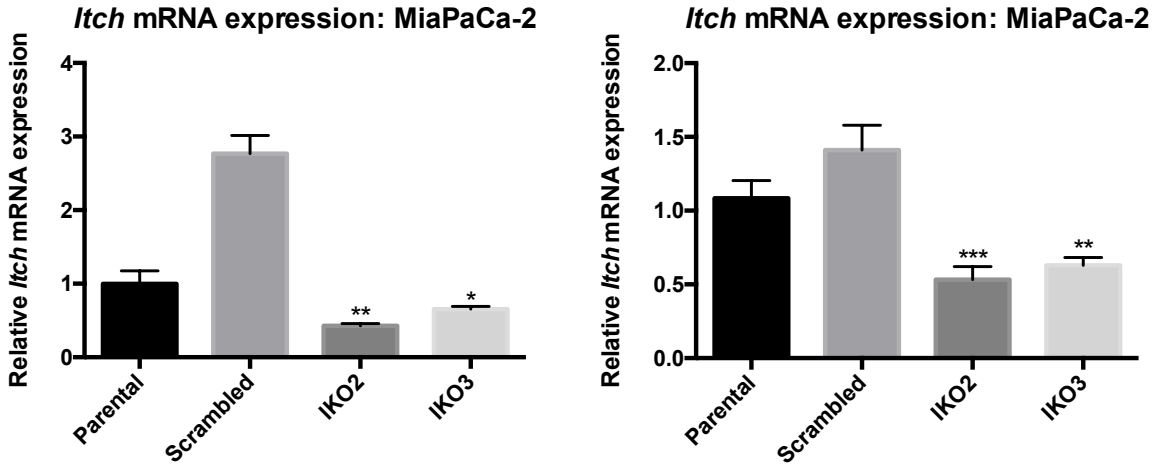

B.

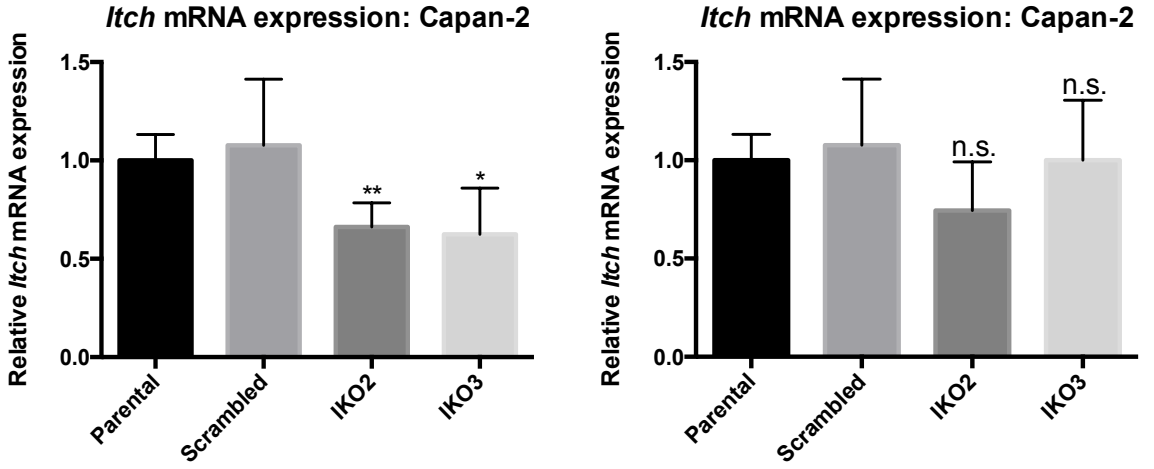

Supplementary Figure 5: qPCR of MiaPaCa-2 and Capan-2 isogenic cell lines IKO2 and IKO3 generated from additional lentiviral constructs:

Itch mRNA expression of cells transduced with pLentiCRISPRv2 with alternative sgRNAs was measured by qPCR to assess degree of Itch knockdown with biological replicates. In MiaPaCa-2 cells IKO2 isogenic cells had a ~40% reduction in *Itch* mRNA compared to parental controls and IKO3 had a 40-50% knockdown (**A.**). In Capan-2 cells specific degree of knockdown was inconclusive for IKO3 cells as percentage knockdown was too varied between biological replicates (**B.**). Mean percentage Itch knockdown for IKO2 cells ranged from 40-30%. Statistical significance was calculated using a Student's t-test. Number of asterixis donates degree of statistical significance between constructs and parental control conditions (* = $p < 0.05$, ** = $p < 0.01$, *** = $p < 0.001$).

A.

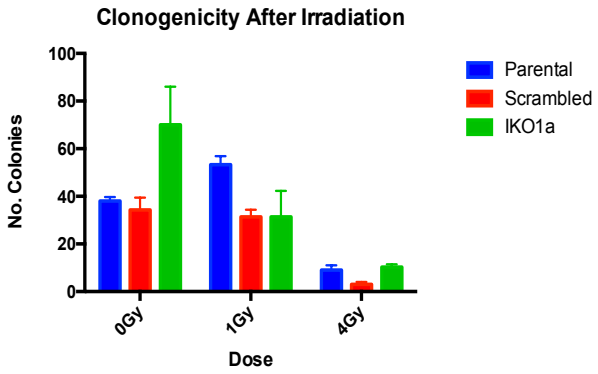

B.

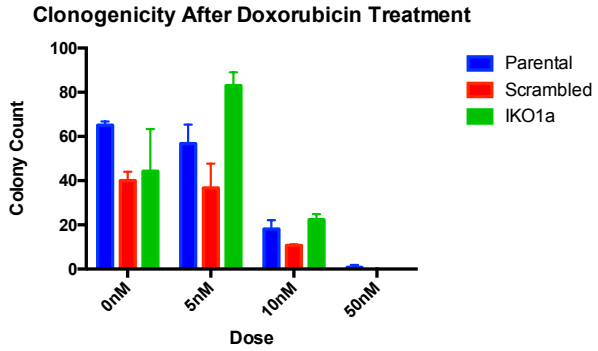

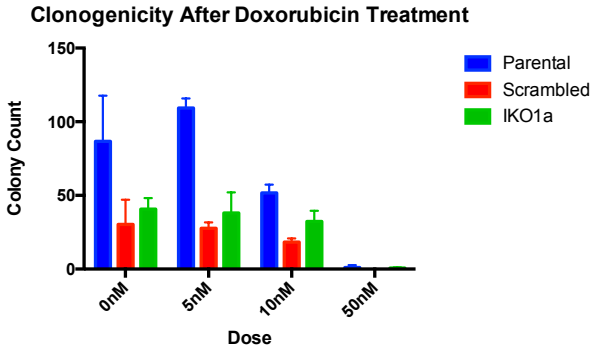

C.

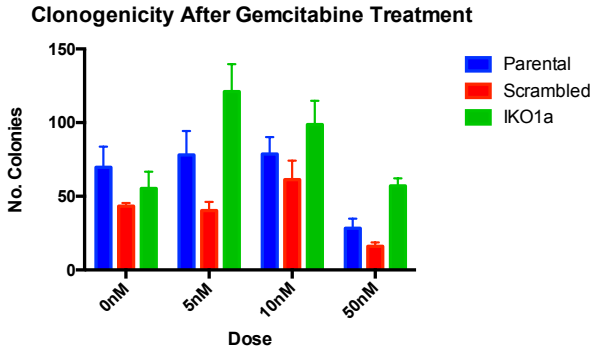

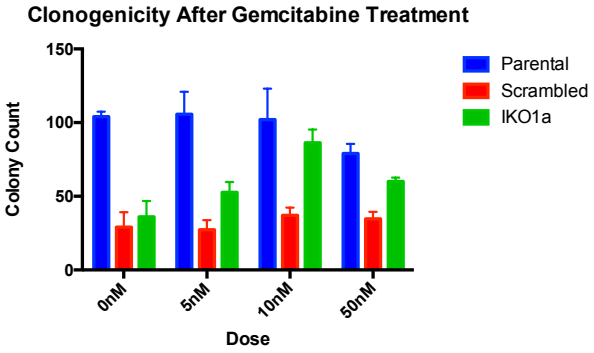

Supplementary Figure 6: Biological repeats of clonogenic assays in MiaPaCa-2 isogenic cell lines:

Clonogenicity of Parental (blue), Scrambled (red), and IKO1a (green) cells with or without treatment. **A.** Cells were irradiated at either 0, 1 or 4Gy before being distributed at a low cell density on a 6-well plate (250 cells/well). Repeat of radiation data mirrored what was seen in prelimary experiment. **B.** & **C.** cells were passaged onto 24-plates (125 cells/well) and were treated with either 0, 5, 10 or 50nM doxorubicin/gemcitabine respectively. Drug-containing media was replaced with fresh media after 24 hours. Clonogenicity data for drug regimens was inconsistent with preliminary data and was repeated again however results remained inconsistent with each other. This could be due to issues with colony distinction and counting on Celigo. If repeated further, recommended to cross-validate with manual counting.

A.

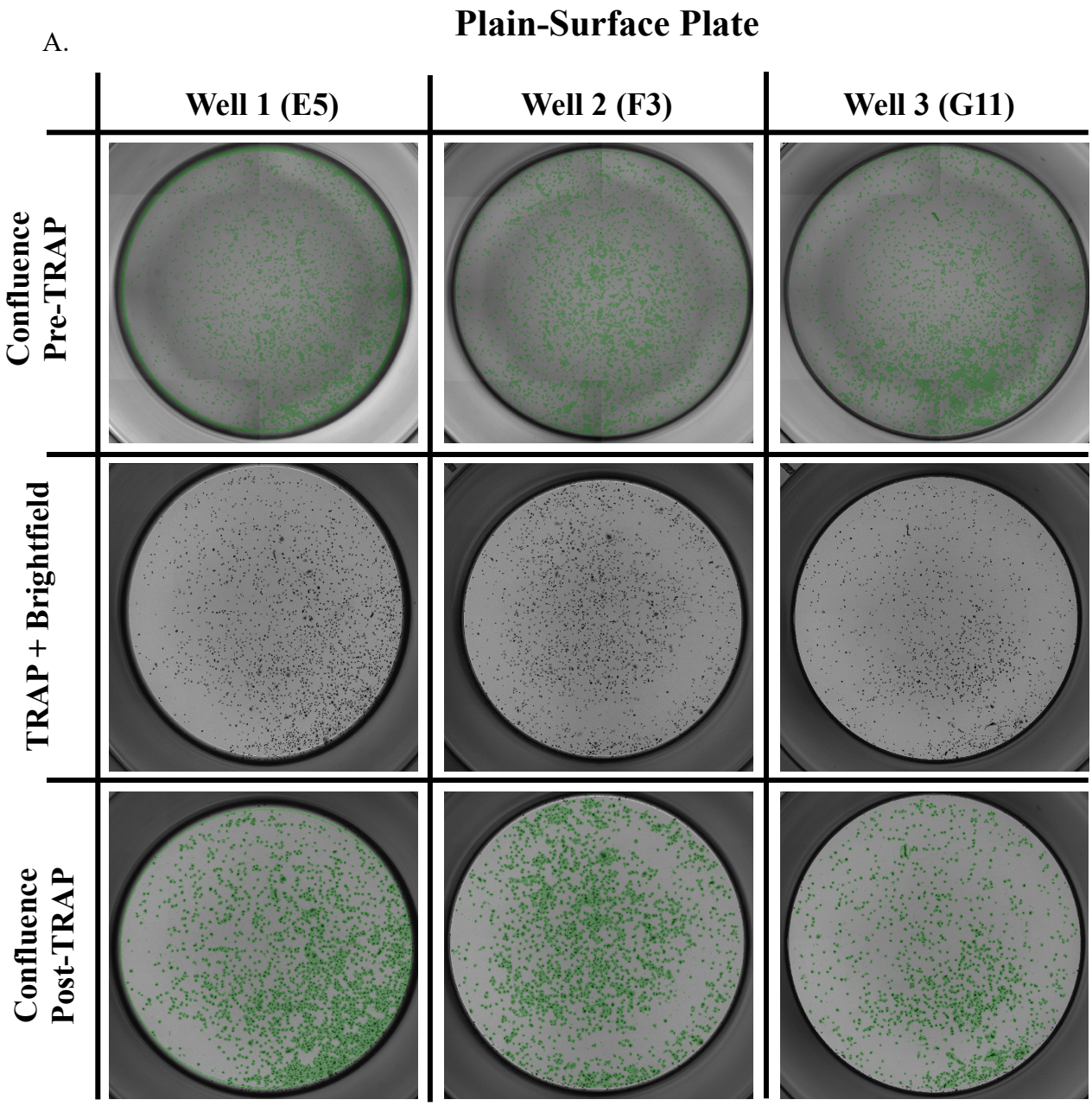
Plain-Surface Plate
Well 1 (E5)
Well 2 (F3)
Well 3 (G11)
Confluence Pre-TRAP
TRAP + Brightfield
Confluence Post-TRAP

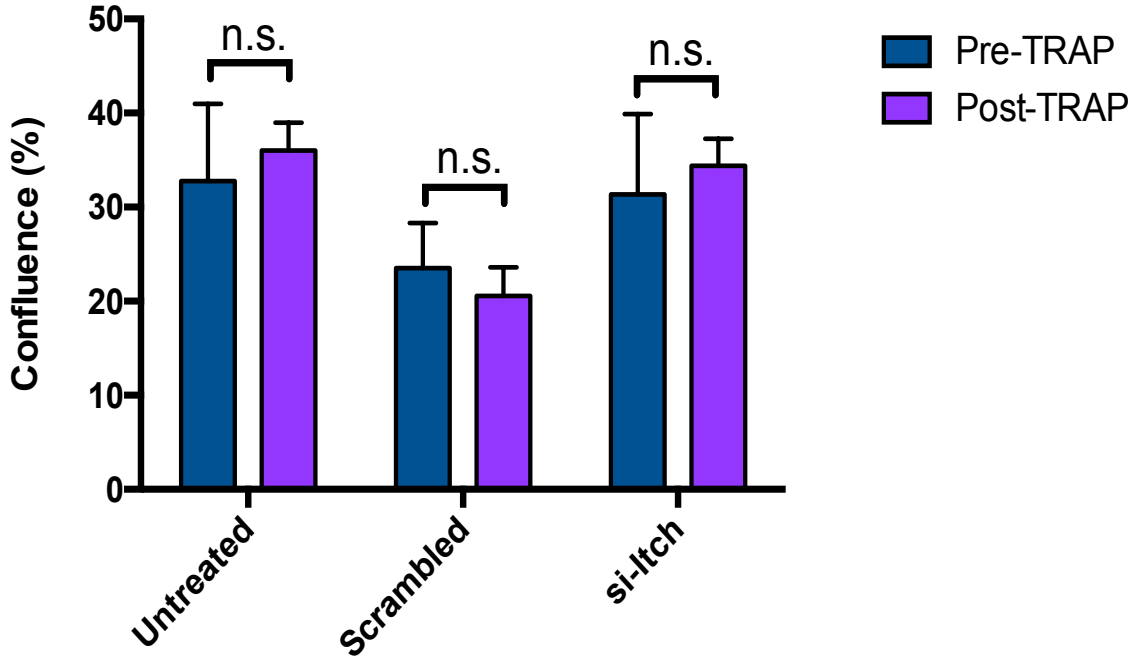
Confluence (%)
50
40
30
20
10
0
n.s.
n.s.
n.s.
Untreated
Scrambled
si-Itch
Pre-TRAP
Post-TRAP

B.

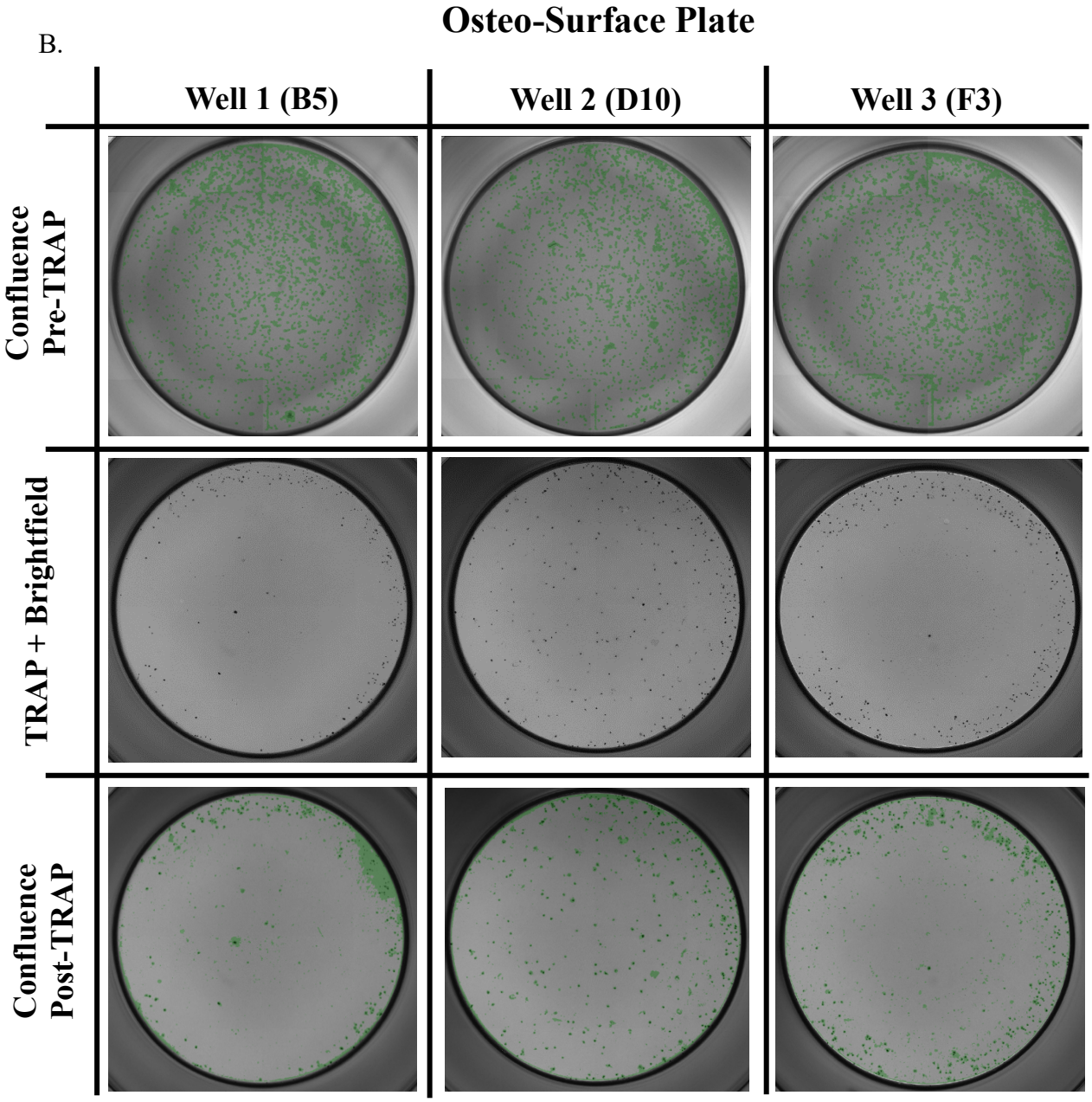
Osteo-Surface Plate
Well 1 (B5)
Well 2 (D10)
Well 3 (F3)
Confluence Pre-TRAP
TRAP + Brightfield
Confluence Post-TRAP

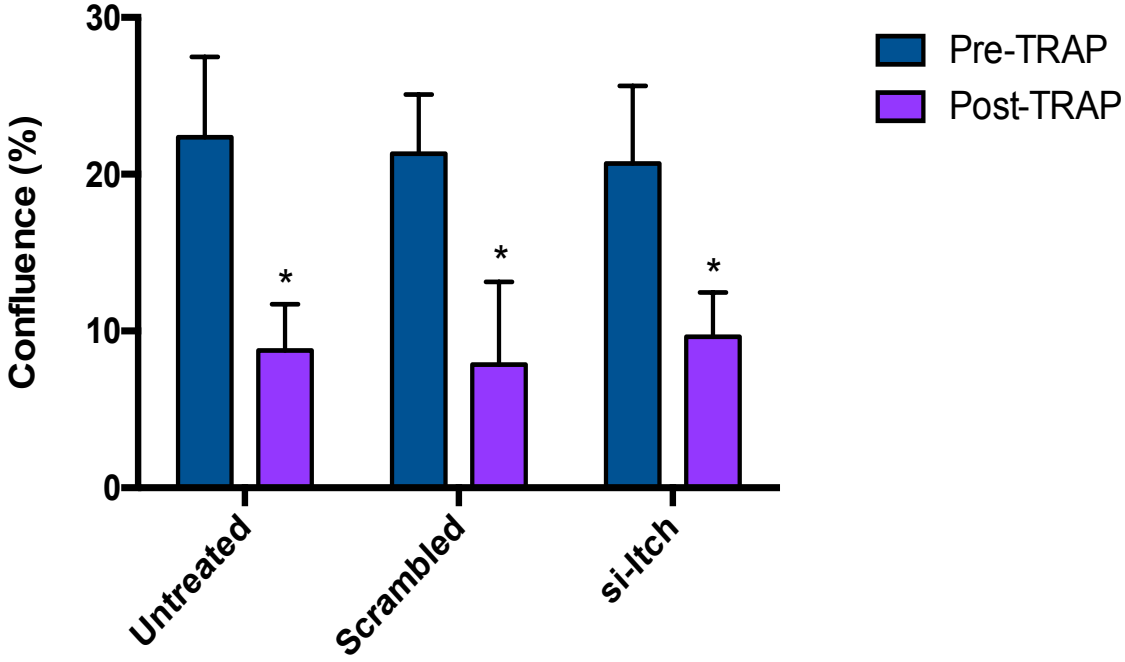
Confluence (%)
30
20
10
0
Pre-TRAP
Post-TRAP
*
*
*
Untreated
Scrambled
si-Itch

Supplementary Figure 7: Osteoclasts are less adherent to osteo-surface plate through analysis of well confluence pre- and post-TRAP staining:

Confluence algorithm designed to select for osteoclasts was used to analyse well confluence in both the plain-surface plate (**A.**) and the osteo-surface plate (**B.**). The algorithm was run both before TRAP staining (top row of images – blue bars in graphs) and after TRAP staining (bottom row of images – purple bars). In the plain surface plate there was no significant difference in mean well confluence across all three treatment regimens (untreated, scrambled, and si-Itch) as determined by students t-test. Meanwhile in the osteo-surface plate the TRAP-staining protocol caused significant cell loss with >50% reduction in confluence across all three treatment regimens ($p = 2.52x10^{-11}$, $p = 1.45x10^{-10}$, and $p = 2.97x10^{-10}$ for untreated, scrambled, and si-Itch respectively). As confluence remained unchanged for the plain-surface plate, the results indicate that cells are less adherent to the osteo-surface plate. Statistically significant difference between pairs of means was determined by Student's t-test and are donated by a *****.

A.

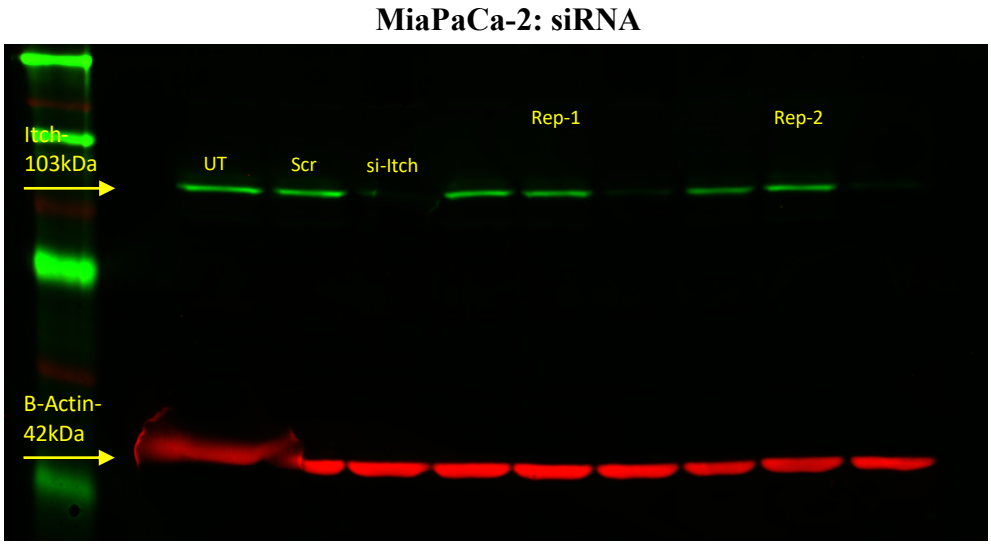

B.

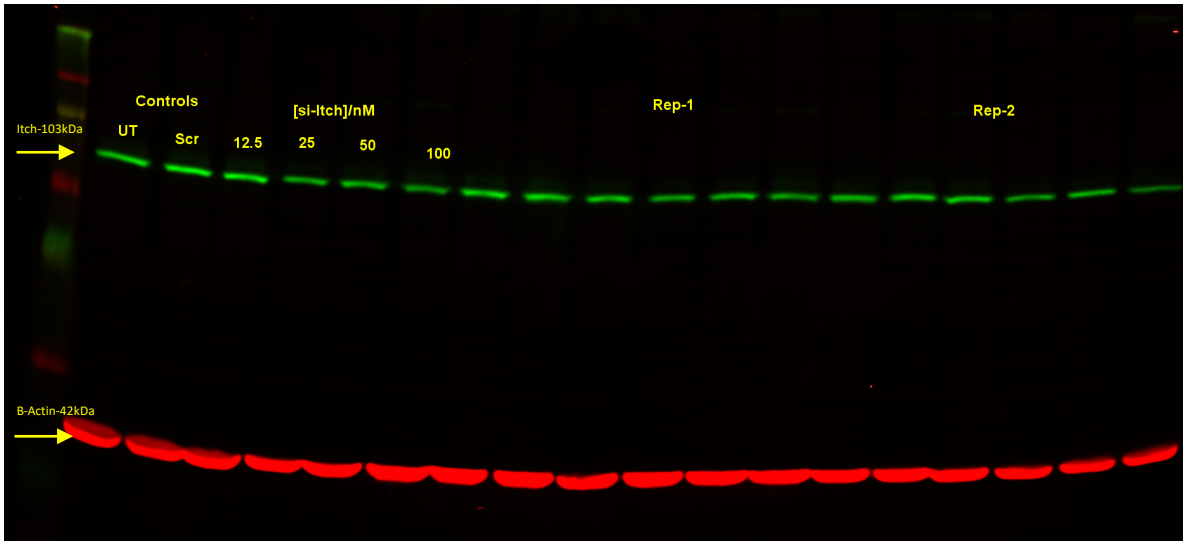

Supplementary Figure 8: Original western blot images of siRNA-mediated *Itch* knockdown in pancreatic cell lines:

Licor images of membranes labelled for Itch (green) and β-Actin (red) protein. In MiaPaCa-2 cells (**A.**) 12.5 nM siRNA duplex solution (si-Itch) was sufficient to reduce Itch protein compared to untreated (UT) and a scrambled siRNA control (Scr). (**B.**) In Capan-2 cells original trials with 12.5nM did not significantly decrease Itch protein levels. Experiment was therefore repeated with increasing concentrations of siRNA (lanes 3-6) up to 100 nM.

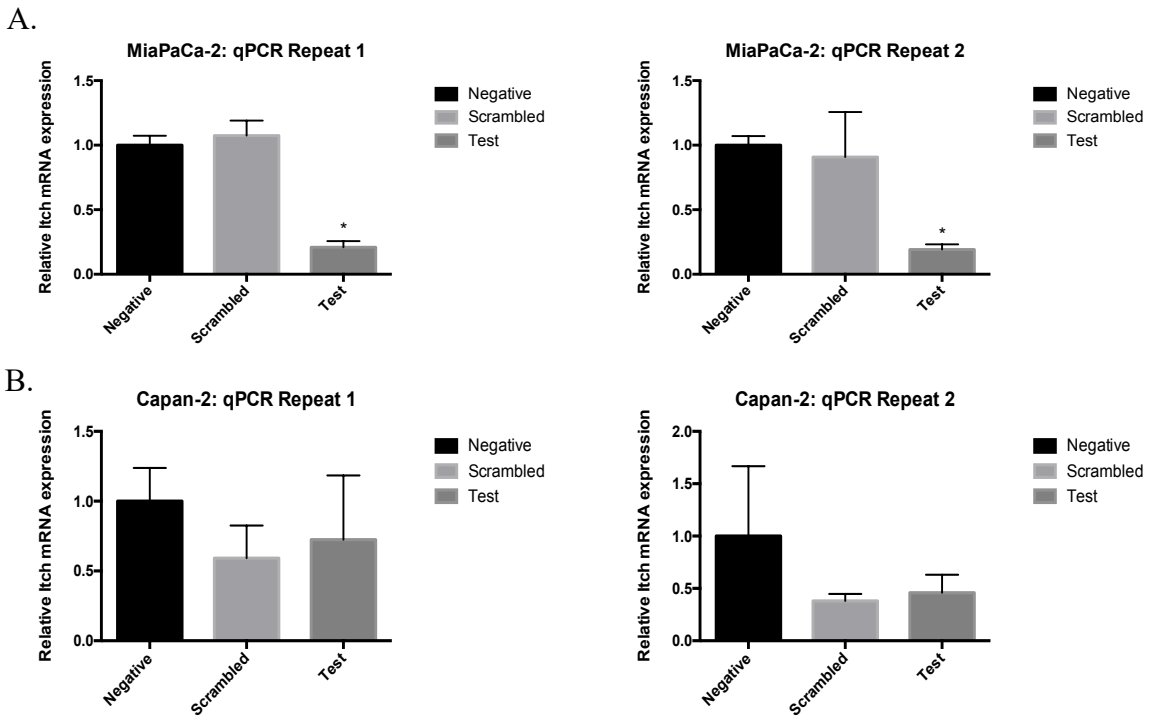

Supplementary Figure 9: Biological repeats of qPCR runs to assess siRNA-mediated knockdown of *Itch* in MiaPaCa-2 and Capan-2 cells:

qPCR runs performed in biological repeat samples of MiaPaCa-2 (**A.**) and Capan-2 (**B.**) cells treated with *Itch*-targeting siRNA. In both repeats for MiaPaCa-2 cells a statistically significant 80% *Itch* knockdown was achieved ($p<0.0001$) using 12.5 nM siRNA. Meanwhile for Capan-2 cells, as was seen previously, knockdown at mRNA level was not significantly different to negative controls despite protein results suggesting otherwise. Statistically significant difference between pairs of means was determined by Student's t-test and are donated by a *

A.

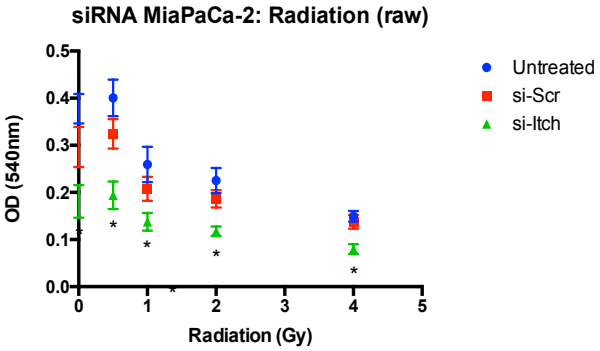
siRNA MiaPaCa-2: Radiation (raw)
OD (540nm)
Radiation (Gy)
Untreated
si-Scr
si-Itch

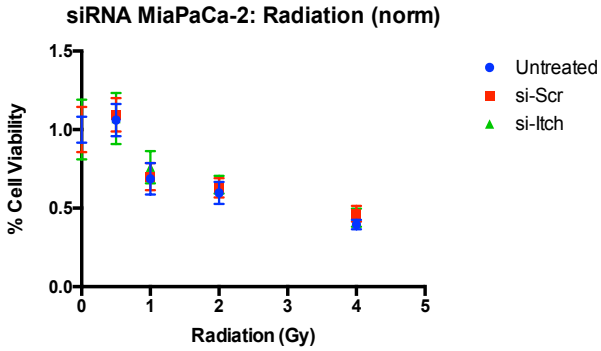
siRNA MiaPaCa-2: Radiation (norm)
% Cell Viability
Radiation (Gy)
Untreated
si-Scr
si-Itch

B.

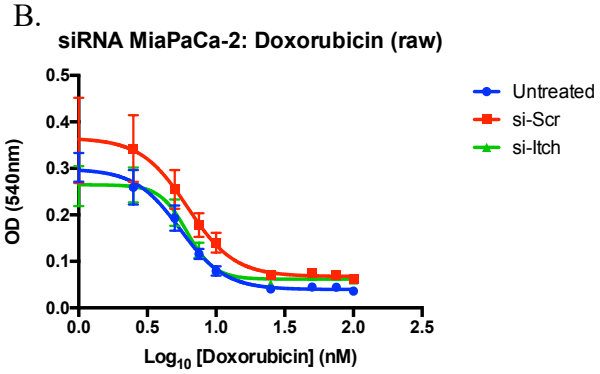
siRNA MiaPaCa-2: Doxorubicin (raw)
OD (540nm)
Log10 [Doxorubicin] (nM)
Untreated
si-Scr
si-Itch

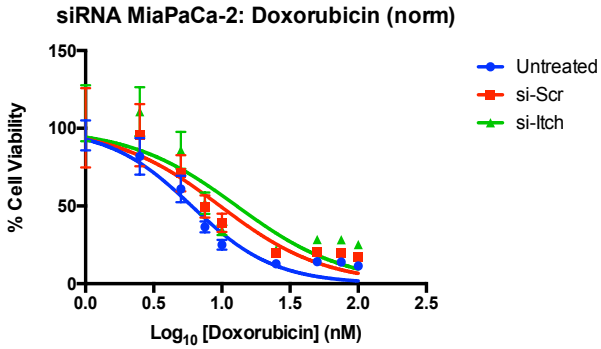
siRNA MiaPaCa-2: Doxorubicin (norm)
% Cell Viability
Log10 [Doxorubicin] (nM)
Untreated
si-Scr
si-Itch

C.

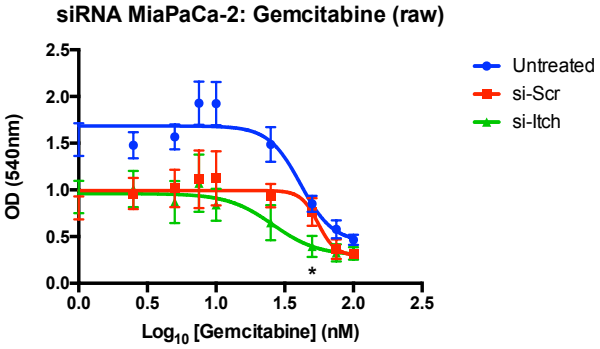
siRNA MiaPaCa-2: Gemcitabine (raw)
OD (540nm)
Log10 [Gemcitabine] (nM)
Untreated
si-Scr
si-Itch

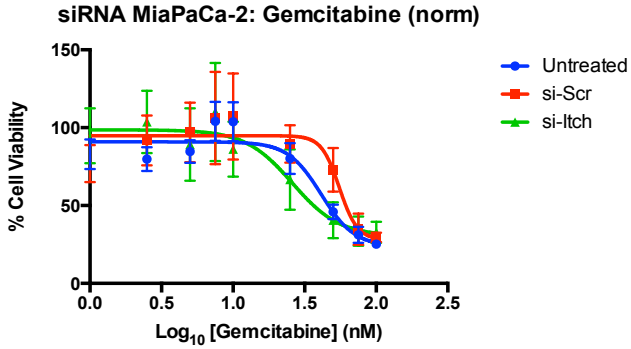
siRNA MiaPaCa-2: Gemcitabine (norm)
% Cell Viability
Log10 [Gemcitabine] (nM)
Untreated
si-Scr
si-Itch

D.

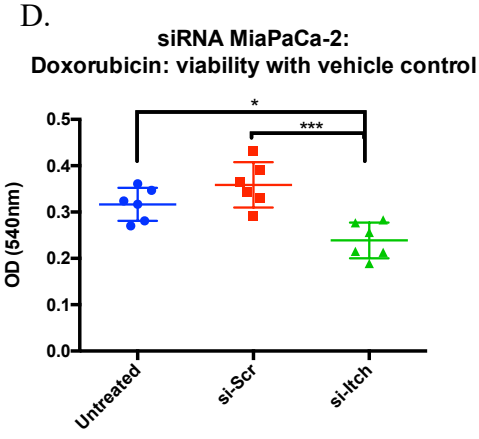
siRNA MiaPaCa-2:
Doxorubicin: viability with vehicle control
OD (540nm)
*
***
Untreated
si-Scr
si-Itch

E.

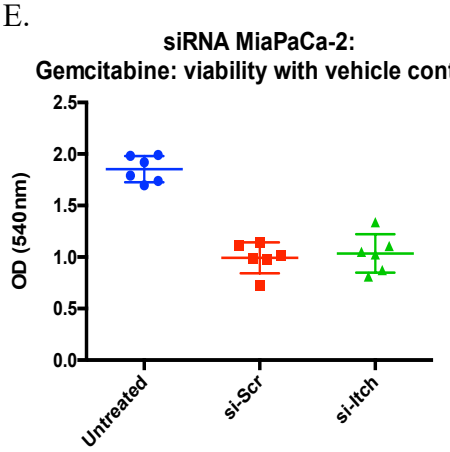
siRNA MiaPaCa-2:
Gemcitabine: viability with vehicle control
OD (540nm)
Untreated
si-Scr
si-Itch

Supplementary Figure 10: Biological repeat of MiaPaCa-2 siRNA-mediated transient *Itch* knockdown cell survival experiments:

Resultant (left) and normalised (right) SRB cell-survival curves for MiaPaCa-2 cells treated with siRNA in combination with additional treatment. **A.** Cells treated with 0-4 Gy γ-radiation; resultant data showed significant reduction in OD readout in si-Itch cells compared to untreated cells for doses 0, 0.5, 1, 2 and 4 Gy ($p = 9.21\times10^{-11}$, 8.03×10^{-11}, 3.57×10^{-8}, 5.86×10^{-10}, and 2.95×10^{-11} respectively). No statistically significant increase in sensitivity was observed upon normalisation of the data. **B.** Cells treated with 0-100 nM doxorubicin (plotted as $\log_{10}$[doxorubicin]); no statistically difference was seen for both resultant and normalised data. **C.** Cells treated with 0-100 nM gemcitabine (plotted as $\log_{10}$[gemcitabine]); resultant data showed significant reduction in OD readout for si-Itch with 50 nM gemcitabine compared to si-Scr ($p = 6.46\times10^{-4}$). No statistically significant increase in sensitivity was observed upon normalisation of the data. Radiation data was normalised to cells that did not receive radiation. Doxorubicin and gemcitabine data were normalised to a vehicle control. A * donates statistically significant difference in mean as determined by Student's t-test. **D.** & **E.** Viability of cells treated with just the vehicle control shows significant decrease in cell viability when just the si-Itch is present compared to untreated cells in the case of the doxorubicin regimen. Number of asterixis donates degree of statistical significance of a one-way ANOVA between conditions (* = $p < 0.05$, *** = $p < 0.001$).

A.

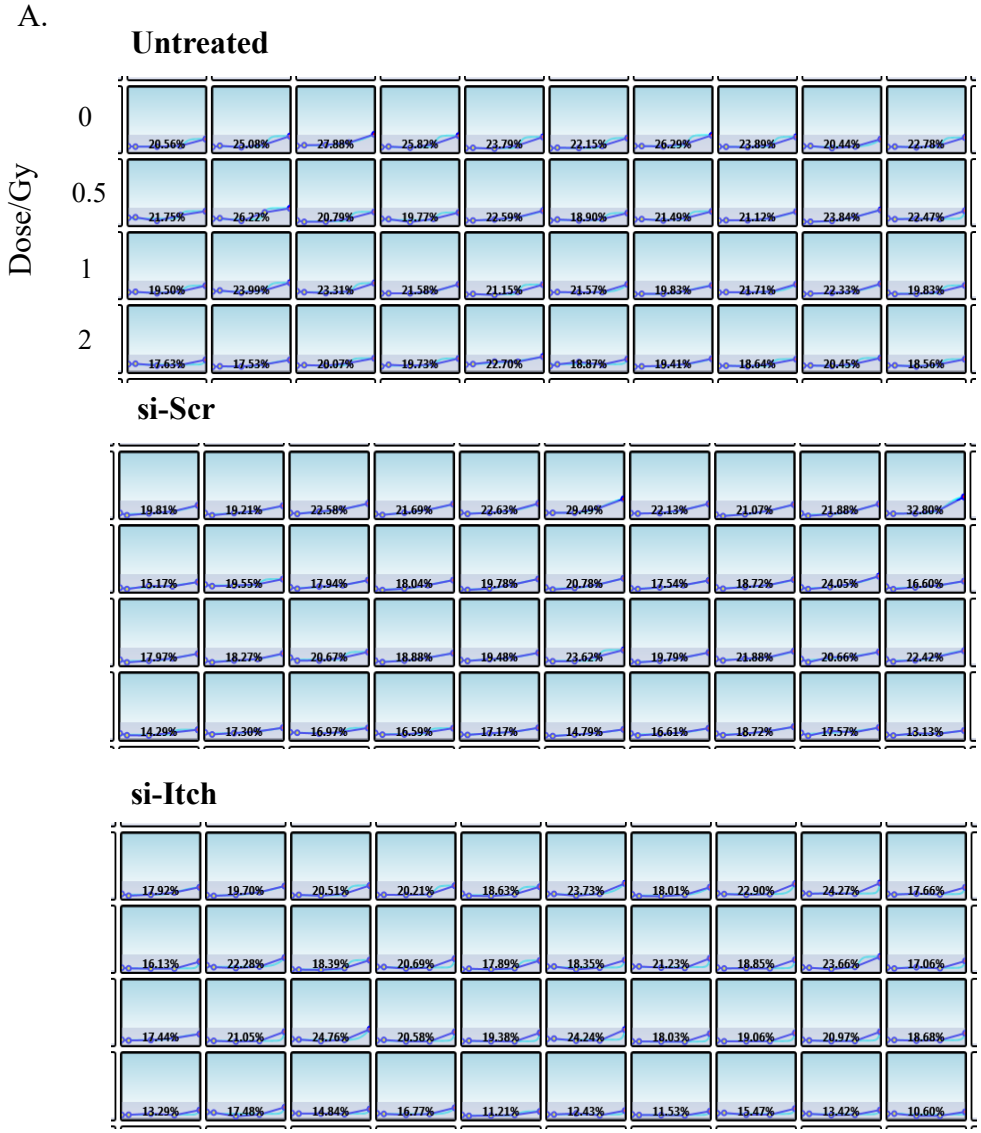
Untreated
Dose/Gy
0
0.5
1
2
20.56% 25.08% 27.88% 25.82% 23.79% 22.15% 26.29% 23.89% 20.44% 22.78%
21.75% 26.22% 20.79% 19.77% 22.59% 18.90% 21.49% 21.12% 23.84% 22.47%
19.50% 23.09% 23.31% 21.58% 21.15% 21.57% 19.83% 21.71% 22.33% 19.83%
17.63% 17.53% 20.07% 19.73% 22.70% 18.87% 19.41% 18.64% 20.45% 18.56%
si-Scr
19.81% 19.21% 22.58% 21.69% 22.63% 29.49% 22.13% 21.07% 21.88% 32.80%
15.17% 19.55% 17.94% 18.04% 19.78% 20.78% 17.54% 18.72% 24.05% 16.60%
17.97% 18.27% 20.67% 18.88% 19.48% 23.62% 19.79% 21.88% 20.66% 22.42%
14.29% 17.30% 16.97% 16.59% 17.17% 14.79% 16.61% 18.72% 17.57% 13.13%
si-Itch
17.92% 19.70% 20.51% 20.21% 18.63% 23.73% 18.01% 22.90% 24.27% 17.66%
16.13% 22.28% 18.39% 20.69% 17.89% 18.35% 21.23% 18.85% 23.66% 17.06%
17.44% 21.05% 24.76% 20.58% 19.38% 24.24% 18.03% 19.06% 20.97% 18.68%
13.29% 17.48% 14.84% 16.77% 11.21% 12.43% 11.53% 15.47% 13.42% 10.60%

B.

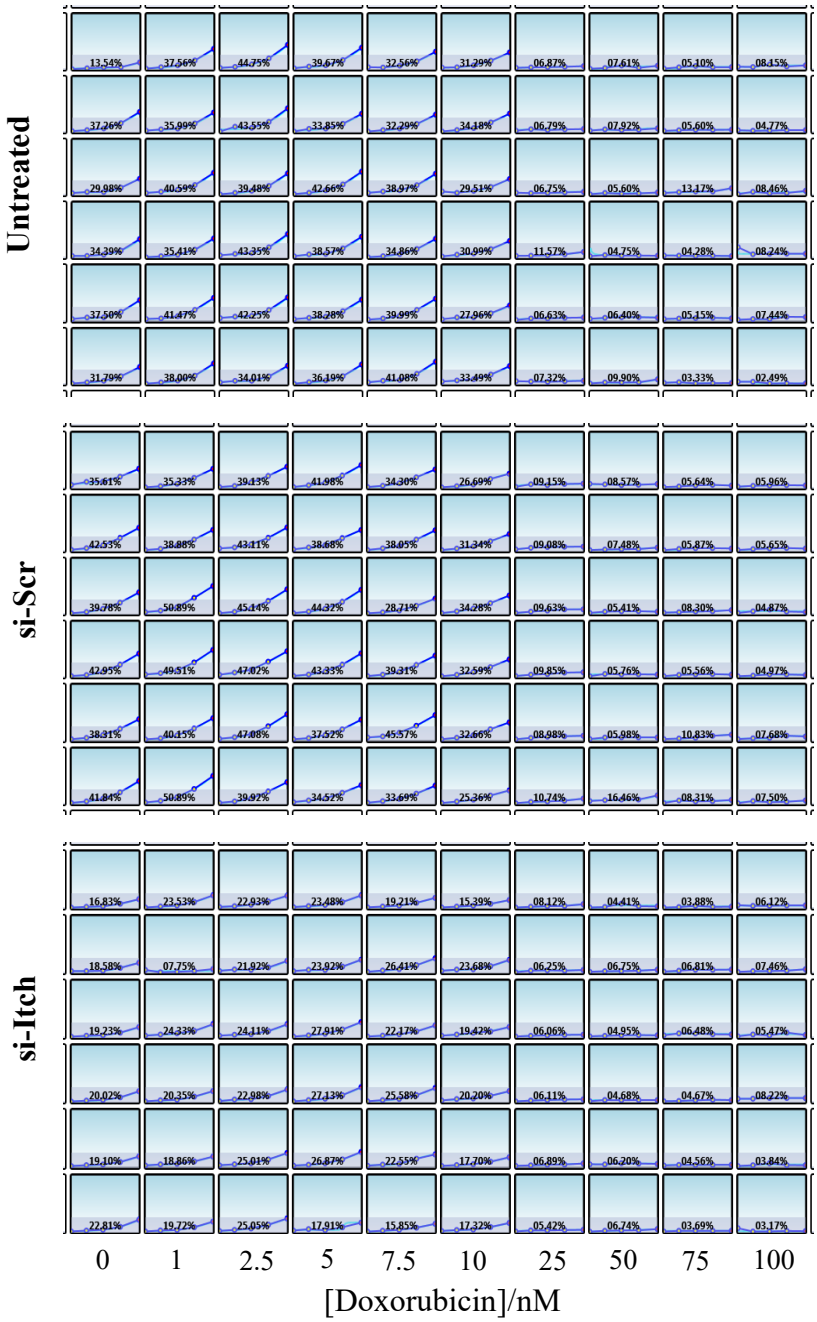
Untreated
si-Scr
si-Itch
0
1
2.5
5
7.5
10
25
50
75
100
[Doxorubicin]/nM

C.

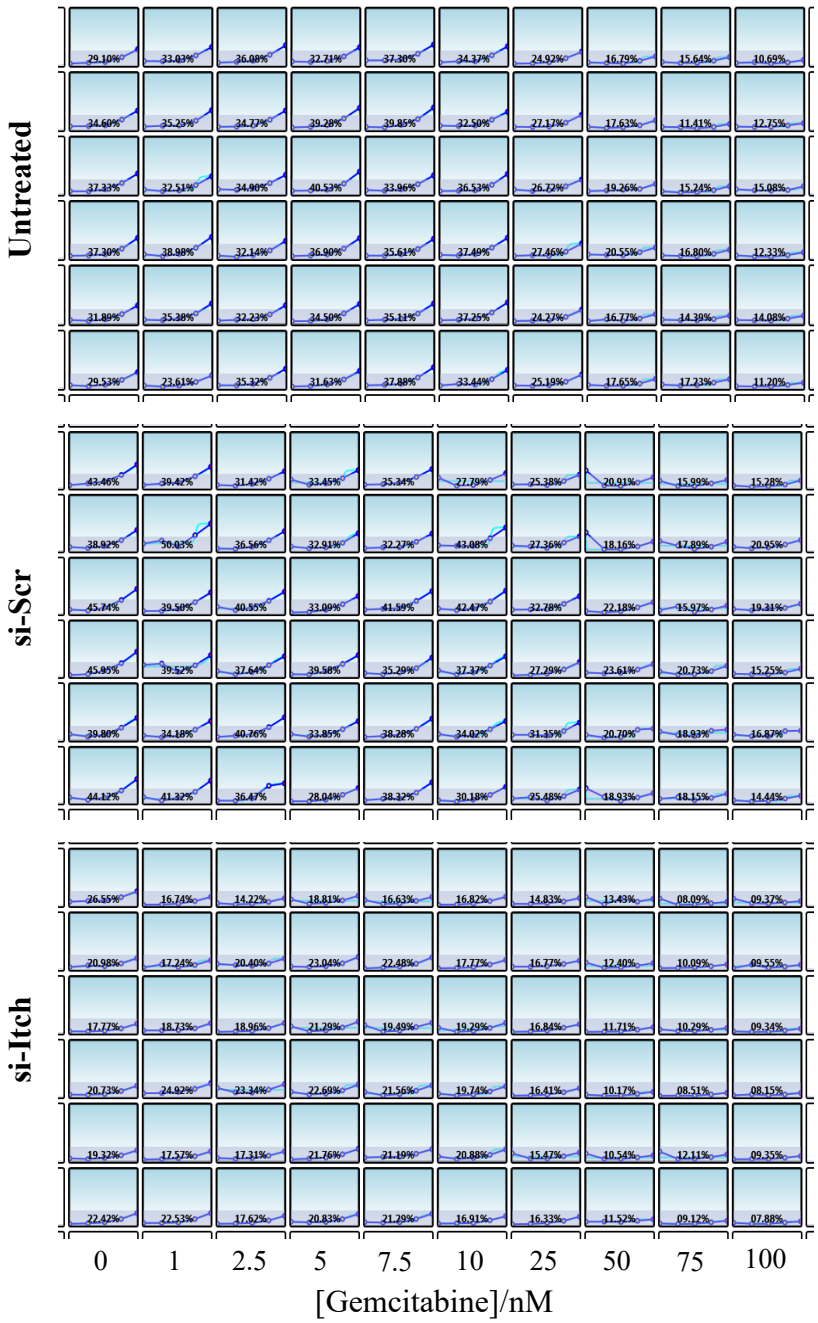

Supplementary Figure 11: Sample confluence curves generated from Celigo:
During the siRNA cytotoxicity experiments well confluence was recorded every 24 hours for irradiated (**A.**), doxorubicin-treated (**B.**), and gemcitabine-treated (**C.**) cells. Celigo algorithm detects and records all objects from a series of images from each well that fulfil a specific set of criteria programmed by the user. Images are then stitched together and a total percentage confluence per well is provided. Subsequent time-points can be recorded and used to plot graphs for each well showing the change in well confluence over time.

A.

B.

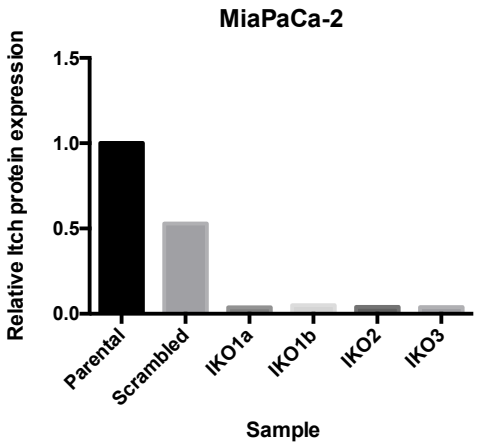

C.

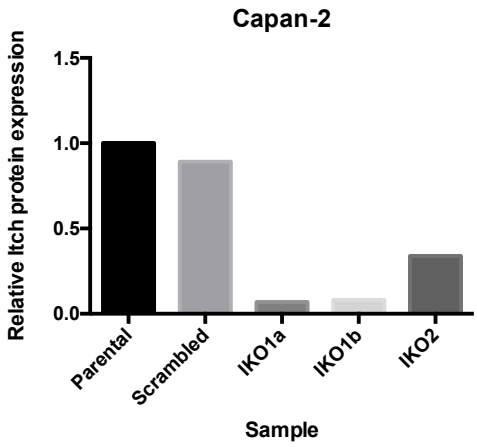

Supplementary Figure 12: initial western blot characterisation of CRISPR-mediated stable Itch knockdown in pancreatic cell lines:

Whole western blot membrane image of initial characterisation of stable Itch knockdown (**A.**). Lanes 1-3 contain lysates from cell-lines reported to be positive controls for Itch expression (MCF-7, HL60, and K562 respectively). However little green fluorescence was detected in K562 cell lysates. MiaPaCa-2 negative controls (in terms of knockdown activity) i.e. parental and scrambled in lanes 4 & 5 respectively had greater band intensity for Itch than the CRISPR+ isogenic cell lines (IKO1a/b, IKO2, and IKO3) in lanes 6, 7, and 8. Lanes 9-13 consist of lysates from Capan-2 cells with untreated and scrambled controls in lanes 9 & 10 and CRISPR+ isogenic cell lines in the subsequent two lanes. Qualitatively all CRISPR+ cells had reduced band intensity for Itch whilst having comparable β-Actin bands (housekeeping gene used - red fluorescent bands) with negative controls. Quantification and normalisation of fluorescence confirmed a <10-fold reduction in Itch protein in CRISPR^{+} MiaPaCa-2 cells compared to parental cells (**B.**). Meanwhile in Capan-2 cells, quantification of band fluorescence intensity showed a knockdown of >90% for IKO1a/b cells and ~70% for IKO2 cells.

A.

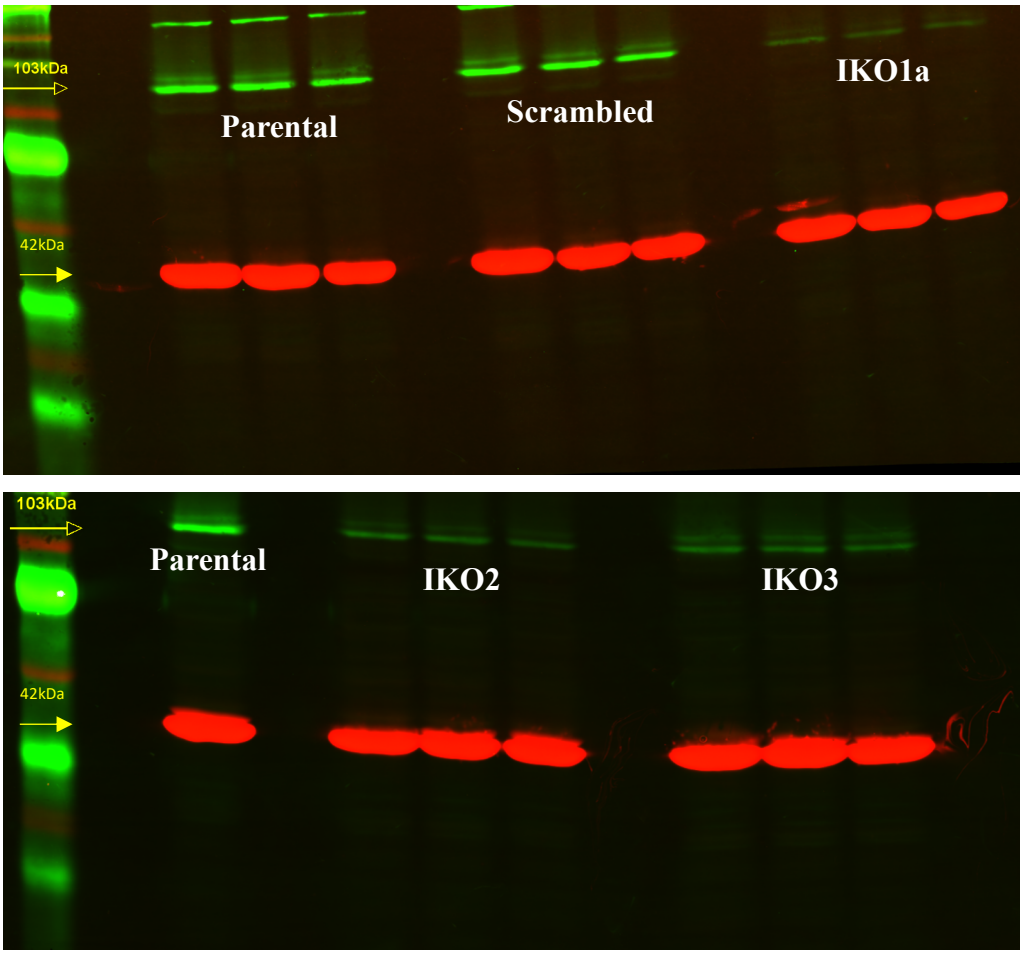

B.

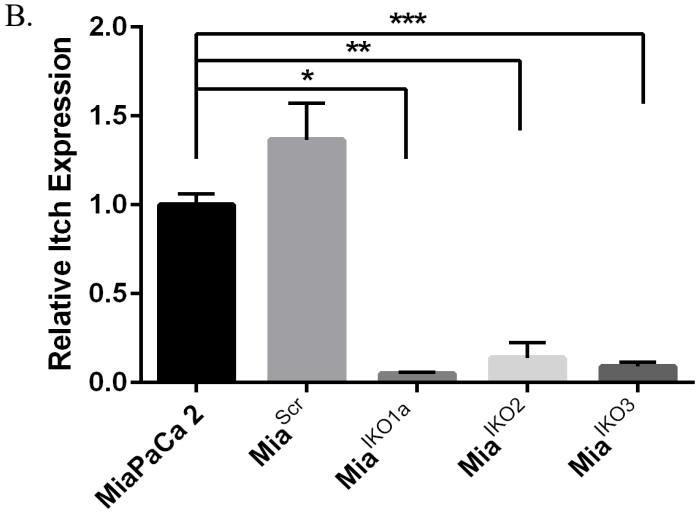

Supplementary Figure 13: Biological repeat of western blot for CRISPR transduced MiaPaCa-2 cells:

Western blot image of isogenic MiaPaCa-2 cells looking at Itch protein level with technical replicates (A.). Band fluorescence intensity was quantified and plotted (B.) – also featured in CRISPR chapter (see Figure 19), bands featured in CRISPR chapter are the same samples as this western blot however arranged in a different order to provide a better qualitative comparison.

A.

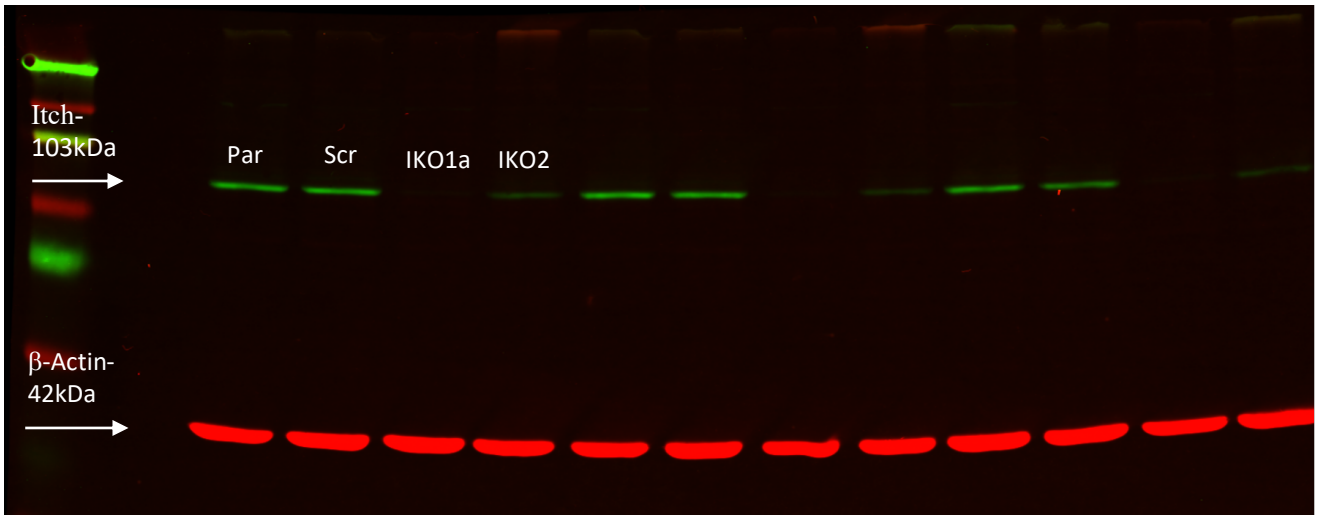

B.

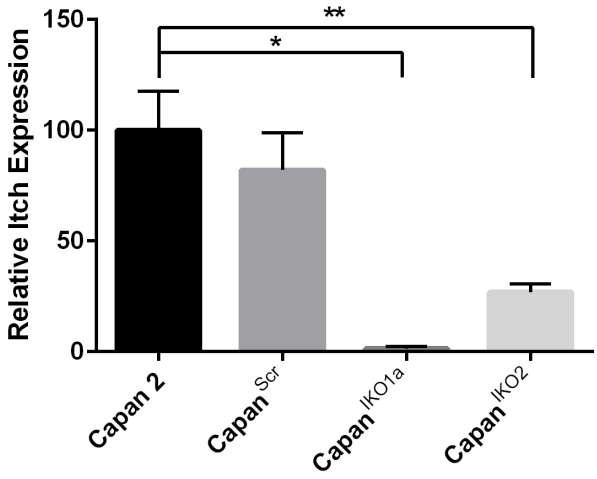

Supplementary Figure 14: Biological repeat of western blot to validate CRISPR in Capan-2 cells:

Western blot image of isogenic Capan-2 cells looking at Itch protein levels in parental (Par), scrambled (Scr), IKO1a and IKO2 cells (A.). Band fluorescence was quantified Band fluorescence intensity was quantified and plotted (B.) – also featured in CRISPR chapter (see Figure 19).

A.

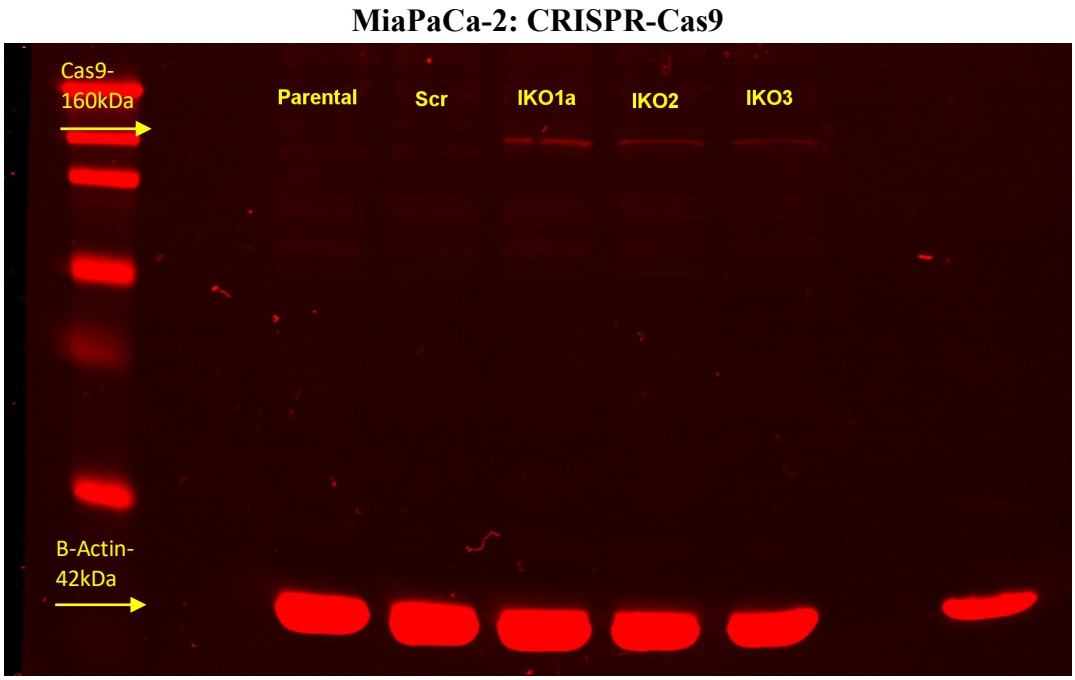

B.

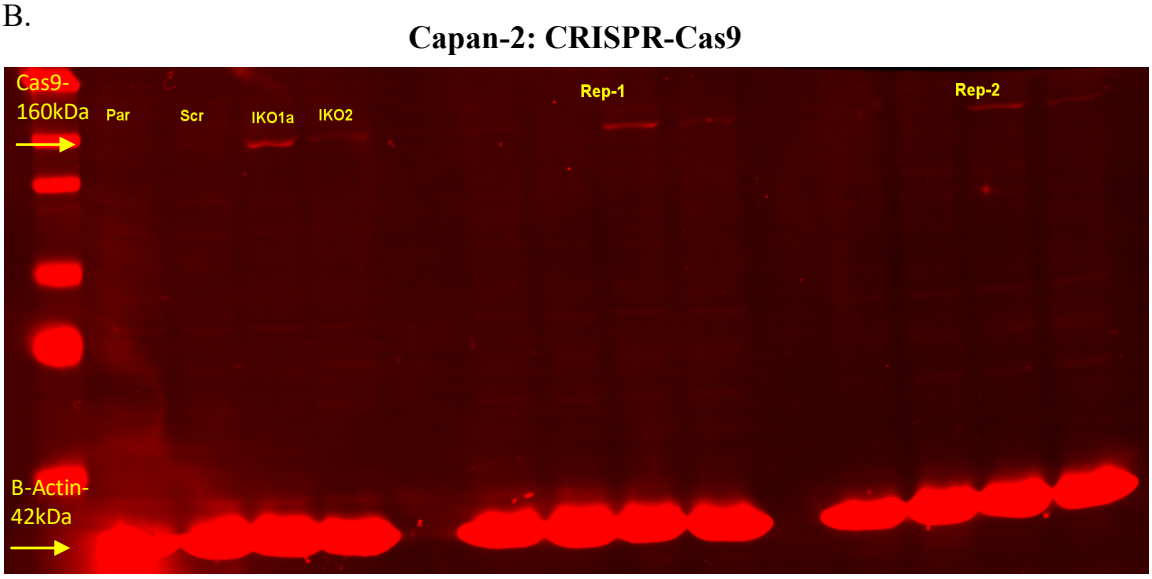

Supplementary Figure 15: Original western blot images of Cas9 expression in *Itch*-targeting CRISPR+ cell lines:

Licor image membrane probing for Cas9 and β-Actin protein (both mouse primary antibodies hence both have red fluorescence) in MiaPaCa-2 (A.) amd Capan-2 (B.) cell lines. Isogenic cell lines transduced with an Itch targeting construct showed increased expression of Cas9 compared to parental controls (Par). Interestingly, despite being transduced with lentiviral particles that shuld allow expression of Cas9, scrambled cells had no bands appear at 160kDa as is seen with the other CRISPR^{+} cells.

A.

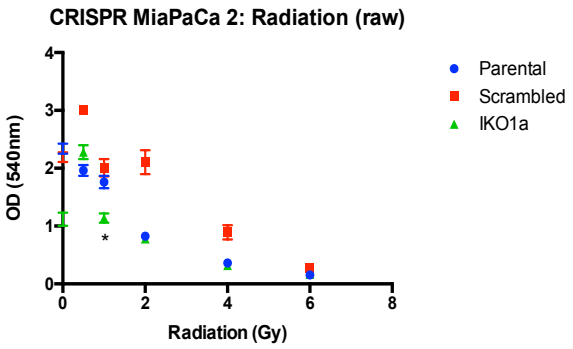
CRISPR MiaPaCa 2: Radiation (raw)
OD (540nm)
Radiation (Gy)
Parental
Scrambled
IKO1a

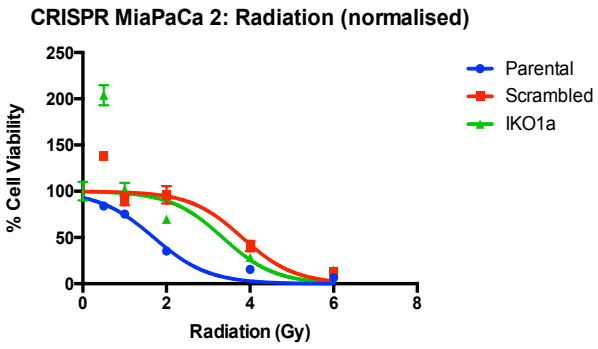
CRISPR MiaPaCa 2: Radiation (normalised)
% Cell Viability
Radiation (Gy)
Parental
Scrambled
IKO1a

B.

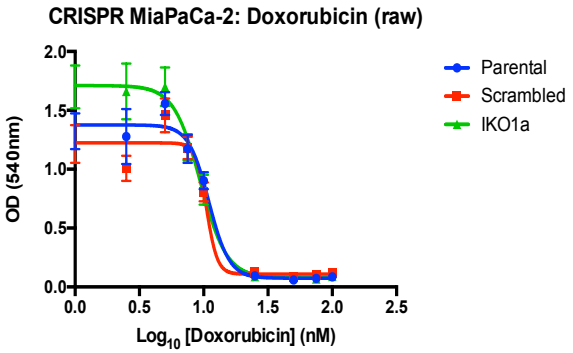
CRISPR MiaPaCa-2: Doxorubicin (raw)
OD (540nm)
Log10 [Doxorubicin] (nM)
Parental
Scrambled
IKO1a

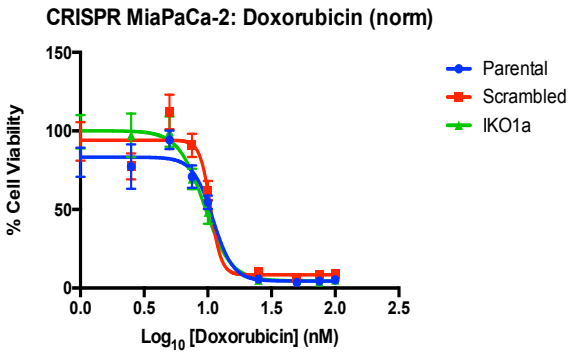
CRISPR MiaPaCa-2: Doxorubicin (norm)
% Cell Viability
Log10 [Doxorubicin] (nM)
Parental
Scrambled
IKO1a

C.

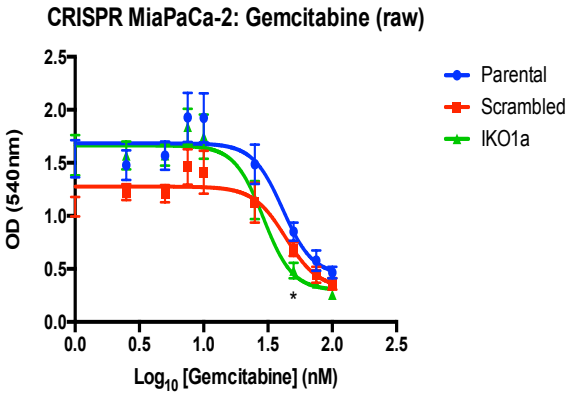
CRISPR MiaPaCa-2: Gemcitabine (raw)
OD (540nm)
Log10 [Gemcitabine] (nM)
Parental
Scrambled
IKO1a

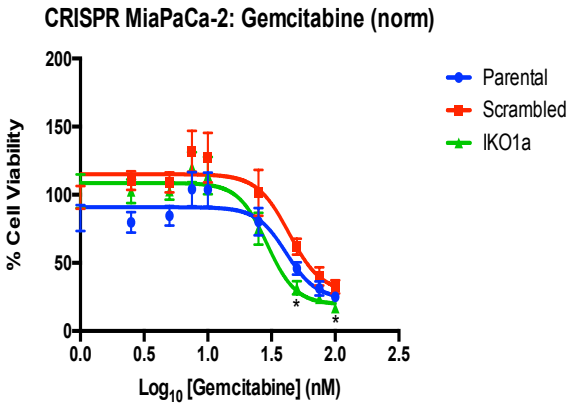
CRISPR MiaPaCa-2: Gemcitabine (norm)
% Cell Viability
Log10 [Gemcitabine] (nM)
Parental
Scrambled
IKO1a

G.

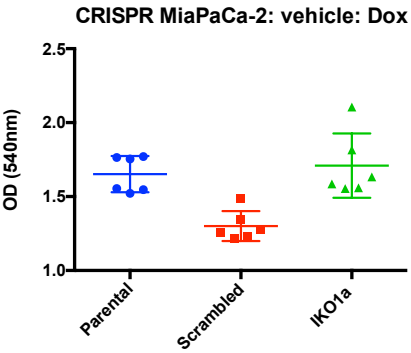
CRISPR MiaPaCa-2: vehicle: Dox
OD (540nm)
Parental
Scrambled
IKO1a

H.

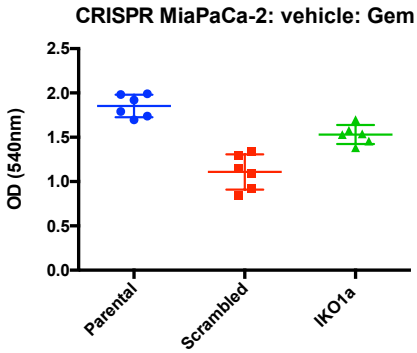
CRISPR MiaPaCa-2: vehicle: Gem
OD (540nm)
Parental
Scrambled
IKO1a

Supplementary Figure 16: Biological repeat of MiaPaCa-2 CRISPR-mediated stable *Itch* knockdown cell survival experiments:

Resultant (left) and normalised (right) SRB cell-survival curves for MiaPaCa-2 CRISPR-treated isogenic cell lines in combination with additional treatment. **A.** Cells treated with 0-6 Gy γ-radiation; resultant data showed significant reduction in OD readout in IKO1a cells compared to parental cells for doses 0 and 1 Gy ($p = 1.16\times10^{-6}$ & 1.09×10^{-9} respectively). No statistically significant increase in sensitivity was observed upon normalisation of the data. **B.** Cells treated with 0-100 nM doxorubicin (plotted as $\log_{10}$[doxorubicin]); no statistically difference was seen for both resultant and normalised data. **C.** Cells treated with 0-100 nM gemcitabine (plotted as $\log_{10}$[gemcitabine]); resultant data showed significant reduction in OD readout for IKO1a with 50 nM gemcitabine compared to parental cells ($p = 1.26\times10^{-5}$). Normalisation of the data revealed an increase in sensitivity of IKO1a cells to 50 and 100 nM ($p = 3.85\times10^{-4}$ & 1.32×10^{-3} respectively). Radiation data was normalised to cells that did not receive radiation. Doxorubicin and gemcitabine data were normalised to a vehicle control. A * donates statistically significant difference in mean as determined by Student's t-test. **D.** & **E.** Viability of cells treated with just the vehicle control. Number of asterixis donates degree of statistical significance of a one-way ANOVA between conditions.

A.

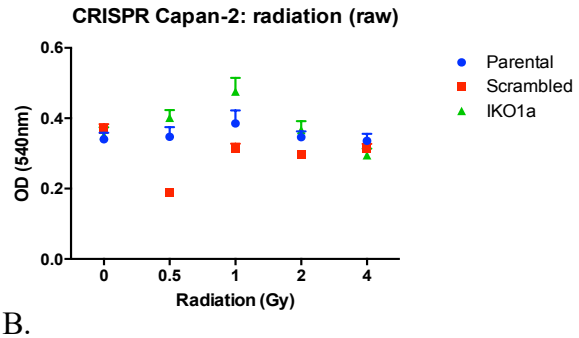
CRISPR Capan-2: radiation (raw)
OD (540nm)
Radiation (Gy)
Parental
Scrambled
IKO1a

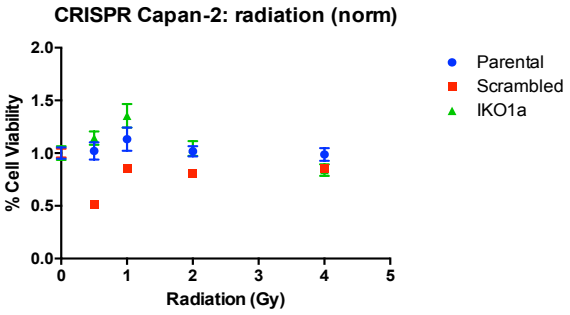
CRISPR Capan-2: radiation (norm)
% Cell Viability
Radiation (Gy)
Parental
Scrambled
IKO1a

B.

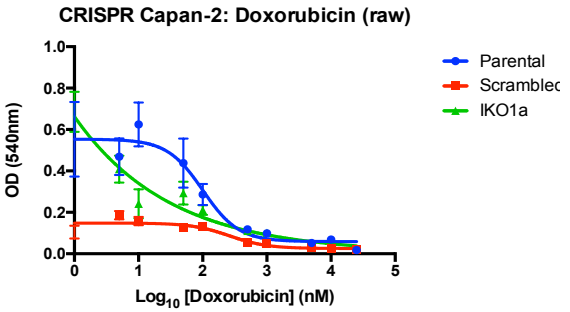
CRISPR Capan-2: Doxorubicin (raw)
OD (540nm)
Log10 [Doxorubicin] (nM)
Parental
Scrambled
IKO1a

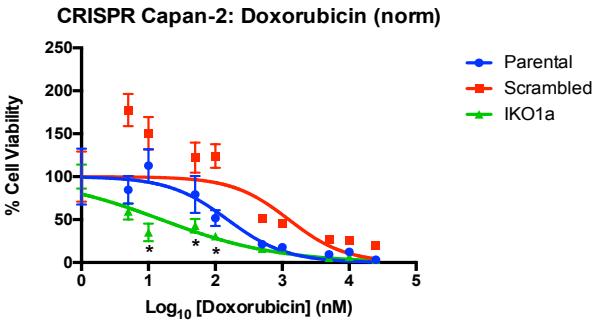
CRISPR Capan-2: Doxorubicin (norm)
% Cell Viability
Log10 [Doxorubicin] (nM)
Parental
Scrambled
IKO1a

C.

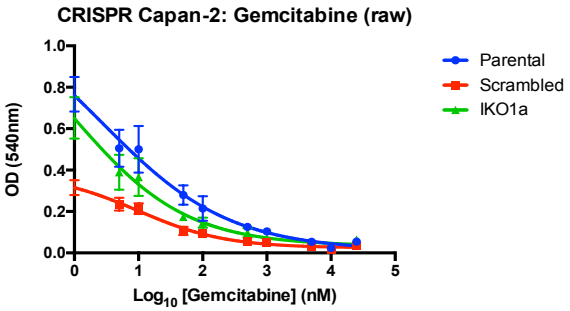
CRISPR Capan-2: Gemcitabine (raw)
OD (540nm)
Log10 [Gemcitabine] (nM)
Parental
Scrambled
IKO1a

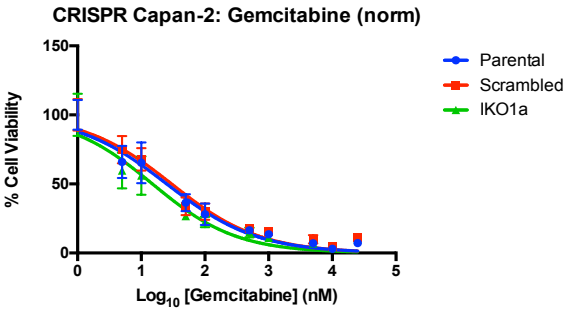
CRISPR Capan-2: Gemcitabine (norm)
% Cell Viability
Log10 [Gemcitabine] (nM)
Parental
Scrambled
IKO1a

D.

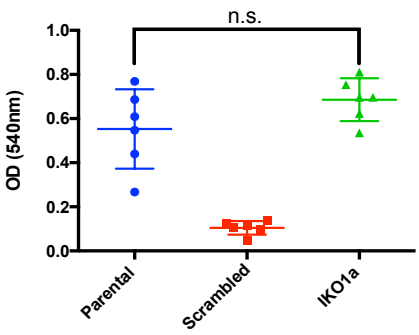
CRISPR Capan-2:
Doxorubicin: viability with vehicle control
n.s.
OD (540nm)
Parental
Scrambled
IKO1a

E.

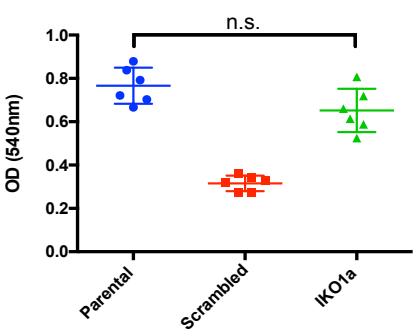
CRISPR Capan-2:
Gemcitabine: viability with vehicle control
n.s.
OD (540nm)
Parental
Scrambled
IKO1a

Supplementary Figure 17: Biological repeat of Capan-2 CRISPR-mediated stable *Itch* knockdown cell survival experiments:

Resultant (left) and normalised (right) SRB cell-survival curves for Capan-2 CRISPR-treated isogenic cell lines in combination with additional treatment. **A.** Cells treated with 0-4 Gy γ-radiation; no statistically significant decrease in resultant OD readout or increase in cell sensitivity of IKO1a cells. ($p = 1.16\times10^{-6}$ & 1.09×10^{-9} respectively). No statistically significant increase in sensitivity was observed upon normalisation of the data. **B.** Cells treated with 0-100 nM doxorubicin (plotted as $\log_{10}$[doxorubicin]); upon normalisation of the data increase in sensitivity of IKO1a cells was found at 10, 50, and 100 nM doxorubicin ($p = 5.39\times10^{-6}$, $p = 3.00\times10^{-3}$, and $p = 3.67\times10^{-4}$ respectively) **C.** Cells treated with 0-100 nM gemcitabine (plotted as $\log_{10}$[gemcitabine]); ; no statistically significant decrease in resultant OD readout or increase in cell sensitivity of IKO1a cells resultant data showed significant reduction in OD readout for IKO1a. Radiation data was normalised to cells that did not receive radiation. Doxorubicin and gemcitabine data were normalised to a vehicle control. A * donates statistically significant difference in mean as determined by Student's t-test. **D.** & **E.** Viability of cells treated with just the vehicle control. Number of asterixis donates degree of statistical significance of a one-way ANOVA between conditions.

A.

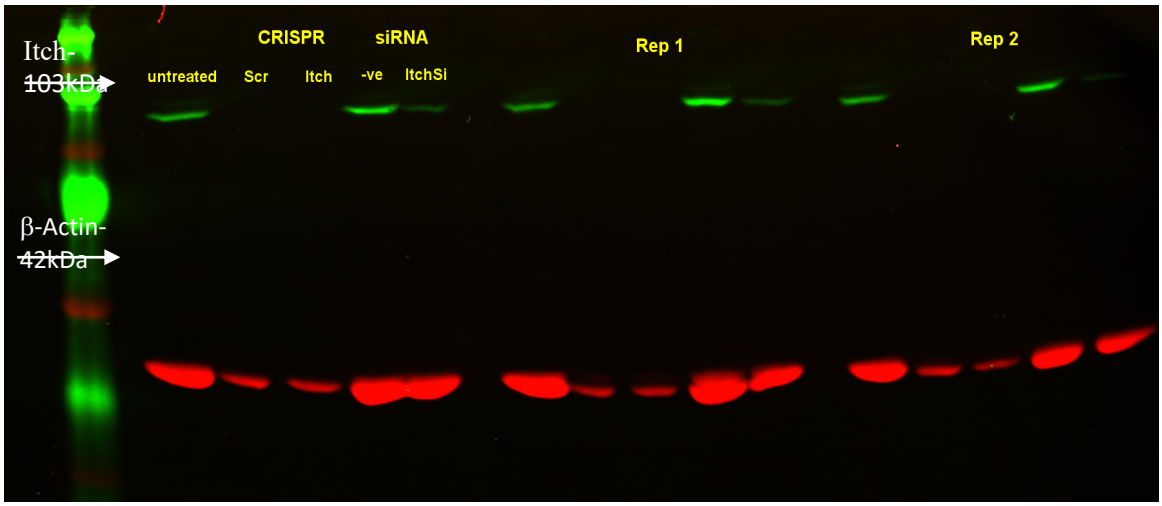

B.

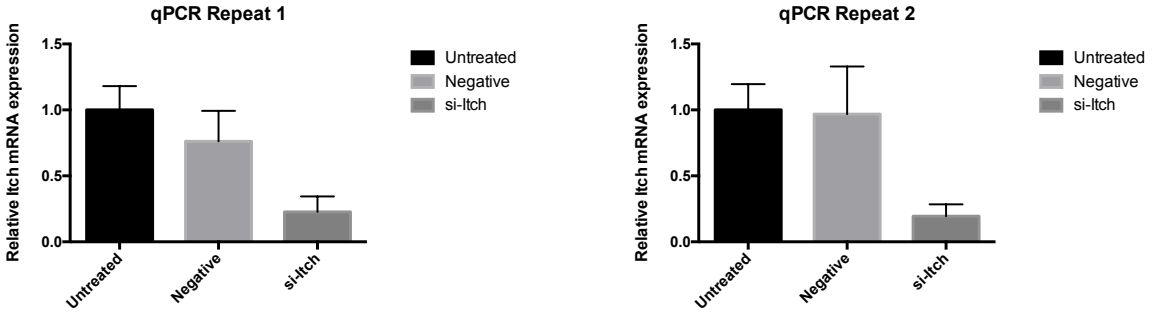

Supplementary Figure 18: siRNA-mediated *Itch* knockdown in PBMCs:

Image of whole western blot membrane (**A.**) including technical replicates (Rep 1/Rep 2). Lanes 2 & 3 for each block of 5 donate PBMCs transduced with pLentiCRISPRv2 (Scr-scrambled and Itch-CRISPR-Itch respectively) and lanes 4 & 5 donate PBMCs transfected with siRNA (-ve-scrambled and ItchSi-Itch siRNA respectively). qPCR was performed on additional PBMCs to act as biological replicates and further verify transient *Itch* knockdown (**B.**). Consistent with qPCR data described in results, *Itch* mRNA levels were reduced by 75-80% in si-Itch treated PBMCs compared to untreated controls.